UNIVERSITY OF SOUTHAMPTON

FACULTY OF NATURAL AND ENVIROMENTAL SCIENCES

School of Chemistry

A modular approach for a controlled immobilization of enzymes

by

MARTA MENEGHELLO

Thesis for the degree of Doctor of Philosophy

April 2018

UNIVERSITY OF SOUTHAMPTON

ABSTRACT

FACULTY OF NATURAL AND ENVIROMENTAL SCIENCES

Chemistry

Thesis for the degree of Doctor of Philosophy

A MODULAR APPROACH FOR A CONTROLLED IMMOBILIZATION OF ENZYMES

by Marta Meneghello

Stable, site-specific immobilization of redox proteins and enzymes is of great interest for the development of biosensors and biofuel cells, where the long-term stability of enzymatic electrodes as well as the possibility of controlling the orientation of the biomolecules at the electrode surface have a great importance. For such applications, it would be desirable to immobilise redox proteins and enzymes in a specific orientation on the electrode in order to improve direct electron transfer.

In this work, we describe such an approach using site directed mutagenesis to introduce cysteine residues at specific locations on the enzyme surface, and the reaction between the free thiol of the cysteine and maleimide groups attached on the electrode surface to immobilise the mutated enzymes. Using cellobiose dehydrogenase (CDH) as a model system, different types of electrodes (carbon and gold-based, flat and nanostructured) were firstly modified with maleimide groups using a modular approach based on electrografting and solid-phase synthesis. Therefore, the electrodes were used to covalently immobilise CDH variants bearing the free cysteine in different locations at their surface. The key point of this method is that the main elements of the modification can be independently varied to tune the architecture of the electrode surface as required, by simply changing the “bricks” of the structure.

The CDH-modified electrodes were tested for direct and mediated electron transfer, showing excellent long-term storage stability as well as good catalytic responses. The mechanisms of the direct and mediated electron transfer were fully investigated, as well as the kinetics of the CDH electrodic reactions, also employing computer simulations.

Table of Contents

Academic Thesis: Declaration of Authorship ..... **v**

Acknowledgements ..... **vi**

Abbreviations ..... **ix**

Chapter 1: Introduction **1**

1.1 Biofuel cells 2

1.1.1 Enzymatic fuel cells 3

1.1.2 Direct and mediated electron transfer 4

1.2 Immobilization of enzymes onto electrode surfaces 6

1.2.1 Reversible and irreversible immobilization techniques 7

1.2.2 Covalent and site-specific immobilization methods 8

1.3 Modification of electrode surfaces 11

1.4 Cellobiose dehydrogenase 14

1.4.1 Effect of pH and divalent cations on the IET of CDH 17

1.4.2 Applications of CDH 18

1.4.3 Protein engineering 19

1.5 Research objectives and overview 20

Chapter 2: Experimental part **25**

2.1 General 26

2.1.1 Chemicals 26

2.1.2 Instrumentation 27

2.1.3 Carbon electrodes 29

2.1.4 Gold electrodes 29

2.1.5 Cleaning and determination of surface area for gold electrodes 30

2.2 Synthesis of non-commercial reagents 31

2.2.1 Synthesis of $BocNHCH_2C_6H_4$ diazonium tetrafluoroborate 31

2.2.2 Synthesis of *N*-maleoyl-β-alanine 32

2.3 Modification of carbon electrodes 33

2.3.1 Fabrication of GC/CNT electrodes 33

2.3.2 Attachment of linker and passivating group 33

2.3.3 General method for deprotection of Boc group 34

2.3.4 Coupling of 6C-spacer 35

2.3.5 Coupling of maleimide 35
2.4 Solid-phase functionalization of CNTs 36
2.4.1 Functionalization of CNTs with anthraquinone 36
2.4.2 Functionalization of CNTs with maleimide 36
2.5 Modification of gold electrodes 37
2.5.1 Grafting of the diazonium salt 37
2.5.2 Deprotection of Boc group 39
2.5.3 Coupling of anthraquinone 39
2.5.4 Coupling of spacer and passivating group 40
2.5.5 Coupling of maleimide 40
2.6 Immobilization of CDH variants at maleimide-modified electrodes 41
2.7 Analysis and characterization techniques 42
2.7.1 Cyclic voltammetry of CDH-modified electrodes 42
2.7.2 Cyclic voltammetry of AQ-modified electrodes 42
2.7.3 Surface plasmon resonance (SPR) spectroscopy 43
2.7.4 Time-of-Flight Secondary-Ion Mass Spectrometry (ToF-SIMS) 44
2.8 Simulation of catalytic voltammograms 45

Chapter 3: Covalent immobilization of CDH at GC/CNT electrodes 47
3.1 Modification of the carbon electrodes 48
3.1.1 Introduction 48
3.1.2 Electrode modification and enzyme immobilization 50
3.1.3 *Mt*CDH variants used in this work 51
3.2 Direct electron transfer of immobilised CDH 52
3.2.1 Non-catalytic voltammetry 52
3.2.2 Steady-state catalysis 56
3.2.3 Michaelis-Menten catalytic behaviour 58
3.2.4 Control experiment: D- and L-glucose 61
3.2.5 Direct electron transfer of different CDH variants 62
3.3 Mediated electron transfer of immobilised CDH 68
3.3.1 Mediated electron transfer of different CDH variants 68
3.3.2 Comparison between DET and MET results 72
3.3.3 Potential shift of MET catalytic current 74
3.4 Mechanisms of the direct and mediated electron transfer 77

3.4.1 Effect of calcium chloride on the DET and MET 78
3.4.2 Effect of calcium chloride on two different CDH variants 83
3.4.3 Control experiment with papain 85
3.5 Stability of the CDH-modified electrodes 90
3.5.1 Stability over the time 90
3.5.2 Covalent immobilization *vs.* physical adsorption 93
3.5.3 Control experiment: effect of Triton X-100 98
3.6 Solid-phase functionalization of CNTs 105
3.6.1 Introduction 105
3.6.2 Functionalization of CNTs with anthraquinone 106
3.6.3 Solid-phase functionalization of CNTs with maleimide 112
3.7 Conclusion 114

Chapter 4: Simulations of CDH catalytic voltammograms 117
4.1 Kinetic model for the CDH electrode reactions 118
4.1.1 Mechanisms of the direct and mediated electron transfer 118
4.1.2 Modelling the CDH kinetics at the electrode surface 120
4.1.3 Derivation of a potential-dependent Michaelis-Menten equation 123
4.2 Simulations of catalytic voltammograms 129
4.2.1 Definition of parameters and constants 129
4.2.2 Estimation of k_{med} 132
4.2.3 Estimation of K_M 136
4.2.4 Estimation of k_{cat} 139
4.2.5 Relationship between k_{cat} and K_M 145
4.2.6 Estimation of k_{int} 147
4.3 Simulation of different CDH variants 151
4.3.1 Introduction 151
4.3.2 Simulation of the MET of the four CDH variants 153
4.3.3 Estimation of m_{enz} and k_{int} for DET data 155
4.3.4 New equation to simulate two enzyme populations 158
4.3.5 Simulation of the DET of the four CDH variants 160
4.4 Interaction between CDH and ferrocene 164
4.4.1 Limit of our model 164
4.4.2 Michaelis-Menten interaction between CDH and ferrocene 168

4.4.3 Estimation of K_M^{med} and k_{cat}^{med} 170
4.4.4 New simulations of DET and MET experiments 172
4.4.5 New estimation of K_M and k_{cat} 175
4.5 Conclusion 178

Chapter 5: Covalent immobilization of CDH at flat electrodes 183
5.1 Immobilization of CDH at flat GC electrodes 184
5.1.1 Comparison between GC and GC/CNT electrodes: covalent immobilization of anthraquinone 184
5.1.2 Immobilization of CDH at flat GC electrodes 191
5.2 Covalent modification of gold electrodes 195
5.2.1 Method: electrochemical grafting of a diazonium salt 195
5.2.2 Characterization by anthraquinone coupling and CV 197
5.2.3 Characterization of gold functionalization by ToF-SIMS 199
5.2.4 Characterization of gold functionalization by SPR 204
5.3 Immobilization of CDH at gold electrodes 209
5.3.1 Procedure 209
5.3.2 Control experiment with a GC/CNT electrode 211
5.3.3 MET of CDH immobilised at flat gold electrodes 213
5.3.4 DET of CDH immobilised at flat gold electrodes 217
5.3.5 Effect of a different pH 219
5.3.6 Control experiment: effect of D- and L-glucose 221
5.3.7 Covalent immobilization *vs.* physical adsorption 222
5.3.8 Stability over the time 224
5.3.9 Effect of different spacers 226
5.3.10 Characterization of CDH immobilization by SPR 230
5.3.11 Effect of different CDH variants on the immobilization process 235
5.3.12 Electrochemical analysis of CDH-modified SPR substrates 237
5.4 Conclusion 241

Chapter 6: Conclusions 245
6.1 Future outlook 249

List of References 251

Academic Thesis: Declaration of Authorship

I, Marta Meneghello

declare that this thesis and the work presented in it are my own and has been generated by me as the result of my own original research.

A modular approach for a controlled immobilization of enzymes

I confirm that:

1. This work was done wholly or mainly while in candidature for a research degree at this University;
2. Where any part of this thesis has previously been submitted for a degree or any other qualification at this University or any other institution, this has been clearly stated;
3. Where I have consulted the published work of others, this is always clearly attributed;
4. Where I have quoted from the work of others, the source is always given. With the exception of such quotations, this thesis is entirely my own work;
5. I have acknowledged all main sources of help;
6. Where the thesis is based on work done by myself jointly with others, I have made clear exactly what was done by others and what I have contributed myself;
7. Parts of this work have been published as:

   F.A. Al-Lolage, M. Meneghello, S. Ma, R. Ludwig, P.N. Bartlett, *A Flexible Method for the Stable, Covalent Immobilization of Enzymes at Electrode Surfaces*, ChemElectroChem **2017**, 4 (6), 1528-1534.

Signed: .....

Date: .....

Acknowledgements

The first person I would like to thank is my supervisor Phil Bartlett, for his support and help, for the long chats about this work, always ending with useful advice and brilliant ideas.

Thanks also to my group, past and present, in particular Eva, Charlie, Hisham, Eugene, David and Gabriella. A special thank goes to Firas, who had shared with me a great part of this work, through good times and bad ones, being a great co-worker and friend. In the electrochemistry group, I would like to thank also Saiful and Guy for the nice chats and help, and Alistair.

In the rest of the chemistry department, I would like to thank the groups of Ramon Rios-Torres (especially Marta Meazza) and Richard Brown for having welcomed me, sometimes unconsciously, and allowed carrying out some organic synthesis, such as the diazonium salt, with the risk of seeing their laboratories exploding. Thanks also to the people working in the glassware workshop for solving a lot of problems with a lot of electrodes. A great thank also to Jeremy Kilburn and his group (in particular Marloes Peeters), which were at the Queen Mary University of London, for giving me a valuable input to start this work.

I would like to thank also Marie Curie, for having given the name to my scholarship, and the European Union for the funding, but especially for the great project and consortium of people I could work with. Thanks to the "Bioenergy" project, in these years I had the opportunity to meet a lot of people working on this topic, gain a lot of experience and travel across Europe for meetings, workshops and secondments. I would like to thank all the people I had the pleasure to work with and that helped me with many experiments (either in my university or in theirs): Magdalena Murawska, Nicolas Mano and Alexander Kuhn (CNRS of Bordeaux, France); Galina Pankratova, Jani Tuoriniemi and Lo Gorton (University of Lund, Sweden); Till Siepenkoetter, Serguei Belochapkine and Edmond Magner (University of Limerick, Ireland); Hussein Kanso, David Hernandez Santos and María Begoña González García (DropSens, Oviedo, Spain). Thanks also to Valentina, Francesca, Sabine, Chiara and Elena that was always a pleasure to meet somewhere in Europe for project duties, conferences or other

travels. Finally, a special thank goes to Su Ma and Roland Ludwig (BOKU-University, Vienna, Austria) for having provided a very important element of this work (the enzyme!), and for being always ready to answer my many questions and giving useful advice. Especially Su Ma, for having also shared with me a flat in Oviedo for a month!

Thanks also to all the nice people I have met in Southampton, especially to Mr Jerry and Phoebe: the life in England would not have been the same without you!

And finally I want to thank my parents, my brother Massimo and Giulia, for their support and for always asking about my work, even if they could not understand it… Lastly, I really need to thank Victor for having spent with me all these years of PhD, supporting me in the good and bad times (mostly good, I must say), giving also advice about organic chemistry issues, allowing me to use his fume hood in the Brown group for my organic chemistry experiments, carrying out all the NMR spectra of this work and, finally, for never being tired of me for all this! And for being sat in front of me during all the writing of this thesis (that was quite long!).

Abbreviations

ACN	Acetonitrile
AQ	Anthraquinone
AuSPE	Gold screen-printed electrode
BFC	Biofuel cell (or biological fuel cell)
Boc	*tert*-Butyloxycarbonyl
CDH	Cellobiose dehydrogenase
CNT	Carbon nanotube
CV	Cyclic voltammetry (or cyclic voltammogram)
DET	Direct electron transfer
DMF	Dimethylformamide
EDC	*N*-Ethyl-*N*′-(3-dimethylaminopropyl)carbodiimide
EDTA	Ethylenediaminetetraacetic acid
FAD	Flavin adenine dinucleotide
Fc	Ferrocene
GC	Glassy carbon
GC/CNT	Glassy carbon modified with multiwall carbon nanotubes
HDA	Hexanediamine
IET	Interdomain (or internal) electron transfer
MET	Mediated electron transfer
*Mt*CDH	Cellobiose dehydrogenase from *Myriococcum thermophilum*
NHS	*N*-Hydroxysuccinimide
NMR	Nuclear magnetic resonance
RI	Refractive index
RT	Room temperature
SAM	Self-assembled monolayer
SCE	Saturated calomel electrode
SPR	Surface plasmon resonance
TBATFB	Tetrabutylammonium tetrafluoroborate
ToF-SIMS	Time-of-flight secondary-ion mass spectrometry

Chapter 1:

Introduction

This Chapter will start with an overview on biofuel cells, which are one of the main applications this work is intended to. We will focus, in particular, on enzymatic fuel cells as the purpose of this work was the immobilization of enzymes at electrode surfaces. The methods to do that will be described afterwards, focussing especially on the covalent techniques that can be used for a controlled immobilization of the biocatalysts. Therefore, we will give an overview on the procedures employed for the modification of electrode surfaces, since the introduction of organic functionalities at the sensor surface is essential for the covalent immobilization of enzymes. Finally, the enzyme used in this work, cellobiose dehydrogenase, will be briefly described.

1.1 Biofuel cells

Biological fuel cells or, simply, biofuel cells (BFCs) are systems capable of transforming chemical energy into electrical energy by using enzymes as the catalysts and natural compounds, such as glucose or ethanol, as the fuel [1-5]. The conversion is achieved by coupling an oxidation reaction supplying electrons at the anode (*e.g.* the oxidation of glucose to gluconolactone) with a reduction reaction utilizing electrons at the cathode (*e.g.* the reduction of oxygen). So that we may call the device a biofuel cell, these two reactions or, at least, one of them (generally the anodic reaction, which consumes the fuel) must be catalysed by biological catalysts, such as enzymes or whole microorganisms. The two reactions are electronically separated inside the system to force electrons to flow through an external circuit, while ion movement inside the cell maintains charge balance and completes the electrical circuit (see Figure 1.1).

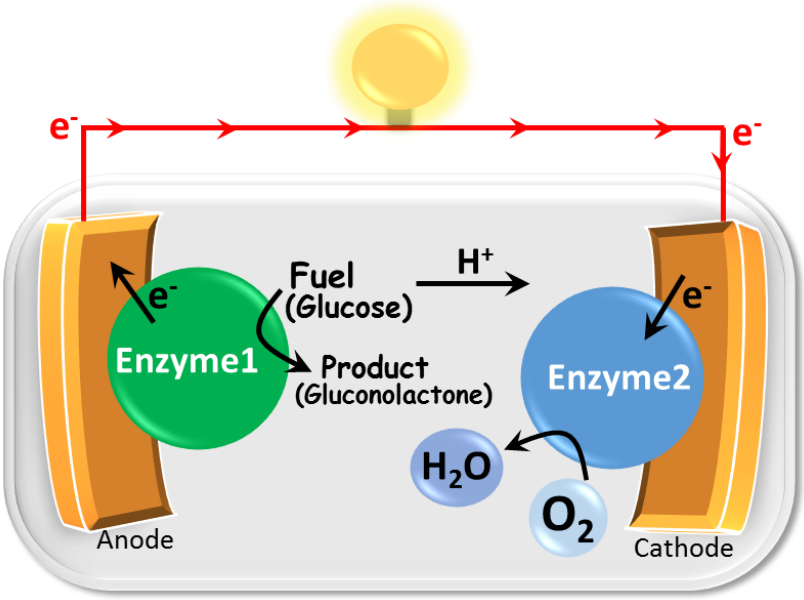

Figure 1.1. *Schematic representation of the simplest model of enzymatic biofuel cell, without membrane and redox mediators.*

An important benefit of BFCs over conventional (inorganic) fuel cells is the low cost of their components, as the chemical reactions are driven by abundant and renewable bio-fuels and biological catalysts, instead of using fossil fuels and expensive rare metal catalysts [5]. Another significant environmental advantage of the BFCs is that they can be disposable and completely biodegradable devices.

Moreover, the use of redox enzymes offers some interesting advantages, such as low operational temperature, working pH close to neutral, as well as high activity and selectivity toward the enzyme substrates [4]. This latter characteristic can simplify the design of a biofuel cell, since fuel and oxidant do not need to be in two distinct compartments or separated by a membrane, opening the way for an extreme miniaturization of the devices.

However, to this day, applications of biofuel cells have been rather limited because the maximum power output is still orders of magnitude lower than for conventional fuel cells, batteries or solar cells [3]. This is due to the low power density of enzymatic electrodes because of the huge dimensions of enzymes if compared with other catalysts, such as metal atoms. For that, while solar energy probably has the highest potential among all forms of alternative energy to solve future energy problems, BFCs are of great interest for a variety of niche applications, such as implantable medical devices or environmental self-powered sensors [3,6]. For instance, a BFC could use the glucose and the oxygen dissolved in the body fluids as fuel and oxidant, respectively, and power microvalves, drug dispensers, pacemakers, sensors or smart contact lenses [7-11].

Biofuel cells can be classified according to the biocatalyst used: systems using isolated enzymes for at least part of their operation are known as enzymatic fuel cells, while those utilising whole organisms are called microbial fuel cells [5]. There are some differences between these two types of BFCs: for example, isolated enzymes are substrate specific, while the diverse enzyme contents of a whole organism can be used for a wide range of fuels. Since this work aims to find new strategies for the immobilization of enzymes at electrode surfaces, we will focus our discussion on enzymatic fuel cells.

1.1.1 Enzymatic fuel cells

Almost all biochemical processes in living organisms are catalysed by enzymes. A group of these proteins, the so-called oxidoreductases (or redox enzymes), is responsible for reactions involving electron transfer. Different subclasses of oxidoreductases are defined according to the type of substrate they act on, as well as the reaction mechanism (*e.g.* dehydrogenases, oxidases, peroxidases) [5].

Enzymatic fuel cells use oxidoreductases as catalysts, either at both cathode and anode, or at just one of the electrodes. Enzymes usually employed in anodes include dehydrogenases, enzymes with a NADH or NADPH cofactor, and those with a FAD cofactor usually deeply buried inside the protein. Glucose oxidase, the most common enzyme in BFC anodes and carbohydrate biosensors, belongs to the latter group [5]. For biological cathodes, the enzymes are typically multi-copper oxidases, which are capable of a four-electron reduction of O_2 to water, such as laccases [12-14] and bilirubin oxidases (BOD) [15,16].

Despite the interesting advantages described above arising from the use of enzymes as biocatalysts, there are still some issues to be solved. The major problems are the short lifetime of enzymes and their instability when functioning in a foreign environment, and the low power density of enzymatic electrodes. The short lifetime (a few hours) is an intrinsic characteristic of enzymes even in their natural conditions, but it can be increased by an efficient immobilization [5]. On the other hand, as we have already mentioned in the previous Section, the low power density is due to the large dimensions of enzymes that, although extremely active in comparison to the catalytic site of a metal electrode, cannot form a densely packed monolayer like metal atoms. Other issues are connected with transport limitations of substrates and products of redox reactions and inefficient direct electron transfer between the electrode surface and the enzyme active centre, which is usually buried inside the protein [4].

1.1.2 Direct and mediated electron transfer

One answer to solve the electronic coupling problem is to employ redox mediators to shuttle electrons between the enzyme active site and the electrode surface, in a mechanism known as mediated electron transfer (MET, see Figure 1.2-A) [17-19]. The mediator is normally a small organic molecule or a metal complex. It may be soluble and free in solution or immobilised onto the electrode together with the enzyme. Importantly, the mediator must be capable of efficient electron transfer at a particular potential, which should be thermodynamically favourable with respect to the enzyme redox potential, that is more positive for anodic enzymes and more negative for cathodic enzymes [19].

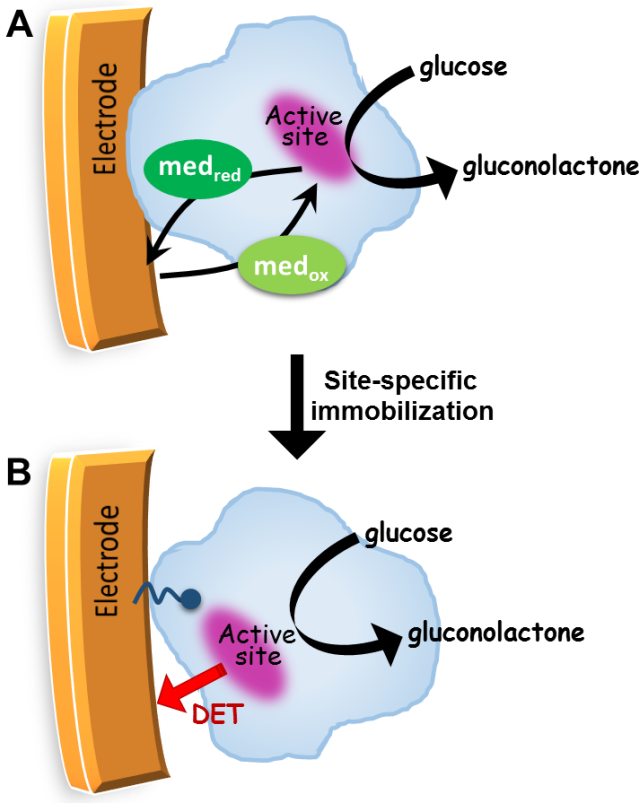

Figure 1.2. *A) Schematic representation of the mediated electron transfer (MET) of a glucose oxidising enzyme with the active site buried inside the protein or in the wrong orientation. B) Representation of a site-specific immobilization to achieve direct electron transfer (DET).*

Although a mediator is essential if the active site is occluded and, consequently, unable to exchange electrons directly with the electrode surface, its use implies some disadvantages. In fact, a mediator adds an extra step to the electron transfer chain, usually lowering the catalytic rate and decreasing the BFC voltage, since anodic and cathodic potentials will be closer. In addition, mediators may not be biocompatible, preventing BFCs to be used for applications such as implantable or biodegradable devices [4].

Therefore, other answers to the electronic coupling problem would be preferred. For example, the enzyme can be immobilised on the electrode in such a way that direct electron transfer (DET) is engaged, without using a redox mediator (see Figure 1.2-B). Indeed, DET is possible if the active site itself or, more commonly, an electron relay centre lies close to the electrode surface. However, most of the sugar oxidising enzymes, such as glucose oxidase, present the catalytic centres fairly deeply inside the protein, so that achieving efficient DET is a key challenge and the use of redox mediators is indispensable [4,20].

Nevertheless, a small group of oxidoreductases is able to communicate directly with the electrodes without the need of any mediator. One of these promising enzymes for bioelectrochemistry applications is the flavocytochrome cellobiose dehydrogenase (CDH), which will be used in this work. An overview on cellobiose dehydrogenase will be given in Section 1.4. For the moment, we will proceed with the discussion of the techniques that can be employed for the immobilization of enzymes at electrode surfaces, focusing in particular on the covalent immobilization. This presents the advantage of being able to control the orientation of the enzyme, bringing the active site close to the electrode surface, if the immobilization occurs at a specific site of the protein: in this case we can talk of "site-specific" immobilization.

1.2 Immobilization of enzymes onto electrode surfaces

Immobilization is a technical process in which enzymes are fixed to or within solid supports, creating a heterogeneous immobilised enzyme system, which often mimics the enzyme natural mode in living cells [21]. The first industrial use of immobilized enzymes was reported in 1966 by Chibata and co-workers, who developed the immobilization of *Aspergillus oryzae* aminoacylase for the resolution of synthetic racemic D-L amino acids [22]. Other major applications of immobilised enzymes are the industrial production of sugars, amino acids and pharmaceuticals [23]. However, in this Section we will focus on procedures of enzyme immobilization at electrode surfaces to be suitable for applications such as biosensors or biofuel cells.

An efficient immobilization system generally maintains the enzyme activity and stabilises its structure, making it more robust and resistant to environmental changes. Thus, the inherent short lifetime of enzymes can be extremely increased upon immobilization [5]. In addition, we should be able to control the orientation of the enzyme at the electrode surface to minimise the electron transfer distance, so that DET is engaged without using diffusing redox mediators. Finally, the method should be generally applicable, working for a wide range of enzymes and electrode types, and the immobilization procedure should be easy to carry out. In this work, we present the results of our recent attempts to meet this challenge.

1.2.1 Reversible and irreversible immobilization techniques

The enzymes can be attached to the support via interactions ranging from reversible physical adsorption and ionic linkages to stable covalent bonds. Physical methods are characterised by weak interactions such as hydrogen bonds, hydrophobic interactions, Van der Waals forces, affinity binding, ionic binding or mechanical containment of the enzyme within the support [24-26]. The simplest immobilization method is non-specific adsorption, which is mainly based on physical adsorption or ionic binding. Enzymes can be adsorbed onto electrodes of all types, but may denature and block electron transfer [27]. Other non-covalent interactions are hydrophobic adsorption [25,28], affinity binding [29] and chelation or metal binding [30]. These are all reversible methods for enzyme immobilization, highly attractive mostly for economic reasons because, once the enzymatic activity decays, the support can be regenerated and re-loaded with fresh enzyme [26].

However, the most widely used methods for enzyme immobilization are irreversible procedures such as entrapment in polymers [31,32] or lipid bilayer films [33,34] and, finally, formation of covalent bonds. Entrapment of enzymes in membranes or polymers allows the substrates and the products to pass through, retaining the big biocatalyst. This method requires the synthesis of the polymeric network in the presence of the enzyme. Cross-linking is another irreversible method of enzyme immobilization, performed by formation of intermolecular cross-linkages between the enzyme molecules thanks to bi- or multifunctional reagents, *e.g.* glutaraldehyde [35]. However, for a more stable immobilization with the possibility of controlling the orientation of the enzyme at the electrode surface, the formation of covalent bonds between the enzyme and the support is preferred.

1.2.2 Covalent and site-specific immobilization methods

Covalent bonds are generally formed through reaction between the functional groups of the protein surface with functional groups present on the support, which can be characteristic groups of the electrode material or introduced at its surface using different methods as we will see in Section 1.3. For example, the exposed amino groups of lysine residues readily react with supports bearing activated carboxylic groups. A common reagent used to activate carboxylic acids forming the corresponding esters is *N*-hydroxysuccinimide (NHS): the esters then will form stable amide bonds with the lysine residues of the protein (Scheme 1.1-A). The nucleophilicity of the amino groups also allows reaction with epoxide-functionalised materials, which have the advantage of being relatively stable to hydrolysis at neutral pH (Scheme 1.1-B). Nevertheless, lysine residues are quite common and abundant in proteins, resulting in random orientations of the enzymes immobilised using these methods.

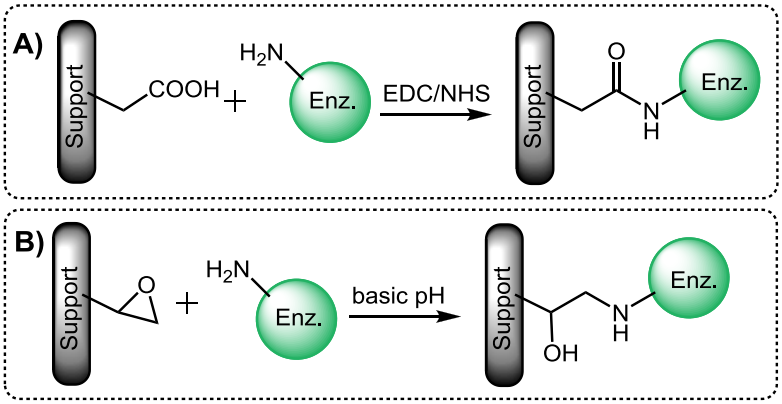

Scheme 1.1. *Reactions of (A) a carboxylic group and (B) an epoxide group immobilised onto a support with the amino groups of enzymatic lysine residues.*

Other functional groups used for protein immobilization are the carboxylic groups of aspartic and glutamic acid residues, which are usually converted to their corresponding active esters *in situ* using a carbodiimide coupling reagent and an auxiliary nucleophile, *e.g.* EDC and NHS (Scheme 1.2). The active esters can then react with amine-bearing supports. The advantage of this combination of reagents is that both EDC and NHS are water-soluble and may be used in aqueous media. However, this method presents the same disadvantages as the previous ones, since aspartic and glutamic acid residues are rather abundant in proteins.

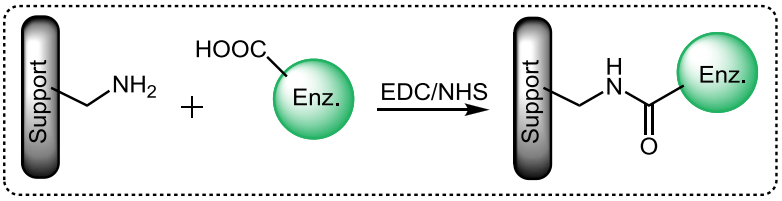

Scheme 1.2. *Reaction of an amino group immobilised onto a support with the carboxylic groups of enzymatic residues (aspartic or glutamic acids).*

To address the issue of random enzyme orientations at electrode surfaces, in recent years several selective immobilization methods able to proceed under mild physiological conditions have received increasing attention [36]. Some of these methods rely on the labelling of proteins with an azide moiety, which can then react with alkynes (Huisgen 1,3-dipolar cycloaddition or "click chemistry" [37,38]) or be activated with a phosphine to react with a variety of electrophiles (Staudinger ligation [39-41], see Scheme 1.3). In any case, for a site-selective attachment, this method also requires the use of an enzymatic site-selective labelling procedure of the azide moiety. Moreover, activation reagents or catalysts are necessary for quantitative reaction yields.

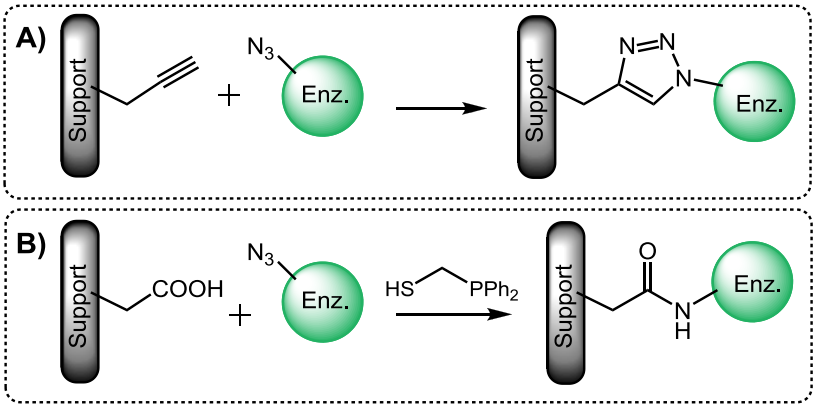

Scheme 1.3. *Reactions of (A) an alkyne and (B) an electrophile (carboxylic group in this case) immobilised onto a support with an azide moiety introduced at the protein surface. Reactions name: A) Huisgen 1,3-dipolar cycloaddition or "click chemistry"; B) Staudinger ligation.*

A promising recent example of site-specific immobilization is the use of the thiol-ene click reaction to attach a cysteine tagged enzyme to a vinyl group at the electrode surface using a tris-(2-carboxyethyl)phosphine catalyst [42] (Scheme 1.4-A). Another method is given by the introduction of genetically encoded affinity tags in the protein structure. Probably, the most well-known tag is the

polyhistidine tag (His-tag), usually consisting of six sequential histidine residues that can chelate metals such as Cu(II), Co(II), Zn(II) or Ni(II) [43,44]. However, the strength of the binding interaction is relatively weak (k_d ≈ 1-10 μM) and, also, the selectivity of this method is rather low since several proteins have been identified that are also able to bind metal ions, thus competing with the desired histidine tag. In addition, this method is usually used to attach the tag at either the N- or C-terminus of the polypeptide chain, and the His-tag is a bulky group.

In this work we adopted a site-selective immobilization method that employs the coupling of an amino acid residue, namely cysteine, with unsaturated carbonyls, such as maleimide, to form stable thioether bonds (Scheme 1.4-B). It has been shown that maleimide groups strongly favour conjugate addition with thiols at physiological pH (6.5-7.5) without the need of any other reagent or catalyst, while under these conditions amines are predominantly protonated and unreactive [21]. As proteins generally have very few surface-exposed cysteine residues, this method can be highly site-selective especially if combined with site-directed mutagenesis [45,46] to engineer the removal of all but one surface cysteine or to insert a single cysteine on the surface. The absence of the requirement for any added reagent or catalyst for the maleimide/thiol coupling reaction and its mild conditions represent a significant advantage making the process very efficient in its use of engineered enzyme.

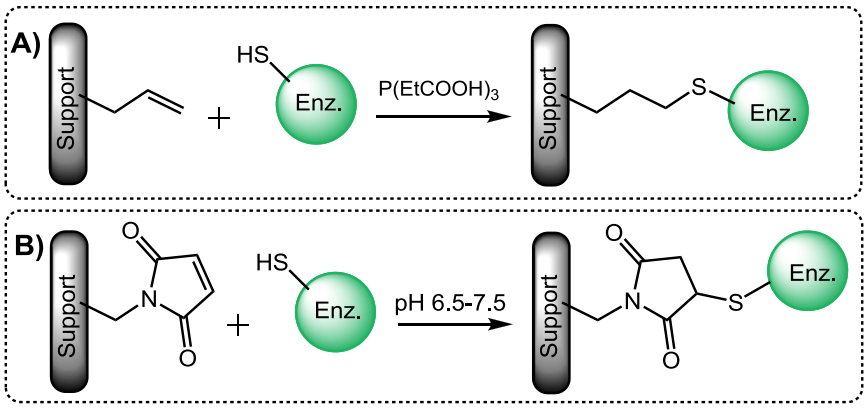

Scheme 1.4. *Reactions of (A) a vinyl group and (B) a maleimide group immobilised onto a support with the thiol group of an enzymatic cysteine residue.*

It is clear that the covalent immobilization of enzymes requires electrode surfaces functionalised with monolayers of organic molecules appropriate to accommodate the biomolecule of choice using one of the reactions described

here above. The next Section will give an overview on the electrode modification, giving special attention to those techniques that can ensure a stable attachment of the desired biocatalyst or recognition molecule on the surface, even when a potential is applied to the underlying electrode.

1.3 Modification of electrode surfaces

The modification of electrode surfaces has been an active area of research for over 40 years dating back to pioneering studies by Lane and Hubbard [47] and Murray et *al.* [48,49]. The first two scientists exploited the tendency of olefins to chemisorb irreversibly on platinum electrodes in order to attach a variety of reactive entities to the electrode surface. On the other hand, Murray used organosilanes to react with the hydroxyl groups present on metal oxide surfaces (SnO_2, RuO_2, TiO_2, Pt/PtO, Au/Au(oxide), Si/SiO_2) in order to functionalise the electrodes with amino groups [50]. Therefore, a wide range of interesting molecules can be coupled to the amino-modified surface by using conventional solid-phase synthesis.

One of the most popular methods for the monolayer modification of metal surfaces is based upon the spontaneous adsorption of thiols to form so-called self-assembled monolayers (SAMs) [51-53]. Adsorption of thiols or disulphides results in the oxidation of the –SH or cleavage of the S-S bond, and the formation of an Au-S bond that is characterised by a partial covalent bond [54]. SAMs have many advantages including easy preparation, formation of densely-packed structures and the possibility of introducing a great number of functional groups at the monolayer surface. However, there are limitations concerning the thermal and mechanical stability [55] and the gold-thiol bond can suffer from oxidative or reductive desorption [56,57]. As a result, there has been an increasing interest in approaches that retain the chemical flexibility of the SAM approach but having stronger bonding between the electrode surfaces and the monolayer of assembled molecules.

Alternative methodologies for the functionalization of carbon and metal surfaces are nowadays well developed. In particular, the electrochemical oxidation of primary amines [58,59] and reduction of aryl diazonium salts [60,61] have been

shown to be versatile methods for the attachment of a wide variety of organic species. The covalent attachment of the organic molecules occurs in two steps: first, the formation of a radical species by applying a positive or negative potential and, second, the chemical grafting of the radical to the electrode surface (Scheme 1.5).

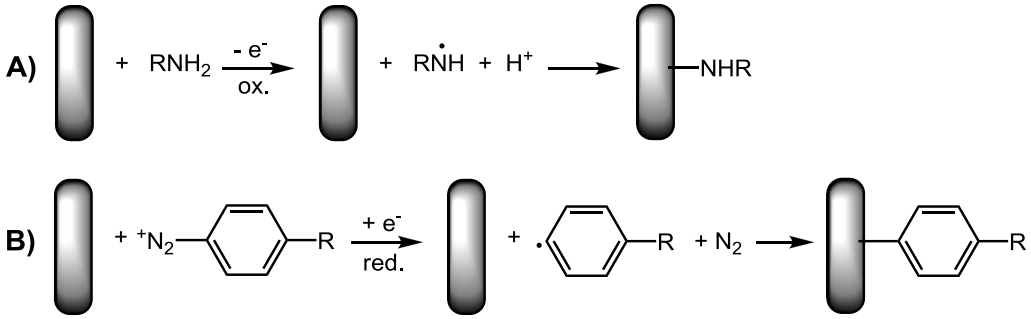

Scheme 1.5. *Two-steps electrochemical attachment of (A) a primary amine and (B) an aryl diazonium salt at a carbon surface (adapted from [59]).*

Aryl diazonium salts form robust covalent bonds with the surface of conducting and semiconducting materials [61]. Films of diazonium salts on gold substrates have been found more stable than thiol monolayers [62], so that diazonium chemistry has been successfully used to immobilise a wide variety of chemically sensitive groups and biomolecules at electrode surfaces. On the other hand, amines can form stable covalent bonds upon electrochemical oxidation only with carbon [59]. However, given the growing interest in different types of carbon materials for electrochemical applications, the oxidation of amines has been widely used to modify electrodes with redox probes or biomolecules, starting from the work of Deinhammer *et al.* [63].

Recently, Bartlett and co-workers described a novel application of these methods, in which a linker bearing a Boc-protected amino group is grafted onto carbon or gold surfaces via oxidation of primary amines or reduction of aryl diazonium salts [64-67]. After removal of the Boc protecting group (Scheme 1.6), a wide range of molecules can be coupled to the amino-modified surface using conventional solid-phase coupling methodology.

The advantages of using the Boc protecting group are that the conditions for covalent attachment to the electrode can be separately optimised and that the reaction is easily controlled electrochemically and monitored through the

current passed. The Boc protecting group appears to prevent the formation of bridged structures or polymeric layers in the diamine case. In the case of diazonium coupling, this approach allows using a single diazonium salt to couple a range of molecules to the electrode surface, avoiding the necessity to synthesise a variety of different diazonium salts and overcoming problems of poor stability for some of these salts. In addition, the presence of the bulky Boc group on the diazonium salt discourages the formation of polymeric layers on the surface by blocking coupling of further aryl radicals at the 3 and 5 positions of the aryl groups already attached to the surface. Therefore, the Boc protective group is readily and cleanly removed in acid to leave a primary free amine, which can be reacted using a variety of well-characterised solid-phase coupling reagents.

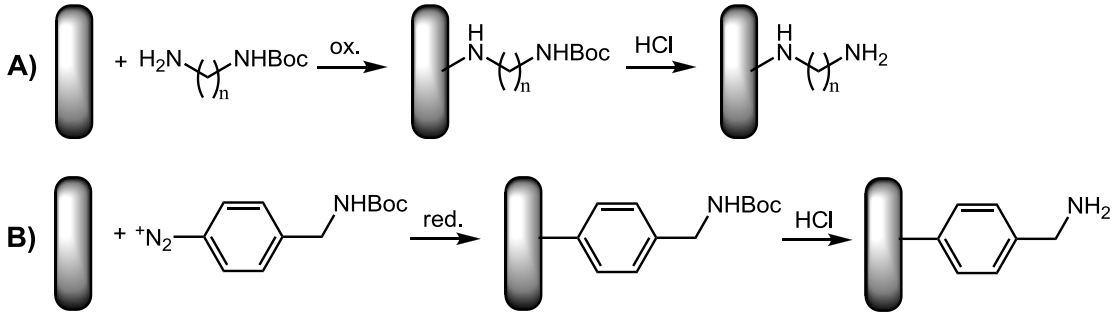

Scheme 1.6. *Schematic representation of the electrochemical attachment of (A) a mono-Boc protected diamine and (B) a Boc protected diazonium salt onto a carbon electrode, and removal of the Boc protecting group (adapted from [64]).*

In this work, we used both of these two methods, employing the electrochemical oxidation of amines to modify carbon electrodes as well as the reduction of a diazonium salt in the case of gold electrodes. In both cases, we obtained surfaces functionalised with amino groups that can be further modified using solid-phase synthesis to immobilise the molecules of choice. In our case, we wanted to immobilise maleimide since, as said in the previous Section, it can then be used for the site-specific immobilization of enzymes bearing only one free cysteine at their surface.

The maleimide modification has already been employed in combination with diazonium salt chemistry to immobilise biomolecules at electrode surfaces [68], also using a maleimide-functionalised aryl diazonium salt [69]. However, this would imply the synthesis beforehand of the maleimide-diazonium salt, which may not be very stable. In our procedure, instead, the different modification steps

were performed separately so that only one Boc protected diamine or one Boc protected diazonium salt are sufficient to produce a huge variety of different molecular architectures at the electrode surface. This method for the formation of maleimide-functionalised electrodes has been developed in our group and already tested for the immobilization of cytochrome c [70]. In this work, we applied this method to the site-specific immobilization of a promising redox enzyme, cellobiose dehydrogenease, that can be used as a valid alternative to glucose oxidase as the anodic catalyst in biofuel cells or recognition molecule in biosensors. The next Section will give an overview on this enzyme.

1.4 Cellobiose dehydrogenase

Cellobiose dehydrogenase (CDH, cellobiose: acceptor 1-oxidoreductase, EC 1.1.99.18) is an extracellular monomeric enzyme, between 85 and 101 kDa in mass depending on degree of glycosylation, secreted by various wood-degrading fungi [71-74]. It carries two prosthetic groups: a flavin adenine dinucleotide (FAD) cofactor and a haem cofactor located in two different domains: the FAD in a dehydrogenase domain and the haem in a cytochrome domain. The two

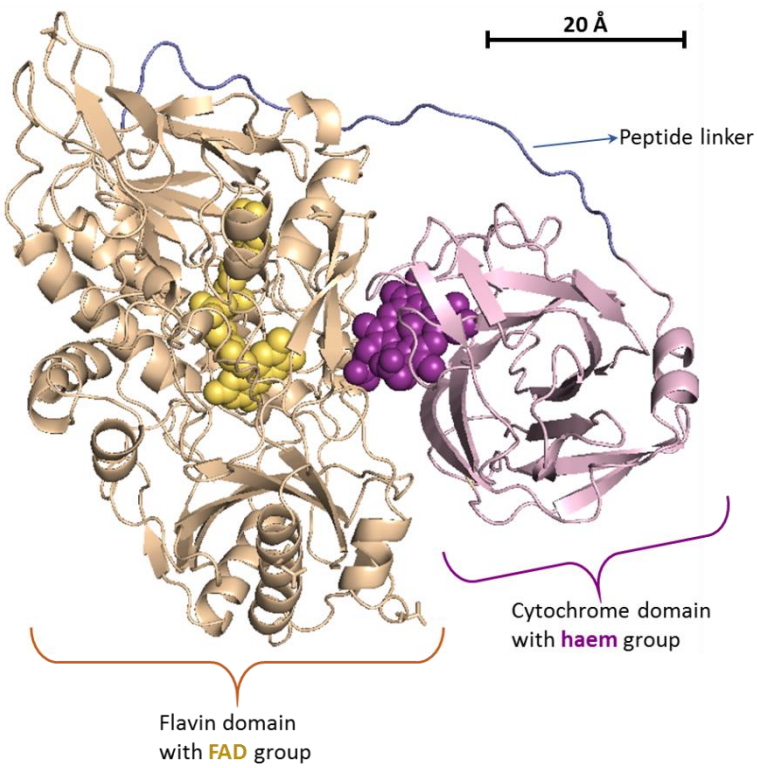

Figure 1.3. *Cartoon representation of the secondary structure of cellobiose dehydrogenase. The flavin domain with the FAD group is in beige/yellow and the cytochrome domain with the haem group is in pink/purple.*

domains are connected through a flexible peptide linker of around 20 amino acids (Figure 1.3).

CDH is involved in the degradation process of cellulose, during which it oxidises cellobiose, a disaccharide formed as a product of the cellulose cleavage. Apart for cellobiose, this enzyme can efficiently oxidise many other sugars showing a greater affinity for disaccharides, such as lactose, which are more similar to the CDH natural substrate, than for monosaccharides like glucose. In this work, however, we used mainly glucose as substrate, and sometimes lactose, since it has a greater interest both in biosensors and biofuel cell applications.

CDH displays the properties of a typical dehydrogenase: it catalyses the oxidation at the C1 position of a saccharide, which is converted to a lactone by losing two electrons and two protons [71] (see Scheme 1.7). All results indicate that the oxidation of carbohydrates is carried out by the FAD cofactor, which takes up the two electrons to be fully reduced to $FADH_2$ [71]. Therefore, $FADH_2$ is oxidised back by donating electrons to one- or two-electron acceptors. Common electron acceptors include several quinones, phenoxyradicals, complexes of Fe^{3+}, Cu^{2+} and osmium, while molecular oxygen is a poor acceptor. In the absence of such acceptors, the FAD cofactor can transfer the electrons to the haem group in a process called interdomain (or internal) electron transfer (IET). Therefore, the haem can donate electrons to large soluble one-electron acceptors such as cytochrome c or, in the absence of electron acceptors or mediators, to an electrode surface in a direct electron transfer (DET) process [73].

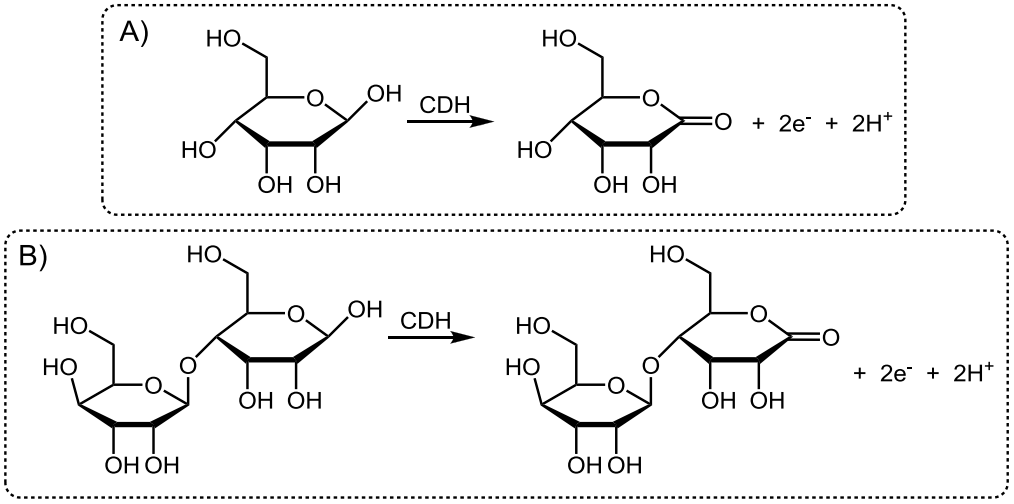

Scheme 1.7. *Oxidation of (A) glucose and (B) lactose to the corresponding lactones catalysed by CDH.*

In this work, we investigated the mechanisms of the direct and mediated electron transfer of *Mt*CDH immobilised at electrode surfaces. This was done by studying the cyclic voltammograms obtained at CDH-modified electrodes, both observing the redox potential of the enzyme and calculating the number of exchanged electrons, which should be 2 in the case of the DET of FAD and 1 in the case the haem gives the DET. All literature results indicate that the haem is responsible for the DET at electrode surfaces, while only one publication shows evidence for the DET from the FAD cofactor [75], even though this was observed only for some class I CDHs and not for class II CDHs, to which *Mt*CDH belongs. Other proofs for the DET and MET mechanisms (see Figure 1.4) were provided by using calcium chloride. In fact, divalent cations, as well as solution pH, were found to strongly affect the IET of CDH [76-78], so that they can be used to study also the DET and MET when the enzyme is immobilised at the electrodes. The next Section will give an overview on this topic, focussing in particular on the *Mt*CDH that was used in this work.

Concerning the MET, we could have two different types of mediated electron transfer depending on the mediator that is used. Quinones, phenoxyradicals and metal complexes, which normally accept electrons from the FAD, will react directly with this cofactor, therefore excluding the IET from this MET mechanism

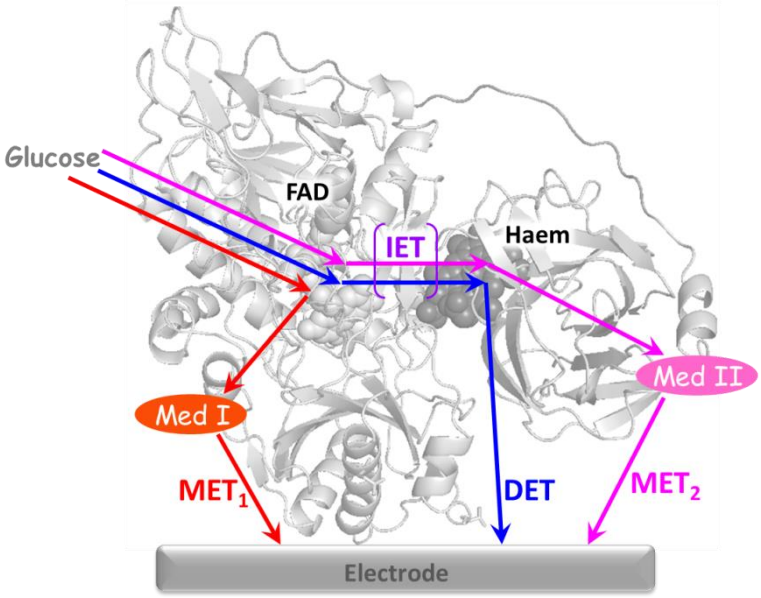

Figure 1.4. *Schematic representation of the DET pathway (blue), and two different MET pathways: MET_1 with a mediator that reacts directly with the FAD cofactor (red) and MET_2 with a mediator that reacts with the haem cofactor (pink). The IET is present in both the DET and MET_2 pathways.*

(red in Figure 1.4). On the other hand, electron acceptors for the haem group, such as cytochrome c and ferricyanide, will react with this cofactor making the second MET pathway longer and passing through the IET (pink in Figure 1.4).

1.4.1 Effect of pH and divalent cations on the IET of CDH

The efficiency of the interdomain electron transfer strongly depends on the pH and the ions dissolved in solution. In fact, at neutral or alkaline pH, electrostatic repulsion between the two domains occurs, disfavouring the adoption of a closed conformation, so that IET is reduced or even eliminated [78]. This directly affects the DET with an electrode, as well as the activity towards big one-electron acceptors such as cytochrome c, since in both cases the electron pathway passes through the haem cofactor (see Figure 1.4). On the other hand, the activity towards acceptors that exchange electrons directly with FAD is not affected.

This effect was shown to be different for CDHs of different origins: in fact, it may be related to structural features of the enzyme. The CDH used in this work, from *Myriococcum thermophilum* (*Mt*CDH), presents a high number of negatively charged amino acids in the interfacial region between the two domains (seven in the cytochrome domain and eight in the flavin domain) [78]. In addition, the distance between the haem and the FAD was found longer than for other CDHs. The presence of these negatively charged amino acids in the interfacial region creates an electrostatic repulsion between the two domains, especially at neutral or alkaline pH, when such amino acids are mostly deprotonated. This can explain why *Mt*CDH showed more efficient DET at acidic pH, when the amino acid residues in the interfacial region are at their isoelectric point, while CDHs of different origins can give DET also at neutral pH.

The electrostatic repulsion between the two domains at neutral pH can also be neutralised by divalent alkali earth metal cations [76-78]. Indeed, concentrations of divalent cations greater than 3 mM have been shown to exert a bridging effect between the cytochrome and the flavin domains, thereby increasing IET rates, with a consequent positive effect on DET. This effect is not caused by the presence of distinct binding sites for divalent cations on the enzyme, but most probably by unspecific shielding of close opposite charges at both sides of the domain's interface.

1.4.2 Applications of CDH

The growing interest in this enzyme derives indeed from its ability of giving DET with an electrode surface, thanks to its haem cofactor that acts as an "internal mediator" shuttling electrons from the FAD group to the electrode. For that, there is no need to add any mediator, avoiding the decrease in the voltage of a biofuel cell in the case where CDH is used as a catalyst, or increasing the possibilities for biosensors and BFCs to be biodegradable and biocompatible since many mediators can be toxic substances.

CDH has been used to construct a variety of biosensors for the detection of different carbohydrates such as glucose and lactose [79-84], but also ATP [85], catecholamines [86] and pollutants like diphenolic compounds [87]. It has also been employed as an anodic biocatalyst in BFCs fuelled with glucose, lactose or cellobiose [88-92]. Electrical contact between CDH and electrodes has been provided by direct electron transfer [93-96], several redox mediators [97] and redox polymers [98,99]. In recent years, various nanostructured electrodes, especially made with carbon nanotubes, have been used to increase the efficiency of DET [80,81,90].

Another way to improve the stability of the CDH-modified electrodes and decrease desorption of the enzyme is represented by covalent immobilization. Some authors report the covalent immobilization of CDH using glutaraldehyde as cross-linker at gold electrodes modified with SAMs of thiols [82,95] or at carbon electrodes modified with diazonium salts [90]. Another publication reports the covalent immobilization of CDH employing the reaction between its glutamic or aspartic acid residues with amino-modified ITO electrodes [91]. However, as we have already said, SAMs present some limitations, especially in electrode applications, as gold-thiol bonds can be destroyed at extremes of potential or pH. Moreover, the techniques employing glutaraldehyde as cross-linker or amino-modified electrodes to react with the carboxylic groups present at the enzyme surface do not have the possibility of controlling the orientation of CDH at the electrode surface.

In this work, we used for the first time a site-specific immobilization method for CDH, employing maleimide-modified electrodes to react with *Mt*CDH variants

genetically engineered to bear only one free cysteine residue at the surface of the flavin domain. We had four different *Mt*CDH variants available to use, with the free cysteines in different positions, so that we could evaluate which immobilization site gives the most efficient DET. The variants were produced using a technique called site-directed mutagenesis by Dr Su Ma and Dr Roland Ludwig at the BOKU-University of Vienna (Austria). Here below, we will give a short overview on the methods used to genetically modify proteins.

1.4.3 Protein engineering

Protein engineering is commonly used in molecular biology to change some characteristics of enzymes, such as substrate specificity, solubility, stability, activity, selectivity, thermal stability or tolerance to organic solvents or to extremes of pH [100]. This usually involves the modification of the amino acid sequence of the enzyme at the DNA sequence level by using chemical or genetic techniques. There are two different basic approaches to engineer proteins:

- Rational design: mutations are introduced at specific site in the protein-encoding gene. Positions to mutagenize are based on the knowledge of possible relationships between the amino acids sequence/secondary structure of the protein with its function or catalytic mechanism. Recently computational predictive algorithms have been developed and used to preselect promising target sites [101-103].

- Directed evolution: this approach involves repeated cycles of random mutagenesis of the gene to create a library of genes with slightly different sequences. The enzyme variants thus obtained are submitted to genetic selection or to high-throughput screening to identify those mutations with improvements in the desired property [104-106].

Directed evolution is a very powerful technique for improving the stability of enzymes or changing the substrate specificity since, in many cases, changes that contribute to these properties are far from the active sites and difficult to target by a rational design. On the other hand, a rational design such as site-directed mutagenesis is useful when the amino acid to alter is known, so that we can make specific and intentional changes to the DNA sequence of the microorganism

producing the enzyme. Given that in this work we wanted to change only one amino acid at the CDH surface to be replaced with a cysteine residue, site-directed mutagenesis seemed the most appropriate technique. We will not enter in more specific details about this method, as it was performed by our co-workers at the BOKU-University of Vienna and is not the purpose of this thesis. The mutation sites of the four different CDH variants used in this work will be described in Section 3.1.3 (see Figure 3.1).

1.5 Research objectives and overview

The aim of this work is the covalent, site-specific immobilization of a redox enzyme for efficient direct electron transfer with electrode surfaces. For the direct electron transfer, the position and orientation of the enzyme active centre, which can be hidden inside the protein, has to be controlled in order to minimise the electron transfer distance and thus avoid the necessity of using diffusing redox mediators. To this purpose, electrode surfaces have to be functionalised with monolayers of organic molecules appropriate to accommodate the enzyme of choice, taking into account steric considerations. Indeed, the binding group on the electrode surface should be able to access the target functional group of the protein (often artificially introduced by protein engineering) and be laterally distributed to accommodate the bulky macromolecule. Moreover, the polarity/charge of the modified electrode surface around the binding group should be compatible with the protein surface around the target functional group, to prevent repulsion or denaturation of the enzyme.

In the present work, a promising redox enzyme, cellobiose dehydrogenase (CDH), was used as model system and covalently immobilised at carbon and gold electrodes. The recent interest in this enzyme derives from its ability of giving direct electron transfer, thanks to its second active site that acts as a “built-in mediator” and shuttles electrons between the FAD active centre and the electrode. For that reason cellobiose dehydrogenase can be a valid substitute of glucose oxidase in glucose biosensors or biofuel cell anodes. Up to now, covalent immobilization of CDH has been reported using cross-linkers or the reactivity of the carboxylic groups of enzymatic amino acid residues towards amino-modified

electrode surfaces. However, these methods do not ensure the best orientation of the enzyme for the DET, as cross-linker reagents and amines can react with several functional groups on the protein surface. In this work, we will show an innovative method for the covalent, site-specific immobilization of CDH at electrodes modified with maleimide groups, which only react with cysteine residues introduced at the surface of CDH by genetic engineering. In this way, CDH molecules should be held at the electrode surface in a fixed orientation, depending on the position of the introduced cysteine residue. Four different CDH variants were used in this work, bearing one free cysteine in four different locations at the surface of the flavin domain. Discrimination between the variants can also be carried out to understand which position for the cysteine residue can ensure the best orientation of the enzyme to efficiently exchange electrons with the electrode surface.

Chapter 3 will describe the method employed for the immobilization of CDH at carbon electrodes, using in particular glassy carbon electrodes modified with multiwall carbon nanotubes (GC/CNT) as model for high surface area electrodes. These were modified with maleimide groups by using a modular approach that combines electrochemical and solid-phase synthesis. In this approach, the key elements of the modification can be independently varied to tune the architecture of the electrode surface as required, by simply changing the "bricks" of the structure. The modification began with the electrografting of two different primary amines to form a mixed monolayer on the electrode surface, essential for the dilution of the maleimide groups. Therefore, using solid-phase synthesis, other molecules were immobilised on the surface to make the tether enough long and flexible, ending with maleimide that was suitable for the site-specific immobilization of the cysteine-modified CDH variants. The CDH-modified electrodes were tested for the direct and mediated electron transfer, using glucose as the substrate and a ferrocene derivative as the mediator. In addition, several tests to verify the stability of the enzymatic electrodes and the mechanism of the direct and mediated electron transfer were performed.

At the end of the Chapter, a new method for the solid-phase functionalization of carbon nanotubes with maleimide will be described. In this way, a great amount of maleimide-functionalised CNTs can be prepared at once, stored and used when

necessary to modify different types of electrodes (we used gold screen-printed electrodes, but also carbon electrodes could be easily modified with this method). After the maleimide-functionalised CNTs are adsorbed on the electrodes, cysteine-modified CDH variants can be easily immobilised on them.

In Chapter 4 we will analyse in depth the kinetics of the CDH catalytic reactions at the electrode surface, trying to find out the rate limiting step (or steps) and the values of the kinetic constants of each reaction step. The meaning of the parameters extracted by the Michaelis-Menten fitting in Chapter 3 will be also explained. For that, we will need to derive a potential-dependent Michaelis-Menten equation, suitable for the CDH electrodic reactions. The equation will be used to simulate the catalytic voltammograms experimentally recorded at CDH-modified electrodes, reported in Chapter 3, in order to estimate the values of the kinetic constants involved in the direct and mediated electron transfer processes of CDH. In this way, we should be able to understand which reactions affect the current and why the DET current is different for the four different CDH variants.

Since all the CDH variants, when immobilised at GC/CNT electrodes, showed high catalytic currents for the DET, we thought that a better discrimination between them could be given upon immobilization on flat electrodes. This will be shown in Chapter 5, starting with the covalent immobilization of CDH at glassy carbon (GC) electrodes and then moving to flat gold electrodes. For the first ones, the same method already described for the modification of GC/CNT electrodes in Chapter 3 was employed. Moreover, flat GC and GC/CNT electrodes were compared thanks to the immobilization of a redox probe, namely anthraquinone. On the other hand, the immobilization of CDH at gold electrodes was carried out using a procedure similar to that employed with carbon electrodes, but changing some “bricks” of the molecular architecture. For instance, the electrografting of primary amines was substituted with the electrografting of a diazonium salt, as the amines do not react with gold. However, the use of maleimide as the reactive group and the idea of a mixed monolayer to dilute the maleimide at the electrode surface were unvaried. The new procedure for the modification of gold electrodes was analysed using different techniques, such as cyclic voltammetry upon the immobilization of anthraquinone, time-of-flight secondary-ion mass spectrometry (ToF-SIMS) and surface plasmon resonance (SPR) spectroscopy.

Finally, the CDH-modified gold electrodes were tested for the direct and mediated electron transfer, using both glucose and lactose as the substrates. The effectiveness of the covalent immobilization and the stability of the enzymatic electrodes were also verified through several experiments.

To begin, in the following Chapter, the chemicals, the instrumentations and the experimental procedures used in this work will be described.

Chapter 2:

Experimental part

The experimental procedures presented in this Chapter are a general description of the methods used in this work. Details of the specific experimental conditions can be found in the following Chapters of results and discussion for each experiment reported in this thesis.

2.1 General

2.1.1 Chemicals

The following chemicals were used for the modification of electrodes:

- *N*-Boc-1,6-hexanediamine (Sigma-Aldrich);
- *N*-(2-aminoethyl)acetamide (Sigma-Aldrich);
- tetrabutylammonium tetrafluoroborate (TBATFB) (Sigma-Aldrich);
- *N*-hydroxysuccinimide (NHS) (Sigma-Aldrich);
- *N*-(3-dimethylaminopropyl)-*N*′-ethylcarbodiimide (EDC) (Sigma-Aldrich);
- *N*-Boc-6-aminohexanoic acid (Sigma-Aldrich);
- *N*-Boc-β-alanine (Sigma-Aldrich)
- butyric acid (Sigma-Aldrich)
- *N*-maleoyl-β-alanine (synthesised as described below using maleic anhydride and β-alanine from Sigma-Aldrich);
- $BocNHCH_2C_6H_4$ diazonium tetrafluoroborate (synthesised as described below using *tert*-butyl-*N*-(4-aminobenzyl)carbamate, tetrafluoroboric acid and sodium nitrite from Sigma-Aldrich);
- anthraquinone-2-carboxylic acid (Sigma-Aldrich);

Buffer solutions were prepared with Tris base and monobasic sodium phosphate (Sigma-Aldrich), acetic acid glacial (BDH), calcium chloride (Fisher Scientific) and titrated with hydrochloric acid (37%, BDH) and sodium hydroxide (laboratory grade, Fisher Chemical). D- and L-glucose were purchased from BDH, β-lactose was from Sigma-Aldrich. Ferrocenecarboxylic acid (used as mediator) was from Fluka. Papain crude and Triton x-100 were from Sigma-Aldrich.

The solvents acetonitrile (ACN, HPLC grade), 1,4-dioxane (laboratory grade), dimethylformamide (DMF, laboratory grade) and ethanol (analytical grade) were purchased from Fisher Chemical. Sulphuric acid (electronic grade) and hydrogen peroxide (laboratory grade) used to prepare the piranha solution were also from Fisher Chemical.

Myriococcum thermophilum cellobiose dehydrogenase (*Mt*CDH) variants, recombinantly expressed in *Pichia pastoris*, were kindly supplied by Dr Su Ma

and Dr Roland Ludwig (BOKU-University of Natural Resources and Life Sciences, Vienna, Austria). All the variants were supplied dissolved in 50 mM sodium acetate buffer (pH 5.5), with concentrations and activities reported in Table 2.1, and stored in the freezer at -4 °C.

Table 2.1. *Concentration and specific activity for the four MtCDH variants used in this work.*

Variant	Concentration Bradford (g/L)	Cytochrome C specific activity* (U/mg)
D813	14.79	1.025
T701	14.07	2.727
E522	11.34	1.377
E674	15.98	2.78

** The enzyme activity is defined as the amount of enzyme that reduces 1 µmol of the respective electron acceptor (cytochrome C in this case) per minute under the specified conditions. The cytochrome C specific activity, therefore, measures the activity of the holoenzyme CDH (whole enzyme containing all the active sites) and was determined by Dr Su Ma (BOKU-University, Vienna, Austria) using lactose as substrate. The reaction was detected by the concomitant reduction of cytochrome C at 550 nm (ε_{550} = 19.6 mM^{-1} cm^{-1}), in sodium acetate buffer (pH 4). Cytochrome C changes colour from orange to a more reddish tone [78,107].*

2.1.2 Instrumentation

All electrochemical solutions were prepared with reagent grade water (18 MΩ cm) from a Purite purification system. Pureshield argon (BOC) was used to purge electrochemical solutions as stated. Electrochemical measurements were performed in glass cells with a standard three-electrode arrangement, connected with either a µAutolab type III or an Autolab PGSTAT 302 (Ecochemie, The Netherlands). The glass cells used were generally 10 mL cells (but also a 20 mL cell was used in some cases) provided with five necks that could be perfectly closed using screw tops (see Figure 2.1). Three of the necks were used to insert the three electrodes (working, reference and counter), one was used to insert a needle purging gas argon, and the fifth neck was normally close during running experiments and open only to add a solution in the cell (*e.g.* glucose solution).

The counter electrode was a platinum gauze and the reference was a home-made saturated calomel electrode (SCE). Different types of working electrodes were used in this work. In general, they can be classified in two main groups, carbon electrodes and gold electrodes, and they will be described in more details in the next Section.

For some experiments, other specific instruments were used (*e.g.* an SPR spectroscope and a ToF-SIMS spectrometer). The details of these instruments will be given in the dedicated Sections.

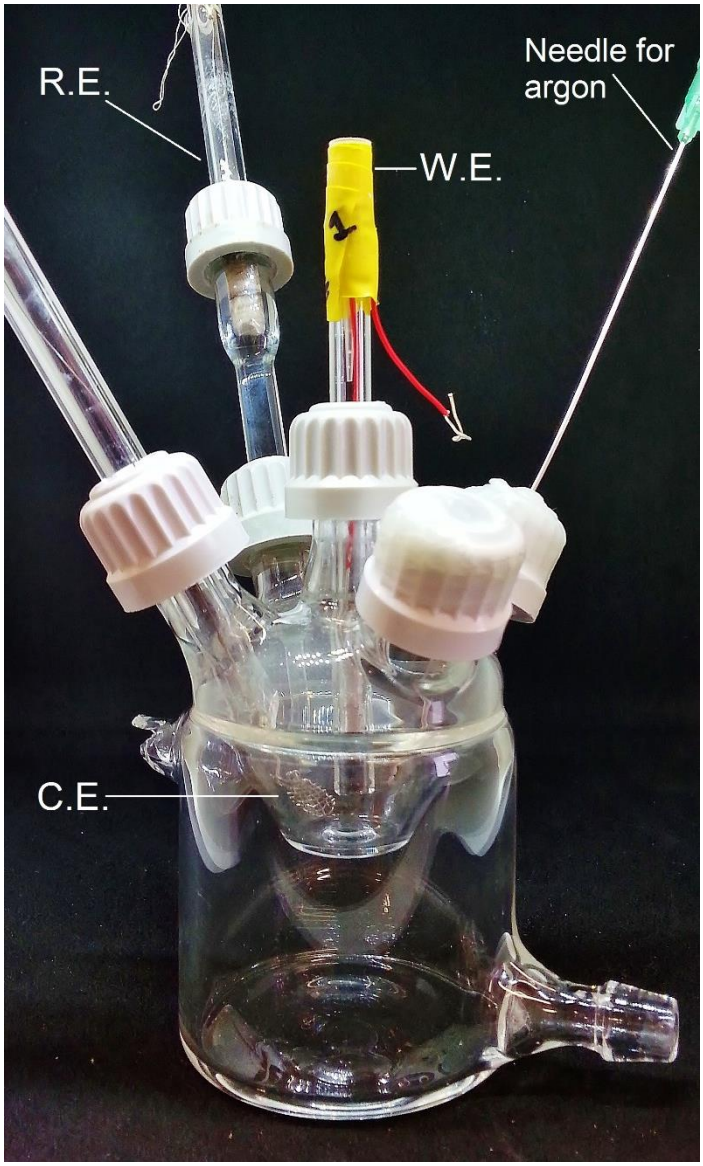

Figure 2.1. *Picture of the typical electrochemical cell used in this work.*

2.1.3 Carbon electrodes

Glassy carbon (GC) working electrodes were 3 mm diameter (area = 0.071 cm^2) glassy carbon disc (HTW Hochtemperatur - Werkstoffe GMBH, Germany) sealed in glass tubes and contacted by a copper wire using melted indium (Aldrich). Prior to modification, the electrodes were polished by using silicon carbide polishing paper (grade 1200), then alumina slurries (1.0 and 0.3 μm, Buehler) on polishing cloths (Buehler), followed by sonication for 5 min in deionised water and then ethanol.

2.1.4 Gold electrodes

The gold electrodes used in this work (Figure 2.2) were mainly flat electrodes, in particular:

- commercial gold disc electrodes, 2 mm diameter (PalmSens, Houten, The Netherlands);
- commercial gold screen-printed electrodes (AuSPEs), 4 mm diameter (DropSens, Oviedo, Spain).

For some experiments, other gold substrates were used, in particular:

- gold-coated glass microscope slides prepared by magnetron sputtering, by deposition of a ≈ 10 nm thick titanium adhesion layer followed by a ≈ 100 nm thick gold layer. The gold slides were normally cut in small pieces of about 5 x 10 mm, and used mainly for the ToF-SIMS experiment.
- gold-coated glass substrates for SPR analysis (≈ 2 cm diameter).

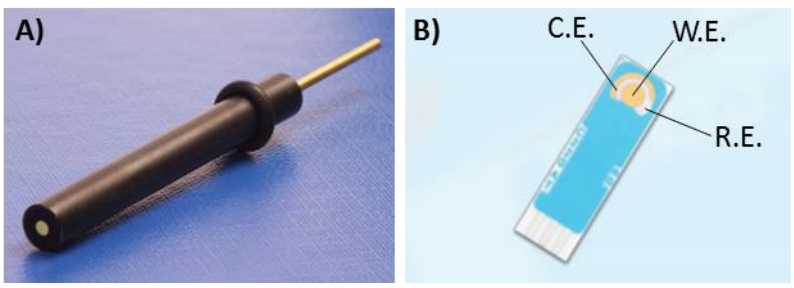

Figure 2.2. *Gold electrodes used in this work: A) commercial gold disc electrode (adapted from www.palmsens.com) and B) gold screen-printed electrode from DropSens (adapted from www.dropsens.com).*

2.1.5 Cleaning and determination of surface area for gold electrodes

Commercial gold disc electrodes were cleaned in piranha solution for 5 min (H_2SO_4/H_2O_2 3:1, since it is a very energetic and potentially dangerous solution, it must be handled very carefully: all work involving piranha solution must be conducted inside a fume cupboard; safety glasses, lab coat and gloves must be worn; piranha solution should be handled in glass or Pyrex containers, it is not compatible with plastic; always add hydrogen peroxide to sulfuric acid slowly, never vice versa). After the treatment in piranha solution, the electrodes were polished by rubbing on alumina slurries (0.3 and 0.05 μm, Buehler) on polishing cloths (Buehler), followed by sonication for 5 min in deionised water and then ethanol.

The active area of gold disc electrodes was determined by cyclic voltammetry in 0.1 M sulphuric acid, scanning the electrode potential from 0.0 to 1.5 V *vs.* SCE at 0.1 V/s (for about five cycles, see Figure 2.3). The area under the reduction peak at about 0.85 V (a_i) was integrated to find out the charge (Q) and, therefore, the effective active area (A) using the following equation:

$$A = \frac{Q}{\sigma} = \frac{a_i}{v\,\sigma} \qquad \text{(Eq. 2.1)}$$

where σ is the surface charge density and v is the scan rate. A value of 390 μC/cm^2 was used for the surface charge density of polycrystalline gold [108].

In the case of the gold-coated slides, the surface area calculated in this way was divided for the geometrical area giving the roughness factor (ρ), which was found to be 1.25 (average between four different electrodes).

The gold screen-printed electrodes were cleaned by immersion in acetonitrile or ethanol for a few minutes before use. The procedure to find the active area by CV in sulphuric acid was not used with these electrodes to avoid damages as they are mainly constituted of plastic materials and gold ink. In any case, screen-printed electrodes (SPEs) are ready to be used and no general pre-treatment protocol is established. Moreover, they are disposable electrodes that were used only for one single experiment.

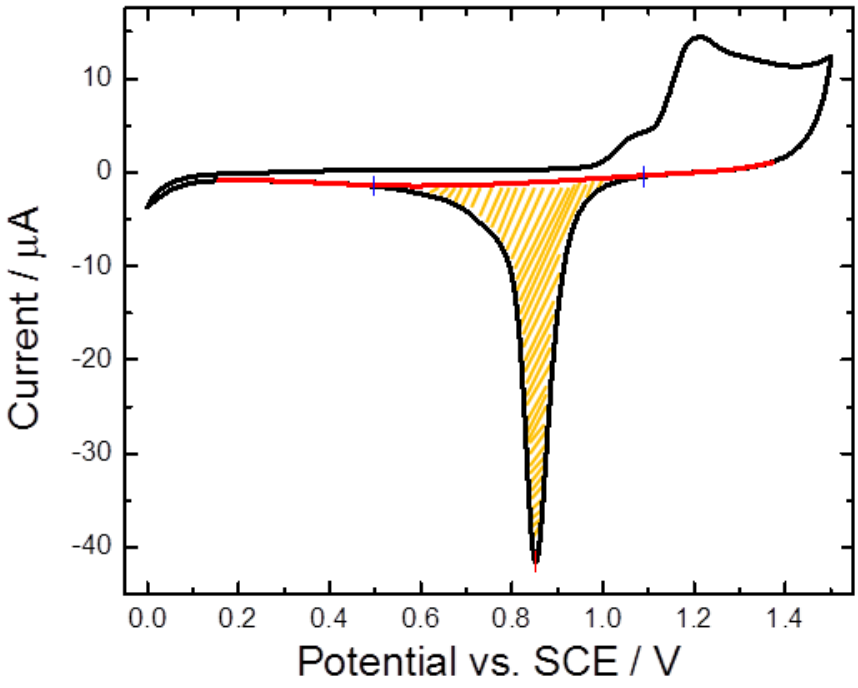

Figure 2.3. *Cyclic voltammogram (5th cycle shown) recorded at a gold disc electrode (2 mm diameter) in 0.1 M sulphuric acid. The potential was swept at 0.1 V/s. The red line is the baseline constructed with Origin 9.1 to integrate the area under the reduction peak (orange) for calculating the electrode active area.*

2.2 Synthesis of non-commercial reagents

2.2.1 Synthesis of $BocNHCH_2C_6H_4$ diazonium tetrafluoroborate

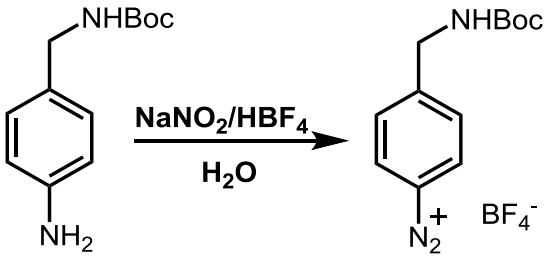

Scheme 2.1. *Synthesis of Boc-protected diazonium salt from tert-butyl-N-(4-aminobenzyl)carbamate, tetrafluoroboric acid and sodium nitrite in water.*

The diazonium salt was prepared following a literature procedure [109]: *tert*-butyl *N*-(4-aminobenzyl)carbamate (200 mg, 1 mmol) was dissolved in tetrafluoroboric acid (40%, 0.12 mL, 1 mmol) and water (2 mL). The solution was cooled on ice and sodium nitrite (62 mg, 1 mmol) dissolved in 0.2 mL of water was added dropwise under an inert atmosphere while the solution was stirred. After adding $NaNO_2$, the reaction mixture was left at room temperature

for 2 hours, and then put in the freezer overnight. It was filtered under vacuum and washed with diethyl ether to give the diazonium salt as an orange solid, which was dried under vacuum pump.

^{1}H NMR (400 MHz, DMSO-d_6), δ ppm 1.40 (9H, m), 4.35 (2H, d, *J* = 5.87 Hz), 7.79 (2H, d, *J* = 8.68 Hz), 8.61 (2H, d, *J* = 8.68 Hz).

2.2.2 Synthesis of *N*-maleoyl-β-alanine

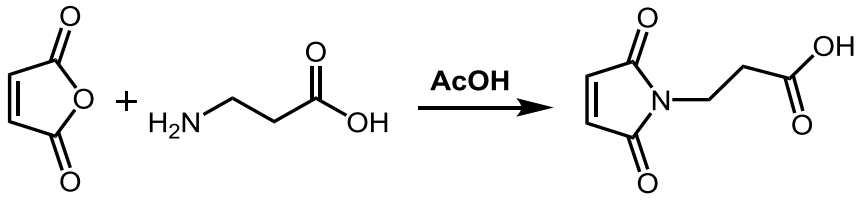

Scheme 2.2. *Synthesis of N-maleoyl-β-alanine from maleic anhydride and β-alanine in acetic acid.*

This synthesis was carried out for the first time at the Queen Mary University (London) with the kind help of Dr Marloes Peeters, in the research group of Prof Jeremy Kilburn. 4.97 g of maleic anhydride (51 mmol, 1 eq.) and 4.59 g of β-alanine (51 mmol, 1 eq.) were dissolved in 37 mL of acetic acid. The solution was stirred and heated to reflux for 90 min. Then toluene was added to lower the boiling point and the solvent was removed under vacuum (50 mbar). An extraction in water/ethyl acetate (50:50) was performed, the organic phase was desiccated with magnesium sulphate and filtered on paper. After removing the solvent under vacuum, the product was recrystallized in ethyl acetate and left in the freezer overnight. Then filtered on Buchner, washed with ethyl acetate and dried under high vacuum.

^{1}H NMR (400 MHz, chloroform-d), δ ppm 2.74 (2H, t, *J* = 8 Hz), 3.87 (2H, t, *J* = 8 Hz), 6.74 (2H, s), 9.94 (1H, s, broad).

2.3 Modification of carbon electrodes

2.3.1 Fabrication of GC/CNT electrodes

Glassy carbon electrodes were modified with carbon nanotubes to increase their surface area. Multi-walled carbon nanotubes (MWCNT, > 8% carboxylic acid functionalised avg., 9.5 nm diameter, 1.5 μm length) were purchased from Sigma-Aldrich. 10 mg of MWCNT were dispersed in 10 mL of DMF, with the aid of ultra-sonication, to give a 1 mg/mL black suspension. Therefore, 5 μL of the MWCNT dispersion were placed onto the clean surface of each glassy carbon electrode and allowed to dry at room temperature for 1-2 days.

2.3.2 Attachment of linker and passivating group

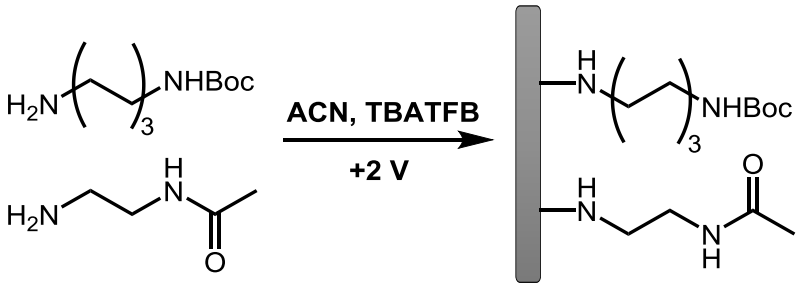

Scheme 2.3. *Electrochemical grafting of N-Boc-1,6-hexanediamine (linker) and N-(2-aminoethyl)acetamide (passivating group) at carbon electrodes.*

10 mL of a solution containing *N*-Boc-1,6-hexanediamine (linker, 2 mM), *N*-(2-aminoethyl)acetamide (passivating group, 18 mM) and TBATFB (supporting electrolyte, 0.1 M) in acetonitrile was prepared and degassed with argon in the electrochemical cell. The carbon electrode of choice was immersed in the cell and the potential was held at +2 V *vs.* SCE for 180 s (see chronoamperogram in Figure 2.4). Then the electrodes were washed with acetonitrile and the linker was deprotected in HCl solution as described in the next paragraph.

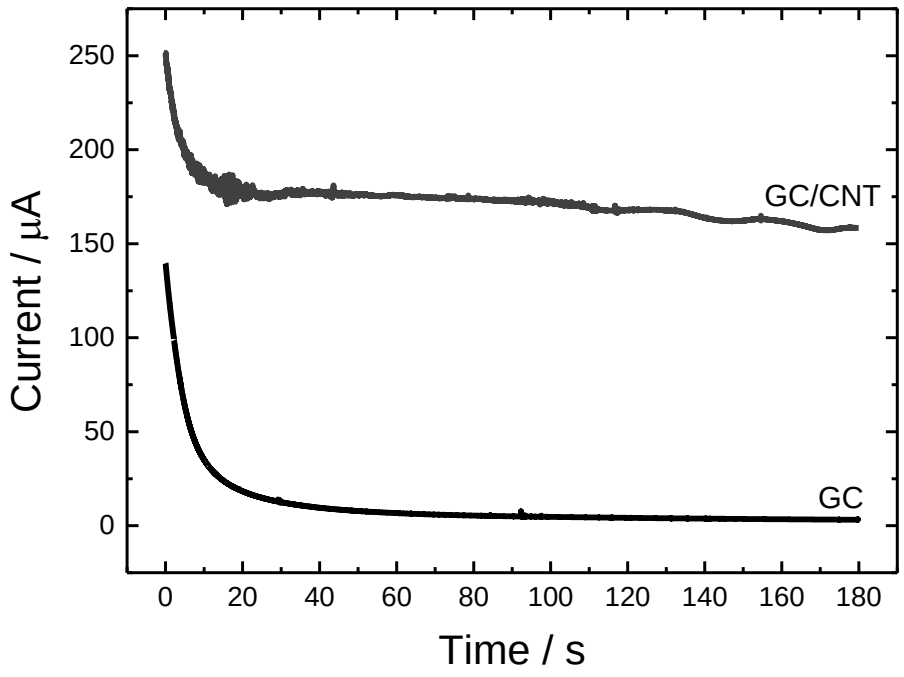

Figure 2.4. *Typical chronoamperograms for the attachment of linker and passivating group at GC and GC/CNT electrodes from a solution containing 2 mM N-Boc-1,6-hexanediamine, 18 mM N-(2-aminoethyl) acetamide and 0.1 M TBATFB in acetonitrile. The electrode potential was held at +2 V vs. SCE for 180 s.*

2.3.3 General method for deprotection of Boc group

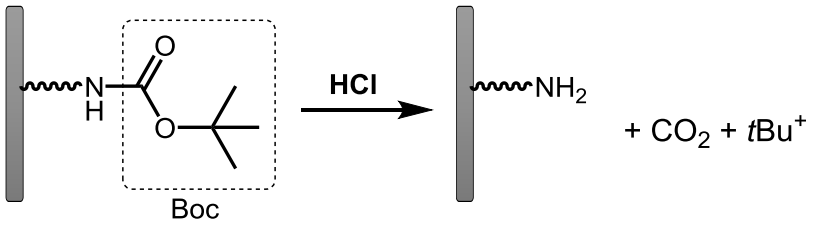

Scheme 2.4. *Deprotection of tert-butyloxycarbonyl amines.*

Electrodes modified with Boc-protected amino groups were immersed in 4 M HCl in 1,4-dioxane for 45 min, strongly stirring the solution. Then they were washed with acetonitrile and water, and dried.

2.3.4 Coupling of 6C-spacer

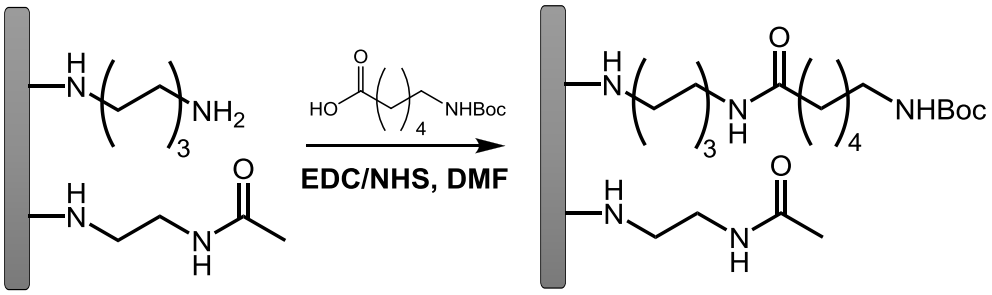

Scheme 2.5. *Coupling of N-Boc-6-aminohexanoic acid.*

A solution containing *N*-Boc-6-aminohexanoic acid (6C-spacer, 10 mM), NHS (60 mM) and EDC (0.1 M) in DMF was prepared and stirred for 15 min. Electrodes were immersed in it for 16 h, then washed with acetonitrile and water and dried. Therefore, the 6C-spacer was deprotected in HCl solution as described in Section 2.3.3.

2.3.5 Coupling of maleimide

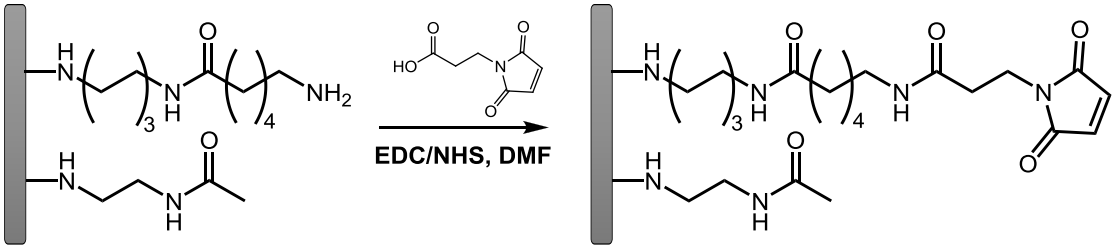

Scheme 2.6. *Coupling of N-maleoyl-β-alanine.*

A solution containing *N*-maleoyl-β-alanine (25 mM), NHS (60 mM) and EDC (0.1 M) in DMF was prepared and stirred for 15 min. Electrodes were immersed for 16 h, then washed with acetonitrile and water and dried.

2.4 Solid-phase functionalization of CNTs

2.4.1 Functionalization of CNTs with anthraquinone

For a better visualization of the procedure see Scheme 3.6. 20 mg of carboxylic acid-functionalised CNTs were placed in a 100 mL round-bottom flask (RBF) with 20 mL of DMF. 64 mg of $BocNHCH_2C_6H_4$ diazonium tetrafluoroborate were added in the flask to have a 10 mM concentration. The solution was stirred and heated at 60 °C in a water bath under reflux, overnight. Then, the solution was filtered on paper. The CNTs obtained (CNTs 1) were washed with acetone and ethanol and dried in the oven at 40 °C for 3 h.

For the first method, the CNTs 1 were dissolved in DMF to have a 1 g/L suspension, sonicated for 5 min and drop cast onto a gold SPE (SPE 1, 10 μL). Once dry, the Boc deprotection of the diazonium salt was carried out by placing the SPE 1 in 1 M HCl in water for 1 h. Finally, coupling of anthraquinone-carboxylic acid was performed in an acetonitrile solution containing 0.1 M EDC and 60 mM NHS (overnight).

For the second method, the CNTs 1 were dissolved in 4 M HCl in dioxane (15 mL) and stirred strongly at RT for 1 h. Then, they were filtered on paper and washed with dioxane, water and ethanol. Once dry, coupling of AQ was carried out by dissolving the CNTs in 10 mL of 25 mM anthraquinone-carboxylic acid, 0.1 M EDC and 60 mM NHS in DMF, stirred overnight at RT. Then, the CNTs (CNTs 2) were separated by centrifuge: the liquid phase was taken off and the solid phase was washed twice with acetone and once with ethanol. The solid phase was collected and dried at RT. Finally, the CNTs 2 were dissolved in a DMF/water (4:1) solution (1 g/L), sonicated for 5-10 min and drop cast onto gold SPEs (SPEs 2).

2.4.2 Functionalization of CNTs with maleimide

For a better visualization of the procedure see Scheme 3.7. 20 mg of carboxylic acid-functionalised CNTs were placed in a 100 mL RBF with 20 mL of DMF. 70 mg of $BocNHCH_2C_6H_4$ diazonium tetrafluoroborate were added in the flask to have a 10 mM concentration. The solution was stirred and heated at 60 °C in oil bath under reflux for 8 h. Then, the solution was filtered on paper. The CNTs obtained

were washed with acetone and ethanol, and dried at RT in the fume hood. For the Boc deprotection, the CNTs were dissolved in 4 M HCl in dioxane (15 mL) and stirred strongly at RT for 1 h. Then, they were filtered on paper and washed with dioxane, water and ethanol.

Once dry, coupling of 6C-spacer was carried out by dissolving the CNTs in 15 mL of 5 mM *N*-Boc-6-aminohexanoic acid, 45 mM acetic acid, 0.1 M EDC and 60 mM NHS in DMF, stirred overnight at RT. Then, the CNTs were filtered on paper, washed with acetone and ethanol, and dried at RT. Boc deprotection was carried out as before to obtain the CNTs 3. Finally, coupling of maleimide was carried out by dissolving the CNTs 3 in 10 mL of 25 mM *N*-maleoyl-β-alanine, 0.1 M EDC and 60 mM NHS in DMF, stirred overnight at RT. Then, the CNTs (CNTs 4) were filtered on paper, washed with acetone and ethanol, and dried at RT.

The CNTs 4 were dissolved in a DMF/water (4:1) solution to have a 1 g/L suspension, and sonicated for 15 min. Around 20 µL of the suspension were drop cast on each gold SPE (SPE 4) and let dry overnight. Afterwards, 10 µL of the CDH solution of choice (in phosphate buffer, pH 7) were placed on each SPE 4 and react at RT for 1 h.

2.5 Modification of gold electrodes

2.5.1 Grafting of the diazonium salt

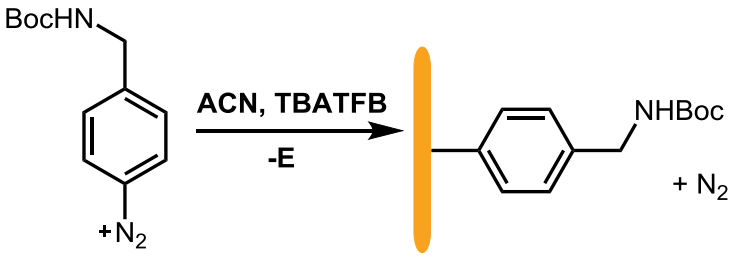

Scheme 2.7. *Electrochemical grafting of diazonium salt onto a gold surface.*

A solution containing 5 mM $BocNHCH_2C_6H_4$ diazonium tetrafluoroborate and 0.1 M TBATFB in acetonitrile was prepared and degassed with argon for 30 min. The electrochemical reduction of the Boc-protected diazonium salt onto a gold surface was carried out by cycling the electrode potential from 0.0 to -0.7 V *vs.*

SCE for 10 cycles at 50 mV/s. Figure 2.5 shows a typical CV for this process at a flat gold electrode: in the first cycle a well-defined reduction peak at about -0.45 V is visible. This peak is attributed to the reduction of the diazonium salt and formation of the corresponding aryl radical in solution, which then couples onto the gold surface. No oxidation peaks are observable, meaning that this redox process is not reversible. Further cycling the electrode potential leads to the complete disappearance of the cathodic reduction peak. This current decay corresponds to the attachment of the linker, which bears the bulky Boc group, completely blocking the electrode surface.

After that, the gold electrode was washed with acetonitrile and water, and dried.

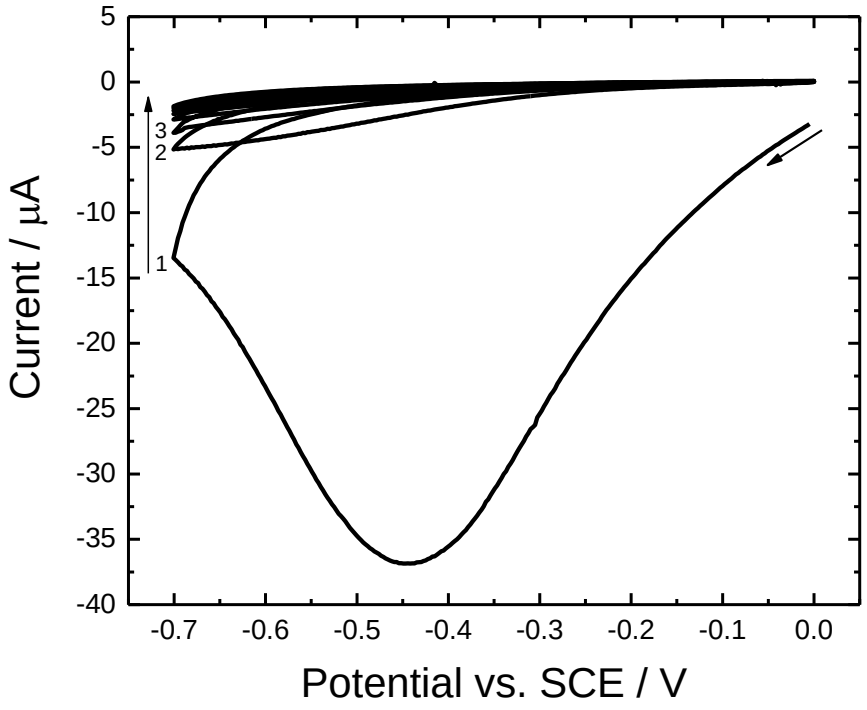

Figure 2.5. *Typical cyclic voltammogram for the attachment of diazonium salt at a flat gold electrode from a solution containing 5 mM* $BocNHCH_2C_6H_4$ *diazonium tetrafluoroborate and 0.1 M TBATFB in acetonitrile. The electrode potential was cycled from 0.0 to -0.7 V vs. SCE at 50 mV/s for 10 cycles.*

2.5.2 Deprotection of Boc group

Electrodes modified with Boc-protected amino groups were immersed in 4 M HCl in 1,4-dioxane for 45 min, strongly stirring the solution (see Scheme 2.4). Then they were washed with acetonitrile and water, and dried.

In the case of screen-printed electrodes and SPR gold electrodes the conditions were slightly changed as the components of these electrodes (or the instruments used) were quite delicate and could be damaged by solvents such as dioxane and DMF. Therefore, the hydrochloric acid was dissolved in water instead of dioxane and its concentration was reduced to 1 M. No significant changes were observed in the deprotection process since such electrodes were found able to react with carboxylic acids as in the previous case. In any case, the specific conditions used for these particular experiments are reported in the results and discussion.

2.5.3 Coupling of anthraquinone (AQ)

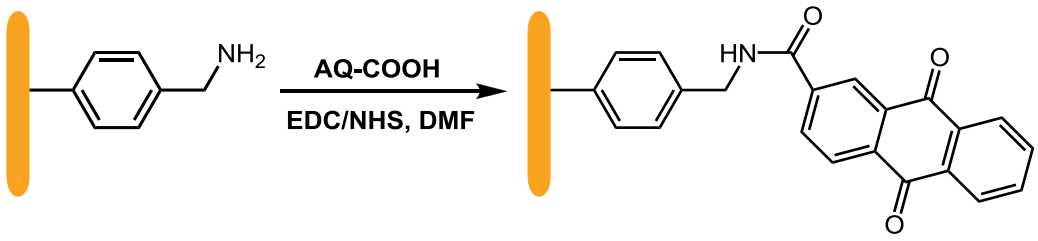

Scheme 2.8. *Coupling of anthraquinone-2-carboxylic acid (AQ-COOH).*

Electrodes modified with amino groups were placed in a solution containing 25 mM anthraquinone-2-carboxylic acid, 0.1 M EDC, 60 mM NHS in DMF, and gently stirred for 16 h. Then electrodes were washed with acetonitrile and water, and dried.

2.5.4 Coupling of spacer and passivating group

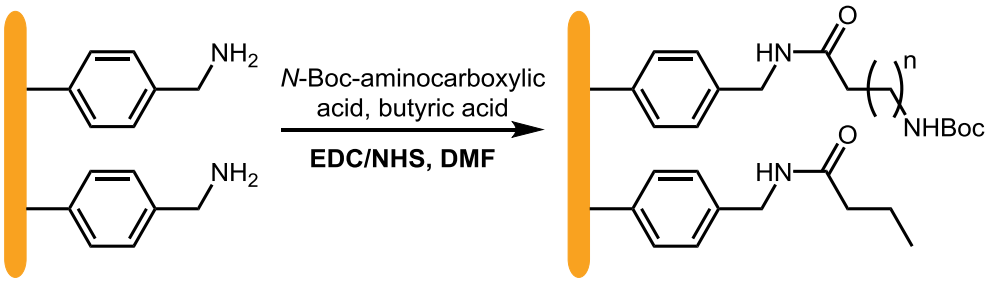

Scheme 2.9. *Coupling of spacer and passivating group. In this work a 3C-spacer (n = 1) or a 6C-spacer (n = 4) were used.*

Electrodes modified with the diazonium salt, after deprotection of the Boc group, were placed in a solution containing 5 mM *N*-Boc-6-aminohexanoic acid (6C-spacer) or *N*-Boc-β-alanine (3C-spacer), 45 mM butyric acid (capping group), 0.1 M EDC, 60 mM NHS in DMF (acetonitrile or water in the case of SPEs and np-Au electrodes) and gently stirred for 16 h. Then electrodes were washed with acetonitrile and water, and dried. After that, Boc deprotection of the spacer was carried out as described above.

2.5.5 Coupling of maleimide

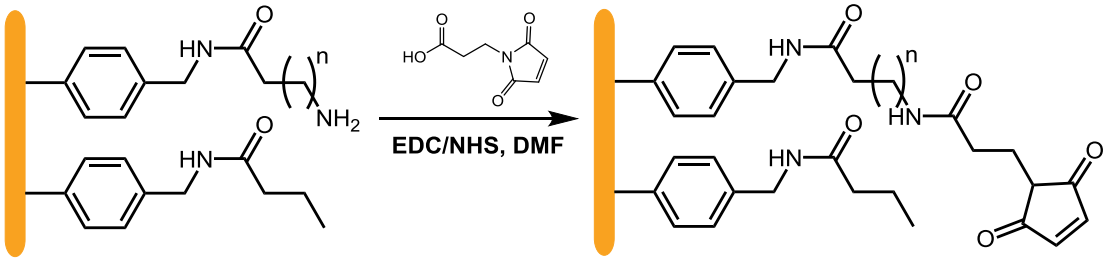

Scheme 2.10. *Coupling of N-maleoyl-β-alanine (n is equal to 1 or 4).*

A solution containing *N*-maleoyl-β-alanine (25 mM), NHS (60 mM) and EDC (0.1 M) in DMF (acetonitrile or ethanol in the case of SPEs and np-Au electrodes) was prepared and stirred for 15 min. Electrodes were immersed for 16 h, then washed with acetonitrile and water and dried.

2.6 Immobilization of CDH variants at maleimide-modified electrodes

Before using the enzyme solution for the immobilization on maleimide-modified electrodes, the buffer in which CDH was dissolved (pH 5.5 acetate buffer, 50 mM) was exchanged with a pH 7.0 phosphate buffer (50 mM). This was done using mini dialysis devices provided with a polyethersulfone (PES) membrane (Fisher Scientific) with 10 kDa cut off. About 10 or 20 µL of enzyme solution were placed in each membrane and the dialysis devices were immersed in gently stirred 50 mM phosphate buffer (250 mL) for 10 minutes. Therefore, other 250 mL of fresh buffer were placed in and the dialysis units were immersed for other 20 minutes. Finally, the dialysis units were immersed in 500 mL of fresh buffer in the fridge for 2 hours.

Eventually, a different method was used for the dialysis using mini concentrator devices (0.5 mL) provided with a PES membrane and 10 kDa cut off (Thermo Scientific). About 10 or 20 µL of CDH solution (pH 5.5) were placed inside the concentrator, which was fill up to 100 µL with 50 mM phosphate buffer (pH 7). The device was placed in the centrifuge at 6000 rmp for about 8 min. Therefore, the concentrator was filled up with the same phosphate buffer again and placed in the centrifuge as before. The operation was repeated for 4-5 times and, finally, about 10-20 µL of CDH solution were recovered from the device.

After dialysis, a few µL (from 3 to 10, depending on the electrode type) of CDH in 50 mM phosphate buffer (pH 7) were placed on the surface of each maleimide-modified electrode, which was then covered and stored in the fridge (4 °C) overnight. The electrodes were then immersed in the same buffer used for the electrochemical measurements to wash away the enzyme in excess, and used for the analysis. After that, the electrodes were stored in the fridge, wet with the same buffer used for the analysis, and tested again when required.

2.7 Analysis and characterization techniques

2.7.1 Cyclic voltammetry of CDH-modified electrodes

Cyclic voltammetry measurements of CDH-modified electrodes were carried out in 50 mM buffers (acetate for pH 5.5 and Tris for pH 7.4), containing 30 mM $CaCl_2$ if stated. Analysis of MET were carried out by adding 1 mM ferrocenecarboxylic acid (or lower concentrations if required) in the buffer and sonicating it for 15-20 min until it was dissolved. All solutions were deoxygenated by bubbling argon for 30 min before applying the potential, and for a few minutes after every addition of glucose or other substrates. Glucose stock solutions were prepared in the same buffer used for the measurement with a concentration of 1 M, and added in the electrochemical cell in different aliquots to reach the desired concentration for the analysis. Lactose solutions were prepared in the same way, normally with a concentration of 0.5 M.

CVs were carried out using the software Nova 1.10, normally sweeping the potential at 1 mV/s from -0.35 to 0.1 V *vs.* SCE for the DET experiments, and at 2 mV/s from 0.0 to 0.4 V for the MET analyses. All collected data were then exported in Origin 9 to be analysed.

2.7.2 Cyclic voltammetry of AQ-modified electrodes

CV measurements of AQ-modified electrodes were carried out in 0.1 M phosphate buffer (pH 7), deoxygenated with argon gas for 30 min before the analysis. The potential was normally swept from -0.25 to -0.65 V *vs.* SCE at different scan rates (usually 25, 50, 100, 150 and 200 mV/s).

2.7.3 Surface plasmon resonance (SPR) spectroscopy

All the experiments with SPR spectroscopy were performed at the University of Lund (Sweden) in the laboratory of Prof Lo Gorton, in collaboration with Dr Jani Tuoriniemi (Goteborg University, Sweden) and Dr Su Ma (BOKU-University, Vienna, Austria).

SPR measurements were performed using a double-channel Autolab ESPRIT instrument (Eco Chemie, Delft, The Netherlands). The polarized laser light (λ = 670 nm) was directed to the bottom side of the gold disc via a hemispheric lens and the reflected light was detected using a photodiode (see Figure 5.7). SPR curves were scanned on the forward and backward movements of the mirror and the minima in reflectance were determined. The modification of the gold disc was followed as the SPR angle shifted within a dynamic range of 4000 millidegrees (m°) and the minima were determined using the AUTOLAB SPR software.

For the SPR experiments, gold-coated SPR substrates (≈ 2 cm diameter, see Figure 5.7-B, from Xan Tec Bioanalytics GmbH, Dusseldorf, Germany) were cleaned in piranha solution (5:1:1 $H_2O/H_2O_2/NH_3$) for 5 min and then rinsed with water and ethanol. For the SPR analysis of CDH immobilization only, the gold discs were functionalised with maleimide outside the SPR instrument according to the method previously described for gold electrodes in Section 2.5. Once modified with maleimide, the gold disc was then inserted in the SPR instrument, washed with 50 mM phosphate buffer (pH 7) and around 10 μL of the *Mt*CDH solution of choice (in the same buffer at pH 7) were dropped in each channel of the SPR cuvette (see Figure 2.6). The immobilization reaction was followed by the SPR angle shift and stopped when the angle shift seemed quite constant by rinsing the channels with the same phosphate buffer.

For some experiments, all the modification procedure was carried out inside the SPR instrument following the same method previously described in Section 2.5, but using a 1:1 water/acetonitrile solution to dissolve the diazonium salt, a 1 M HCl solution in water for the Boc deprotection and ethanol instead of DMF for the coupling of carboxylic acids in order to avoid damages of the instrument.

Some electrochemical measurements of CDH-modified SPR substrates were also performed inside the SPR instrument (in addition to the electrochemical grafting of the diazonium salt), using the SPR cuvette as the electrochemical cell (Figure 2.6). This was equipped with a pseudo Ag/AgCl reference electrode and a platinum disc counter electrode, fixed inside the cuvette. The two void channels of the plastic cuvette formed a close rectangular shape on a small portion of the gold disc substrate, isolating an area of about 0.5 cm^2. For the CV analysis of the CDH-modified substrate, the channels were filled with 20-30 µL of 50 mM Bis-Tris buffers (at pH 5.5 or 7.4), containing 30 mM $CaCl_2$ for pH 7.4 only, to measure the background current. For the catalytic current, the buffer contained also 10 mM lactose. The measurement were performed with an Autolab PGSTAT 30 (Ecochemie, The Netherlands) equipped with GPES 4.9 software.

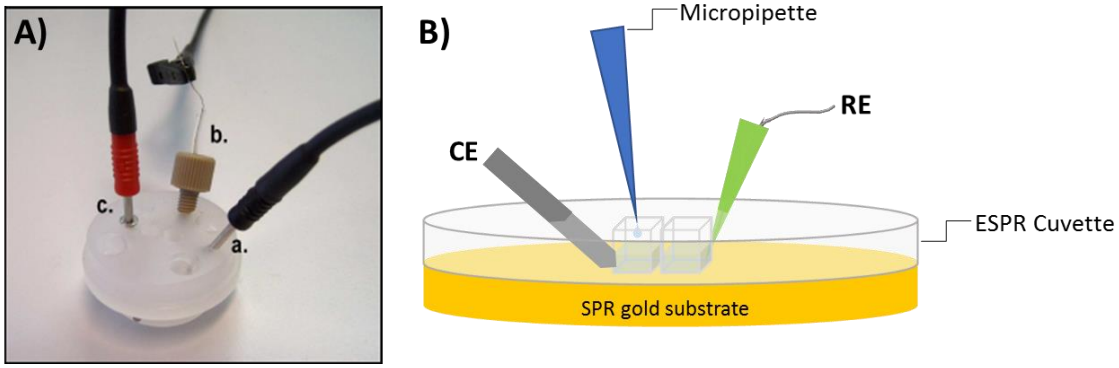

Figure 2.6. *A) Picture of the electrochemical SPR cuvette with the three electrode connections: a) counter electrode (CE), b) reference electrode (RE) and c) contact for the gold working electrode (adapted from the Autolab ESPRIT manual). B) Schematic representation of the same ESPR cuvette placed on an SPR gold substrate: the two void channels inside (total area ≈ 0.5 cm^2) can be filled with a solution using a micropipette.*

2.7.4 Time-of-Flight Secondary-Ion Mass Spectrometry (ToF-SIMS)

All the ToF-SIMS measurements have been carried out at the University of Limerick (Ireland) in the laboratory of Prof Edmond Magner, thanks to the help of Till Siepenkoetter (PhD student) and Serguei Belochapkine (technician).

Flat gold substrates prepared by magnetron sputtering were used. These were simple microscope glass slides prepared by deposition of a ≈ 10 nm thick titanium adhesion layer followed by a ≈ 100 nm thick gold layer. The substrates

were cleaned with DMF and then used for the covalent modification with diazonium salt as previously described in Section 2.5.

Time-of-flight secondary-ion mass spectrometry (ToF-SIMS) data were acquired using a ToF-SIMS IV spectrometer (ION-TOF GmbH). The analysis chamber was maintained at a working pressure of 5×10^{-9} – 5×10^{-10} mbar under operating conditions. A pulsed 25 keV Bi^+ primary ion source (Liquid Metal Ion Gun, LMIG) at a current of about 0.3 pA (with pulse width of 4 ns), raster over a scan area of 300 x 300 μm, was used as the analysis beam. The analyser had a typical mass resolution (m/Δm) of 9000 at mass 29 u. The complete vacuum system and all electronic devices were computer controlled by a Windows™ based PC.

For the ToF-SIMS analysis of the pure diazonium salt, a silicon wafer spin-coated with the sample was used. The silicon wafer was first cleaned in a vacuum chamber by H_2-O_2 plasma. Then, a 0.5 % diazonium salt solution in acetonitrile was spin-coated onto the silicon wafer in order to produce a uniform thickness layer of the sample.

2.8 Simulation of catalytic voltammograms

The simulations of the CDH catalytic voltammograms were performed using the software Excel 2013, by writing the equation for the current that was derived in Section 4.1.3 and plotting the data of current *vs.* potential. For the figures reported in Chapter 4, the data were exported in Origin 9, plotted and, eventually, fitted with the Michaelis-Menten equation, written using the "Nonlinear Curve Fit" in the "Fitting" function of the software.

Chapter 3:

Covalent immobilization of CDH at GC/CNT electrodes

In this Chapter, we will show the stable, site-specific immobilization of a redox enzyme, cellobiose dehydrogenase from *Myriococcum thermophilum* (*Mt*CDH), at high surface area carbon electrodes. Glassy carbon electrodes modified with carbon nanotubes (GC/CNT) were modified with maleimide groups by using a modular approach that combines electrochemical and solid phase synthesis. In this approach, the key elements of the modification can be independently varied to tune the architecture of the electrode surface as required, by simply changing the "bricks" of the structure. The CDH-modified electrodes were tested for the DET and MET; in addition, several tests to verify the stability of the enzymatic electrodes and the mechanism of the direct and mediated electron transfer were performed. In the last Section, we will show a different method to functionalise the CNTs with maleimide groups before adsorbing them on the electrodes.

This work has been carried out in collaboration with my colleague Firas Al-Lolage (University of Southampton); Dr Roland Ludwig and Dr Su Ma (BOKU-University, Vienna, Austria), who kindly provided the *Mt*CDH variants.

3.1 Modification of the carbon electrodes

3.1.1 Introduction

The method for the covalent, site-specific immobilization of cysteine-modified CDH on carbon electrodes follows previous work in our group [70,110]. Glassy carbon electrodes modified with multiwall carbon nanotubes (GC/CNT) were chosen as models for carbon-based electrodes because of their high surface area combined with a relatively low capacitance. These were modified with maleimide groups using electrochemical surface attachment and solid phase synthesis methodology [70,110]. A key aspect of our procedure is the creation of a modified surface on the electrode in a stepwise manner, allowing the single elements of the construction to be independently varied. In this case, these elements are a "linker", a "spacer", a "reactive group" and a "passivating group" (Scheme 3.1).

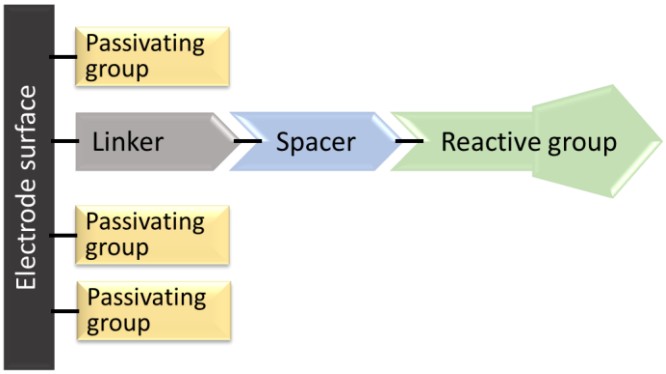

Scheme 3.1. *Schematic representation of the stepwise modified electrode, with the key elements highlighted.*

The "linker" provides the attachment between the electrode and the rest of the modification connecting to the enzyme: it has two functionalities that allow it to be electrochemically grafted on the electrode surface and then chemically linked with other molecules. The "spacer" can be introduced after the linker to lengthen the linkage; it has two functional groups, one to react with the linker and the other one with the reactive group, and it can be of different length. The "reactive group" is the final component in the linkage; it is chemically attached to the linker or spacer through one of its functionalities and has a second functional group suitable to react with the target group on the desired protein or

biomolecule. Finally, the "passivating group" is, normally, a small molecule co-grafted at the electrode surface with the linker to form a two-component monolayer on the electrode in order to dilute the reactive groups and provide a film compatible with the surface of the enzyme around the attachment point, thus to reduce denaturation of the protein.

The partial coverage of the reactive group is a significant aspect of our design. In fact, redox enzymes are large, three-dimensional objects with non-uniform surfaces. Dilution of the reactive group on the surface of the electrode and the choice of a suitable length of linkage allow the maleimide to react with the cysteine at the enzyme surface without steric restrictions. In fact, in a previous work [70], our group showed that a full coverage of maleimide produced the same result as a control experiment without any reactive group, suggesting that non-specific binding was the predominant mode of protein retention on the electrode surface in both the cases. This is because, with the linker forming a compact monolayer of uniform thickness, the bulky protein could not be sterically accommodated onto the electrode (see Scheme 3.2-B). On the other hand, dilution of the binding group on the surface resulted in increased coverage of the protein, reaching the maximum value for electrodes modified with a mixture of amines containing 10 % of the linker (see Scheme 3.2-A).

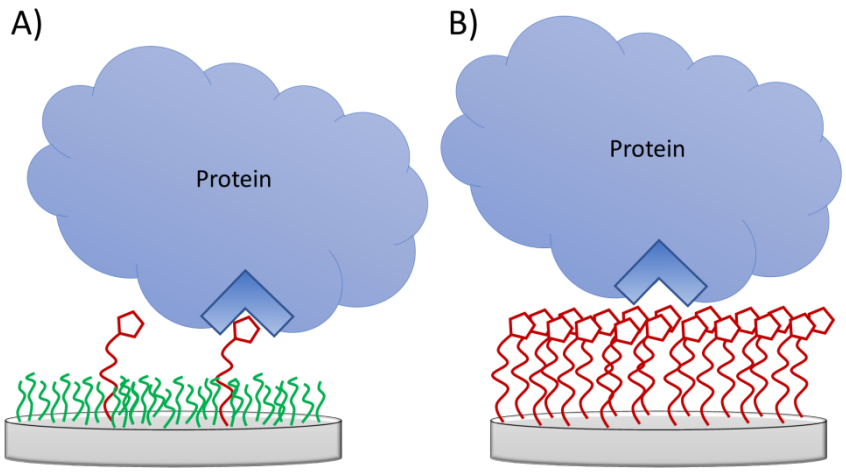

Scheme 3.2. *Schematic representation of electrode surfaces with (A) partial coverage and (B) full coverage of the reactive group. The reactive group is represented by the red pentagon, the passivating group is in green and the protein with relative target group in blue.*

3.1.2 Electrode modification and enzyme immobilization

GC/CNT electrodes were modified with a mixture of two primary amines (see Scheme 3.3) in order to dilute the ultimate number of maleimide groups in the final film. A mono-Boc-protected diamine was chosen as the linker due to its efficient electrografting to carbon surfaces through electrochemical oxidation to give a stable attachment [58,59]. This represents a versatile, modular method for electrode modification since, after removal of the Boc protecting group, a wide range of molecules can be coupled to the amino-modified surface using conventional solid phase synthesis methodology [65,111] to build up the desired molecular architecture on the electrode and to tune the electrode properties [112,113].

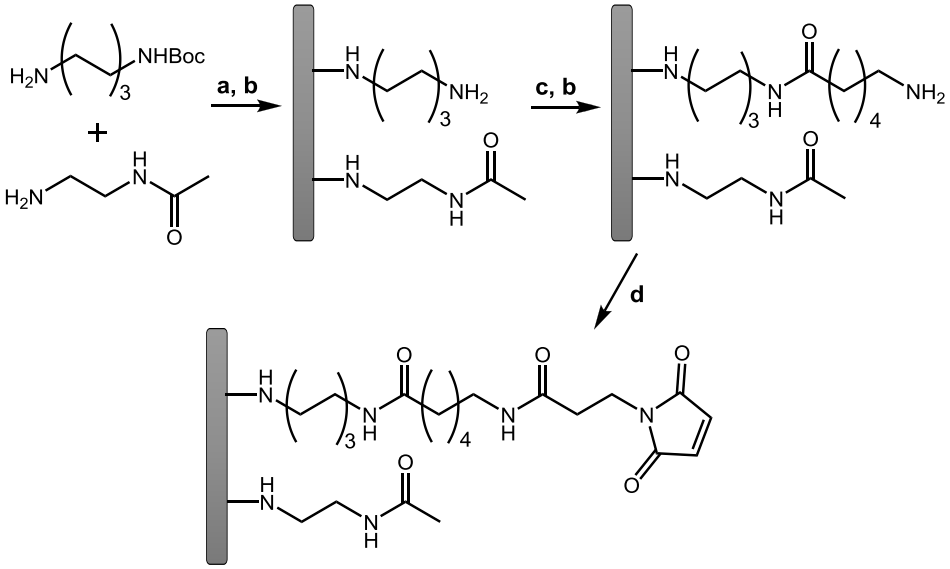

Scheme 3.3. *Sequential electrochemical and solid-phase preparation of maleimide-modified electrodes. Reagents and conditions: a) 2 mM N-Boc-1,6-hexanediamine, 18 mM N-(2-aminoethyl)acetamide, 0.1 M TBATFB in deoxygenated acetonitrile, constant potential of +2 V vs. SCE for 180 s; b) 4 M HCl in 1,4-dioxane (45 min); c) 10 mM N-Boc-6-aminohexanoic acid, 0.1 M EDC, 60 mM NHS in DMF (16 h); d) 25 mM N-maleoyl-β-alanine, 0.1 M EDC, 60 mM NHS in DMF (16 h).*

A more detailed description of the modification procedure can be found in the Experimental Part (Chapter 2): here we will illustrate the main steps. The linker (*N*-Boc-1,6-hexanediamine, Boc-HDA) and the passivating group (*N*-(2-aminoethyl)acetamide) were grafted onto the carbon electrodes through electrochemical oxidation from an acetonitrile solution containing 10 % of the linker and 90 % of the passivating group. The electrode potential was held

constant at +2 V *vs.* SCE: at this potential both amines are oxidised forming the corresponding amine radicals. If we assume similar reactivity for the two radicals formed, we expect the ratio of their surface coverages to be similar to the ratio of their solution concentration. After electrografting, the Boc protecting group was removed and a six-carbon-long spacer was added to the 1,6-hexadiamine linker in order to lengthen the linkage, making it more flexible and accessible to the enzyme. The six-carbon-long spacer was introduced by coupling *N*-Boc-6-aminohexanoic acid onto the amino-modified surface. Overall, this gives a tether approximately 3 nm long and was chosen to ensure that the maleimide binding group can easily reach the cysteine residue at the CDH surface. After removal of the Boc protecting group, *N*-maleoyl-β-alanine was coupled to the amino-modified surface to produce the maleimide-modified electrode. One of the advantages of maleimide is that it couples spontaneously to free thiols in aqueous solution, at neutral pH, allowing very efficient use of small quantities of purified enzyme. Coupling of the *Mt*CDH variants was carried out by drop casting 3 μL of CDH solution (at pH 7.0) on the electrode and leaving it overnight at 4 °C.

3.1.3 *Mt*CDH variants used in this work

In this work, we investigated four different CDH variants, genetically engineered to bear a free cysteine in different positions at the surface of the flavin domain (see Figure 3.1). The positions for introduction of the cysteine residues were selected to ensure mobility of the cytochrome domain after immobilization, because this is necessary for the direct electron transfer. The cysteine mutation for the variant E522 (red in Figure 3.1) is on top-centre of the CDH molecule and requires the cytochrome domain not only to move away from the dehydrogenase domain, but also to rotate to contact the electrode with its haem cofactor. The position T701 (blue), in the bottom-centre of the molecule, requires a smaller movement of the cytochrome domain and no reorientation of the haem towards the electrode. The position E674 (green) is in the bottom of the flavin domain, far from the cytochrome domain: it is probably the mutation that would have the longest distance between the haem and the electrode surface, thus having less probability for the DET. Finally, the mutation D813 (orange) is on the top-left in Figure 3.1, close to the peptide linker connecting the two domains: once

immobilised on the electrode, it will require a small movement of the cytochrome domain to be in contact with the electrode surface. For a better visualization of the four different CDH variants in the correct orientation on the electrode surface see also Figure 3.10 in Section 3.2.5.

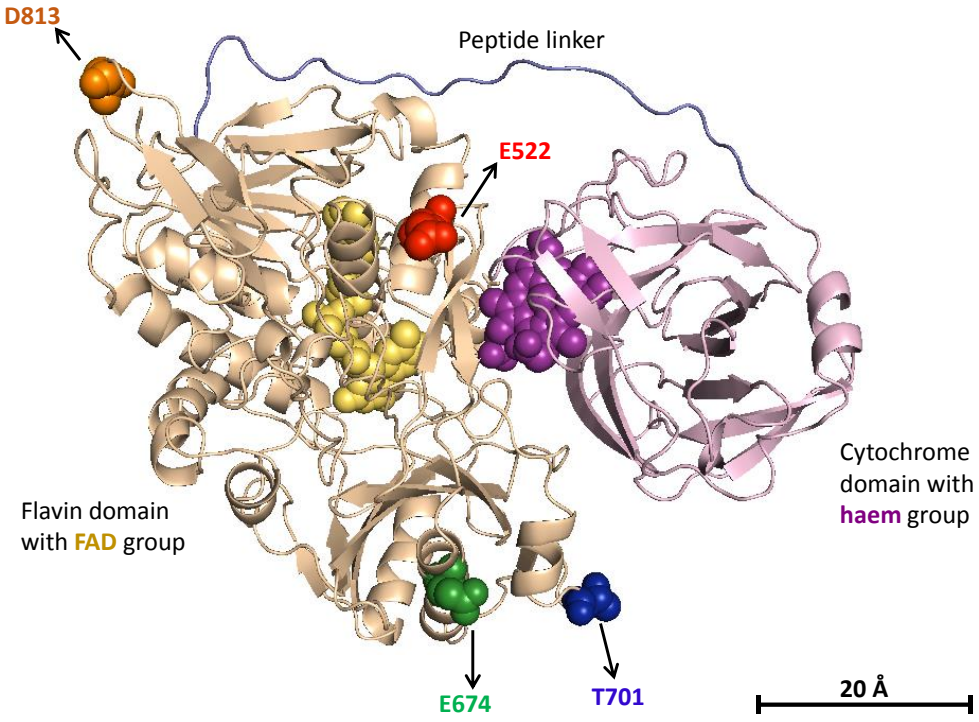

Figure 3.1. *Cartoon representation of the secondary structure of MtCDH. The sites of the E522, T701, E674 and D813 mutations are highlighted in red, blue, green and orange, respectively; the flavin domain with the FAD group in beige/yellow and cytochrome domain with the haem group in pink/purple. The peptide chain linking the two domains is in light-blue. Note, this is a simplified representation of the location of the four mutations, they are not all present in one enzyme, but in four distinct variants.*

3.2 Direct electron transfer of immobilised CDH

3.2.1 Non-catalytic voltammetry

Now we have immobilised CDH on the GC/CNT electrodes, the ability of the enzyme to produce direct electron transfer with the electrode surface was investigated. Figure 3.2-A shows a voltammogram of *Mt*CDH (variant E522) immobilised at a maleimide-modified GC/CNT electrode. In the absence of substrate, sweeping across the potential range at 10 mV/s produces redox peaks

due to DET between the electrode and one of the redox centres of the enzyme. In Figure 3.2-A, the outer trace (grey line) is a cyclic voltammogram recorded at pH 5.5 (50 mM acetate buffer, containing 30 mM $CaCl_2$). The capacitive, or background, current was subtracted using the software Origin 9: the baseline for the capacitive current was created by setting the "subtract baseline" mode in the "peak analyser" function. Therefore, an adequately high number of points (generally around 100) was manually placed on the curve, except for the potential range where the peaks are located (between -0.2 and 0.0 V for the forward scan and between -0.05 and -0.22 V for the backward scan). Then the points were interpolated using the "BSpline" function to produce the baseline.

After subtracting the capacitive current, the resulting faradaic voltammogram (black line in Figure 3.2-A) can be integrated to find out the charge (Q) and, therefore, the absolute amount of electroactive enzyme in this particular experiment (m_{enz}) (the surface coverage cannot be calculated since the exact active area of a GC/CNT electrode is not known as we will explain in Section 5.1.1) by using the Faraday law:

$$Q = n\, m_{enz}\, F \qquad \text{(Eq. 3.1)}$$

where F is the Faraday constant (96485 A s mol^{-1}) and n is the number of electrons exchanged at the electrode surface for each molecule of enzyme. Since the active centre responsible for the DET should be the haem group, as we will verify later through several experiments, n will be equal to 1. This will be confirmed by studying the shape of the CDH catalytic voltammograms using the Nernst equation in Section 3.2.2. From integration of the reduction and oxidation peaks, we can obtain the average integration area (a_{int}), from which the charge can be calculated using the following equation:

$$Q = \frac{a_{int}}{v} \qquad \text{(Eq. 3.2)}$$

where v is the scan rate. Therefore, the amount of electroactive enzyme will be given by rearranging Eq. 3.1 and substituting Q with Eq. 3.2:

$$m_{enz} = \frac{a_{int}}{n\, F\, v} \qquad \text{(Eq. 3.3)}$$

For the voltammogram reported in Figure 3.2-A, m_{enz} was found to be $\approx$ 8 pmol.

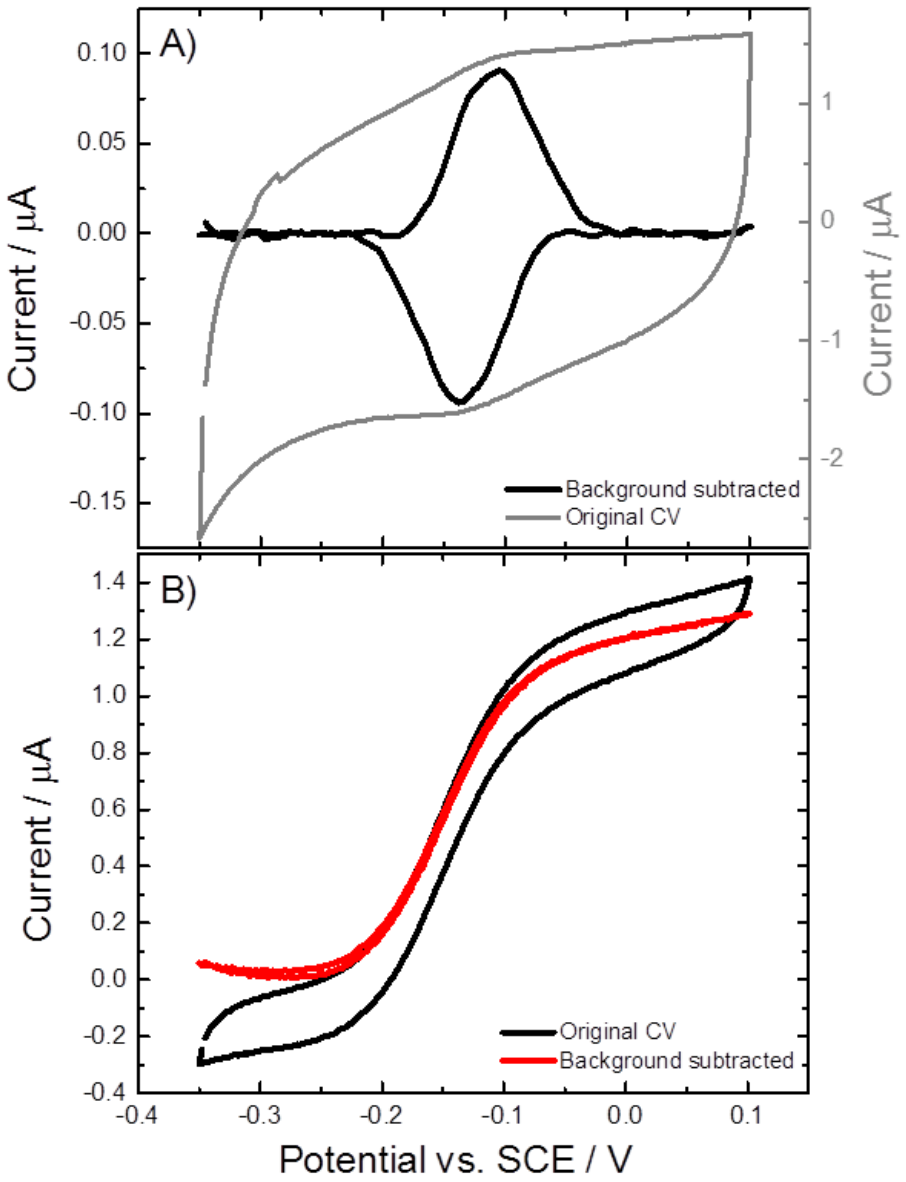

Figure 3.2. *Cyclic voltammograms for a E522-CDH modified GC/CNT electrode, in the (A) absence and (B) presence of 70 mM glucose. CVs were recorded in argon-saturated 50 mM acetate buffer (pH 5.5), containing 30 mM $CaCl_2$, scanning the potential at (A) 10 mV/s and (B) 1 mV/s. A) CV without glucose has been background subtracted and smoothed (black), the original CV is also reported in a different scale (grey). B) CV with glucose has been background subtracted too (red line): in this case the background is the CV recorded in the same conditions without glucose.*

The redox couple observable in Figure 3.2-A presents a redox potential ($E_{1/2}$) of about -0.12 V *vs.* SCE and, as we have already mentioned, can be attributed to the one-electron transition of the haem group, one of the two CDH active sites. In fact, the other active site, FAD, should not be able to exchange electrons directly with the electrode surface. The fact that the redox peaks observed in Figure 3.2-A are due to the haem group was also confirmed by an experiment performed at a

different pH, such as 7.4 (Figure 3.3). In this condition, the redox potential was found to be at about -0.13 V *vs.* SCE. The small difference in the redox potential between the two pHs (about 10 mV) can be attributed to experimental error or to the manual background subtraction, as the faradaic current is very small. Otherwise, we can assume that there is a pH-dependence due to changes in the ionization states of the amino acid residues surrounding the haem group, which would induce a perturbation in the haem redox potential [114,115]. In any case, this perturbation is too small (about 10 mV passing from pH 5.5 to pH 7.4) to be attributed to the FAD active site, whose reduction-oxidation potential strongly depends on the pH [75,116,117], decreasing of 59 mV per pH unit (between pH 4 and pH 7), according to the Nernst equation for a 2 proton-2 electron redox process. In fact, if this were the case, going from pH 5.5 to pH 7.4, we would expect a decrease in the redox potential of about 120 mV, which did not occur. Further experiments proving that the haem group, not the FAD, is responsible for the DET of CDH will be shown later in this Chapter.

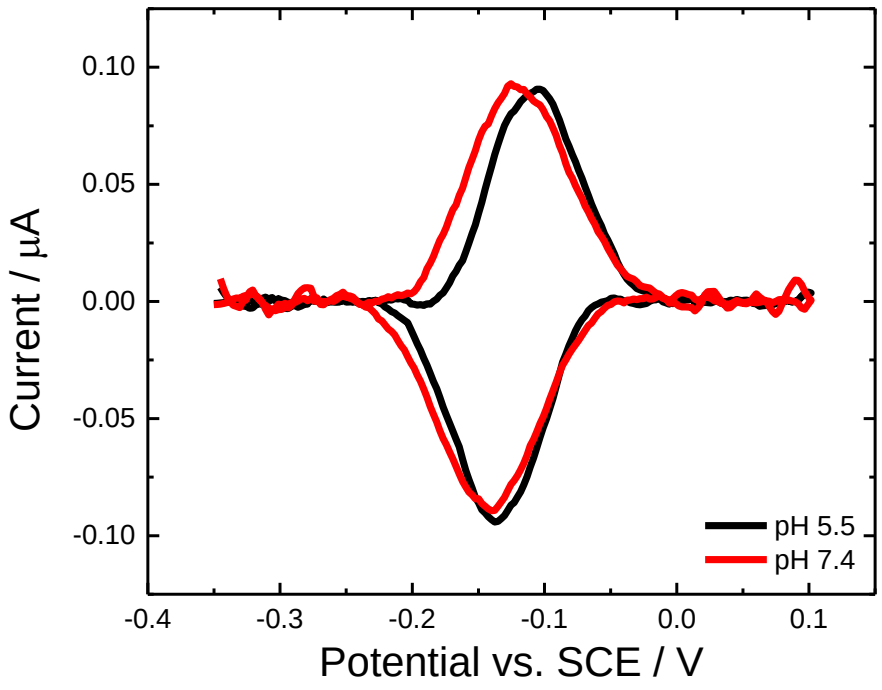

Figure 3.3. *Cyclic voltammograms for E522-CDH modified GC/CNT electrodes recorded in argon-saturated 50 mM acetate buffer pH 5.5 (black) and 50 mM Tris buffer pH 7.4 (red), both containing 30 mM $CaCl_2$, scanning the potential at 10 mV/s. CVs have been background subtracted and smoothed.*

3.2.2 Steady-state catalysis

Figure 3.2-B shows a voltammogram recorded for the same CDH-modified GC/CNT electrode placed in a solution containing the substrate, D-glucose. A slower scan rate (1 mV/s) was used to ensure steady state. The resulting voltammogram is a "direct read-out" of the rate of catalysis as a function of the electrode potential (driving force). At an applied potential higher than the CDH equilibrium potential, electrons flow from the glucose to the electrode via the FAD and haem active centres. The resulting, positive, limiting current is directly proportional to the rate of glucose oxidation for that given concentration of substrate, when regeneration of the active site by the electrode is not the limiting step. We can subtract the background current (CV recorded in the absence of glucose) from the original voltammogram (black line), obtaining then a sigmoidal curve (red line) that starts at about 0.0 μA and reaches its plateau at about 1.3 μA.

Looking closer at the voltammogram in Figure 3.2-B, we can notice at first glance that the oxidation process starts at about -0.2 V *vs.* SCE. According to studies by Gorton *et al.* [96], this should be the redox potential of the haem group, while FAD should be oxidised at more negative potentials [75,117]. This further proves that the haem group exchanges electrons with the electrode surface in the DET mechanism, not the FAD cofactor. A deeper analysis can be carried out using the following modified form of the Nernst equation:

$$E = E' + \frac{0.059}{n}\mathrm{Log}\left(\frac{i_\mathrm{L} - i}{i}\right) \qquad \text{(Eq. 3.4)}$$

where E' is the formal potential, n is the number of exchanged electrons and i_L the limiting current. Applying this equation to some points taken in the middle part of steady-state catalytic voltammograms subtracted for the background current, such as the red curve in Figure 3.2-B, a linear relation between the applied potential and $\mathrm{Log}((i_\mathrm{L}-i)/i)$ was found (Figure 3.4). Linear fits of these plots procured a more precise value of E' for the haem cofactor, given by the intercept. For the plot in Figure 3.4, E' was found to be -0.15 V *vs.* SCE. In addition, the slope of the linear fit can provide information about the number of exchanged electrons (n), which was found to be 0.85 and can be approximated to

1. This is a further proof that the haem group is responsible for the DET at the electrode surface, as its redox process involves one electron, while the FAD cofactor would need to exchange two electrons to be oxidised [117].

The obedience to the Nernst equation shown in Figure 3.4 implicates that the electron transfer between the haem and the electrode is always very fast and reversible, so that thermodynamic equilibrium is maintained at the electrode surface. As a consequence, the haem/electrode reaction cannot be considered as the rate limiting step in the CDH catalytic process, and it will not affect the current intensity since only the rate limiting step does.

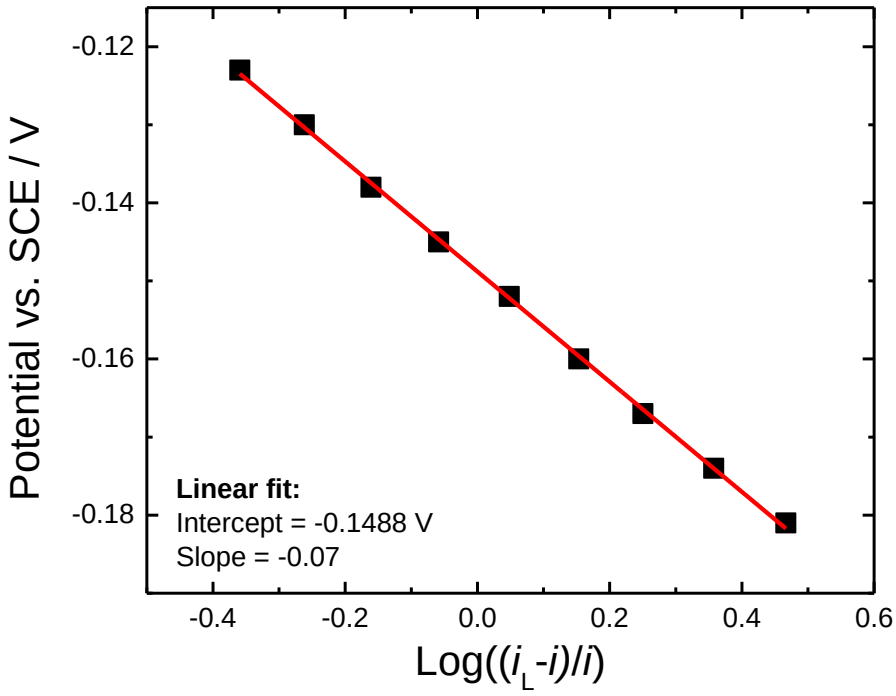

Figure 3.4. *Some potential points taken in the middle region of the background subtracted CV reported in Figure 3.2-B (red line) plotted against the Log((*i_L*-i)/i) (see Eq. 3.4). Data were fitted with a linear fit (red line).*

3.2.3 Michaelis-Menten catalytic behaviour

A GC/CNT electrode modified with the CDH variant E522 was tested for DET by cyclic voltammetry at increasing concentrations of D-glucose. As we can see in Figure 3.5, increasing the concentration of substrate in solution leads to increase in the catalytic current in the positive region of the voltammogram. The original CVs (Figure 3.5-A) were subtracted for the background current, which is the CV recorded in the absence of glucose (black line in Figure 3.5-A), to obtain a sort of sigmoidal curves shown in Figure 3.5-B.

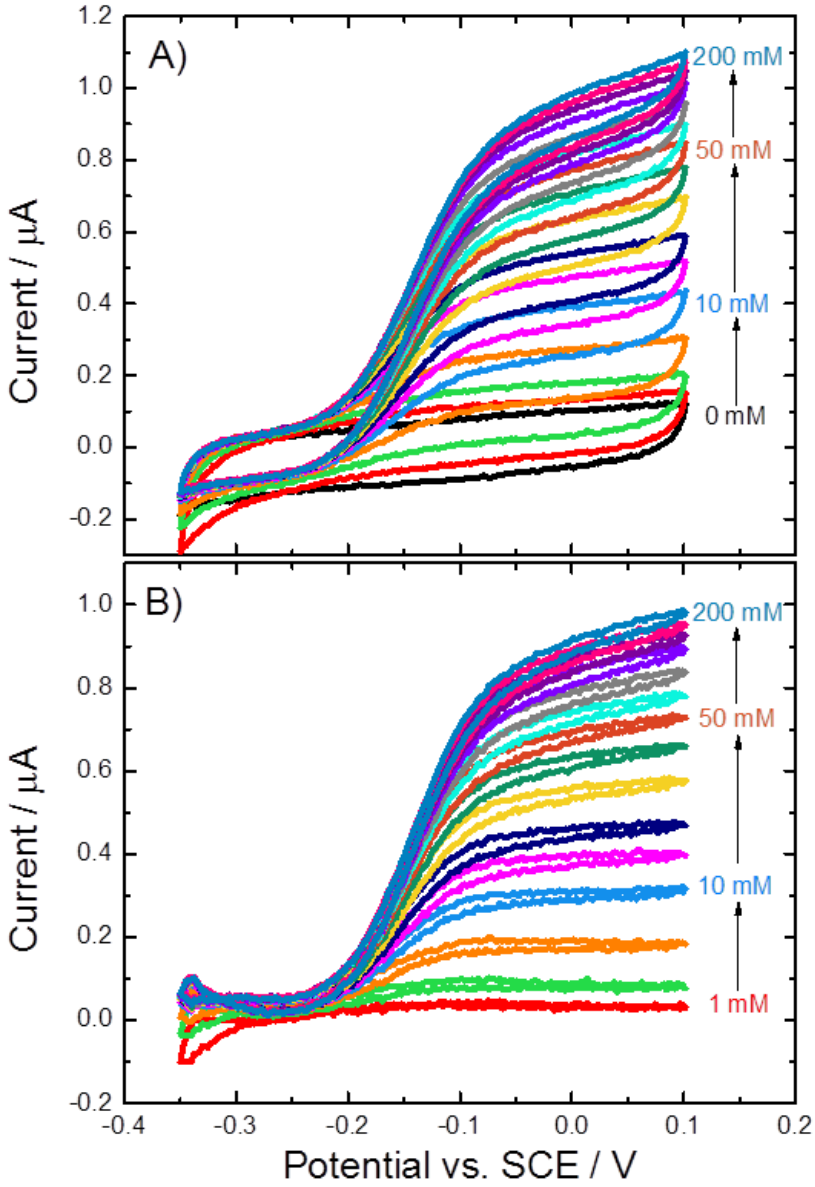

Figure 3.5. *A) Cyclic voltammograms for a E522-CDH modified GC/CNT electrode, recorded in argon-saturated 50 mM acetate buffer (pH 5.5), containing 30 mM $CaCl_2$ and different concentrations of D-glucose from 0 to 200 mM. The electrode potential was swept at 1 mV/s. B) Same CVs subtracted for the background current (black line in Figure A).*

The limiting current taken at 0.0 V *vs.* SCE in the voltammograms of Figure 3.5-B can be plotted versus the glucose concentration (Figure 3.6), showing a typical Michaelis-Menten-like plot. The experimental data can be fitted with a potential-dependent Michaelis-Menten equation (red line in Figure 3.6), in which the dependent variable is represented by the current:

$$i = \frac{{i_{\max}}^{\mathrm{APP}}[\mathrm{S}]}{[\mathrm{S}] + {K_{\mathrm{M}}}^{\mathrm{APP}}} \qquad \text{(Eq. 3.5)}$$

where [S] is the substrate concentration, ${K_{\mathrm{M}}}^{\mathrm{APP}}$ is the apparent Michaelis-Menten constant (relative to glucose oxidation in this case) and ${i_{\max}}^{\mathrm{APP}}$ is the maximum current that can be reached upon saturation. Eq. 3.5 will be derived and fully described for the electrodic reactions of CDH in Chapter 4. For the moment, we can just observe that for the lowest substrate concentrations (between 0 and 5 mM glucose) the current increases linearly with [S]. In this case, the current must be controlled by a kinetic step involving the substrate, such as the glucose/FAD reaction.

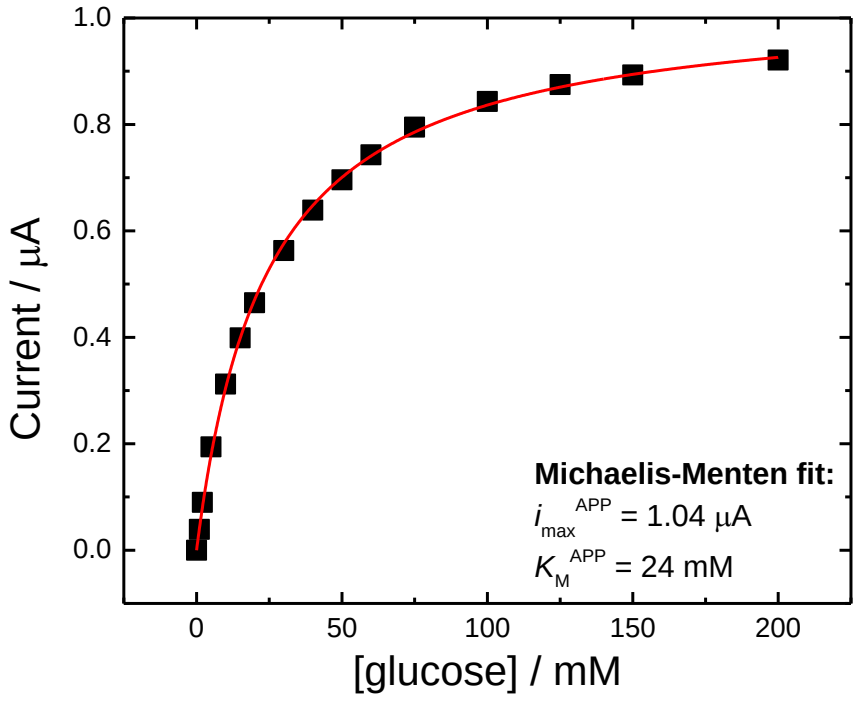

Figure 3.6. *Values of the current taken at 0.0 V in the CVs reported in Figure 3.5-B, plotted vs. glucose concentration. The CVs were recorded at a E522-CDH modified GC/CNT electrode, in argon-saturated 50 mM acetate buffer (pH 5.5), containing 30 mM $CaCl_2$ and different concentrations of D-glucose. Data were fitted with Eq. 3.5 (red line).*

Therefore, for the first part of the plot, Eq. 3.5 can be approximated as follow:

$$\text{for} \quad [\text{S}] \ll {K_\text{M}}^{\text{APP}} \quad \Longrightarrow \quad i = \frac{{i_\text{max}}^{\text{APP}}}{{K_\text{M}}^{\text{APP}}}[\text{S}] \qquad \text{(Eq. 3.6)}$$

Afterwards, in the middle part of the plot, a mixed control is realised: the current is affected by both the glucose/FAD reaction and some other kinetic step. In this middle part, any approximation can be done and the Michaelis-Menten equation should be used in form given by Eq. 3.5. Finally, in the last part of the plot (at about 150-200 mM glucose), the current reaches saturation and Eq. 3.5 can be approximated as follow:

$$\text{for} \quad [\text{S}] \gg {K_\text{M}}^{\text{APP}} \quad \Longrightarrow \quad i = {i_\text{max}}^{\text{APP}} \qquad \text{(Eq. 3.7)}$$

$$\text{with} \quad {i_\text{max}}^{\text{APP}} = nFm_\text{enz}{k_\text{cat}}^{\text{APP}} \qquad \text{(Eq. 3.8)}$$

where n is the number of electrons involved in the process, F is the Faraday constant, m_{enz} is the number of moles of electroactive enzyme and k_{cat}^{APP} is the apparent catalytic constant. Given that for each molecule of glucose oxidised two electrons are exchanged at the electrode surface, n is equal to 2. Looking at Eq. 3.7 and 3.8, we can conclude that for the highest substrate concentrations the current becomes limited by both the amount of electroactive enzyme (m_{enz}) and some other step that is independent on the substrate and can be described by the parameter k_{cat}^{APP}. We can exclude as rate limiting step the glucose/FAD reaction, as it involves the substrate, and the haem/electrode reaction that we have proved being too fast in the previous section. Therefore, k_{cat}^{APP} can depend on the FAD/haem reaction (IET) or on the intrinsic activity of the enzyme. At the moment, we cannot say which one of the two factors is limiting the current, or whether there are other factors: this will be attempted in Chapter 4.

Considering m_{enz} equal to 8 pmol, as we have found in Section 3.2.1 (even though it may be slightly different for each electrode as we cannot precisely control the electrode active area), and since the fitting provided the value of i_{max}^{APP} as 1.04 µA, k_{cat}^{APP} was found to be 0.7 s^{-1} using Eq. 3.8. The value reported in the literature for *Mt*CDH with glucose is 14 s^{-1} [73]. The difference between the two values can be attributed to the error in the value of m_{enz} used to calculate k_{cat}^{APP} and, more importantly, to the fact that both the k_{cat} (the one we calculated and

the one found in the literature) are actually apparent k_{cat} and their value depends on the experimental conditions used since many different factors can affect k_{cat}^{APP}, as we will see in more details in Chapter 4.

Also the value of K_M^{APP} extracted from the fitting in Figure 3.6, 24 mM, is much lower than the value found in the literature, 250 mM [73]. However, both these values are also apparent K_M and, as we have already said for k_{cat}^{APP}, they can depend on the experimental conditions used. For a more detailed explanation of the difference between the "real" and the apparent K_M/k_{cat}, and how the latter can be affected by the experimental conditions, we refer you to Chapter 4. For the moment, we will carry on with showing the experimental results proving the DET between CDH and GC/CNT electrodes.

3.2.4 Control experiment: D- and L-glucose

In order to prove that the catalytic current observed in the previous Section is due to the oxidation of the glucose by the immobilised enzyme, a simple control experiment using D- and L-glucose was performed. In fact, the enzyme is selective for the D-glucose, while it does not oxidise the other isomer, so that adding L-glucose in the electrochemical cell should not produce any increasing catalytic current. This selectivity can only be attributed to the enzyme: indeed, other possible catalysts present in the cell or on the electrode, such as metals, would oxidise both the isomers of the sugar. Figure 3.7-A shows the voltammograms (after background subtraction) recorded at a E522-CDH modified GC/CNT electrode upon addition of different aliquots of L- and D-glucose in the cell. It is clear, also looking at Figure 3.7-B that shows the value of the current after every addition, that there is no change in the current upon addition of L-glucose in the cell (see dashed CVs in Figure 3.7-A). Contrarily, upon each addition of an aliquot of D-glucose the catalytic current increases (see solid CVs). As we have already mentioned, this chiral selectivity can only be explained by the catalysis of the reaction by the enzyme.

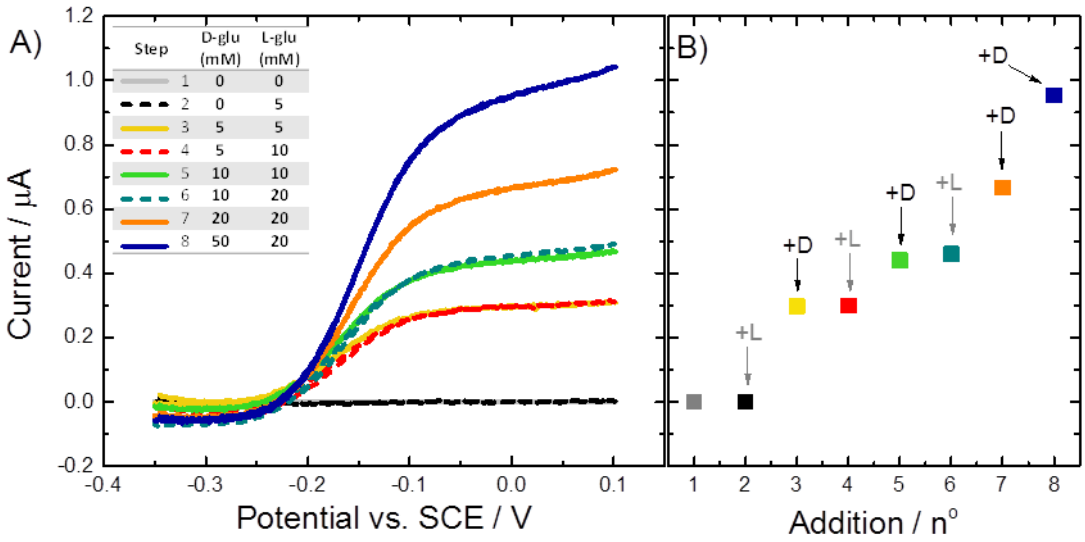

Figure 3.7. *A) Background subtracted CVs for a E522-CDH modified GC/CNT electrode, recorded in argon-saturated 50 mM acetate buffer (pH 5.5), containing 30 mM $CaCl_2$ (grey line) and increasing concentrations of L- and D-glucose. The solution compositions are reported in the inset. The electrode potential was swept at 1 mV/s. B) Plot of the background subtracted currents measured at 0.0 V after each addition of D- and L-glucose.*

3.2.5 Direct electron transfer of different CDH variants

As we have already mentioned, we used four different *Mt*CDH variants genetically engineered to bear the free cysteine in different positions at the surface of the flavin domain. Since the free surface cysteine reacts with maleimide groups previously introduced at the electrode surface, we would expect the different CDH variants to be immobilised with different orientation on the electrode, depending on the position of their cysteine residues (see Figure 3.10). Therefore, we might expect the different variants to have different direct electron transfer distances (distance between the haem group and the electrode surface) and, consequently, different direct electron transfer rates. In other words, we would expect different activities for the four CDH variants, when the same amount of enzyme is immobilised on the electrode.

To prove that, maleimide-modified GC/CNT electrodes were used to immobilise the four different CDH variants. The reaction between maleimide and the cysteine residue should be fast and occurring at neutral pH and room temperature, without the need of any other reagent or catalyst. The CDH-modified electrodes were tested by cyclic voltammetry in deoxygenated 50 mM

acetate buffer (pH 5.5), containing 30 mM $CaCl_2$ and increasing concentrations of D-glucose. The addition of the sugar increases the anodic current at around -0.2 V *vs.* SCE, as we have previously observed for the variant E522 (Figure 3.5), showing the direct electron transfer between the enzyme and the electrode. Figure 3.8 reports all the voltammograms recorded for the three remaining CDH variants: T701, E674 and D813. About 16 voltammograms were recorded for each electrode, at increasing concentration of D-glucose going from 0 to 200 mM.

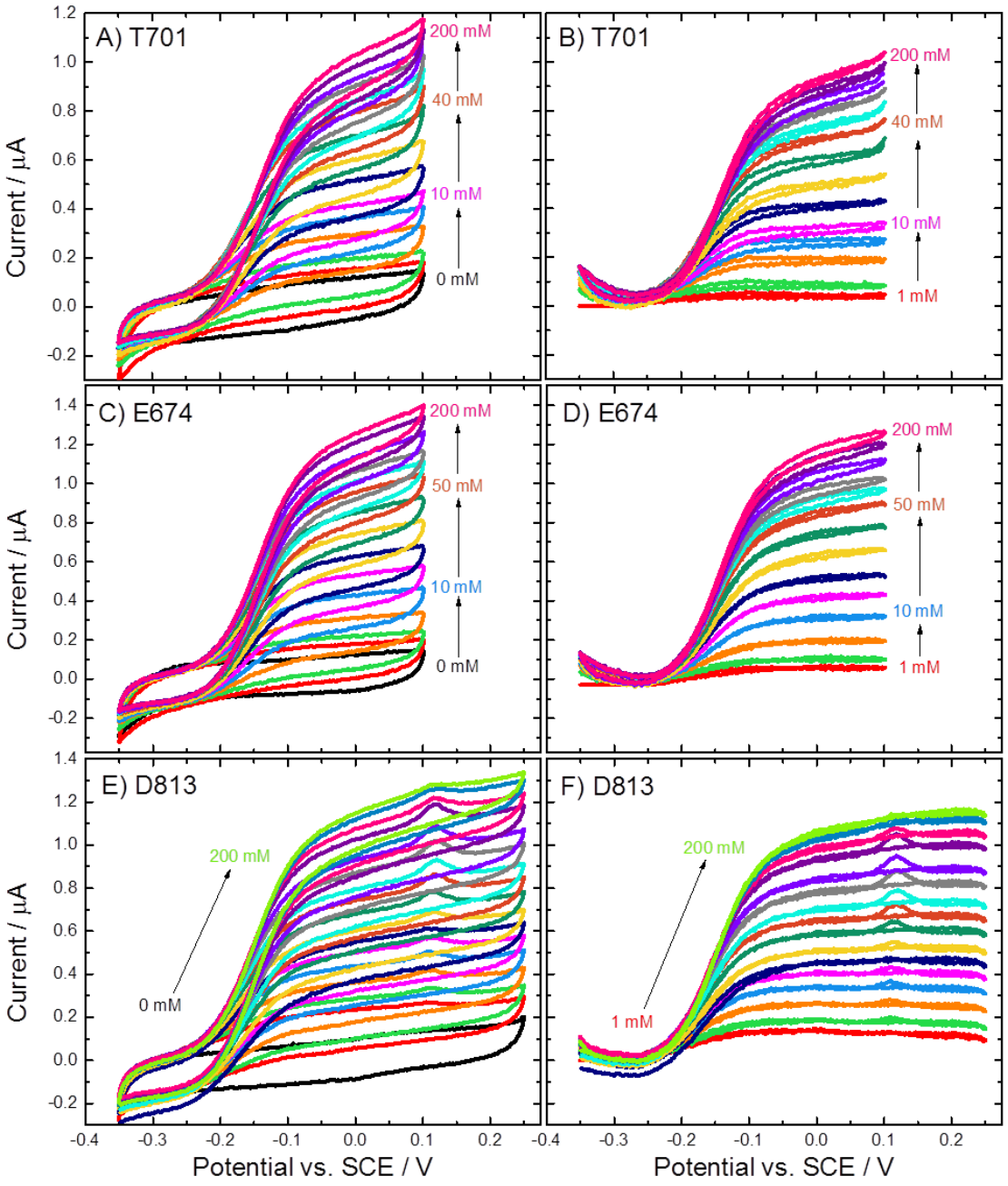

Figure 3.8. *(A, C, E) Original and (B, D, F) background subtracted CVs recorded at (A-B) T701, (C-D) E674 and (E-F) D813-CDH modified GC/CNT electrodes, in argon-saturated 50 mM acetate buffer (pH 5.5), containing 30 mM $CaCl_2$ and different concentrations of D-glucose from 0 to 200 mM. The potential was swept at 1 mV/s.*

The original voltammograms (Figure 3.8-A, C, E) have been background subtracted, meaning that each CV was subtracted for the voltammogram recorded in the absence of glucose (black lines). The subtracted CVs are shown in Figure 3.8-B, D, F: they all look like sigmoidal curves.

Looking at Figure 3.8, we can observe that the redox potential is the same for all the three CDH variants, with the anodic catalytic current always starting at about -0.2 V *vs.* SCE. A deeper analysis can be performed by using the Nernst equation (Eq. 3.4) as already done in Section 3.2.2 for the variant E522: we can plot some potential points taken in the middle region (between -0.2 and -0.1 V *vs.* SCE) of some voltammograms of Figure 3.8 *vs.* the Log($(i_L-i)/i$). Figure 3.9 shows these plots obtained using the CVs recorded with 100 mM glucose, after background

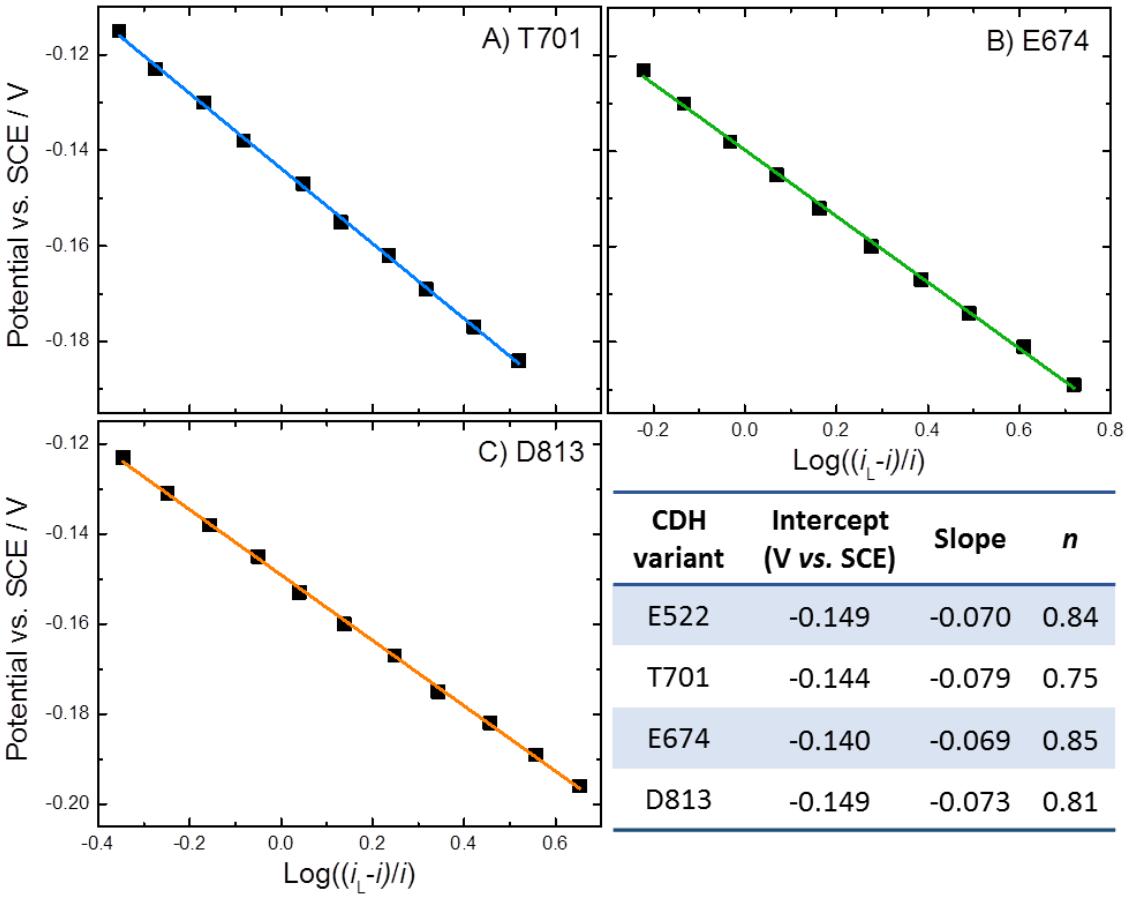

CDH variant	Intercept (V *vs.* SCE)	Slope	*n*
E522	-0.149	-0.070	0.84
T701	-0.144	-0.079	0.75
E674	-0.140	-0.069	0.85
D813	-0.149	-0.073	0.81

Figure 3.9. *Potential points taken in the middle region of background subtracted CVs for each CDH variant, reported in Figure 3.8-B, D and F (for 100 mM glucose), plotted against the Log($(i_L-i)/i$) (see Eq. 3.4). Data were fitted with linear fits. The table reports the values of intercept and slope extracted from the linear fitting for the four CDH variants (see Figure 3.4 for E522), and the number of exchanged electrons (n) calculated from the slopes.*

subtraction, for the remaining three CDH variants (CVs reported in Figure 3.8-B, D and F). All the three plots obey to the Nernst equation, as the points can be perfectly fitted with a linear fit, indicating that the electron transfer between the haem and the electrode is always very fast and reversible for all the CDH variants. Moreover, from the linear fitting we can extract the values of *E*' for the haem group (intercept) and the number of electrons exchanged during the oxidation (*n* = 0.059/slope). The table in Figure 3.9 reports these values: *E*' is always around -0.14/-0.15 V *vs.* SCE for all the variants, while *n* is about 0.8, which can be approximated to 1.

Going back to the discussion of Figure 3.8, we can see that the voltammograms for the variants D813 (Figure 3.8-E and F) were recorded using a larger potential range than for the other enzymes, going from -0.35 to 0.25 V *vs.* SCE instead of stopping at 0.1 V. This is because the variant D813, despite its position at the bottom in Figure 3.8, was the first one analysed in our work and, at the beginning, we were not sure about where to expect the catalytic current, so that we used a larger potential range. Thereafter, for the other variants we reduced the potential range of our CVs to the minimum necessary to see the catalytic current, thus going from -0.35 to 0.1 V *vs.* SCE. This was done also to reduce the time required for the experiments, since the scan rate used was 1 mV/s: this means that recording a full CV going from -0.35 to 0.1 V takes 900 s, which is 15 min. Given that we normally recorded two full cycles for each experiment (because it is always recommended to ignore the first cycle as it is necessary to reach a steady state condition [118]), it took 30 min for each single CV, while it would have taken longer using a larger potential range. In any case, we always take the value of the current at 0.0 V, so the changes in the potential range did not affect the results. Moreover, in some of the voltammograms of D813 (Figure 3.8-E and F) an unusual peak at about 0.12 V is visible: this could be due to an impurity present on the electrode or in the cell, which would have not been visible by stopping the CV at 0.1 V.

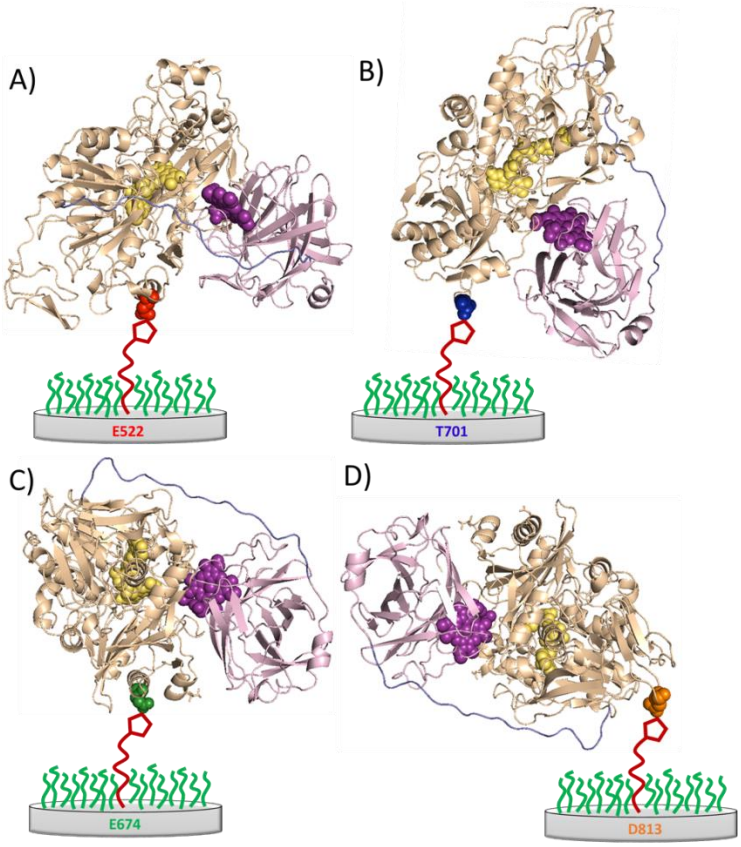

Figure 3.10. *Cartoon representations of the secondary structure of the four different MtCDH variants attached to the electrode surface in different orientations through the cysteine-maleimide bond. A) E522, B) T701, C) E674 and D) D813.*

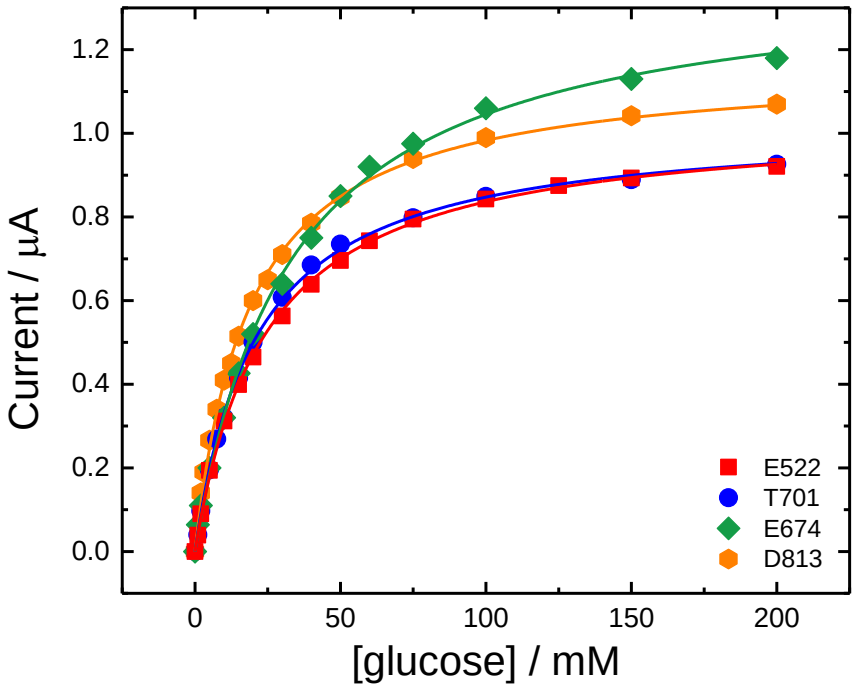

Figure 3.11. *Values of the current taken at 0.0 V in the CVs reported in Figure 3.5-B (for E522) and Figure 3.8-B, D and F (for the other three variants) plotted vs. glucose concentration. Data were fitted with Eq. 3.5 (lines).*

The limiting current taken at 0.0 V *vs.* SCE in the subtracted voltammograms was then plotted versus the sugar concentration obtaining plots attributable to the Michaelis-Menten behaviour for all the CDH variants (Figure 3.11). These plots are not exactly the same for all the variants, a part for E522 and T701 (red and blue plots in Figure 3.11) that are very similar. Fitting the data with the Michaelis-Menten equation (Eq. 3.5), we can obtain the values of i_{max}^{APP} and K_M^{APP} for the four enzymes (reported in Table 3.1): they are slightly different between the four variants, with the K_M^{APP} going from 19 to 32 mM and i_{max}^{APP} between 1.02 and 1.39 μA.

As we have said above, the difference in the plots of Figure 3.11 can be attributed to a different kinetics for the four CDH variants, probably due to a different orientation of the enzymes on the electrodes. Given that, the variants E674 and D813 would have the fastest kinetics and, therefore, the best orientations since they produced the highest current in Figure 3.11 (green and orange plots). Looking at the cartoon representations of the four CDH variants immobilised on the electrode surface (Figure 3.11), we would expect the variant D813 (D) to have a good orientation of the cytochrome domain since, with a small movement of the peptide linker, the haem group can be brought in close proximity to the electrode surface. This seems more difficult for the variant E674 (C), which produced the highest current, though.

We may think that a small distance between the haem and the electrode surface is not the only factor determining a high DET current. Another factor may be, for example, the interdomain electron transfer (IET) rate, which is affected by the distance between the two domains of CDH. It is possible that, for some orientations of the enzyme on the electrode, the two domains are closer to each other than for other orientations, maybe because of favourable electrostatic interactions between them or between one domain and the electrode surface. This would have a positive effect on the IET rate, therefore increasing the DET current. However, it is difficult at this point to distinguish between the effect due to the IET rate and the one of the DET distance. A deeper investigation of these two factors will be carried out in Chapter 4, where we will try to simulate the experimental voltammograms and analyse each single element that contributes to them.

Another factor affecting the current, as we can see from Eq. 3.8, is the amounts of electroactive enzyme, which depends on the absolute amount of immobilised enzyme. This can be different from one electrode to another since it is difficult to precisely control the amount of CNTs drop casted on each electrode and, consequently, their active area. For that, an analysis using a soluble mediator should help to estimate the total amount of CDH immobilised on each electrode. In fact, the mediator should react with all the enzyme molecules present at the electrode surface indistinctly from their orientation or distance from the surface. Moreover, the mediator we chose in this work, ferrocene, reacts directly with the FAD group, as we will prove later in Section 3.4. It follows that the haem group is excluded from the MET mechanism, and so is the interdomain electron transfer.

3.3 Mediated electron transfer of immobilised CDH

3.3.1 Mediated electron transfer of different CDH variants

To exclude the fact that the difference in the plots current/glucose concentration obtained for the four CDH variants was due to a different amount of CDH molecules immobilised on each GC/CNT electrode, the same electrodes previously tested for the DET were analysed also for the mediated electron transfer (MET). As we have already mentioned, a mediator should react with all the enzyme molecules on the surface of the electrode, transferring electrons between the enzyme and the electrode surface [119]. Mediated electron transfer can, therefore, be employed to relate the current observed for the DET of each variant to the real amount of CDH molecules on the electrode surface.

In our experiments, we used ferrocenecarboxylic acid (often simply named as ferrocene) as the soluble mediator. Many research groups employed ferrocene derivatives as electron acceptors for glucose oxidase, a well-known sugar oxidising enzyme [18,120,121]. With cellobiose dehydrogenase, instead, most of the research groups have been using as mediators quinone derivatives [86,122,123], cytochrome c [97] or osmium complexes [98,99]. In any case, the redox potential of mediators used for the electrocatalytic oxidation should be slightly more positive than the redox potential of the oxidising enzyme. In the

case of CDH, the redox potential was found at about -0.12 V *vs.* SCE (see Section 3.2.1), while the redox potential of ferrocenecarboxylic acid is around +0.3 V *vs.* SCE. Therefore, the ferrocene derivative seemed a good choice of mediator to be used with CDH. However, in the case of CDH, we should not look at the redox potential of the enzyme found by DET, since this is due to the haem group of CDH, as explained above. In fact, ferrocene should interact with the FAD group, as we will verify in Section 3.4, which has a redox potential even more negative than the haem group [75]. This does not preclude the possibility of using ferrocene as mediator for CDH, but it strengthens our choice.

Therefore, 1 mM ferrocenecarboxylic acid was added in the cell and cyclic voltammograms were recorded at CDH-modified GC/CNT electrodes, with increasing concentrations of glucose. The electrode potential was swept at 2 mV/s, instead of 1 mV/s as in the case of the DET, to make the experiments faster. Indeed, with this scan rate, going from 0.0 to 0.4 V and making two full cycles for each CV for the reason explained in the previous section, it took 800 s for each CV (about 13 min). In any case, for reasonably low scan rates in order to establish the steady state, the catalytic current is not affected by the scan rate but only by the rate of the catalytic reaction, as we will show in Chapter 4.

Figure 3.12 shows all the CVs recorded for the electrodes modified with the four different CDH variants: the original CVs are reported in Figure 3.12-A, C, E, G; while Figure 3.12-B, D, F, H reports the background subtracted CVs, which are the original CVs subtracted for the voltammogram recorded in the absence of substrate (black lines). At a first glance, we can see that the potential range used for the MET experiments is different from the one previously employed for the DET (see Figures 3.5 and 3.8): for the MET we used a more positive potential range going from 0.0 to 0.4 V *vs.* SCE. This is because the redox potential of the ferrocene is around 0.3 V *vs.* SCE, as we can observe looking at the CVs recorded in the absence of glucose (black lines in Figure 3.12-A, C, E, G). However, when we add glucose in the cell, we can note that the current starts increasing much earlier than in the absence of substrate: while for 0 mM glucose the increase starts around 0.22 V, with glucose it starts around 0.1 V *vs.* SCE.

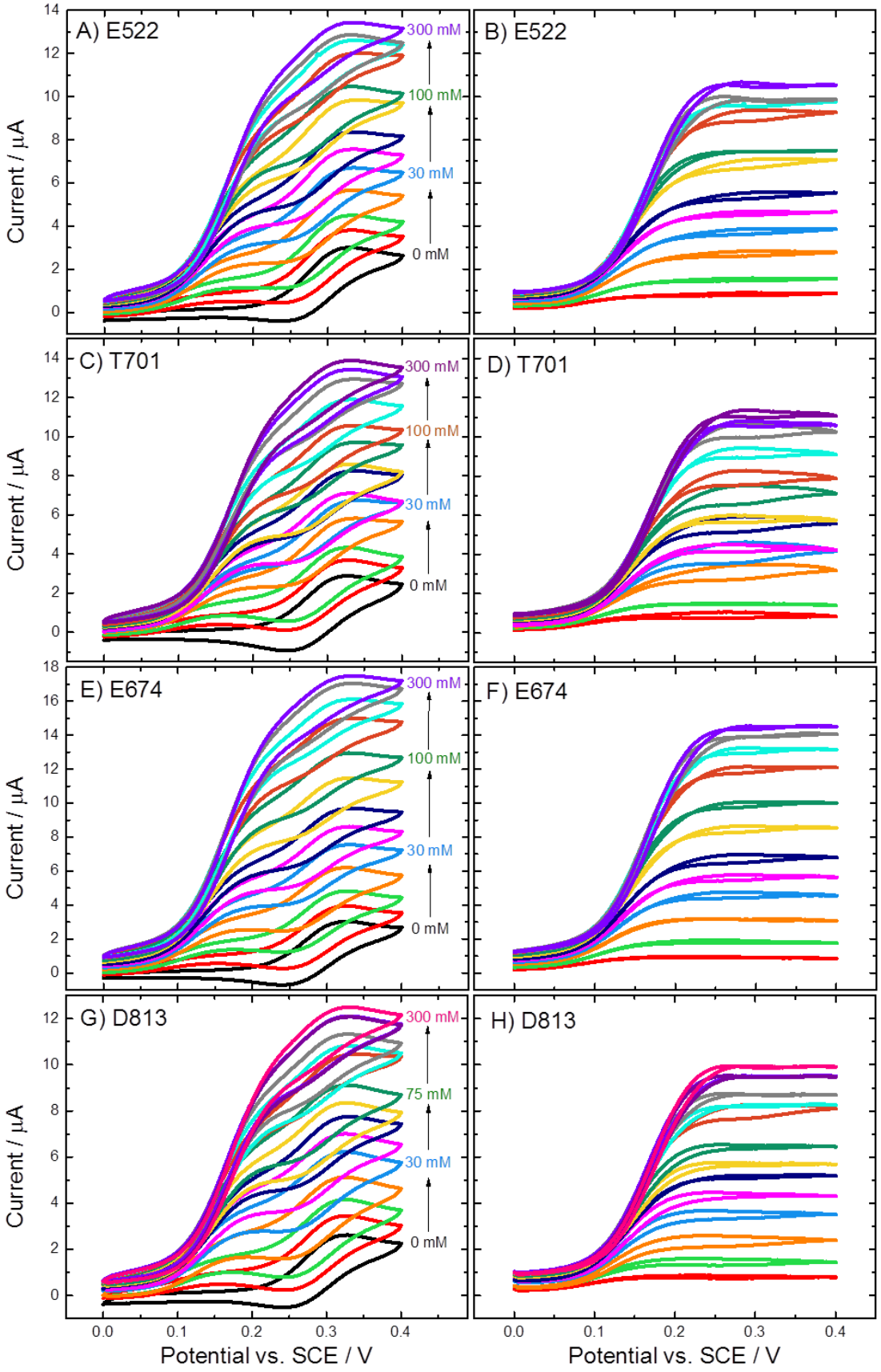

Figure 3.12. *(Left) Original and (right) background subtracted CVs recorded at (A-B) E522, (C-D) T701, (E-F) E674 and (G-H) D813-CDH modified GC/CNT electrodes, in argon-saturated 50 mM acetate buffer (pH 5.5), containing 30 mM $CaCl_2$, 1 mM ferrocene and different concentrations of D-glucose from 0 to 300 mM. The potential was swept at 2 mV/s.*

Moreover, in the original CVs (Figure 3.12-A, C, E, G) we can sometimes observe a kind of double-peak curve, with the first peak around 0.2 V and the second one around 0.3 V, which corresponds to the potential of the oxidation peak of the ferrocene. In fact, the last part of most of the voltammograms, between 0.2 and 0.4 V, looks like the CV of the ferrocene (black lines) but shifted up. After subtracting the background (Figure 3.12-B, D, F, H), the peaks due to the ferrocene disappear and the voltammograms look like sigmoidal curves with the catalytic current starting at about 0.1 V and reaching a limiting current around 0.20-0.25 V *vs.* SCE. The reason why the catalytic current starts at more cathodic potentials than the ferrocene redox potential, producing such unusual double-peak voltammograms, will be investigated in Section 3.3.3. For the moment we will analyse the MET current of the four different electrodes, since they all have the same behaviour in term of potential shift of the catalytic current.

Figure 3.13 shows the values of the current taken at 0.4 V *vs.* SCE in the voltammograms reported in Figure 3.12-B, D, F, H, plotted versus the glucose concentration from 0 to 200 mM. We can immediately note that three of the CDH variants (E522, T701 and D813) produced the same current, while E674 gave a slightly higher catalytic current. Since we assume that the mediator reacts with all the enzyme molecules present on the electrode surface, we can relate the intensity of the MET catalytic current to the total amount of CDH on the electrodes. Therefore, we can conclude that the amount of CDH molecules was basically the same for three of the four modified electrodes, while it was higher for the electrode modified with the variant E674. This was probably due to a higher surface area for this electrode, because of a greater amount of CNTs.

Comparing the DET and MET results of the four variants (Figures 3.11 and 3.13), we can conclude that the higher DET current of D813 (orange) is probably due to a better kinetics of this variant, since the MET current is the same as for the variants E522 and T701 (red and blue). On the other hand, the high DET current of E674 (green) can be attributed to a higher amount of enzyme immobilised on the electrode, given that also its MET current is higher than for the other three variants. However, for this discussion, we would need to know which one is the rate limiting step in each case, since it may be different for the DET and MET. This will be investigated in Chapter 4, where we will explain in more details the

differences observed in the current intensities of the four CDH variants. For the moment, we will discuss the parameters extracted by fitting the experimental data with the Michaelis-Menten equation, making a comparison between DET and MET.

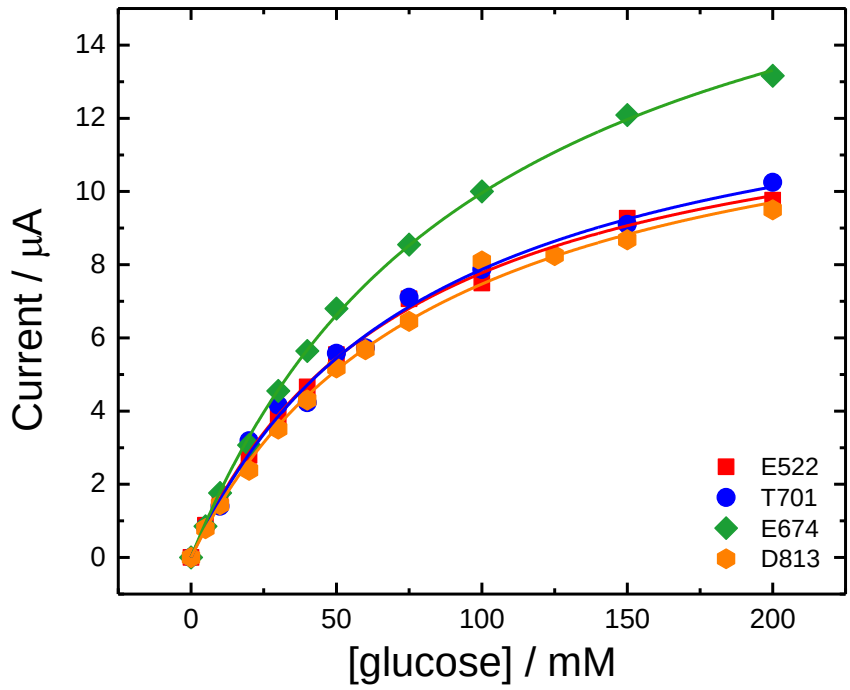

Figure 3.13. *Values of the current taken at 0.4 V in the CVs reported in Figure 3.12-B, D, F, H (for the four CDH variants) plotted vs. glucose concentration. Data were fitted with Eq. 3.5 (lines).*

3.3.2 Comparison between DET and MET results

Fitting the data in Figures 3.11 and 3.13 with the Michaelis-Menten equation (Eq. 3.5), we can extract the values of i_{max}^{APP} and K_M^{APP} for the four different CDH variants, for the DET and MET experiments (Table 3.1). We have already discussed the values of i_{max}^{APP} for the four enzymes here above, since this parameter is clearly visible in the graphs. However, we can note that, in general, i_{max}^{APP} extracted from the DET data is much lower than the one extracted from the MET data. This means that the mediated electron transfer is probably faster or that, in this case, the current due to the glucose oxidation is not limited by other factors. In the DET case, instead, the current is probably limited by some steps that are not present in the MET mechanism, such as the interdomain electron transfer or the reaction between the haem and the electrode. This point

will be further investigated in Chapter 4, where we will try to understand the impact of each reaction step on the current.

Concerning K_M^{APP}, in Table 3.1 we can note that, for the DET, all the CDH variants have similar values close to 20 mM, except for E674 that presents a value of 33 mM. The same can be observed in the case of the MET: all the variants have values close to 80 mM, except for E674 that presents a higher value of K_M^{APP}, equal to 101 mM. We do not have any reason at the moment to explain this, or the fact that the K_M^{APP} extracted from the DET data is always much lower than the one extracted by fitting the MET data. In theory, the Michaelis-Menten constant, K_M, measures the affinity between the enzyme and the substrate: therefore, it should be the same for the four CDH variants given that they are the same enzyme, and the only thing that changes is one amino acid residue at the surface of the flavin domain. Given that, K_M should be the same also for the DET and MET. However, the parameter extracted by the fitting is an apparent K_M, which may depend also on different factors other than the affinity between the enzyme and the substrate. As we have already mentioned in Section 3.2.3, K_M^{APP} can also depend on the experimental conditions used to find it: this will be further investigated in Chapter 4, with a more detailed discussion.

In the next section, we will examine the reason why the MET catalytic current starts at more cathodic potentials than the ferrocene redox potential, as we have already observed in the voltammograms in Figure 3.12.

Table 3.1. *Values of K_M^{APP} and i_{max}^{APP} for the four CDH variants extracted by fitting the DET and MET data in Figures 3.11 and 3.13, respectively, with Eq. 3.5.*

CDH variant	DET		MET	
	i_{max}^{APP} (µA)	K_M^{APP} (mM)	i_{max}^{APP} (µA)	K_M^{APP} (mM)
E522	1.037 ± 0.007	24.0 ± 0.5	13.5 ± 0.3	75 ± 4
T701	1.025 ± 0.007	21.0 ± 0.4	14.2 ± 0.6	80 ± 7
E674	1.39 ± 0.02	33 ± 1	20.1 ± 0.3	101 ± 3
D813	1.17 ± 0.01	18.7 ± 0.5	13.8 ± 0.5	85 ± 7

3.3.3 Potential shift of MET catalytic current

As we have observed in Section 3.3.1, the MET catalytic current starts increasing at more cathodic potentials than the ferrocene redox potential. We thought that this unusual behaviour might be related to the concentration of ferrocene in solution. To investigate this, we tried to record some cyclic voltammograms at a E522-CDH modified GC/CNT electrode, keeping the substrate concentration constant (50 mM) and increasing the concentration of mediator in solution going from 0 to 200 µM (we had already the result for 1000 µM, see Figure 3.12-A and B). Figure 3.14 shows the results: the original CVs are reported in Figure 3.14-A and the CVs background subtracted (for the CV recorded in the absence of ferrocene, black line) are reported in Figure 3.14-B. It is clear that, increasing the concentration of mediator in solution, the catalytic current shifts at more cathodic potentials, going from about 0.3 V with 1 µM ferrocene to about 0.15 V with 200 µM ferrocene. If we compare these results with the CVs recorded with ferrocene in solution but in the absence of substrate (black lines in Figure 3.12), we can note that only for the smallest ferrocene concentration, 1 µM, the potential of the catalytic current is basically the same as the ferrocene oxidation potential (about 0.3 V *vs.* SCE for the ferrocenecarboxylic acid). In addition, from these results we found that even a very small concentration of ferrocene, 1 µM, is able to react with CDH producing a catalytic current. This must be due to an

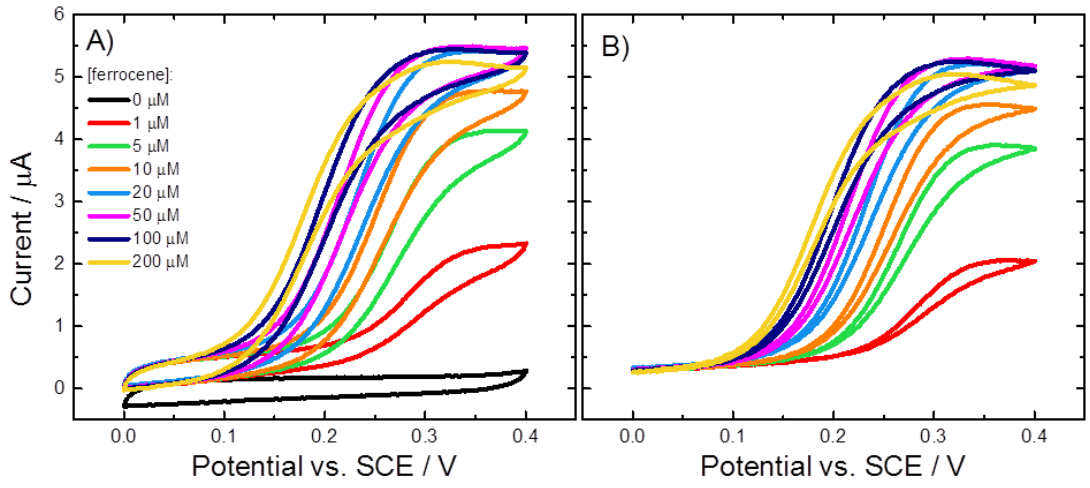

Figure 3.14. *(A) Original and (B) background subtracted cyclic voltammograms for a E522-CDH modified GC/CNT electrode in argon-saturated 50 mM acetate buffer (pH 5.5), containing 30 mM $CaCl_2$, 50 mM glucose and increasing concentrations of ferrocenecarboxylic acid. The potential was swept at 2 mV/s.*

extremely high rate constant for the CDH/ferrocene reaction, which should be responsible also for the potential shift of the MET catalytic current.

For the moment, we will not assign a value to the CDH/ferrocene rate constant, as this will be determined in Chapter 4, Section 4.2.2. Here, we want just to discuss its effect on the catalytic current, in particular its shift towards cathodic potentials when the concentration of ferrocene is increased. This happens because the reaction of CDH at the electrode surface is actually catalysed by the oxidised form of ferrocene, the ferrocenium ion. As we can see in Scheme 3.4, the ferrocenium oxidises the enzyme and, in turn, is reduced to ferrocene. Since the rate constant for such reaction is very high, it follows that an extremely small concentration of ferrocenium ion will be enough to catalyse the reaction. The concentration of ferrocenium ion, $[Fc^+]$, depends on the concentration of ferrocene, [Fc], and the applied potential, E, as described by the Nernst equation (at 298 K):

$$E = E' + \frac{0.059}{n} \mathrm{Log}\left(\frac{[Fc^+]}{[Fc]}\right) \qquad \text{(Eq. 3.9)}$$

where E' is the formal potential of the redox couple Fc^+/Fc in our experimental conditions. By analysing the reduction and oxidation peaks of the CVs recorded with 1 mM ferrocene, in the absence of glucose (black lines in Figure 3.12), E' was found at 0.28 V *vs.* SCE. From Eq. 3.9 we can deduce that, at a given potential, increasing [Fc], $[Fc^+]$ will increase accordingly in order to maintain the equilibrium. We can rearrange Eq. 3.9 as follows in order to find $[Fc^+]$:

$$[Fc^+] = [Fc] \cdot \exp\left\{\frac{n}{0.059}(E - E')\right\} \qquad \text{(Eq. 3.10)}$$

We have previously said that a very small concentration of ferrocenium is enough to produce the catalytic current: such concentration can be called $[Fc^+]_{cat}$ and will be always the same independently of the ferrocene added in solution. Therefore, for increasing [Fc], we need to decrease E in order to maintain constant $[Fc^+]_{cat}$. It follows that, increasing the concentration of ferrocene, the catalytic current will start at "smaller", or more negative, potentials as we found experimentally.

To prove our hypothesis and find $[Fc^+]_{cat}$, we determined the half-wave potential ($E_{1/2}$) for each voltammogram of Figure 3.14 using the Nernst equation in the form of Eq. 3.4. The potential points used for the calculation of $E_{1/2}$ for each concentration of ferrocene are shown in Figure 3.15-A: from 1 to 200 µM ferrocene we used the CVs reported in Figure 3.14-B, while for 1 mM ferrocene the CV previously recorded with 50 mM glucose (dark blue line in Figure 3.12-B) was used. Each set of data of potential *vs.* Log($(i_L\text{-}i)/i$) was fitted with a linear fit, whose intercept is the half-wave potential of each voltammogram and slope is equal to $0.059/n$ (see Eq. 3.4). Since the average value between all the slopes of the linear fits in Figure 3.15-A was 0.067, it follows that n is equal to 0.88, which can be approximated to 1. In fact, this is the number of electrons that ferrocene exchanges with the electrode during its redox process. The intercepts of each linear fit ($E_{1/2}$) were plotted versus the concentration of ferrocene (Figure 3.15-B) and the data were fitted using the following equation, which was rearranged from Eq. 3.9:

$$E = E' + \frac{0.059}{n}\text{Log}[Fc^+]_{cat} - \frac{0.059}{n}\text{Log}[Fc] \qquad \text{(Eq. 3.11)}$$

and can be written as:

$$E = A - B \cdot \text{Log}[Fc] \qquad \text{(Eq. 3.12)}$$

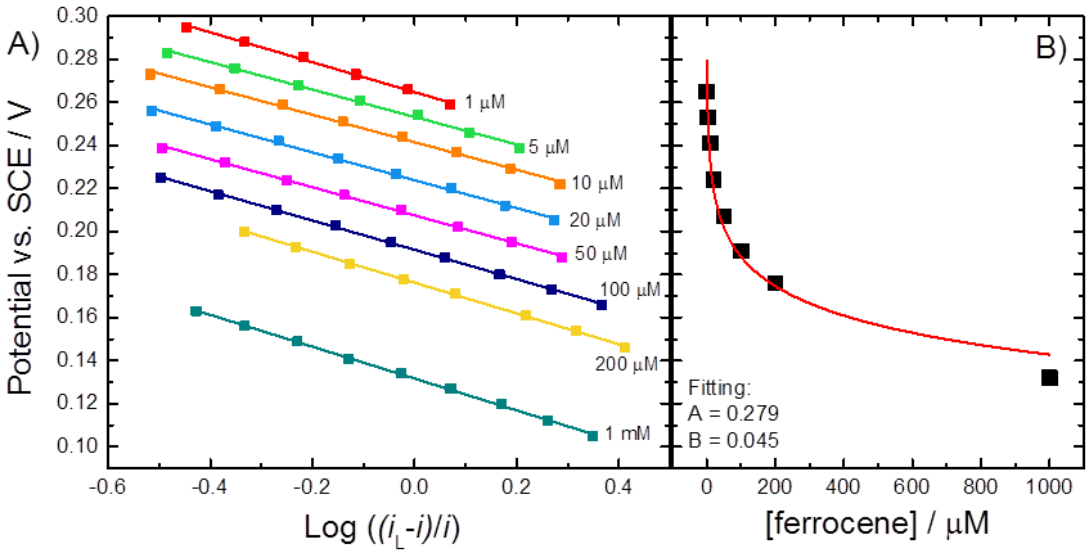

Figure 3.15. *A) Plots of potential vs. Log($(i_L\text{-}i)/i$) (Eq. 3.4) for some points taken in the middle part of the CVs of Figure 3.14-B (for ferrocene concentrations from 1 to 200 µM) and Figure 3.12-B (for 1 mM ferrocene, dark blue line: 50 mM glucose). Lines: linear fitting. B) Plot of half-wave potentials extracted from the linear fitting in Figure A vs. ferrocene concentration. Red line: logarithmic fitting using Eq. 3.12.*

From the fitting parameter A we can calculate the concentration of the ferrocenium ion required for the catalytic current, given that E' for the couple Fc^+/Fc was found to be 0.28 V and n is equal to 1:

$$A = E' + \frac{0.059}{n}\mathrm{Log}[\mathrm{Fc}^+]_{\mathrm{cat}} \quad \Longrightarrow \quad [\mathrm{Fc}^+]_{\mathrm{cat}} = \exp\left\{\frac{n}{0.059}(A - E')\right\} \qquad \text{(Eq. 3.13)}$$

Since from the fitting of the data in Figure 3.15-B it results that A is 0.279 V, $[Fc^+]_{cat}$ was found to be 0.98 μM. We can conclude that a concentration of 1 μM ferrocenecarboxylic acid is enough to catalyse the CDH electrodic reaction, as experimentally found. At this concentration, the catalytic current will start roughly at the same potential as the oxidation potential of Fc^+/Fc, since most of the ferrocene molecules in solution need to be in the oxidised form to reach the concentration of Fc^+ required for the catalysis. For higher ferrocene concentrations, the catalytic current will start earlier (at more cathodic potentials), as we found experimentally.

3.4 Mechanisms of the direct and mediated electron transfer

Now we have shown the DET and MET of four different CDH variants immobilised at GC/CNT electrodes, we would like to investigate in more details the pathways of the two electron transfer mechanisms. For the DET, the electron pathway should go from the substrate to the FAD group, which then transfers the electrons to the haem group in a step called interdomain electron transfer (IET), and finally the electrons are transferred from the haem to the electrode surface (see Scheme 3.4). We have already proved this mechanism through the non-catalytic voltammetry at two different pH, in Section 3.2.1, and the study of the shape of a catalytic voltammogram, in Section 3.2.2, both indicating that the haem group is responsible for the DET at the electrode. About the MET mechanism, we have only mentioned in Section 3.3.1 that the ferrocene should react directly with FAD, therefore excluding the haem group from the MET pathway (see Scheme 3.4). This finds confirmation in the literature, in fact Kracher *et al.* report that the current produced by ferrocene does not depend on IET, but this one-electron acceptor is reduced by the FAD directly [78]. However, we performed some other experiments to confirm the mechanisms shown in

Scheme 3.4 for the DET and MET. Firstly, we studied the effect of a divalent cation, such as Ca^{2+}, on the DET and MET current. Finally, we used another enzyme, papain, able to break the peptide linker connecting the two domains of CDH, analysing the DET and MET current before and after the papain breakage.

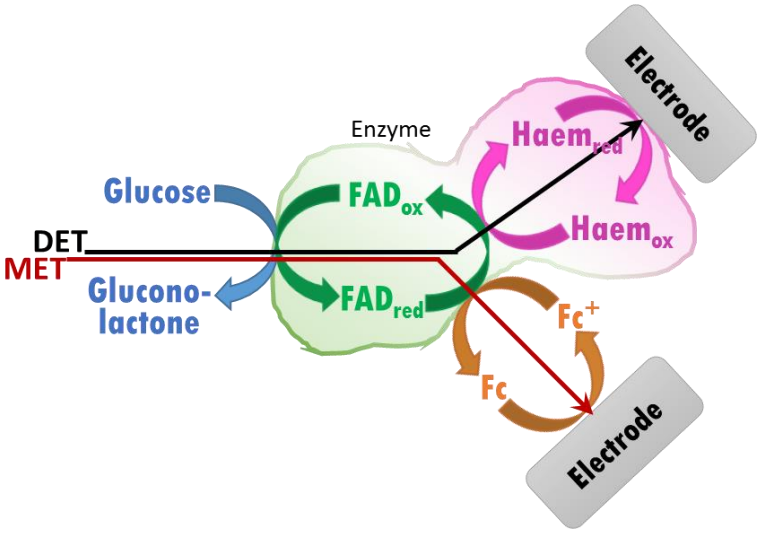

Scheme 3.4. *Schematic representation of the DET (black line) and MET (red line) pathways: CDH is represented by the green/pink shape with the two active centres (FAD and haem) inside it.*

3.4.1 Effect of calcium chloride on the DET and MET

Work by Ludwig *et al.* [76-78,122] revealed that the presence of calcium, as well as other divalent alkali earth metal cations, leads to an increase in the catalytic current generated by *Mt*CDH. Such an increase is due to the adoption of a closer conformation for CDH in the presence of divalent cations, which exert a bridging effect between the two enzymatic domains. This effect is more significant at neutral pH: in fact, in this condition, the amino acids located in the interfacial region between the haem and flavin domain are mainly negatively charged, hence producing an electrostatic repulsion between them. Such repulsion causes the two domains to move apart from each other, thanks also to the great flexibility of the peptide linker connecting them. As a consequence, the interdomain electron transfer (IET) will be slower, also having a negative effect on the DET (see Figure 3.16). As a result, neutral pH is not the optimal condition for the DET of *Mt*CDH, which produces higher current between pH 5.0 and 5.5

[73,74,123], even though it was reported that the optimum pH for the substrate/FAD reaction is pH 8 [78].

This electrostatic repulsion between the two CDH domains can be neutralised by using a more acidic buffer solution, with pH between 4.5 and 5.5, or by adding divalent cations in solution (see Figure 3.16). In these conditions, *Mt*CDH will adopt a closer conformation, so that the IET rate will increase, also having a positive effect on the DET. Given that, the addition of Ca^{2+} in solution should increase the DET current of CDH-modified electrodes. However, this should not have any effect on the MET current: in fact, if the ferrocene interacts directly with FAD excluding the haem group from the MET pathway (see Scheme 3.4), changes in the IET rate would not have any influence on the MET.

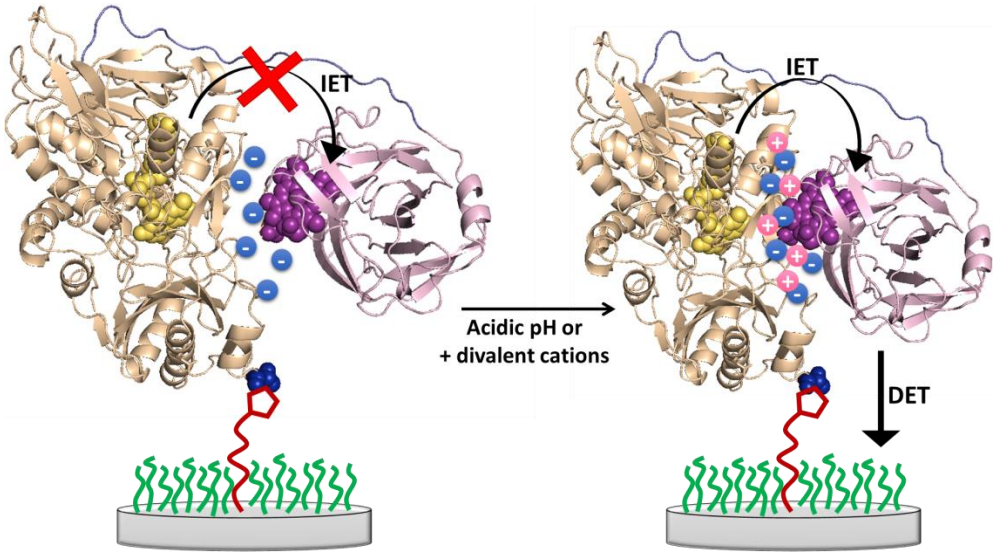

Figure 3.16. *Schematic representation of the effect of acidic pH or addition of divalent cations: before the two CDH domains are far from each other because of electrostatic repulsion due to the negatively charged amino acids; then CDH adopts a closer conformation thanks to the neutralization of electrostatic repulsion.*

In order to study the effect of divalent cations on the DET and MET current, and therefore prove their mechanisms, CDH-modified GC/CNT electrodes were tested at neutral and acidic pH at increasing concentrations of calcium chloride, in the presence of glucose in solution. Figure 3.17 shows the cyclic voltammograms recorded at GC/CNT electrodes modified with the variant E522: A and B report the DET experiments, C and D the MET experiments. In addition, the CVs in A and C were measured in acetate buffer at pH 5.5, the ones in B and D in Tris buffer at pH 7.4. We cannot, and it is not our intention to, compare the four sets of

voltammograms with each other, because they have been recorded using different electrodes (modified with the same CDH variant, though), at different times, so that the amount of immobilised enzyme was most probably different. Moreover, the two experiments for the MET (C and D) were performed using different concentrations of mediator: 1 mM for C and 0.2 mM for D. As a result, the shapes of the voltammograms are different. Finally, we cannot compare the current intensity between experiments carried out at two different pH since, as we have already said, the rate of the substrate/FAD reaction changes with the pH, reaching its maximum around pH 8 [78]. Therefore, especially for the MET that depends only on the substrate/FAD and FAD/ferrocene reactions (with the latter one being very fast and, most probably, independent of the pH), the current intensity would have been different even using the same electrode. Nevertheless,

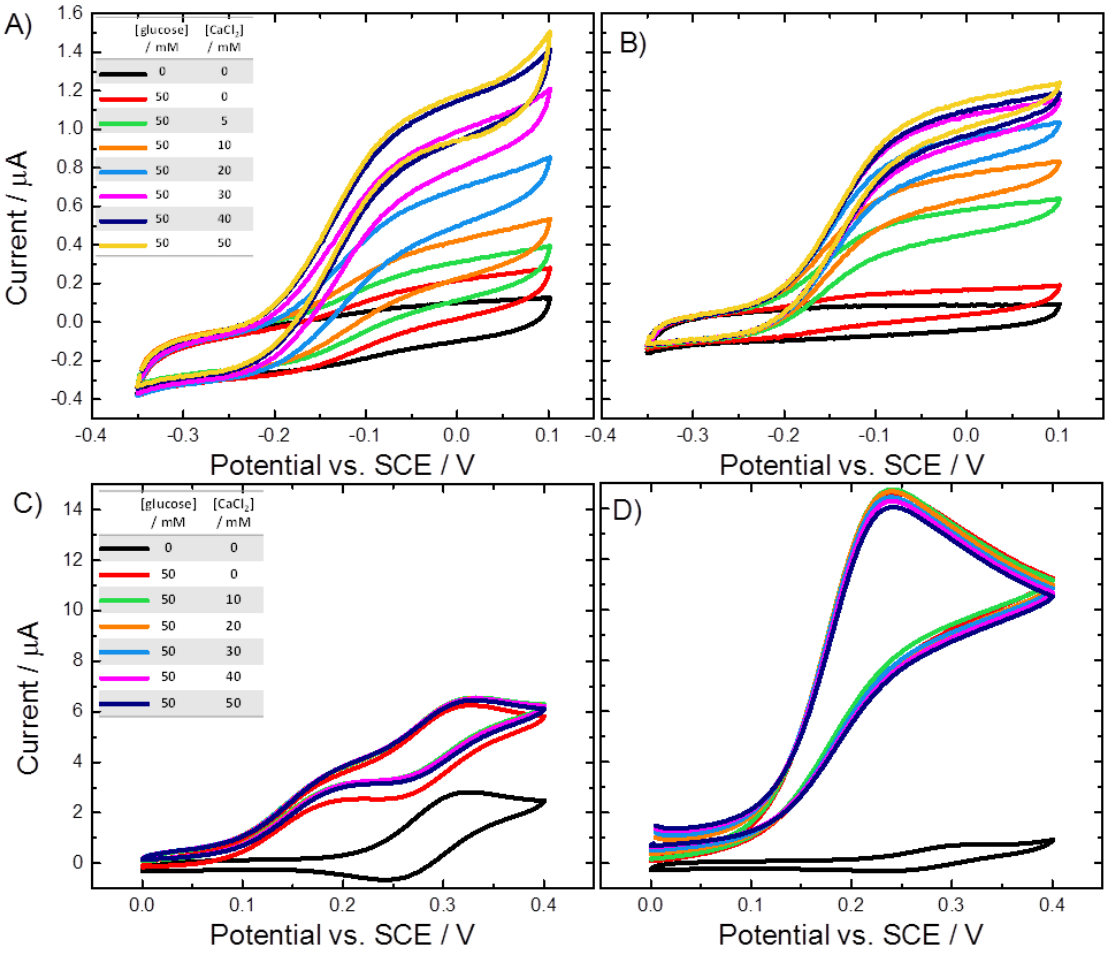

Figure 3.17. *Cyclic voltammograms for the (A-B) DET and (C-D) MET of E522-CDH modified GC/CNT electrodes recorded in argon-saturated (A-C) 50 mM acetate buffer pH 5.5 and (B-D) 50 mM Tris buffer pH 7.4, at increasing concentrations of glucose and $CaCl_2$ (as shown in the tables inside). CVs for the MET were recorded with (C) 1 mM and (D) 0.2 mM ferrocene. The potential was swept at (A-B) 1 mV/s from -0.35 to 0.1 V, and (C-D) 2 mV/s from 0.0 to 0.4 V vs. SCE.*

it is significant to note that the MET current measured at pH 7.4 is much higher than the one for pH 5.5 (compare Figure 3.17-C and D). Such a big difference cannot be attributed only to a different amount of enzyme on the electrodes, but it is due also to the higher activity of FAD at neutral pH.

Even if we cannot directly compare the current intensity between the four experiments (reported in Figure 3.18-A), it is possible, however, to make a comparison between the percentage current increases (Figure 3.18-B). These

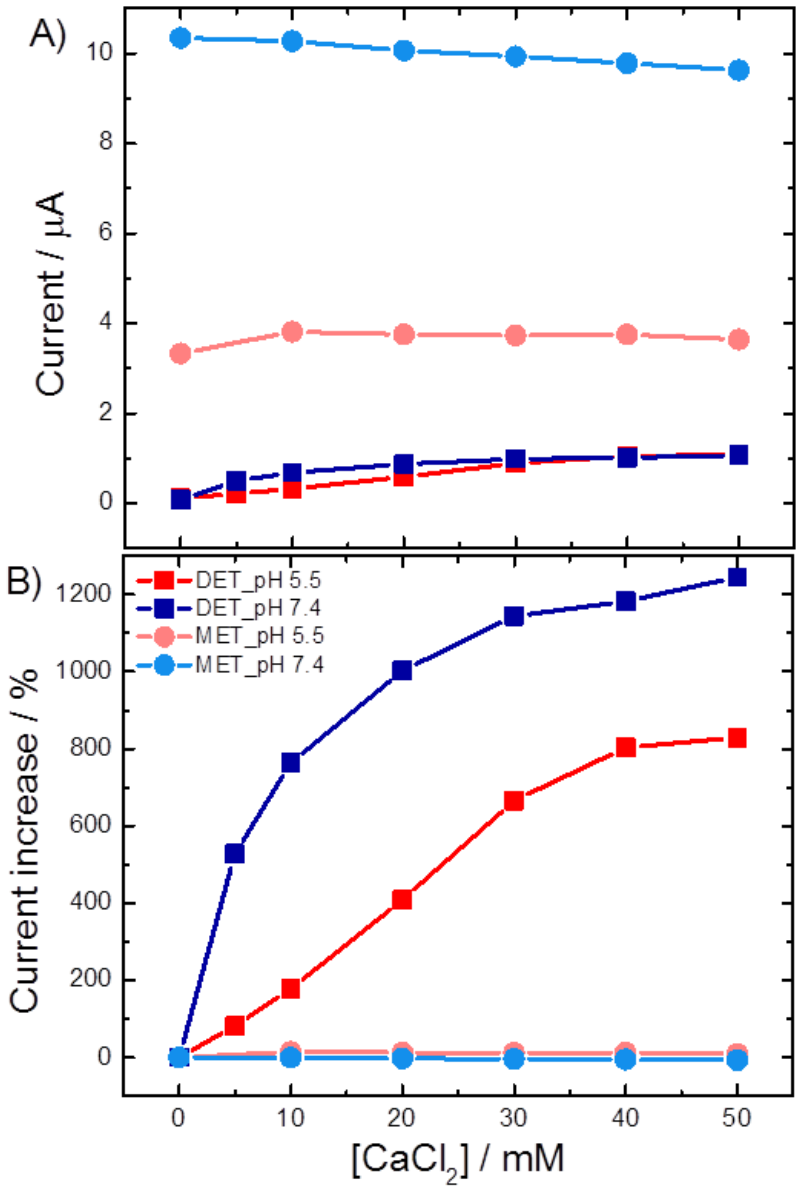

Figure 3.18. *(A) Current and (B) percentages of current increase for the DET (squares) and MET (circles) of E522-CDH modified GC/CNT electrodes, measured at pH 5.5 (red) and pH 7.4 (blue). The data of the current were taken from the CVs of Figure 3.17, at 0.0 V for the DET and 0.4 V for the MET, after background subtraction. The percentages of current increase were calculated for each data set in relation to its current value for 0 mM* $CaCl_2$.

were calculated, for each set of data, in relation to the current for 0 mM $CaCl_2$ (red CVs in Figure 3.17), after subtraction for the background current (black CVs). Looking at Figure 3.18, it is immediately clear that, when the mediator is present in solution (circles), no significant effect upon addition of $CaCl_2$ is visible at any pH (see also CVs in Figure 3.17-C and D). This proves that the ferrocene interacts directly with the FAD group, while the haem domain is excluded from this process. In fact, the presence of divalent cations does not affect the MET catalytic current, meaning that IET is not occurring, or is not relevant to this process.

On the other hand, in the absence of mediator (squares in Figure 3.18-B), Ca^{2+} plays a crucial role in the catalytic process greatly increasing the catalytic current. As expected, this effect is greater at neutral pH (blue squares) than at acidic pH (red squares): the addition of 5 mM $CaCl_2$ increases the current of the 500 % at pH 7.4 and "only" by 80 % at pH 5.5. Further increasing the concentration of calcium chloride up to 50 mM leads to a gain in the percentage of current increase up to 1200 % at neutral pH and about 800 % at acidic pH. This proves that the DET pathway is consistent with the one shown in Scheme 3.4, with the electrons passing from the FAD domain to the haem and from the haem to the electrode surface. In fact, the addition of divalent cations, exerting a bridging effect between the two domains, increases the IET rate and, consequently, the DET catalytic current. Moreover, this effect is more significant at neutral pH, because at acidic pH the electrostatic repulsion between the FAD and haem domain is already less important.

All the experiments carried out in this work with CDH-modified electrodes were performed in buffer solutions containing 30 mM $CaCl_2$, unless otherwise stated. This concentration of calcium, in fact, was found enough to have a sufficiently high DET current, both at pH 5.5 and 7.4. Experiments for the MET were also carried out in the same buffer solutions containing $CaCl_2$, even though it is not necessary, in order to use the same conditions as for the DET (same buffer concentration, same ionic strength).

3.4.2 Effect of calcium chloride on two different CDH variants

Now we have verified the mechanisms of the DET and MET thanks to the effect of divalent cations, we wanted to see if this effect is different for different CDH variants. For that, we have performed the same experiment, only for the DET at pH 5.5, using an electrode modified with another variant, namely T701. The MET is not reported here since it produced the same flat response already observed with the variants E522 (Figure 3.18-B), as expected.

Figure 3.19-A shows the cyclic voltammograms recorded at a T701-CDH modified electrode, at pH 5.5, for increasing concentrations of calcium chloride. Also in this case the DET current increases when Ca^{2+} is added in solution, however we can note some differences with the variant E522 by analysing the percentages of current increase (Figure 3.19-B). Both the enzymes have the same trend until 10 mM $CaCl_2$ with a current increase of the 160-180 %. Further additions of $CaCl_2$ until 50 mM increase the current up to the 800 % for E522 (red) and "only" by 200 % for T701 (blue). This may be due to different distances between the flavin and haem domains of the two variants in the absence of divalent cations, probably due to the different orientations of the two enzymes on the electrode.

We have seen in Section 3.2.5 that the electrodes modified with E522 and T701, with probably the same amount of immobilised enzyme, produced the same DET current in the presence of 30 mM $CaCl_2$ (see Figure 3.11). Therefore, we can suppose that, with a sufficiently high amount of divalent cations, the two CDH variants present their two domains at the same distance between each other, thus producing the same DET current (in this case we are considering the IET as the rate limiting step). However, for smaller or zero concentrations of Ca^{2+}, the two domains of E522 are probably farther apart than for T701. This may be due to different electrostatic interactions or because the variant E522 better accommodates on the electrode surface with the two domains farther apart from each other, when they are freer to move in the absence of Ca^{2+}. Therefore, the addition of $CaCl_2$ has a greater effect on E522, which probably needs a higher concentration of divalent cations to bring the two domains close to each other. On the other hand, a smaller concentration of calcium (10 mM) is enough to place

the domains of T701 in the closer conformation, so that further additions of $CaCl_2$ do not increase the current.

Going on with the verification of the DET and MET mechanisms, the last experiment was performed using another enzyme, namely papain, capable of breaking the peptide linker connecting the two domains of CDH, and analysing the DET and MET current before and after the papain breakage.

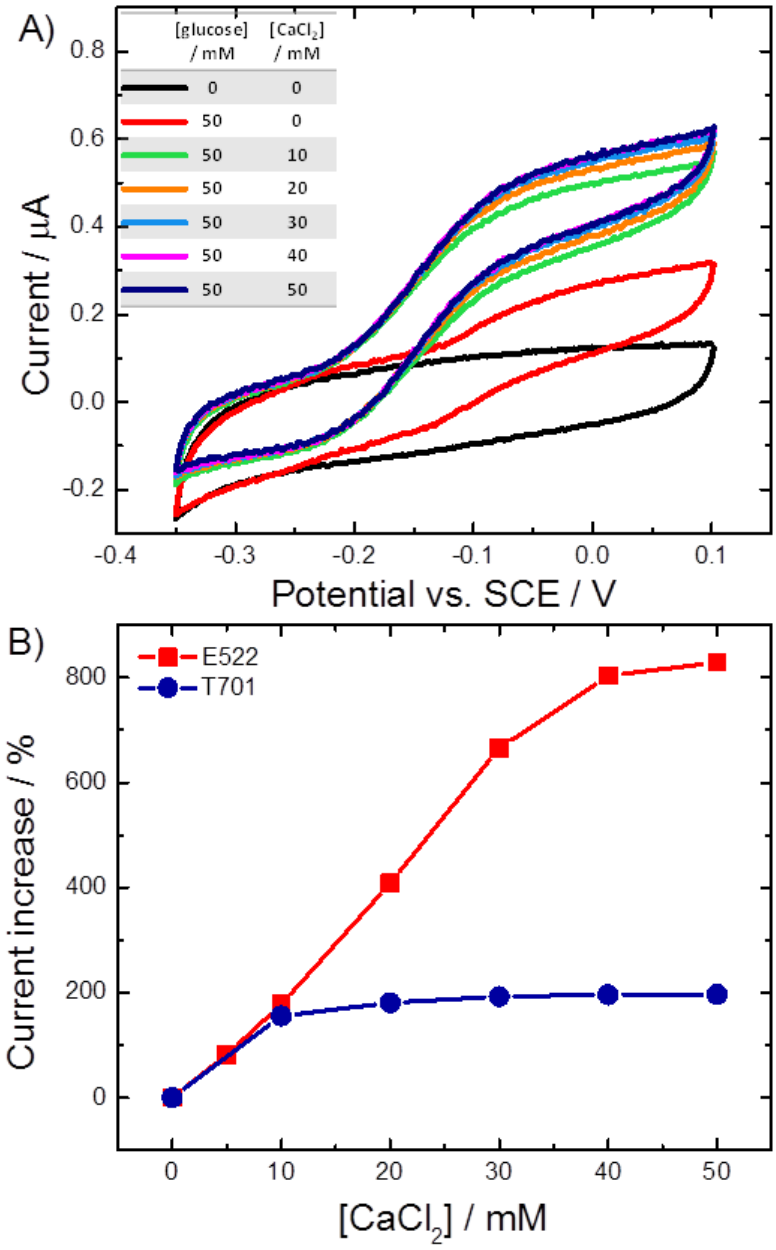

Figure 3.19. *A) Cyclic voltammograms for the DET of a T701-CDH modified GC/CNT electrode recorded in argon-saturated 50 mM acetate buffer (pH 5.5), at increasing concentrations of glucose and $CaCl_2$ (as shown in the table inside). The potential was swept at 1 mV/s. B) Percentages of current increase for the DET of E522 (red) and T701 (blue) modified GC/CNT electrodes, measured at pH 5.5. Data were calculated for each set (CVs in Figure 3.17-A for E522 and CVs here above for T701) in relation to its current value for 0 mM $CaCl_2$.*

3.4.3 Control experiment with papain

In this experiment we used a protease enzyme, papain, to cut the peptide linker connecting the flavin and haem domains of CDH. Papain is an enzyme showing extensive proteolytic activity towards proteins, short-chain peptides, amino acid esters and amide bonds [124]. With CDH, in particular, it is used to separate the two enzymatic domains as the preferential site of cleavage is, indeed, the peptide linker between them [107,125,126]. Therefore, after treatment with papain, we would expect the loss of the DET activity as a consequence of the loss of the haem domain from the enzyme (see Figure 3.20). On the other hand, the MET activity should not be affected as the flavin domain would be still active and attached at the electrode surface, given that the cysteine residue responsible for the immobilization is located on the flavin domain.

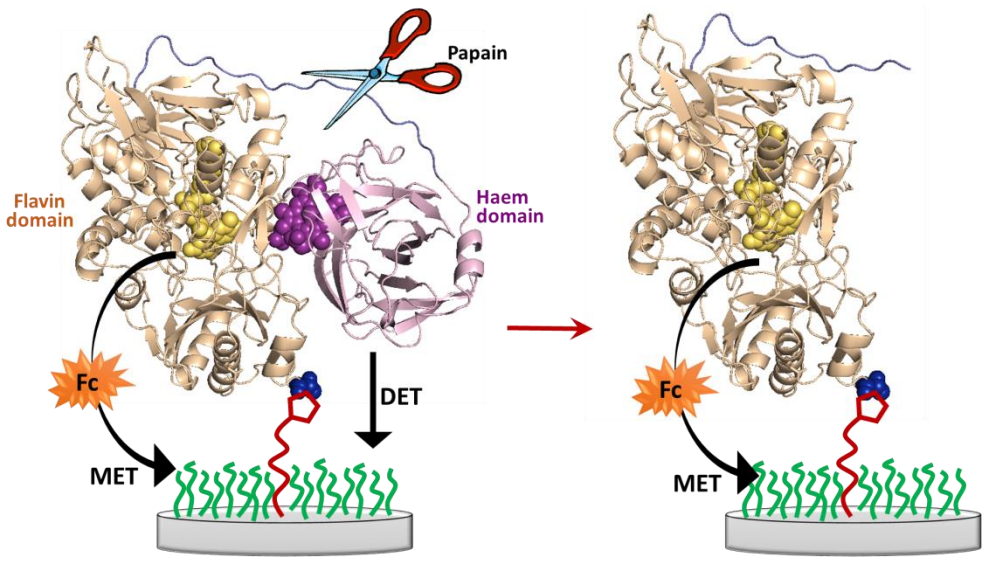

Figure 3.20. *Schematic representation of the action of papain (scissor) toward CDH immobilised at the electrode surface through maleimide/cysteine bond.*

The experiment was carried out with a CDH-modified GC/CNT electrode that was prepared about two months before, stored in the fridge at 4 °C and tested at regular times during this period (see Figure 3.23 for the stability over the time). For the experiment with papain, the electrode was placed in the electrochemical cell filled with 10 mL of 50 mM acetate buffer (pH 5.5), containing 30 mM $CaCl_2$. The cell was deoxygenated by bubbling gas argon before and during the experiment: this was useful also to mix the solution in the cell during the chronoamperometry. A constant potential of +0.2 V *vs.* SCE was applied at the

working electrode for about 10 hours, recording the current every 20 s. The potential for the chronoamperometry was chosen according to the typical cyclic voltammograms for CDH-modified electrodes, since at +0.2 V *vs.* SCE the DET limiting current is fully reached.

Figure 3.21 shows the chronoamperogram recorded during the experiment. Starting with only the acetate/$CaCl_2$ buffer, after 16 min 50 mM glucose was added in the cell showing an increase in the current that reached about 0.37 μA (very similar to the value that the electrode showed during its last 50 days, see Figure 3.23). When the current was stable, at about 33 min, 0.1 mg/mL papain was added in the cell and the current started to decrease slowly. After some time, when the decrease seemed to slow down, other aliquots of papain were added: 0.1 mg/mL after 200 min and 0.3 mg/mL after 385 min, making the final concentration of papain in the cell of 0.5 mg/mL. From the amperogram, we can see that after 10 hours the current decreased of the 50 %. However, the electrode was left in the cell with the papain, under light argon bubbling, overnight (roughly for another 10 hours).

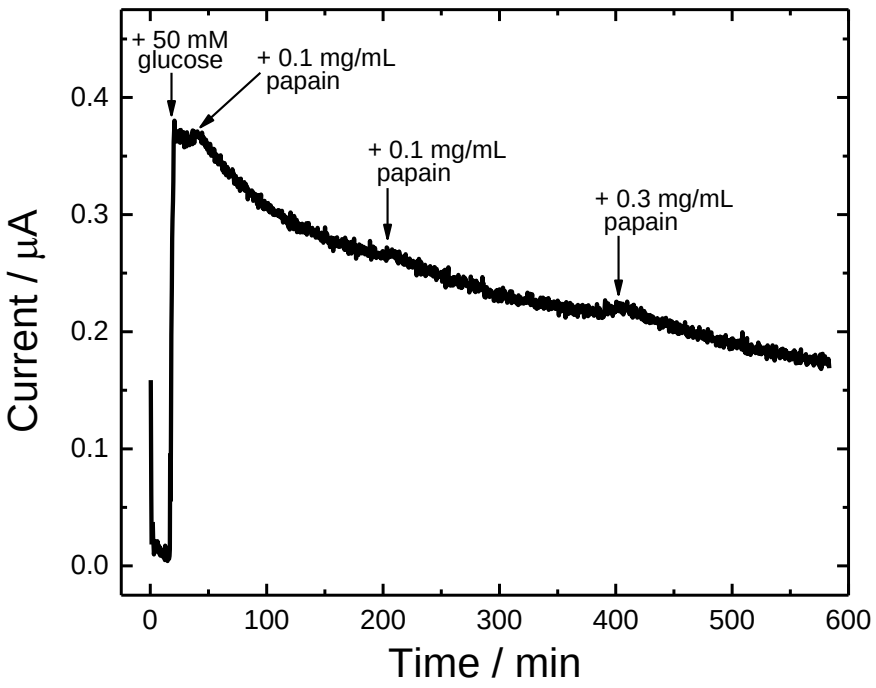

Figure 3.21. *Chronoamperogram recorded at a E522-CDH modified GC/CNT electrode in argon-saturated 50 mM acetate buffer (pH 5.5), containing 30 mM $CaCl_2$. The electrode potential was held at +0.2 V vs. SCE for about 10 h. During this time, the cell was under light argon bubbling and several additions were carried out: 50 mM glucose at 16 min, 0.1 mg/mL papain at 33 min, other 0.1 mg/mL papain at 200 min and 0.3 mg/mL papain at 385 min.*

Cyclic voltammograms for the DET and MET were recorded before and after the papain experiment (Figure 3.22-A and B). The voltammetry was performed using a wide potential range in order to include both the DET and MET currents in the same CV: the electrode potential was swept from -0.35 V to 0.4 V *vs.* SCE, using a scan rate of 2 mV/s. After recording the background in the buffer (black line), 50 mM glucose was added in the cell to measure the DET current (blue line). In this CV we can observe the catalytic current starting at about -0.2 V and reaching a kind of plateau after -0.1 V *vs.* SCE. Then, 20 µM ferrocene was added to measure also the MET current (red line): in this latter CV we can see the DET current in the same position as before, and the MET catalytic current starting at about 0.15 V and reaching a plateau at about 0.3 V. The CVs have been background subtracted to better visualise the DET and MET current (Figure 3.22-C and D): in these graphs, the background is represented by a black dashed line.

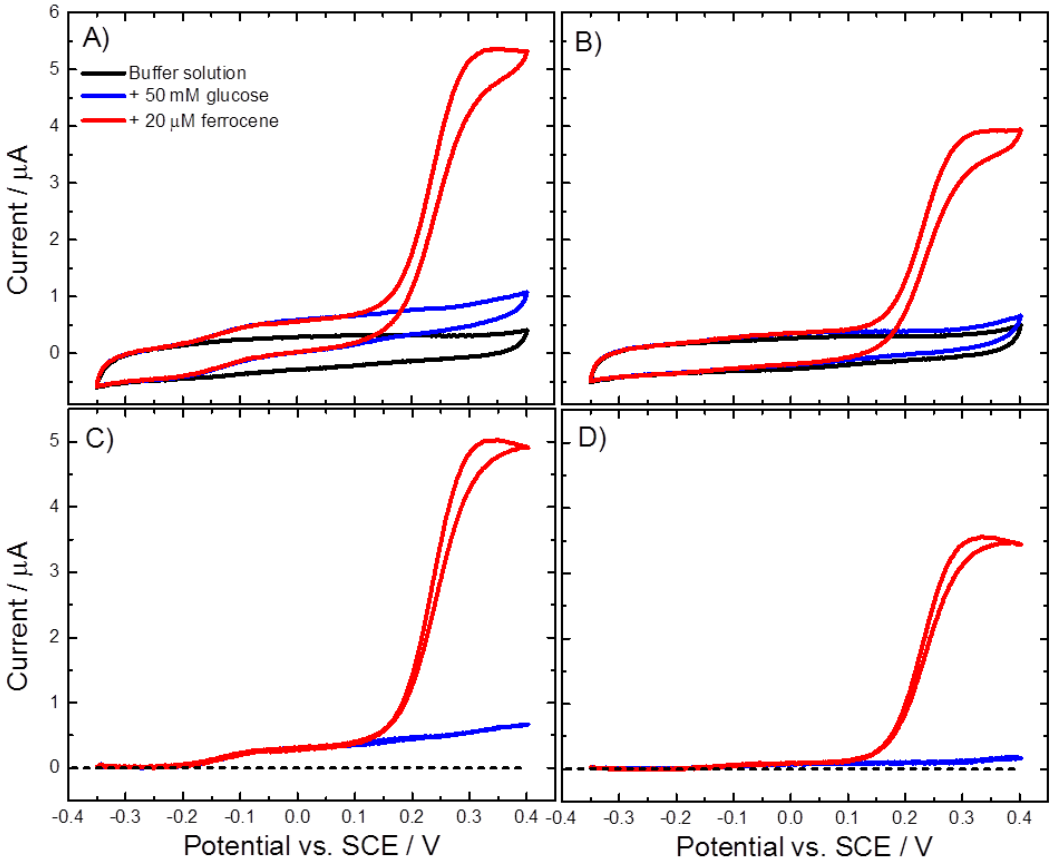

Figure 3.22. *(A-B) Original and (C-D) background subtracted CVs recorded at a E522-CDH modified GC/CNT electrode in argon-saturated 50 mM acetate buffer (pH 5.5), containing 30 mM $CaCl_2$ (black), after the addition of 50 mM glucose (blue) and the addition of 20 µM ferrocene (red). The CVs were recorded (A-C) before and (B-D) after the papain treatment, sweeping the potential at 2 mV/s.*

In the CVs recorded the day before the papain treatment (Figure 3.22-A and C), we can observe quite well both the DET and MET currents. After the papain experiment (Figure 3.22-B and D), we can see that both the DET and MET currents have decreased, even though to different extents: certainly, the DET current decreased more than the MET one, as it is almost no longer visible being very close to the background. Comparing the current before and after the papain treatment (at 0.0 V for the DET and at 0.35 V for the MET in the subtracted voltammograms), we calculated that the DET decreased of the 75 % and the MET of the 30 %.

In theory, we would have expected a decrease of about the 100 % for the DET current, without affecting the MET one. However, the experimental results slightly differ from the theoretical ones. This is because papain breaks peptide bonds indiscriminately and, even if the preferential cleavage site in the CDH molecule is the peptide linker connecting the two domains, which is more exposed, this is not the only site where papain can act. Therefore, the reduction in the DET current can derive from three factors: *i*) cleavage of the peptide linker between the two domains with consequent loss of the haem domain (preferential cleavage); *ii*) damage of the haem domain, which would not be capable of DET; *iii*) damage of the flavin domain, which would be no longer capable of oxidising the glucose. But this third factor would affect also the MET current, which indeed decreased too, even though to a lesser extent.

The fact that the DET current did not decrease by 100 % can be explained by the papain not being able to break completely the CDH linker for mainly two reasons. First, the papain could have had some difficulties to access all the CDH molecules inside the carbon nanotube structure of the electrode, even though its concentration was quite high (0.5 mg/mL) and this enzyme is even smaller than CDH (23 kDa [124] compared with the 94 kDa of *Mt*CDH [73]). Second, the experimental conditions were probably not the most optimal for papain. In fact, most of the authors use papain at pH included between 6 and 7 and temperatures higher than room temperature (around 40 °C) [107,125,126], even if the enzyme should be active for a wide range of temperatures and pH (between 3-9) [124]. Moreover, these authors use cysteine (or other thiols) and EDTA to activate the papain. In our experiment, we wanted to avoid the use of cysteine or other thiols

in solution, since they could exchange the cysteine-modified CDH attached through the maleimide/cysteine bonds on the electrode [127], as well as the use of EDTA, which can inhibit the haem group [128]. We wanted also to follow the papain cleavage by measuring in real-time the DET current in the same conditions used previously to measure the activity of this CDH-modified electrode, which was at room temperature and pH 5.5.

Although the conditions used in our experiment were not the most optimal for the papain cleavage, it is rather significant that the DET current decreased much more than the MET one. In any case, also using the best conditions reported in the literature, the cleavage of the CDH peptide linker is never completely successful: at the end, a chromatographic separation is always necessary to separate the different fragments obtained, which can include intact CDH molecules or smaller portions, in addition to the flavin and haem domains alone [107,125].

It is also significant to look at the trend of the DET current measured after different times from the preparation of this E522-CDH modified electrode, during

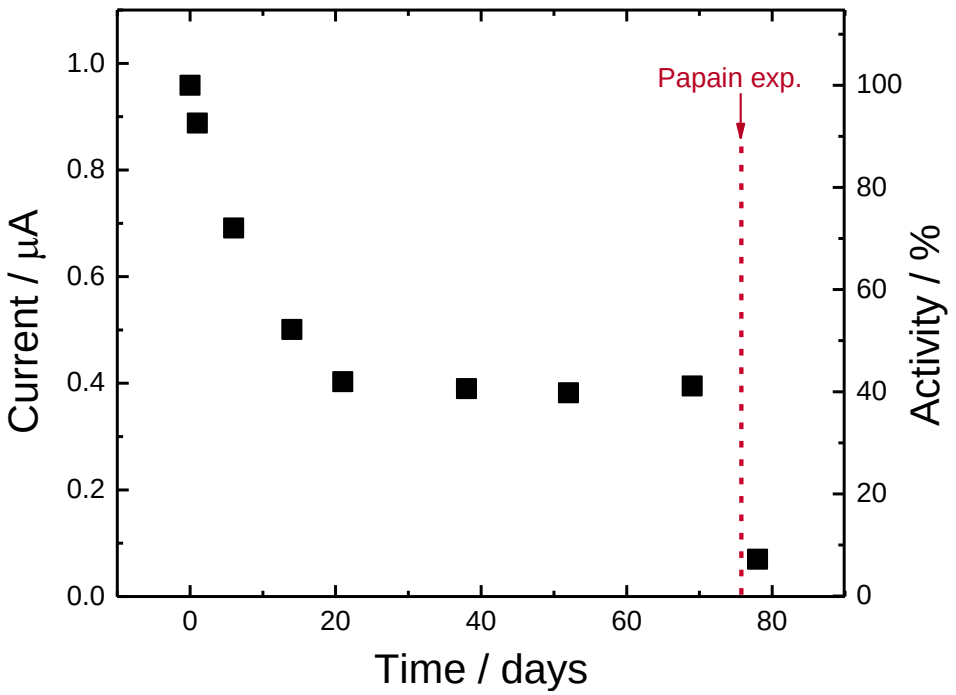

Figure 3.23. *DET current measured at a E522-CDH modified GC/CNT electrode in argon-saturated 50 mM acetate buffer (pH 5.5), containing 30 mM $CaCl_2$ and 50 mM glucose. The current was measured at different times from the preparation of the electrode, which was stored wet with the same buffer at 4 °C. On the 77th day the electrode was treated with papain.*

a period of almost 80 days (Figure 3.23). We can notice that its activity decreased quite rapidly during the first 20 days, reaching the 40 % of its initial value. After that, the current was quite stable at this value for about 50 days. However, after the papain experiment, performed on the 77th day, the DET current further decreased reaching the 7 % of the initial activity. Apart for the last decrease due to the papain treatment, which was expected, these results will be discussed in more detail in the next section, where we will show the stability of our covalently modified electrodes.

3.5 Stability of the CDH-modified electrodes

3.5.1 Stability over the time

As reported in the previous section, a CDH-modified electrode maintained its activity for a very long period, almost 80 days, and finally it lost it only because on the 77th day it was used for the papain experiment (see Figure 3.23). This is a great success for our immobilization method because, generally, enzymes have a short life-time even in their natural environment. However, as said in the Introduction (Section 1.2), good immobilization techniques can improve the stability of enzymes and increase their life-time.

The electrode for the stability experiment (used also for the papain experiment) was prepared according to our covalent immobilization procedure, using a maleimide-modified GC/CNT electrode and the CDH variant E522. Soon after the preparation, the electrode was tested for the DET in 50 mM acetate buffer (pH 5.5), containing 30 mM $CaCl_2$: two CVs were performed, one in the buffer alone as background and the second one after the addition of 50 mM glucose to measure the DET catalytic current. Therefore, the electrode was stored wet with the same buffer used to test it, at 4 °C. From time to time, the electrode was taken out from the fridge and tested it again by cyclic voltammetry, using the same conditions as before. The values of the DET current for 50 mM glucose, taken at 0.0 V *vs.* SCE after background subtraction, were then plotted versus the time passed from the preparation of the electrode (Figure 3.23). In this graph, we can see that the initial activity of the electrode decreases quite sharply during the first 20 days.

This can be due to the desorption of physically absorbed CDH molecules as well as the possible loss of the haem group from bound enzyme, which would make some CDH molecules unable to undergo DET. Note that we do not attribute the decrease in response to loss of CNTs from the GC electrode surface as Figure 3.24, which reports the background CVs recorded for this electrode at different times, shows no change in the capacitive background current over the same period.

After the initial decrease during the first 20 days, the activity of the electrode was found stable at the 40 % of the initial value for about 50 days (Figure 3.23). After that, the electrode was used for the papain experiment and lost almost completely its activity, as already explained in the previous section.

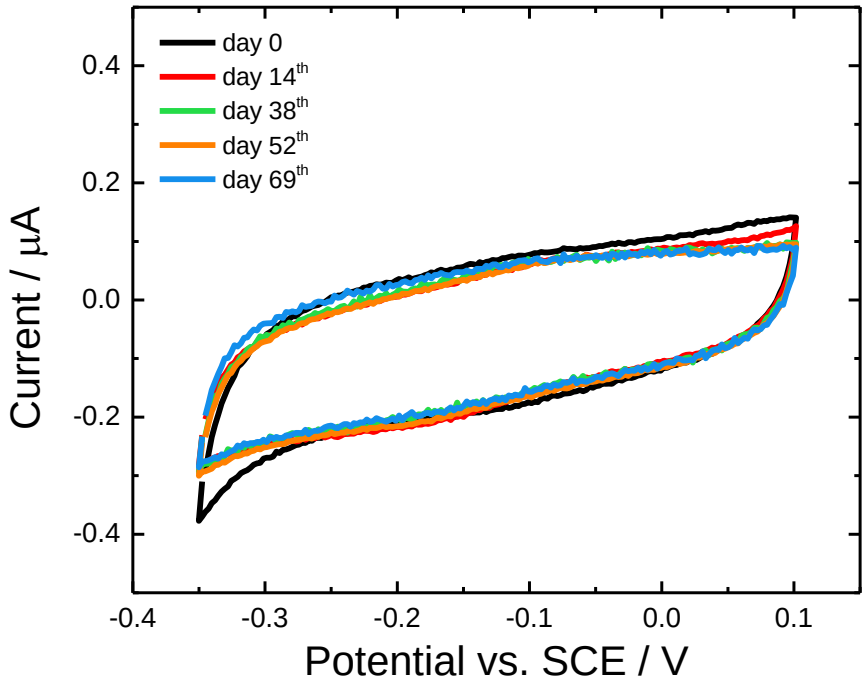

Figure 3.24. *Cyclic voltammograms recorded at a E522-CDH modified GC/CNT electrode (same electrode used for Figure 3.23) in argon-saturated 50 mM acetate buffer (pH 5.5), containing 30 mM $CaCl_2$. The potential was swept at 1 mV/s. CVs were recorded after different times from the preparation of the electrode, as reported in the inset.*

This experiment was repeated with a second electrode, this time measuring the DET current at a different pH, namely 7.4. Moreover, in addition to the maleimide-modified electrode, an unmodified GC/CNT electrode was also tested for the stability over the time. The two electrodes were prepared with the CDH variant E522: the first one would present a covalent immobilization, the second

one a physical adsorption of the enzyme. Soon after the preparation, they were tested by CV in 50 mM Tris/30 mM $CaCl_2$ buffer (pH 7.4), before and after the addition of 50 mM glucose, as already done with the previous electrode tested at pH 5.5. The DET current was plotted versus the time passed from the preparation of the electrodes (Figure 3.25).

The electrode with the covalently immobilised CDH (black squares) was found to be very stable for a long period showing the same activity after two months (about 40 % of the initial activity) as after one week from the preparation. Also in this case, the activity decreased quite rapidly at the beginning, reaching after one week almost the 40 % of its initial value. The same behaviour was observed also in the previous experiment at pH 5.5 (Figure 3.23), with the only difference that the decrease was slightly slower: 20 days instead of just 7. We can believe that this initial decrease was due to the same factors as before: desorption of physically absorbed CDH molecules and/or loss of the haem group from bound enzyme. After that, the activity of the electrode was stable for about 50 days, until when we decided to end the experiment. The small fluctuations in the activity observed during the test are probably due to experimental factors, such as slightly different temperature or concentration of glucose. In any case, it is significant to note that the enzyme immobilised at the maleimide electrode is much more stable than the control electrode with the physically adsorbed CDH (green circles). For this latter electrode, the catalytic response decayed much more rapidly, reaching after 22 days 20 % of the initial activity, which was already much lower than the one of the covalently modified electrode. This is a good indicator of the greater stability of the covalent bonds between maleimide-modified electrodes and cysteine-modified CDH. However, further control experiments comparing covalently immobilised and physically adsorbed CDH are reported in the next sections.

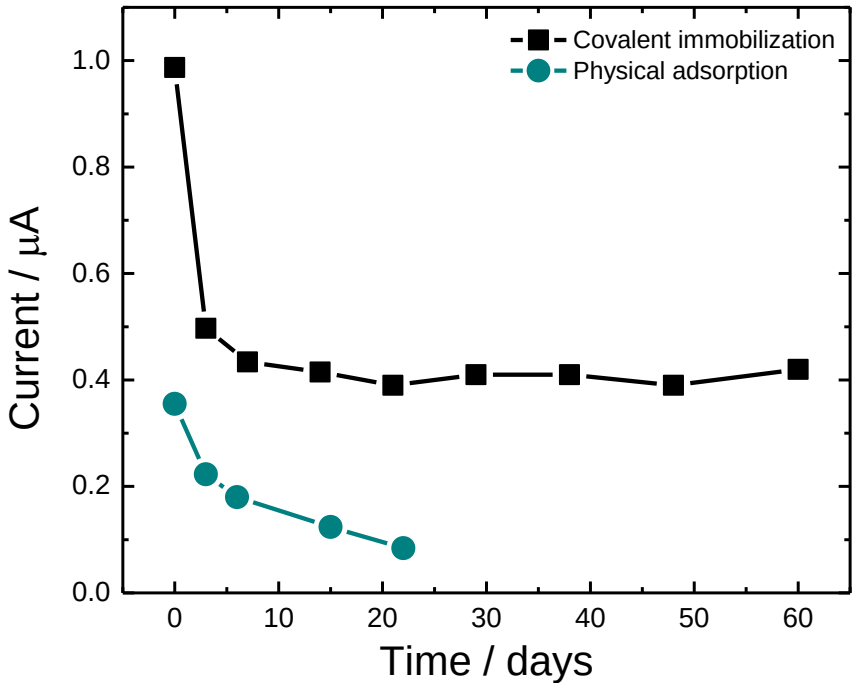

Figure 3.25. *DET current measured at E522-CDH modified GC/CNT electrodes in argon-saturated 50 mM Tris buffer (pH 7.4), containing 30 mM $CaCl_2$ and 50 mM glucose. The current was measured at different times from the preparation of the electrodes, which were stored wet with the same buffer at 4 °C. Black squares: enzyme covalently immobilised at maleimide-modified GC/CNT electrode. Green circles: enzyme physically adsorbed on unmodified GC/CNT electrode.*

3.5.2 Covalent immobilization *vs.* physical adsorption

To verify that CDH was immobilised at the electrode surface through a covalent bond between its free cysteine residue and the maleimide, we carried out some experiments using two different *Mt*CDH variants (E522 and T701) covalently bound and physically absorbed at GC/CNT electrodes. The first experiment was performed at pH 7.4, and it was carried out in collaboration with my colleague Firas Al-Lolage. However, a second experiment at pH 5.5 was also performed, using the same two CDH variants as for the previous one.

For the covalent immobilization, maleimide-modified electrodes were prepared using the procedure described in Section 3.1.2, while the physically-modified ones were prepared by simply drop casting 3 µL of the enzyme solution onto an unmodified GC/CNT electrode. Soon after the preparation, all the electrodes were tested by cyclic voltammetry in 50 mM Tris/30 mM $CaCl_2$ buffer (pH 7.4), at increasing concentrations of glucose in solution (from 0 to 50 mM). Direct

electron transfer was observed for both modification methods in the presence of the substrate. Therefore, the current taken at 0.0 V *vs.* SCE, after background subtraction, was plotted versus the glucose concentration for all the electrodes analysed (Figure 3.26). We can immediately note that the catalytic currents for physically absorbed CDH (circles) were decidedly lower than the ones for the covalently immobilised enzyme (squares): in particular, the current was about 60 % less for the variant E522 (red/pink) and 80 % less for the variant T701 (blue). Moreover, we can see that the curves of current *vs.* glucose concentration are the same for the electrodes physically-modified with the two different variants (circles). In this case, in fact, all the enzyme molecules would lie on the electrode surface in random orientations, most probably the same for both the CDH variants. In contrast, for the two covalently-modified electrodes the curves are different (squares), as expected if the two enzymes are immobilized with different orientations through the cysteine residues located in different positions on the enzyme surface (see Figure 3.10).

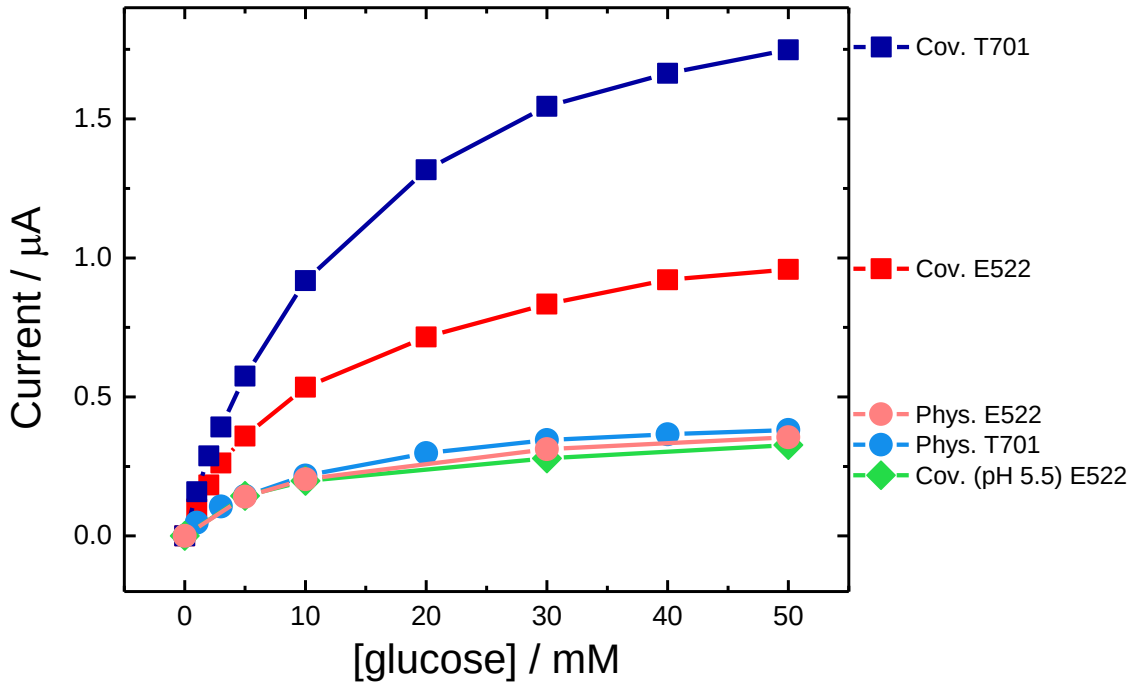

Figure 3.26. *Current for the DET of different CDH modified GC/CNT electrodes, measured in 50 m Tris buffer (pH 7.4), containing 30 mM $CaCl_2$ and increasing concentrations of glucose. Electrodes: (red/pink) E522 and (blue) T701, (squares) covalently immobilised at maleimide-modified GC/CNT electrodes and (circles) physically adsorbed on unmodified GC/CNT electrodes. Green diamond: E522 immobilised at maleimide-modified GC/CNT electrode, but immobilization carried out at pH 5.5. (Experiment performed in collaboration with Firas Al-Lolage).*

Note that the same two CDH variants E522 and T701 immobilised at maleimide-modified electrodes produced almost the same curves of current/glucose concentration at pH 5.5 (see Figure 3.11), while here at neutral pH they are rather different. This should not be attributed to a different amount of immobilised enzyme between the two electrodes analysed at pH 7.4. In fact, the MET analysis showed very similar trends of the current *vs.* glucose concentration for the same two electrodes (data not shown, experiment done by my colleague Firas Al-Lolage), as we found also for the two electrodes analysed at pH 5.5 (see Figure 3.13), meaning that the amount of enzyme was the same in both the cases. Instead, the different results for the two variants at neutral pH (Figure 3.26) might be due to a different conformation of the enzymes on the electrode, with the haem and flavin domains more or less far from each other, producing different IET rates and, consequently, different currents (note that also in this case we are considering the IET as the limiting step). This can be accounted for the different orientation of the two variants on the electrode due to the different position of their cysteine residues. For instance, the variant E522 might better accommodate on the electrode with the two domains more apart from each other, causing a slower IET rate and, therefore, a lower DET current. However, this would mainly occur at neutral pH, when the two domains are freer to move, and not at acidic pH, even though 30 mM $CaCl_2$ was present in both the cases. The same behaviour was observed also by studying the effect of $CaCl_2$ on the two variants in Section 3.4.2. We found that the addition of $CaCl_2$ had a greater effect on E522, which needed a higher concentration of divalent cations to bring the two domains close to each other. For that, a better discrimination between the CDH variants (or at least E522 and T701) should probably be carried out at neutral pH and, preferably, in the absence of $CaCl_2$. On the contrary, acidic pH and relatively high amounts of divalent cations would make the results more uniform between the different variants.

Carrying on with the description of the control experiments shown in Figure 3.26, as final control a maleimide-modified GC/CNT electrode was prepared by reaction with the variant E522 dissolved in a pH 5.5 buffer (50 mM acetate) instead of the usual pH 7 buffer (50 mM phosphate) used for the immobilization procedure (see Section 2.6 in the Experimental Part). The results of this electrode

(green diamonds in Figure 3.26) are comparable with the ones of the physically-modified electrodes (circles), indicating that at pH 5.5 covalent attachment did not take place. This is consistent with the fact that the coupling reaction between cysteine and maleimide occurs at neutral pH (6.5-7.5), while at acidic pH the thiol group of cysteine is not nucleophilic enough to react with maleimide [129,130] (see reaction in Scheme 1.4-B; the pK_a of the cysteine side chain in folded proteins is around 6.8 [131]).

The results in Figure 3.26 are consistent with covalent binding of CDH at the maleimide-modified electrodes. The higher catalytic currents obtained with covalently-modified electrodes can be explained by immobilization of a greater number of enzyme molecules at the surface and/or the fact that the covalently immobilised enzyme is held in a more suitable orientation for DET as compared to the randomly-orientated physically-absorbed CDH. As a final test, we performed a similar experiment at pH 5.5, since a different pH could change the surface charges of both the electrode and the enzyme, hence changing the electrostatic interaction between them and, therefore, the strength of the physical adsorption.

The four electrodes used for this experiment were prepared as before: for the covalent immobilization, maleimide-modified electrodes were prepared using the procedure described in Section 3.1.2, while the physically-modified ones were prepared by drop casting the enzyme solution onto unmodified GC/CNT electrodes. Thereafter, the electrodes were tested by CV in 50 mM acetate/30 mM $CaCl_2$ buffer (pH 5.5), before and after the addition of 50 mM glucose. In this case, we did not perform the analysis for several substrate concentrations, as in the previous experiment, since for the physically-modified electrodes the DET current was so small (see Figure 3.27-B and D) that it was of difficult detection for glucose concentrations lower than 50 mM.

The results are shown in Figure 3.27: at a first glance, we can note the huge difference in the DET current produced by covalently immobilised enzyme (A and C) and physically adsorbed enzyme (B and D). The current for the physically-modified electrodes is about 90 % lower than the one for the maleimide-modified electrodes, for both the CDH variants. We do not attribute this big difference to a

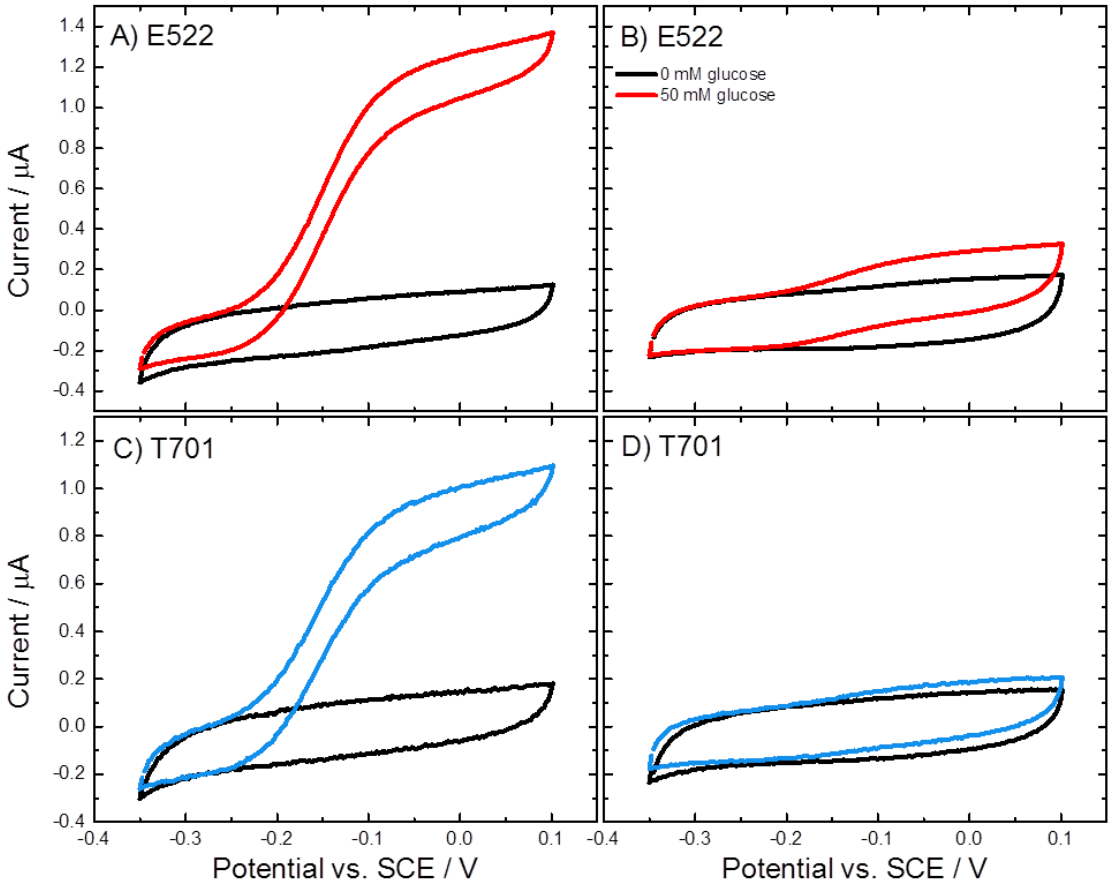

Figure 3.27. *Cyclic voltammograms recorded at (A-B) E522 and (C-D) T701-CDH modified GC/CNT electrodes in argon-saturated 50 mM acetate buffer (pH 5.5), containing 30 mM $CaCl_2$ (black lines), and after the addition of 50 mM glucose (coloured lines). A-C) enzyme covalently immobilised at maleimide-modified GC/CNT electrodes. B-D) enzyme physically adsorbed on unmodified GC/CNT electrodes. The potential was swept at 1 mV/s.*

different active area of the electrodes as the capacitive background currents are roughly the same for all of them (see black lines in Figure 3.27). Instead, this is a further evidence of the greater stability of our covalently-modified electrodes compared with the enzyme only physically adsorbed on unmodified electrodes. Note that the difference in the DET current between covalently and physically-modified electrodes is even bigger than at pH 7.4. This can be accounted for changes in the surface charges of both the electrode and the enzyme passing from pH 7.4 to pH 5.5. In fact, a more acidic pH leads to an increased protonation of the carboxylic acid groups on the CNTs ($pK_a \approx 4.5$ [132]) and CDH (pI ≈ 3.8 [73]), weakening the electrostatic interactions between them and, therefore, reducing the strength of the CDH physical adsorption.

The experiments reported until now in this Section 3.5 clearly proved the efficacy of our immobilization method since electrodes modified with CDH using our covalent procedure were found to be more stable over long periods, capable of retaining more enzyme molecules and with better orientations for the DET, and more stable over pH changes as compared to physically-modified electrodes. However, a further proof will arise from the last experiment of this section, performed with a surfactant, namely Triton X-100.

3.5.3 Control experiment: effect of Triton X-100

Polymers such as polyethylene glycol (PEG) and non-ionic surfactants have been employed to passivate surfaces with the aim of reducing nonspecific adsorption of proteins [133-136]. Here, we tried to use a non-ionic surfactant, namely Triton X-100, to desorb physically adsorbed CDH molecules, thus to further compare maleimide-modified and unmodified GC/CNT electrodes. Triton X-100 has a hydrophilic polyethylene oxide chain (a short PEG chain with an average of 9.5 ethylene oxide units) and an aromatic lipophilic (hydrophobic) group, see Scheme 3.5. It strongly adsorbs on hydrophobic surfaces, such as graphite and CNTs, thanks to hydrophobic interactions with its lipophilic head, forming a monolayer. This monolayer of surfactant causes the surface to become hydrophilic and non-ionic, thus reducing the interactions between it and the proteins, although without denaturing them [135].

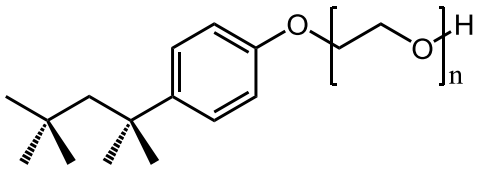

Scheme 3.5. *Structure of Triton X-100.*

For our control experiment, we used some electrodes covalently modified and some physically modified with the CDH variant E522. The electrodes were prepared as already described in the previous section. Upon immersion in the Triton solution, we would expect the physically modified electrodes to lose their catalytic activity: in fact, the surfactant should form a hydrophilic monolayer on the electrode surface, thus reducing the nonspecific adsorption of the enzyme. On the other hand, the covalently modified electrodes should not be affected by the Triton or, eventually, they could lose only a small part of their activity as a consequence of the loss of the physically adsorbed CDH molecules.

Three different electrodes were used: two covalently modified with E522 and one physically modified with the same enzyme. The experiments were carried out using mainly chronoamperometry to monitor in real time the effect of Triton on the electrodes (Figure 3.28-A, C, E); however, cyclic voltammetry was also performed before and after the Triton experiments (Figure 3.28-B, D, F). For the chronoamperometry experiments, the electrodes were placed in the electrochemical cell filled with 10 mL of 50 mM Tris buffer (pH 7.4), containing 30 mM $CaCl_2$. The cell was deoxygenated by bubbling gas argon for 20-30 min before the experiment, and it was kept under light argon bubbling also during it in order to mix the solution. A constant potential of +0.2 V *vs.* SCE was applied. When the current was enough stable, after 10-20 min, 70 mM glucose was added in the cell: the current immediately jumped up for all the three electrodes (see Figure 3.28-A, C, E). However, the current did not reach the same intensity for all of them: this depends on the amount of enzyme that was present on each electrode at the time of the experiment, since not all of the electrodes were used immediately after preparation. In any case, we do not need to compare the current intensities of the electrodes between each other.

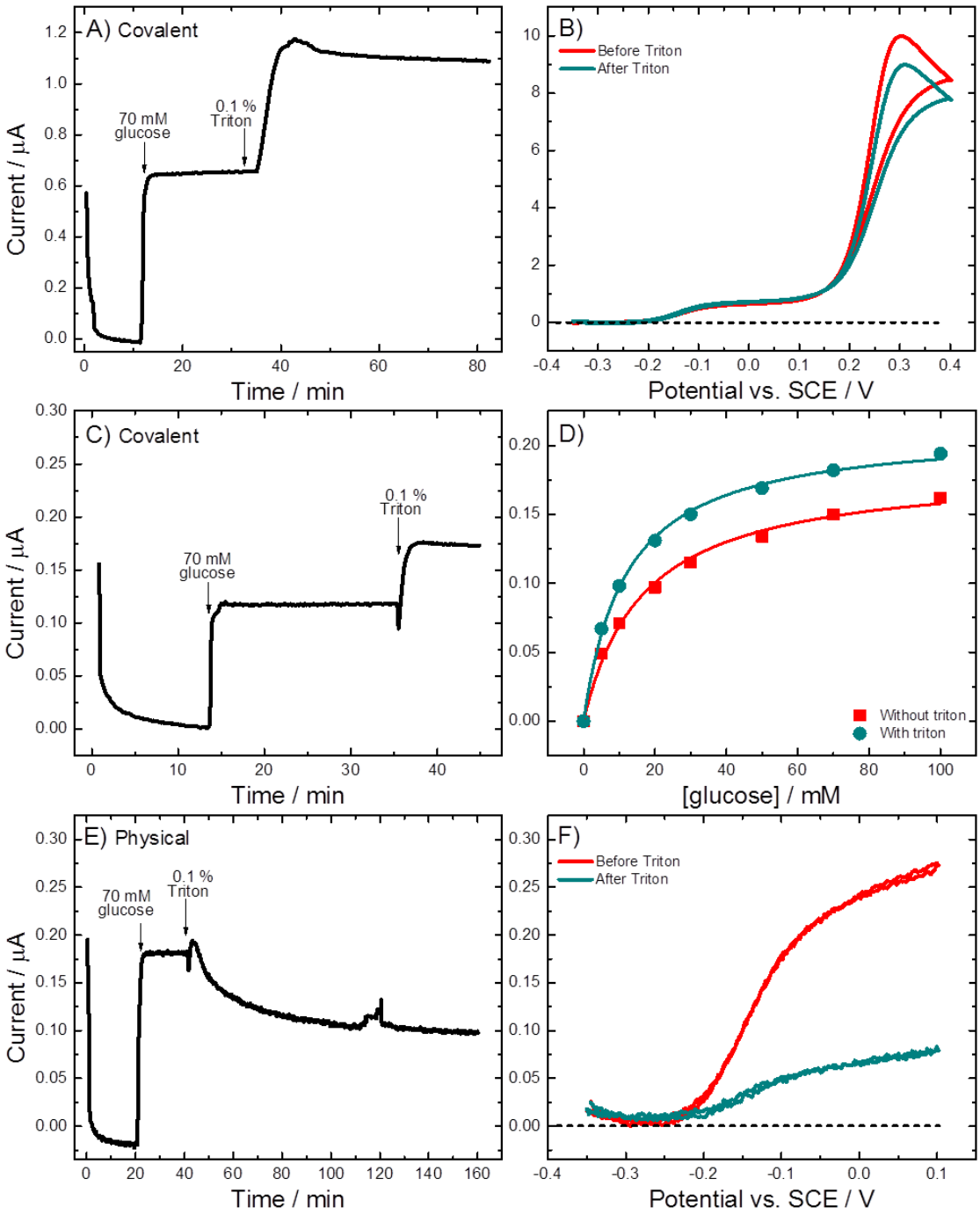

Figure 3.28. *Experiments performed at GC/CNT electrodes modified with the CDH variant E522, in particular: (A-B) electrode 1 covalently-modified, (C-D) electrode 2 covalently-modified and (E-F) physically-modified electrode. A, C, E) Chrono-amperograms recorded holding the potential at +0.2 V vs. SCE, in argon-saturated 50 mM Tris buffer (pH 7.4), containing 30 mM $CaCl_2$. The electrochemical cell was kept under light argon bubbling during the experiments and the additions of 70 mM glucose and 0.1 % Triton were carried out as indicated. B) Background subtracted CVs recorded in the same Tris/$CaCl_2$ buffer containing 70 mM glucose and 20 µM ferrocene, before (red) and after (green) the Triton experiment shown in A. D) Current vs. glucose concentration: experiment carried out in the same Tris/$CaCl_2$ buffer (red) and with the addition of 0.1 % Triton (green). F) Background subtracted CVs recorded in the same Tris/$CaCl_2$ buffer containing 70 mM glucose, before (red) and after (green) the Triton experiment shown in E.*

Once the current was stabilised again, after 30-40 min, 0.1 % Triton X-100 was added in the cell, which became full of soap-like bubbles. However, the effects on the current were different depending on which electrode was present in the cell. We will start our discussion from the physically modified electrode, whose behaviour was quite expected (Figure 3.28-E). The addition of the surfactant, after an immediate small increase, produced a decrease in the current that reached 60 % of the initial value after 120 min. After the chronoamperometry, the electrode was washed with the same Tris/$CaCl_2$ buffer and tested by CV, as was already done before the experiment with Triton. Figure 3.28-F reports the background subtracted CVs: the one recorded after (green) showed a catalytic current much lower than before the Triton experiment (red), with a decrease of the 75 %. Therefore, the effect of Triton is not reversible: a significant part of the physically adsorbed enzyme must have been irreversibly lost from the electrode, as expected. However, not all the CDH molecules have been desorbed from the electrode surface since Triton alone on CNTs produces a partial resistance to nonspecific adsorption of proteins: the total resistance would be achieved by also adding a polymer, such as PEG [135].

What was not expected is the effect of Triton on the current of the covalently modified electrodes. As we can see in Figure 3.28-A and C, after the addition of Triton, the catalytic current increased by 70 % for the first electrode (A) and by 55 % for the second electrode (C). Further experiments could help to understand this unexpected behaviour. For the first electrode, cyclic voltammetry was carried out before and after the Triton experiment (Figure 3.28-B). The CVs were performed in the buffer solution containing 70 mM glucose and 20 µM ferrocene, and using a wide potential range to include both the DET and MET. We can see that, after the electrode was treated with Triton and then washed with the buffer (green line), the MET current (around 0.3 V) decreased by 10 %. On the other hand, the DET current (between -0.1 and +0.1 V) did not undergo such a decrease: instead, it was increased by 10 %, even though this is not very visible in Figure 3.28-B as the current scale is very large to include the MET current. The small decrease in the MET current can be due to the loss of the physically adsorbed CDH molecules from the electrode, as we expected. However, it is not clear why the DET current is even higher than before the Triton experiment, and

why it increased so much when Triton was added in solution (Figure 3.28-A), despite the loss of some enzyme molecules from the electrode surface, as verified by the MET current decrease.

This effect of Triton on the DET current of covalently modified electrodes could be due to different factors. Here below we will list the different steps involved in the CDH catalytic process, explaining which ones could have been affected by the addition of Triton thus increasing the DET current:

1) The substrate/FAD reaction: its rate could increase due to a better diffusion of glucose at the electrode surface or a greater affinity between the enzyme and the substrate. However, we can exclude this hypothesis since, if that were true, the addition of Triton would increase also the MET current, not only the DET. In fact, this could only be true if the mass transport of glucose were the rate limiting step, which is not the case for the DET. Moreover, it was excluded also by the experiment performed at the second covalently modified electrode: the Michaelis-Menten analysis with and without Triton in solution (Figure 3.28-D). As we can see, the current intensity in the presence of Triton (green circles) was higher than before the addition of the surfactant (red squares). However, the Michaelis-Menten fitting provided the values of K_M^{APP}, which were 16 and 12 mM before and after the addition of Triton, respectively. Such a small difference can be attributed to experimental error, so that we can consider the two values of K_M^{APP} being very similar (note that the values of K_M^{APP} for the four CDH variants at pH 7.4 were found between 11 and 14 mM, in experiments performed by Firas Al-Lolage). It follows that the affinity of the enzyme for the substrate does not significantly change upon the addition of the surfactant. In any case, the value of K_M^{APP} depends also on other factors, not only on the K_M, as we will see in the next Chapter.

2) The FAD/haem reaction (IET): Triton could increase its rate, making the two CDH domains closer to each other, like $CaCl_2$ does. To prove that, an experiment with CDH in solution was carried out by my co-worker Dr Su Ma at the BOKU-University of Vienna (Austria). The activity of *Mt*CDH towards the reduction of cytochrome c was tested in solution, in the absence and presence of different concentrations of Triton X-100. The results of the test are reported

in Figure 3.29-A for pH 5.5 and Figure 3.29-B for pH 7.4. The experiment was performed at two different concentrations of substrate, 5 mM (blue) and 50 mM (red). In all the cases, we can see that the enzyme activity does not vary by increasing the concentration of Triton in solution (from 0 to 0.3 %), meaning that the surfactant does not affect the IET rate of CDH. Note that the CDH activity increases only when the glucose concentration is increased (compare blue with red bars), and passing from pH 5.5 to pH 7.4 (compare Figure 3.29-A with 3.29-B). This latter increase is expected since, as we have already said, the substrate/FAD reaction rate changes with the pH, reaching its maximum around pH 8 [78]. Although this might be the case in solution, it does not necessary mean that it has to be the same with the enzyme immobilised at the electrode surface. In fact, the adsorption of Triton could affect the orientation of the enzyme at the electrode surface, probably making the FAD and haem domains closer to each other and improving the IET rate. The surfactant would act in a different way if compared with $CaCl_2$, without eliminating the electrostatic repulsion between the two domains, so that its effect is not visible on the free enzyme in solution but only when it is immobilised.

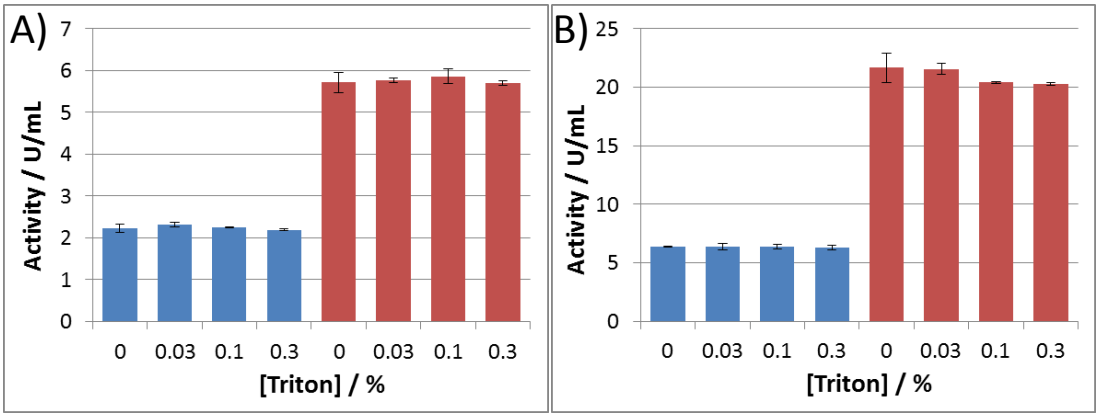

Figure 3.29. *Activity of MtCDH (wild type) in solution tested in (A) 50 mM Bis-Tris buffer (pH 5.5) and (B) 50 mM Tris/30 mM $CaCl_2$ buffer (pH 7.4), using 20 µM cytochrome c and different concentrations of glucose: (blue) 5 mM or (red) 50 mM. The test was carried out for different concentrations of Triton X-100, from 0 to 0.3 %. (Experiment performed by Dr Su Ma at the BOKU-University, Vienna).*

3) The haem/electrode reaction (DET): the adsorption of Triton could make the haem group have a better orientation and/or shorter distance with the electrode surface, so increasing the DET rate. However, we can exclude also this hypothesis since, as we showed earlier in Sections 3.2.2 and 3.2.5, the haem/electrode reaction is always very fast, so that it cannot be the rate limiting step and, even increasing its rate, it cannot affect the current.

4) An increase in the activity of the covalently bound CDH molecules after desorption of the physically adsorbed ones. In fact, it is possible that the desorption of the physically (and randomly) adsorbed CDH molecules makes more space available on the electrode for the covalently bound enzyme, so that it can be better accommodated.

To conclude, the presence of Triton could increase the DET current of covalently modified electrodes thanks to two different effects: by changing the orientation of the immobilised enzyme and making the two domains closer to each other (reversible effect) and, secondly, by making more space available for the covalently immobilised CDH molecules after desorption of the physically adsorbed ones (irreversible effect). However, this should be further investigated also because it can be an interesting way to increase the current intensity of CDH-modified electrodes, or even electrodes modified with other redox enzymes. In any case, even though it is not completely clear how Triton acts to increase the DET current of covalently immobilised CDH, the purpose of this experiment was to prove the greater stability of our covalently modified electrodes if compared with CDH only physically adsorbed at GC/CNT electrodes. This was fully achieved since the addition of Triton in solution caused the DET current to decrease for physically modified electrodes and, on the contrary, to increase for covalently modified ones.

3.6 Solid-phase functionalization of CNTs

3.6.1 Introduction

Until now in this Chapter we have shown the covalent, site-specific immobilization of CDH at GC/CNT electrodes, which were modified through an electrochemical and solid-phase synthesis procedure. However, despite the great flexibility of the method that allows varying the key elements of the modification independently to tune the architecture of the electrode surface as required, the long procedure restricts its applicability for large-scale production of modified electrodes. Moreover, for applications such as biosensors, simple, low-cost and disposable electrodes, such as screen-printed electrodes (SPEs), have recently attracted a great interest. Unfortunately, such electrodes are not always suitable for a long modification procedure involving the use of strong organic solvents and acids, which may damage their materials. For that reason, we decided to try a different way for producing GC/CNT electrodes (or different types of electrodes modified with CNTs) functionalised with maleimide groups, which are suitable for the immobilization of cysteine-modified enzymes.

This new method consists in the solid-phase modification of carbon nanotubes, before adsorbing them on SPEs (or any other type of electrode), employing the spontaneous attachment of diazonium salt to carbon surfaces at high temperatures [137-139]. In this way, a large amount of CNTs can be functionalised at once with maleimide, and then used to modify screen-printed electrodes (or other electrodes) when required for the covalent immobilization of CDH variants.

This work has been carried out at DropSens (Oviedo, Spain), a company specialised in the design and manufacture of SPEs as well as other instrument for electrochemistry research, in collaboration with Dr David Hernandez Santos and Dr María Begoña González García. We decided to adsorb the maleimide-functionalised CNTs on gold SPEs (see Figure 3.30), since the conductivity of the carbon SPEs tested was not as good as that for gold ones, due to the different materials used for their manufacture. Indeed, a good conductivity was of primary

importance for the immobilization of enzymes and detection of their, rather low, direct electron transfer current.

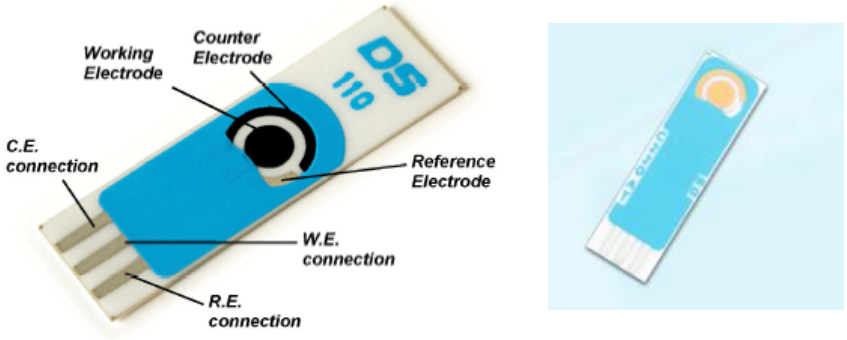

Figure 3.30. *Pictures of a carbon (left) and a gold (right) screen-printed electrodes from DropSens (adapted from www.dropsens.com).*

3.6.2 Functionalization of CNTs with anthraquinone

Before attempting the modification of CNTs with maleimide and, therefore, CDH, the solid phase modification of CNTs was tested using a redox probe, anthraquinone (AQ), following previous work by our group [139]. The modification was carried out using two methods in order to verify that each step of the procedure worked correctly (see Scheme 3.6).

For the first method (Scheme 3.6, steps a-1.c), only the first step (attachment of diazonium salt on CNTs) was performed in solution by mixing the carboxylic acid-functionalised CNTs in DMF with the diazonium tetrafluoroborate, at 60 °C under reflux, overnight. The modified CNTs (CNTs 1) were washed, dried and dissolved in DMF to be drop cast onto a gold screen-printed electrode (SPE 1). The following steps, Boc deprotection of diazonium salt and coupling of anthraquinone, were carried out with the CNTs adsorbed on the electrode, using milder solvents (such as water and acetonitrile) to avoid damaging the SPE.

For the second method (Scheme 3.6, steps a-2.d), the entire solid-phase modification of CNTs was carried out in solution. The first step (a) was the same as before. Then CNTs 1 were washed, dried and dissolved in a 4 M HCl solution in dioxane for the Boc deprotection. After they were washed and dried again, the CNTs were dissolved in a DMF solution containing EDC, NHS and

anthraquinonecarboxylic acid, stirred at room temperature overnight. Finally, the AQ-modified CNTs (CNTs 2) were dissolved in a DMF/water (4:1) solution and drop cast on AuSPEs (SPE 2).

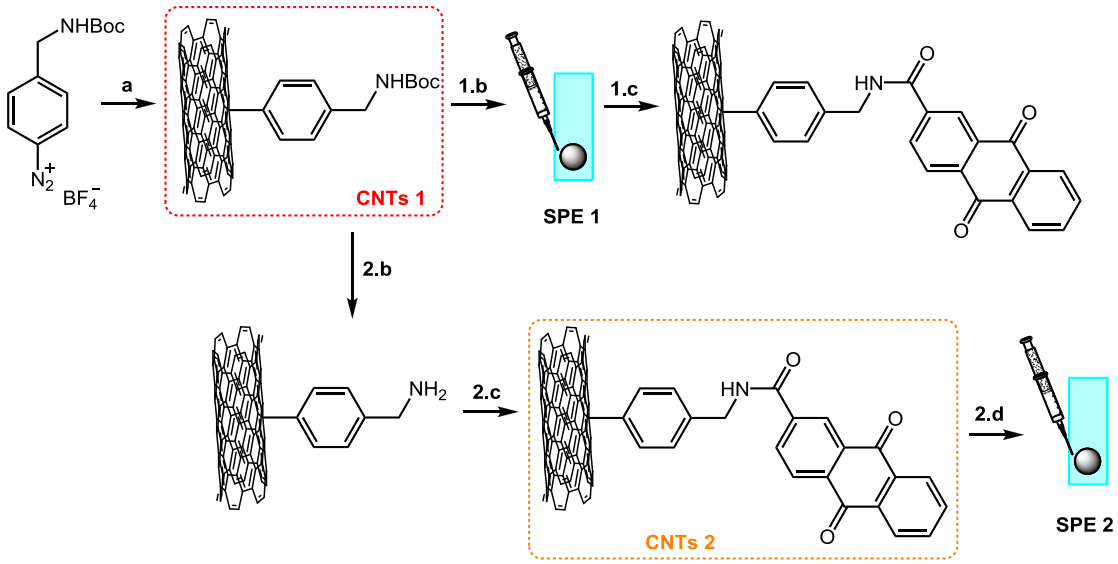

Scheme 3.6. *Sequential modification of CNTs with AQ. Reagents and conditions: a) carboxylic acid-functionalised CNTs and diazonium tetrafluoroborate in DMF, heated at 60 °C under reflux (overnight); 1.b) CNTs 1 were dissolved in DMF and drop cast onto a AuSPE (SPE 1); 1.c) Boc-deprotection in 1 M HCl in water (1 h), then coupling of anthraquinonecarboxylic acid in ACN with EDC/NHS (overnight). 2.b) CNTs 1 in 4 M HCl in dioxane, stirred strongly at RT (1 h); 2.c) CNTs and anthraquinonecarboxylic acid in DMF with EDC/NHS (overnight); 2.d) CNTs 2 were dissolved in a DMF/water (4:1) solution and drop cast onto a AuSPE (SPE 2).*

The screen-printed electrodes modified with CNTs and AQ using the two methods described above were tested by cyclic voltammetry in phosphate buffer (pH 7). Figure 3.31 shows the CVs recorded at different scan rates for a SPE 1 and three SPEs 2: the reversible redox peaks of anthraquinone are clearly visible around -0.48 V *vs.* SCE. At first glance, we can note that the peaks for the SPE 1 (Figure 3.31-A) are lower than those for the SPEs 2 (Figure 3.31-B, C and D).

The surface coverage of AQ (Γ_{AQ}) was calculated by integrating the redox peaks in the CVs recorded at 50 mV/s. From the average integrated area between the anodic and cathodic peaks (a_{int}), the charge (Q) can be found out:

$$Q = \frac{a_{int}}{v} \qquad \text{(Eq. 3.14)}$$

where v is the scan rate (0.05 V/s in our case).

The charge is then related to the number of moles of anthraquinone (m_{AQ}) through the Faraday law:

$$Q = n\, m_{AQ}\, F \qquad \text{(Eq. 3.15)}$$

where F is the Faraday constant (96485 A s mol^{-1}) and n is the number of electrons exchanged during the oxidation or reduction of each molecule of AQ, which is equal to 2. Therefore, m_{AQ} was divided either for the geometrical area of the SPEs (≈ 0.12 cm^2) or for the weight of CNTs loaded on each SPE (≈ 20 µL of a 1 g/L solution, which is 2 ×10^{-5} g) to find two different types of AQ surface coverage (Table 3.2). Looking at the Γ_{AQ} normalised to the electrode geometrical area (Table 3.2, 2nd column), we can see that the value for the SPE 1 is lower than those for the SPEs 2. This difference may be due to the different methods used for the modification or, most probably, to the different loading of CNTs on the SPEs. In fact, for the first method, the CNTs 1 (modified with the diazonium salt, see Scheme 3.6) were dissolved in pure DMF and drop cast on SPE 1. However, the high hydrophobicity of such solution prevented the drop of CNTs from remaining only on the gold electrode, even if a plastic mask with the exact shape of the working electrode was used. As a result, a significant amount of the CNTs was lost from the SPE 1, resulting in a lower amount of AQ on the electrode surface. This is the reason why, for the second method, the CNTs 2 were dissolved in a DMF/water (4:1) solution to make the drop of CNTs less hydrophobic and more inclined to remain on the gold surface. Thanks to this changes, the AQ surface coverage for the SPEs 2 was higher than for the SPE 1, and quite reproducible between the three electrodes (SPEs 2.a-c), with values between 5 and 7 nmol/cm^2. Since in the case of SPEs 2 the amount of CNTs loaded on each electrode was known and there was no significant loss of CNT solution from the electrodes, the surface coverage normalised to the CNT weight was calculated (Table 3.2, 3rd colunm). The values obtained were between 0.03 and 0.04 mmol/g, which are a bit lower than those found in a previous work by Ghanem *et al.* [139], where the AQ surface coverage was 0.2 mmol/g. For the SPE 1 we could not calculate this second type of Γ_{AQ} as the amount of CNTs that remained on the electrode was not known for the reason reported above.

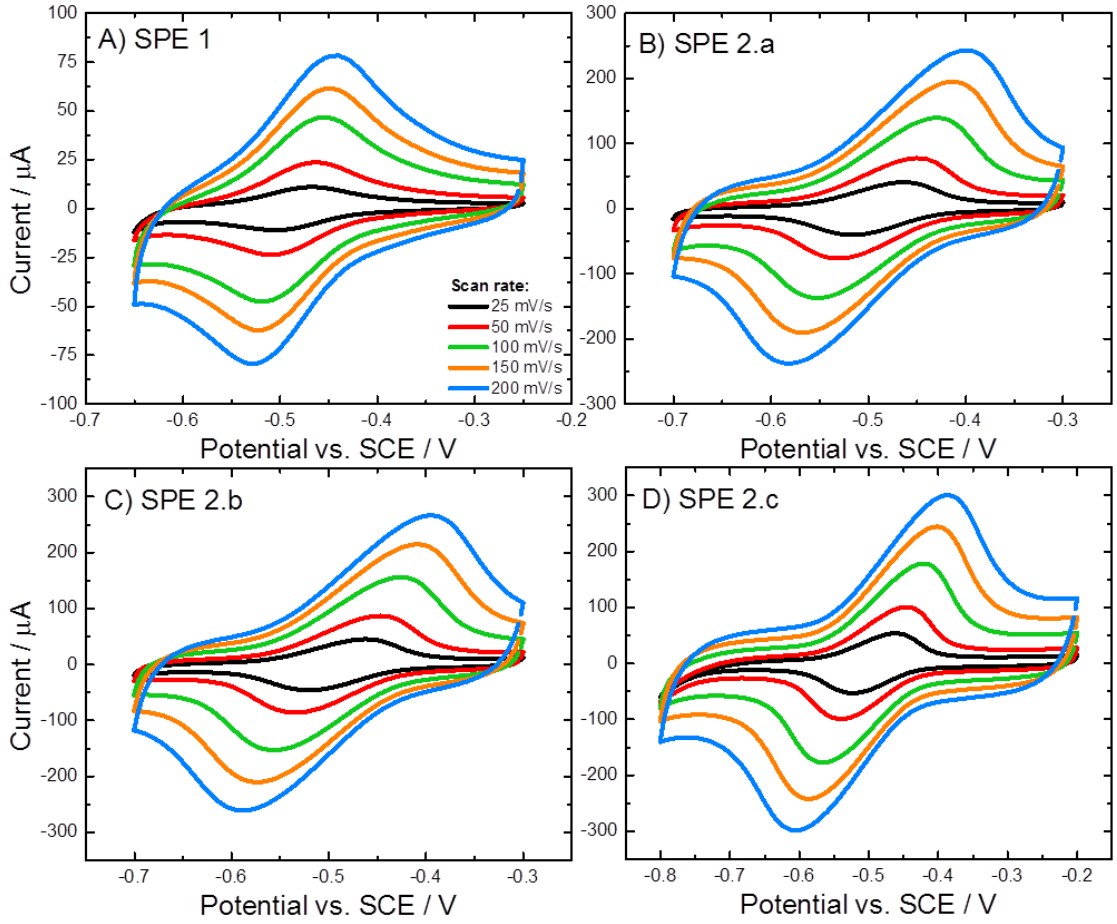

Figure 3.31. *Cyclic voltammograms recorded at (A) a SPE 1 and (B-D) SPEs 2 modified with anthraquinone using the two methods described in Scheme 3.6. CVs were carried out in deoxygenated 50 mM phosphate buffer (pH 7) at different scan rates from 25 to 200 mV/s.*

Table 3.2. *AQ surface coverages for some SPEs 1 and SPEs 2 estimated from the integration of the redox peaks in the CVs recorded at 50 mV/s (red lines in Figure 3.31).*

Electrode	Surface coverage[1] (mol/cm^2)	Surface coverage[2] (mol/g)
SPE 1	1.3×10^{-9}	-
SPE 2.a	5.1×10^{-9}	3.2×10^{-5}
SPE 2.b	5.7×10^{-9}	3.5×10^{-5}
SPE 2.c	7.0×10^{-9}	4.4×10^{-5}

[1]Surface coverage normalised to the geometrical area of SPEs (≈ 0.12 cm²).
[2]Surface coverage normalised to the weight of CNTs loaded on each SPE (≈ 20 µL of a 1 g/L solution, which is 2×10^{-5} g)

The fact that the lower AQ surface coverage for SPE 1 was due to a smaller amount of CNTs adsorbed on the electrode is supported also by its lower capacitive current if compared with the one of the SPEs 2 (see Figure 3.32). From the CVs recorded at 50 mV/s, the amplitude of the capacitive currents was estimated around 15-18 µA for SPE 1 (orange dashed line) and 40 µA for SPEs 2 (green dashed lines). This means that the active area of SPE 1 is smaller than the one of the SPEs 2 because of a lower amount of CNTs.

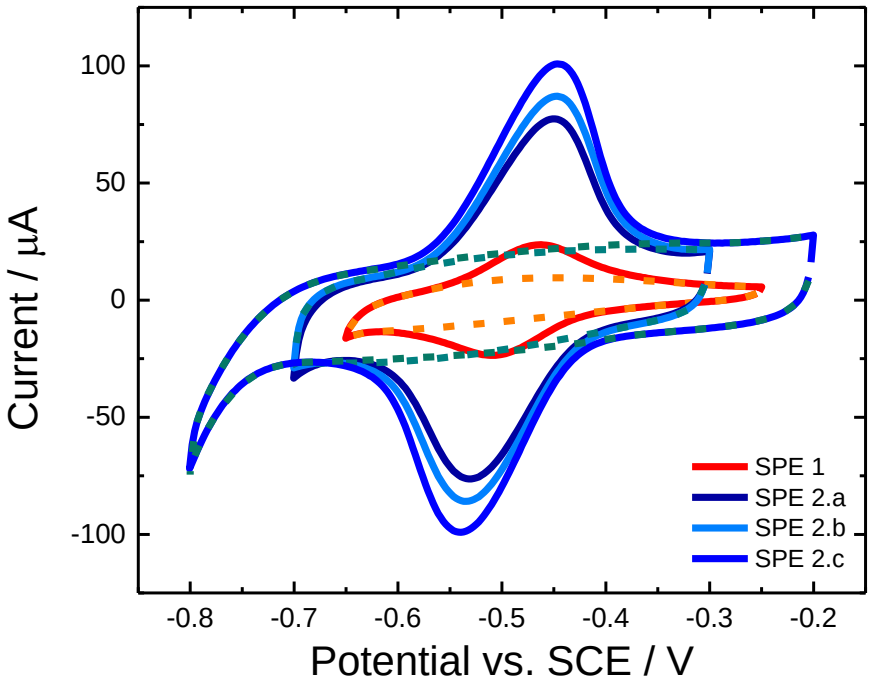

Figure 3.32. *Cyclic voltammograms recorded at a SPE 1 (red) and three SPEs 2 (blue) modified with AQ using the two methods described in Scheme 3.6. The CVs were carried out in deoxygenated 50 mM phosphate buffer (pH 7) scanning the potential at 50 mV/s. The dashed lines represent the capacitive currents.*

From the voltammograms in Figure 3.31 we can also notice that the peak-to-peak separation is more emphasised for the SPEs 2 than for SPE 1. This becomes clearer when we plot the difference between the peak potential (E_p) and the half-wave potential ($E_{1/2}$), both for cathodic and anodic current, versus the scan rate (Figure 3.33). The peak-to-peak separation is about 90 mV at 200 mV/s for SPE 1 (red circles), while it is about 220 mV at the same scan rate for SPE 2.c (blue squares). Such a greater peak-to-peak separation for the SPEs 2 can be explained with a slower electrode kinetics if compared with SPE 1. This may be due to the fact that, when AQ is coupled to the CNTs in solution (second method), all the

CNTs are modified with AQ but, after they were adsorbed on the electrode, not all of them are easily reached by the buffer solution, hence slowing down the kinetics of the immobilised AQ. Otherwise, another possible cause is the fact that the AQ redox reactions generate or consume H^+ and, for high coverage of AQ (such as in the case of SPEs 2), the pH can change locally during cycling, leading to a wider peak-to-peak separation. On the other hand, when the AQ coupling is performed with the CNTs already adsorbed on the electrode (first method), only the CNTs easily reached by the solution would be modified with AQ, being the same CNTs that will be wet by the buffer during the cycling voltammetry.

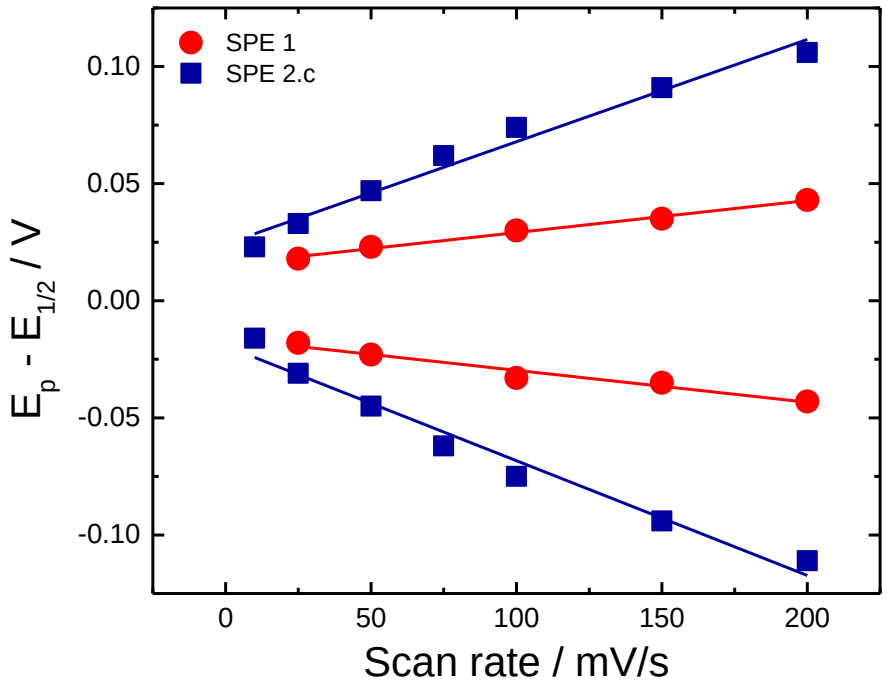

Figure 3.33. *Difference between peak potential and half-wave potential at different scan rates for SPE 1 (red) and SPE 2.c (blue). Lines: linear fitting.*

Finally, the stability of the AQ-modified CNTs (CNTs 2, prepared using the second method) was tested by analysing the SPEs 2 after 5 days from the preparation of the electrodes. All three SPEs 2 showed very intense redox peaks also on the fifth day (see Figure 3.34), with a small decrease in the AQ surface coverage between 10-15 %, which may be due to the loss of some AQ molecules from the electrodes. We do not think there was loss of the CNTs from the electrode surface as the capacitive currents were basically the same as the ones obtained on the first day.

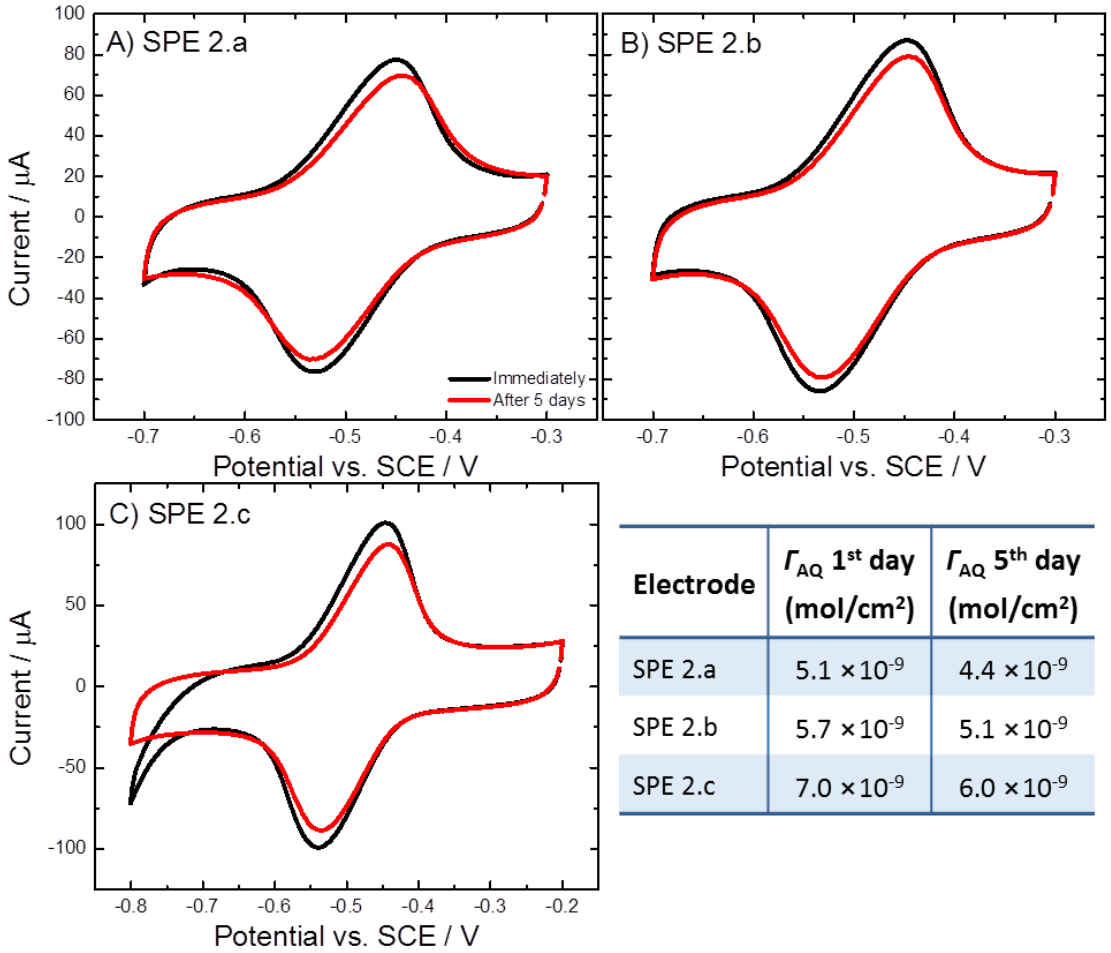

Electrode	Γ_{AQ} 1st day (mol/cm²)	Γ_{AQ} 5th day (mol/cm²)
SPE 2.a	5.1×10^{-9}	4.4×10^{-9}
SPE 2.b	5.7×10^{-9}	5.1×10^{-9}
SPE 2.c	7.0×10^{-9}	6.0×10^{-9}

Figure 3.34. *Cyclic voltammograms recorded at three AQ-modified SPEs 2 on the first (black) and fifth day (red). The CVs were carried out in deoxygenated 50 mM phosphate buffer (pH 7) scanning the potential at 50 mV/s. The table reports the values of AQ surface coverage normalised for the electrode geometrical area (≈ 0.12 cm²) on the first and fifth day.*

3.6.3 Solid-phase functionalization of CNTs with maleimide

Given that the solid-phase modification of CNTs with diazonium salt and anthraquinone was successful, we moved on to the modification of CNTs with maleimide, suitable for the covalent immobilization of cysteine-modified CDH variants. Scheme 3.7 shows the entire modification process of the carboxylic acid-functionalised CNTs. The first step (a: attachment of the diazonium salt) was the same as in Scheme 3.6, producing the CNTs 1 after the Boc deprotection (step b). Then, the 6C-spacer (*N*-Boc-6-aminohexanoic acid) and the passivating group (acetic acid in this case) were coupled to the amino-modified CNTs 1 to form a two-component monolayer on the CNT surface (step c), giving the CNTs 3 after

another step of Boc deprotection. Finally, the maleimide was coupled to the CNTs 3 to give the CNTs 4.

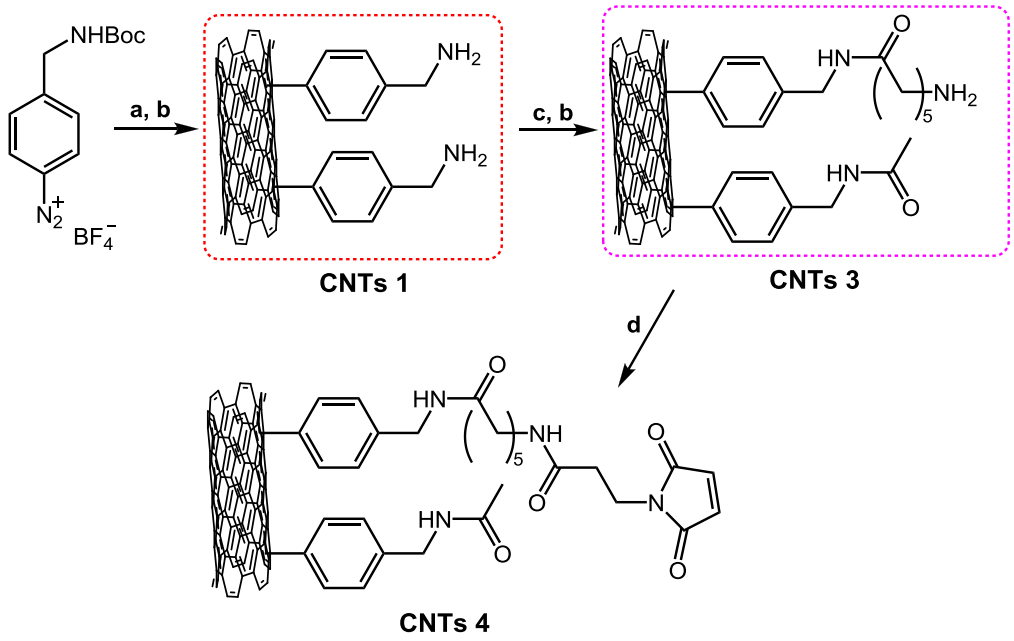

Scheme 3.7. *Sequential solid-phase modification of CNTs with maleimide. Reagents and conditions: a) carboxylic acid-functionalised CNTs and diazonium salt in DMF, heated at 60 °C under reflux (overnight); b) CNTs in 4 M HCl in dioxane, stirred strongly at RT (1 h); c) CNTs 1 dissolved in a DMF solution of N-Boc-6-aminohexanoic acid, acetic acid, EDC and NHS (overnight); d) CNTs 3 dissolved in a DMF solution of N-maleoyl-β-alanine, EDC and NHS (overnight).*

The CNTs 4 were dissolved in a DMF/water (4:1) solution to obtain a 1 g/L suspension. After sonication, the suspension was drop cast on AuSPEs and let dry overnight. Therefore, 10 µL of D813-CDH solution (in phosphate buffer, pH 7) were placed on each SPE and let react for 1 hour at room temperature.

The electrode modified with CNTs 4 and CDH was tested by CV in Tris/$CaCl_2$ buffer (pH 7.4), using glucose as the substrate. The results reported in Figure 3.35-A show a very high catalytic current starting at about -0.2 V *vs.* SCE and reaching 2 µA at 0.0 V when 70 mM glucose was added in solution. A control experiment was performed with a AuSPE modified with the original, unmodified CNTs (SPE 0). The same amount of D813-CDH was drop cast on this second electrode and let react for 1 hour at RT as before. The SPE 0 was tested by CV in the same conditions (Figure 3.35-B) showing a much lower catalytic current that reached a maximum of 0.4 µA with 70 mM glucose. This confirmed the successful modification of CNTs with maleimide since a greater amount of CDH molecules

were immobilised on the SPE 4, producing a higher catalytic current if compared with the unmodified CNTs.

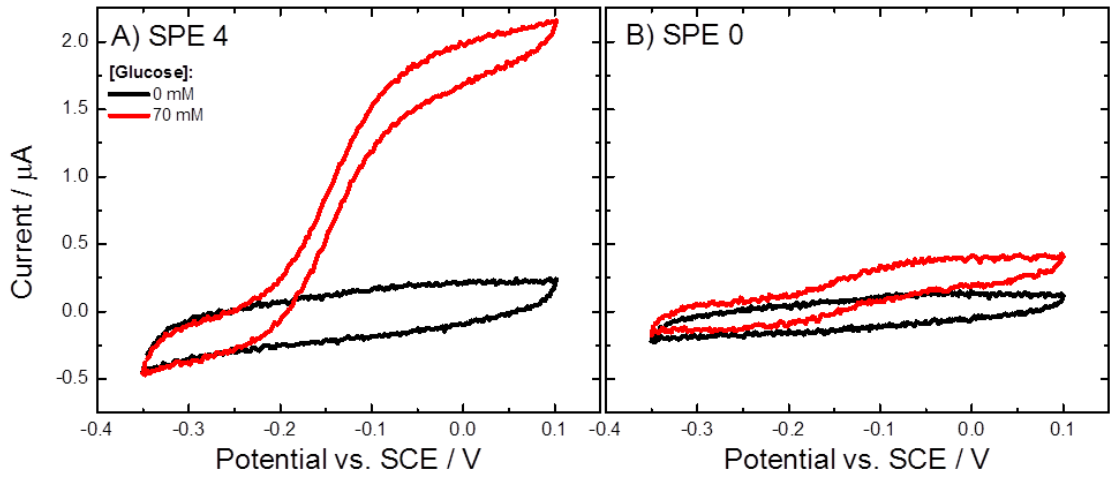

Figure 3.35. *CVs recorded at (A) a SPE 4 and (B) a SPE 0 modified with D813-CDH, in deoxygenated 50 mM Tris buffer (pH 7.4), containing 30 mM $CaCl_2$ (black) and after the addition of 70 mM glucose (red). The potential was swept at 1 mV/s. A) SPE 4 was modified with CNTs 4 (maleimide-functionalised); B) SPE 0 was modified with bare carboxylic acid-functionalised CNTs.*

3.7 Conclusion

In this Chapter we showed the stable, site-specific immobilization of *Mt*CDH variants at carbon electrodes. Such site-specific immobilization was achieved by reacting maleimide-modified electrodes with CDH variants genetically modified to bear only one free cysteine at their surface. The maleimide-modified electrodes were prepared by using a modular approach that combines electrochemical and solid-phase synthesis, starting with the formation of a two-component monolayer at the electrode surface given by the electrochemical oxidation of two amines. Afterwards, solid-phase synthesis was used to attach a spacer and, finally, the reactive group (maleimide).

The CDH-modified electrodes were tested for the DET and MET, mainly in acetate buffer (pH 5.5), using glucose as the substrate. A control experiment using D- and L-glucose, in Section 3.2.4, proved that the observed catalytic current was actually due to the oxidation of the sugar by the enzyme, excluding the interference of other potential catalysts. Moreover, the mechanisms of the DET and MET, as represented in Scheme 3.4, were verified through several

experiments. The DET pathway was confirmed by: *i*) the non-catalytic voltammetry at two different pHs (5.5 and 7.4) in Section 3.2.1; *ii*) the study of the shape of catalytic voltammograms using Eq. 3.4, proving that they are due to a one-electron process, in Sections 3.2.2 and 3.2.5; *iii*) the effect of $CaCl_2$ that was shown to increase the DET, but not the MET current, in Section 3.4.1, and *iv*) the experiment with papain in Section 3.4.3. The two latter experiments confirmed also the mechanism for the MET using ferrocenecarboxylic acid as mediator, which reacts directly with the FAD thus excluding the haem group from the MET pathway. The use of the ferrocene as mediator highlighted the occurrence of a potential shift for the MET catalytic current that depends on the mediator concentration. In Section 3.3.3, this potential shift was attributed to a very high rate constant for the reaction between the ferrocene and CDH, and the fact that the catalytic reaction is due to the oxidised form of the ferrocene, the ferrocenium ion, whose concentration depends on the applied potential and the ferrocene concentration according to the Nernst equation (Eq. 3.9). It was found that a very small amount of Fc^+, around 1 μM, was sufficient to catalyse the reaction and produce the MET current.

The DET and MET of four different CDH variants, bearing the free cysteine residues in different position at the surface of the flavin domain, were analysed. A potential-dependent Michaelis-Menten equation (Eq. 3.5) was employed to fit the plots of the catalytic current *vs.* glucose concentration and extract some kinetic parameters, such as i_{max}^{APP} and K_M^{APP}, for the four different variants (Table 3.1). The MET analysis, in Section 3.3.1, revealed that three of the four electrodes presented the same amount of immobilised enzyme. Therefore, the differences in the DET curves of those three electrodes (Figure 3.11) can be accounted for different IET or DET rates, due to the different orientation of the enzymes on the electrode. In Table 3.1 we can note that there is a big difference between the kinetic parameters extracted from DET data and those from MET data: this will be explained in the next Chapter.

Finally, some tests were performed to prove the great stability of our covalent modification method if compared with physically adsorbed enzyme. The experiments about the stability over the time, in Section 3.5.1, proved that our maleimide-modified electrodes can keep CDH stable and active for more than

two months, at different pH, while physically modified electrodes lost their activity more rapidly. In addition, in Section 3.5.2, covalently modified electrodes were found capable of retaining a greater number of CDH molecules and in a better orientation for the DET if compared with physically modified electrodes. Lastly, a control experiment using Triton X-100, in Section 3.5.3, further confirmed the difference between covalently and physically modified electrodes, as its addition in solution caused the DET current to increase in the case of maleimide-modified electrodes and to decrease in the case of unmodified ones.

The very high storage stability found for our CDH-modified electrodes is not so surprising, in fact it is reported that biosensors using CDH as recognition molecule have a very high stability and can also be used for years, being even more stable than electrodes based on glucose oxidase [71]. Some recent papers report that biosensors based on CDH cross-linked on the electrodes or entrapped in polymers were active for one or more months [79,82,83], in agreement with what we found in this work. Also other enzymes have been found stable for long periods, for example laccase and glucose dehydrogenase entrapped in redox polymers presented a storage stability of several months [140,141].

The last Section (Section 3.6) presented a method to functionalise CNTs with maleimide (or other organic functionalities) before adsorbing them on the electrode surface. This was done through a solid-phase modification of the CNTs in solution employing the spontaneous grafting of diazonium salts to carbon surfaces at high temperatures. The CNTs have been first modified with a redox probe, anthraquinone, in order to verify the applicability of the method already described in a previous work by our group [139]. Therefore, the procedure was adapted to functionalise the CNTs with maleimide, suitable for the covalent immobilization of cysteine-modified CDH variants. The maleimide-modified CNTs were then adsorbed on gold SPEs showing, after reacting CDH for just 1 hour, a catalytic current five times higher than that obtained with unmodified CNTs.

Chapter 4:

Simulations of CDH catalytic voltammograms

In the previous Chapter, we showed the stable, site-specific immobilization of CDH variants at GC/CNT electrodes, reporting several experiments that confirmed the DET and MET of the enzyme, as well as the great stability of the immobilization method. However, we have not analysed in depth the kinetics of the CDH catalytic reactions, so that many doubts remained about the rate limiting step, the kinetic constants of each reaction and the meaning of the parameters extracted by the Michaelis-Menten fitting. In this Chapter, we will try to fill this gap describing step by step the kinetics of the CDH electrode reactions, both for the direct and mediated electron transfer, and assigning to each reaction a kinetic constant. Therefore, we will derive a potential-dependent Michaelis-Menten equation, which was already used to fit the experimental data in Chapter 3 (Eq. 3.5), and use it to simulate the catalytic voltammograms experimentally recorded at CDH-modified electrodes.

4.1 Kinetic model for the CDH electrode reactions

4.1.1 Mechanisms of the direct and mediated electron transfer

The mechanisms of the direct and mediated electron transfers have been briefly explained in Section 1.4 (see Figure 1.4), and then investigated through specific experiments in the previous Chapter, especially in Section 3.4 (see Scheme 3.4). At this point, we will need to fully examine each single reaction that constitutes the electron pathway of the CDH catalytic process at an electrode surface, in order to write all the kinetic constants for each reaction step. From that, we will be able to write a potential-dependent Michaelis-Menten equation that includes all the different rate constants and can simulate the current of the CDH electrodic reaction.

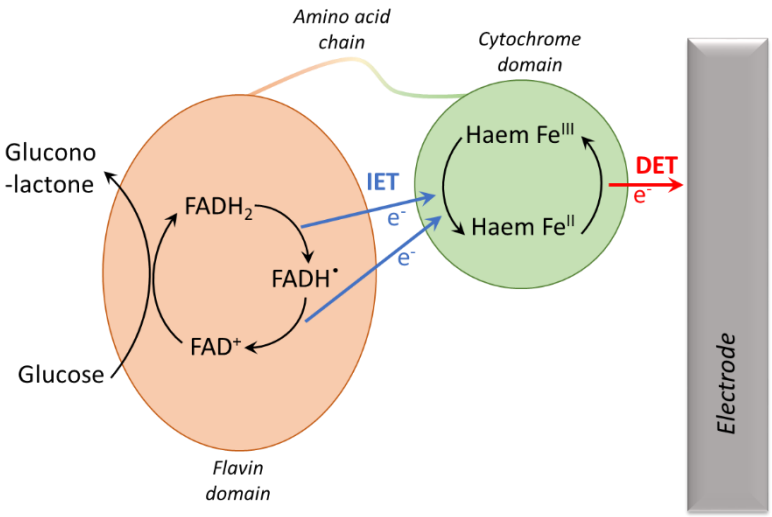

Figure 4.1. *Schematic representation of the DET mechanism of CDH (adapted from [73]).*

Figure 4.1 shows a schematic representation of the oxidation of an aldose sugar (glucose in this case) at an electrode surface via CDH. The mechanism has been proven by several experiments in the previous Chapter, in particular in Sections 3.2.1, 3.2.2, 3.4.1 and 3.4.3, and can be observed also in Scheme 3.4. The first step is the oxidation of glucose to gluconolactone, with the concomitant one-step, two-electron reduction of the FAD group to $FADH_2$ [73]. $FADH_2$ is then oxidised back via two sequential one-electron reactions with the haem group, which is present in the CDH cytochrome domain and acts as a one-electron acceptor for FAD. The

reaction between FAD and haem is denominated interdomain electron transfer (IET): $FADH_2$ is first oxidised to its semiquinone form (the radical $FADH^{\cdot}$) transferring one electron to the haem, then $FADH^{\cdot}$ is oxidised to FAD^+ transferring also the second electron to the haem. In this process, the haem group is reduced (and oxidised back at the electrode surface) twice for each complete oxidation of FAD. During its oxidation, the haem transfers one electron to the electrode surface in a process called direct electron transfer (DET).

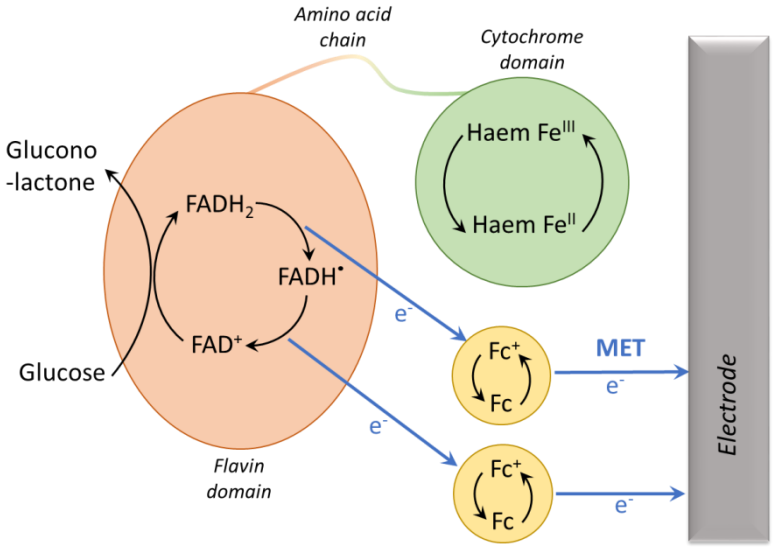

Figure 4.2. *Schematic representation of the MET mechanism of CDH using ferrocene (Fc) as mediator.*

On the other hand, Figure 4.2 shows a schematic representation of the mediated electron transfer (MET) mechanism of CDH with ferrocene as the mediator. The first steps are the same as previously described for the DET mechanism. Therefore, the oxidation of $FADH_2$ to FAD^+ occurs in two steps transferring the electrons to two molecules of ferrocene, which acts as a one-electron acceptor and in turn transfers the electron to the electrode surface.

To simplify the following text, we will denote FAD^+ as F_1, $FADH^{\cdot}$ as F_2 and $FADH_2$ as F_3. Moreover, the two possible oxidation states of haem will be denoted Fe^{II} and Fe^{III}, and the two oxidation states of the mediator ferrocene will be Fc and Fc^+.

4.1.2 Modelling the CDH kinetics at the electrode surface

In order to understand the kinetics of CDH at the electrode surface, we should start from the simplest description of steady-state enzyme kinetics based on the work of Michaelis and Menten [142]. This treatment assumes that the substrate forms a complex with the enzyme in a reversible step and that equilibrium is maintained between the enzyme (E), the substrate (S) and the enzyme-substrate complex (ES). Irreversible breakdown of the enzyme-substrate complex then yields the product (P) and the free enzyme.

The second assumption in this model is that the concentration of the enzyme-substrate complex can be treated using the steady-state approximation, meaning that it does not vary with the time. Clearly, this is not true immediately after the substrate and the enzyme are mixed together, when the concentration of the complex is building up, and will only be true as long as the substrate is not significantly consumed by the course of the reaction [27].

We can assume that the first step of the CDH catalytic reaction occurs as described by the Michaelis-Menten model, with the substrate forming a complex with FAD^+ (F_1), which will then yield the product and $FADH_2$ (F_3). Table 4.1 gives, in more detail, all the reactions involved with the relative kinetic constants. The first step, the substrate/enzyme reaction to produce the enzyme-substrate complex, can also be described using the Michaelis-Menten constant, K_M:

$$K_M = \frac{k_b + k_{cat}}{k_f} \qquad \text{(Eq. 4.1)}$$

$$\text{or} \qquad K_M = \frac{k_b}{k_f} \qquad \text{if} \quad k_b \gg k_{cat} \qquad \text{(Eq. 4.1a)}$$

In the Michaelis-Menten treatment, the reaction rate (ν), which represents the variation of the substrate or product concentrations with the time, is due to the slowest step, called also “rate determining step” or “rate limiting step”. In the case of the CDH catalytic process, we do not know yet which one of the steps reported in Table 4.1 is the slowest one, as we have not determined yet their kinetic constants. In any case, in the steady state all the different reaction steps

will have the same rate so that we can write ν, for example, for the breakdown of the enzyme-substrate complex (second row in Table 4.1) as follow:

$$\nu = \frac{\mathrm{d[P]}}{\mathrm{d}t} = -\frac{\mathrm{d[S]}}{\mathrm{d}t} = [\mathrm{SF_1}]k_{\mathrm{cat}} \qquad \text{(Eq. 4.2)}$$

Table 4.1. *Reaction steps for the DET and MET oxidation of a sugar via CDH, with the relative kinetic constants.*

Step	Reaction	Kinetic constants
Substrate-enzyme reaction	$\mathrm{S + F_1 \rightleftharpoons (SF_1)}$	$k_{\mathrm{f}}, k_{\mathrm{b}}$
	$\mathrm{(SF_1) \longrightarrow P + F_3}$	k_{cat}
Reoxidation of FAD by haem	$\mathrm{F_3 + Fe^{III} \longrightarrow F_2 + Fe^{II}}$	$k_{\mathrm{int(1)}}$
	$\mathrm{F_2 + Fe^{III} \longrightarrow F_1 + Fe^{II}}$	$k_{\mathrm{int(2)}}$
Reoxidation of FAD by mediator	$\mathrm{F_3 + Fc^{+} \longrightarrow F_2 + Fc}$	$k_{\mathrm{med(1)}}$
	$\mathrm{F_2 + Fc^{+} \longrightarrow F_1 + Fc}$	$k_{\mathrm{med(2)}}$
Electrode reactions	$\mathrm{Fe^{II} \longrightarrow Fe^{III} + e^{-}}$	fast
	$\mathrm{Fc \longrightarrow Fc^{+} + e^{-}}$	fast

At this point, given that we are treating an enzymatic reaction occurring at the electrode surface, we need to define what the current is. An electrochemical reaction at the electrode surface converts the flux of substrate, J_S, into a flux of electrons (current) that flows through the external circuit [27], with the current being given by:

$$i = nFA\,J_{\mathrm{S}} = -nFA\,D_{\mathrm{S}}\left(\frac{\mathrm{d[S]}}{\mathrm{d}x}\right)_{x=0} \qquad \text{(Eq. 4.3)}$$

where F is the Faraday constant, A is the electrode area, D_S is the diffusion coefficient of the substrate and n is the number of electrons involved in the reaction of each molecule of substrate at the electrode. Since, in this case, for each molecule of substrate oxidised via CDH, 2 electrons are taken at the electrode surface (see Figures 4.1 and 4.2), n is equal to 2. However, in the case of an enzymatic reaction the current can also be due to the rate of the reaction

occurring at the electrode surface, if there are no mass transport limitations for the substrate. Since this seems to be the case for our electrodes, as the flux of glucose towards the electrode surface is not limited by a membrane or other restrictions, in Eq. 4.3 we can substitute the flux of substrate J_S with ν given by Eq. 4.2:

$$i = 2FA\nu = 2FA[\mathrm{SF}_1]k_{\mathrm{cat}} \qquad \text{(Eq. 4.4)}$$

This is one possible expression for the current due to an enzymatic reaction. In the case of CDH, since there are several steps involved in the enzymatic reaction as shown in Table 4.1, we could write several different expressions for *i*. However, as we said above, in the steady state the rate of each step will be the same so that it makes no difference to use one expression or the other to determine the current, and we chose to use Eq. 4.4. At this point, to have a usable expression for *i*, we need to find an equation for [SF_1]: this is what we will do in the next Section 4.1.3.

Going back to discuss the reaction steps reported in Table 4.1, it is clear that the kinetics of CDH is more complex than the one of other enzymes, such as glucose oxidase, often used in kinetic models. Unlike glucose oxidase, CDH presents a second active site, haem, located in a second domain, the cytochrome domain, which is not directly involved in the substrate oxidation, but acts as an electron acceptor for FAD. Therefore, once $FADH_2$ (F_3) is released from the enzyme-substrate complex, it can be oxidised back by transferring two electrons to the haem (Figure 4.1) or to a soluble electron acceptor, the mediator (Figure 4.2). Since both the haem and the mediator used in this work, ferrocene, are $1e^-$ acceptors, the reoxidation of the flavin group occurs in two steps in both cases passing through a semiquinone intermediate, $FADH^{\cdot}$ (F_2). Each oxidation step is described by a kinetic constant (Table 4.1), so that we will have two kinetic constants for the reoxidation of FAD by haem ($k_{\mathrm{int(1)}}$ and $k_{\mathrm{int(2)}}$) and other two for the reoxidation of FAD by the mediator ($k_{\mathrm{med(1)}}$ and $k_{\mathrm{med(2)}}$).

Finally, the last step reported in Table 4.1 is represented by the electrode reactions, which are the reoxidation of the haem and reoxidation of the mediator by transfer of one electron to the electrode. In Section 3.2.2 we have confirmed that the electron transfer of the haem to the electrode surface is fast and

reversible, and we assume the same for the ferrocene/electrode reaction, so that they can be described using the Nernst equation as we will see below.

It could also be possible that the ferrocene reacts with the haem, adding then an extra step in the reaction mechanism (not reported in Table 4.1). However, this second type of mediated electron transfer was excluded by some experiments reported in Sections 3.4.1 and 3.4.3. In any case, if the reaction of the haem with the electrode is fast, then the Nernst equation applies and the addition of mediator cannot make it any faster. Therefore, we will not take this second type of MET into account in our kinetic model here.

4.1.3 Derivation of a potential-dependent Michaelis-Menten equation

Considering all the assumptions made in the previous Section, we try here to build a potential-dependent Michaelis-Menten model that can be applied to the electrode kinetics of CDH. To do that, we need to find a usable expression for $[SF_1]$ that we can substitute in the equation for the current (Eq. 4.4). Firstly, we can assume that the total amount of immobilised enzyme is given by:

$$[\text{enz}] = [SF_1] + [F_1] + [F_2] + [F_3] \qquad \text{(Eq. 4.5)}$$

and the total amount of mediator will be:

$$[M] = [Fc] + [Fc^+] \qquad \text{(Eq. 4.6)}$$

If we assume that the electron transfer kinetics of the haem and the mediator are fast and reversible, as we have already said, then we can apply the Nernst equation for the two cases:

$$E = E'_{Fe} + \frac{RT}{F} ln\left(\frac{[Fe^{III}]}{[Fe^{II}]}\right) \qquad \text{(for the haem)} \qquad \text{(Eq. 4.7)}$$

$$E = E'_{Fc} + \frac{RT}{F} ln\left(\frac{[Fc^+]}{[Fc]}\right) \qquad \text{(for the mediator)} \qquad \text{(Eq. 4.8)}$$

Therefore, the concentration of ferrocenium ion (the oxidised form of ferrocene, Fc^+), which is responsible for the reoxidation of FAD, will depend on the applied potential and be given by rearranging the Nernst equation for the mediator case (Eq. 4.8), applying the condition given by Eq. 4.6:

$$\frac{[Fc^+]}{[Fc]} = \exp\left\{\frac{F}{RT}(E - E'_{Fc})\right\} \quad \Longrightarrow \quad [Fc^+] = \frac{[M]\exp(\vartheta_{Fc})}{\exp(\vartheta_{Fc}) + 1} \qquad \text{(Eq. 4.9)}$$

$$\text{with} \quad \vartheta_{Fc} = \left\{\frac{F}{RT}(E - E'_{Fc})\right\} \qquad \text{(Eq. 4.9a)}$$

For the haem the situation is more complicated and depends on whether we assume that the haem of a given enzyme molecule can oxidise the FAD of a different enzyme molecule or not. For the moment, we will assume that this is not the case in order to simplify the calculations. In this case, the haem of a particular enzyme molecule could be in the reduced (Fe^{II}) or oxidised (Fe^{III}) state. We can call Φ_{FeII} the probability for the haem to be in the reduced state, and Φ_{FeIII} the probability to be in the oxidised state, so that:

$$\phi_{FeII} + \phi_{FeIII} = 1 \qquad \text{(Eq. 4.10)}$$

Therefore, the probability that the haem of a particular CDH molecule is in its oxidised form, which is responsible for the reoxidation of FAD, will also depends on the applied potential and be given by rearranging the Nernst equation for the haem case (Eq. 4.7), applying the conditions given by Eq. 4.10:

$$\phi_{FeIII} = \frac{\exp(\vartheta_{Fe})}{\exp(\vartheta_{Fe}) + 1} \qquad \text{(Eq. 4.11)}$$

$$\text{with} \quad \vartheta_{Fe} = \left\{\frac{F}{RT}(E - E'_{Fe})\right\} \qquad \text{(Eq. 4.11a)}$$

We can now write the kinetic expressions for all the different states of the enzyme as follow, looking at the reactions in Table 4.1:

$$\frac{\mathrm{d}[\mathrm{F_1}]}{\mathrm{d}t} = -k_\mathrm{f}[\mathrm{S}][\mathrm{F_1}] + k_\mathrm{b}[\mathrm{SF_1}] + k_{\mathrm{int(2)}}[\mathrm{F_2}]\phi_\mathrm{FeIII} + k_{\mathrm{med(2)}}[\mathrm{F_2}][\mathrm{Fc^+}] \qquad \text{(Eq. 4.12)}$$

$$\frac{\mathrm{d}[\mathrm{F_2}]}{\mathrm{d}t} = k_{\mathrm{int(1)}}[\mathrm{F_3}]\phi_\mathrm{FeIII} - k_{\mathrm{int(2)}}[\mathrm{F_2}]\phi_\mathrm{FeIII} + k_{\mathrm{med(1)}}[\mathrm{F_3}][\mathrm{Fc^+}] - k_{\mathrm{med(2)}}[\mathrm{F_2}][\mathrm{Fc^+}] \qquad \text{(Eq. 4.13)}$$

$$\frac{\mathrm{d}[\mathrm{F_3}]}{\mathrm{d}t} = k_\mathrm{cat}[\mathrm{SF_1}] - k_{\mathrm{int(1)}}[\mathrm{F_3}]\phi_\mathrm{FeIII} - k_{\mathrm{med(1)}}[\mathrm{F_3}][\mathrm{Fc^+}] \qquad \text{(Eq. 4.14)}$$

$$\frac{\mathrm{d}[\mathrm{SF_1}]}{\mathrm{d}t} = k_\mathrm{f}[\mathrm{S}][\mathrm{F_1}] - k_\mathrm{b}[\mathrm{SF_1}] - k_\mathrm{cat}[\mathrm{SF_1}] \qquad \text{(Eq. 4.15)}$$

These expressions will be used below to write the concentrations of all the different forms of the enzyme (F_1, F_2 and F_3) and the enzyme-substrate complex, applying the steady-state approximation as described in the Michaelis-Menten model. For that, we assume that the concentrations of SF_1 as well as F_1, F_2 and F_3 do not vary with the time once the steady state is reached, so that:

$$\frac{\mathrm{d}[\mathrm{F_1}]}{\mathrm{d}t} = \frac{\mathrm{d}[\mathrm{F_2}]}{\mathrm{d}t} = \frac{\mathrm{d}[\mathrm{F_3}]}{\mathrm{d}t} = \frac{\mathrm{d}[\mathrm{SF_1}]}{\mathrm{d}t} = 0 \qquad \text{(Eq. 4.16)}$$

Moreover, we assume that $[Fc^+]$ and Φ_{FeIII} are constant at a given potential and that [S] is also constant and the same at the electrode surface as in the bulk solution. Given that, we can now write the concentration of the substrate-enzyme complex, $[SF_1]$, as follows using Eq. 4.15:

$$[\mathrm{SF_1}] = \frac{k_\mathrm{f}[\mathrm{S}][\mathrm{F_1}]}{k_\mathrm{b} + k_\mathrm{cat}} \qquad \text{(Eq. 4.17)}$$

The concentration of $FADH_2$, $[F_3]$, using Eq. 4.14 will be:

$$[\mathrm{F_3}] = \frac{k_\mathrm{cat}[\mathrm{SF_1}]}{k_{\mathrm{int(1)}}\phi_\mathrm{FeIII} + k_{\mathrm{med(1)}}[\mathrm{Fc^+}]} \qquad \text{(Eq. 4.18)}$$

The concentration of FADH, $[F_2]$, using Eq. 4.13 and Eq. 4.18 in substitution of $[F_3]$ will be:

$$[F_2] = \frac{[F_3]\left(k_{int(1)}\phi_{FeIII} + k_{med(1)}[Fc^+]\right)}{k_{int(2)}\phi_{FeIII} + k_{med(2)}[Fc^+]}$$

$$= \frac{k_{cat}[SF_1]\left(k_{int(1)}\phi_{FeIII} + k_{med(1)}[Fc^+]\right)}{\left(k_{int(1)}\phi_{FeIII} + k_{med(1)}[Fc^+]\right)\left(k_{int(2)}\phi_{FeIII} + k_{med(2)}[Fc^+]\right)}$$

$$= \frac{k_{cat}[SF_1]}{k_{int(2)}\phi_{FeIII} + k_{med(2)}[Fc^+]} \qquad \text{(Eq. 4.19)}$$

The concentration of FAD^+, $[F_1]$, using Eq. 4.12 and Eq. 4.19 in substitution of $[F_2]$ will be:

$$[F_1] = \frac{[F_2]\left(k_{int(2)}\phi_{FeIII} + k_{med(2)}[Fc^+]\right) + k_b[SF_1]}{k_f[S]}$$

$$= \frac{k_{cat}[SF_1] + k_b[SF_1]}{k_f[S]} \qquad \text{(Eq. 4.20)}$$

Substituting Eq. 4.17, 4.18, 4.19 and 4.20 in Eq. 4.5, the total amount of immobilised enzyme will be:

$$[enz] = [SF_1]\left\{1 + \frac{k_{cat} + k_b}{k_f[S]} + \frac{k_{cat}}{k_{int(2)}\phi_{FeIII} + k_{med(2)}[Fc^+]} + \frac{k_{cat}}{k_{int(1)}\phi_{FeIII} + k_{med(1)}[Fc^+]}\right\} \qquad \text{(Eq. 4.21)}$$

So that, rearranging Eq. 4.21, the concentration of the substrate-enzyme complex is given by:

$$[SF_1] = \frac{[enz]}{\left\{1 + \frac{k_{cat} + k_b}{k_f[S]} + \frac{k_{cat}}{k_{int(2)}\phi_{FeIII} + k_{med(2)}[Fc^+]} + \frac{k_{cat}}{k_{int(1)}\phi_{FeIII} + k_{med(1)}[Fc^+]}\right\}} \qquad \text{(Eq. 4.21a)}$$

Substituting this expression for $[SF_1]$ in Eq. 4.4, the current will be given by:

$$i = \frac{2FAk_{\mathrm{cat}}[\mathrm{enz}]}{\left\{1 + \frac{k_{\mathrm{cat}} + k_{\mathrm{b}}}{k_{\mathrm{f}}[\mathrm{S}]} + \frac{k_{\mathrm{cat}}}{k_{\mathrm{int(2)}}\phi_{\mathrm{FeIII}} + k_{\mathrm{med(2)}}[\mathrm{Fc^+}]} + \frac{k_{\mathrm{cat}}}{k_{\mathrm{int(1)}}\phi_{\mathrm{FeIII}} + k_{\mathrm{med(1)}}[\mathrm{Fc^+}]}\right\}}$$

(Eq. 4.22)

Knowing that $K_{\mathrm{M}} = (k_{\mathrm{b}} + k_{\mathrm{cat}})/k_{\mathrm{f}}$, as defined in Eq. 4.1, Eq. 4.22 can be rewritten as follow:

$$i = \frac{2FAk_{\mathrm{cat}}[\mathrm{enz}]}{\left\{1 + \frac{K_{\mathrm{M}}}{[\mathrm{S}]} + \frac{k_{\mathrm{cat}}}{k_{\mathrm{int(2)}}\phi_{\mathrm{FeIII}} + k_{\mathrm{med(2)}}[\mathrm{Fc^+}]} + \frac{k_{\mathrm{cat}}}{k_{\mathrm{int(1)}}\phi_{\mathrm{FeIII}} + k_{\mathrm{med(1)}}[\mathrm{Fc^+}]}\right\}}$$

(Eq. 4.22a)

In this equation for the current, we can highlight that the first term at the denominator ($1 + K_{\mathrm{M}}/[\mathrm{S}]$) is due to the enzyme/substrate kinetics, while the other two terms are due to the interdomain electron transfer (IET) or the flavin/mediator kinetics. These two terms can be simply written as $k_{\mathrm{cat}}/k_{\mathrm{x}}(x)$, with $k_{\mathrm{x}}(x)$ representing the reoxidation kinetics of FAD, either due to the haem or to the mediator, and being equal to:

$$k_{\mathrm{x}}(x) = \frac{\left(k_{\mathrm{int(2)}}\phi_{\mathrm{FeIII}} + k_{\mathrm{med(2)}}[\mathrm{Fc^+}]\right)\left(k_{\mathrm{int(1)}}\phi_{\mathrm{FeIII}} + k_{\mathrm{med(1)}}[\mathrm{Fc^+}]\right)}{\left(k_{\mathrm{int(1)}} + k_{\mathrm{int(2)}}\right)\phi_{\mathrm{FeIII}} + \left(k_{\mathrm{med(1)}} + k_{\mathrm{med(2)}}\right)[\mathrm{Fc^+}]} \qquad \text{(Eq. 4.23)}$$

$k_{\mathrm{x}}(x)$ can be simplified depending on whether the IET or the MET is the dominant process, becoming therefore:

$$k_{\mathrm{x}}{}^{\mathrm{int}}(x) = \frac{k_{\mathrm{int(1)}} \cdot k_{\mathrm{int(2)}}}{k_{\mathrm{int(1)}} + k_{\mathrm{int(2)}}}\phi_{\mathrm{FeIII}} \qquad \text{(for IET dominant)} \qquad \text{(Eq. 4.23a)}$$

$$k_{\mathrm{x}}{}^{\mathrm{med}}(x) = \frac{k_{\mathrm{med(1)}} \cdot k_{\mathrm{med(2)}}}{k_{\mathrm{med(1)}} + k_{\mathrm{med(2)}}}[\mathrm{Fc^+}] \qquad \text{(for MET dominant)} \qquad \text{(Eq. 4.23b)}$$

Moreover, if we consider the rates of the two semioxidation reactions being the same, for both the IET and MET case, as we will discuss below, $k_x(x)$ can be simplified as follow:

$$k_x(x) = \frac{k_{int}\phi_{FeIII} + k_{med}[Fc^+]}{2} \quad \text{(Eq. 4.24)}$$

$$k_x{}^{int}(x) = \frac{k_{int}}{2}\phi_{FeIII} \quad \text{(for IET dominant)} \quad \text{(Eq. 4.24a)}$$

$$k_x{}^{med}(x) = \frac{k_{med}}{2}[Fc^+] \quad \text{(for MET dominant)} \quad \text{(Eq. 4.24b)}$$

Therefore, the equation for the current (Eq. 4.22a) can now be written in a simplified form as follow:

$$i = \frac{2FAk_{cat}[enz]}{\left\{1 + \frac{K_M}{[S]} + \frac{k_{cat}}{k_x(x)}\right\}} = \frac{2FAk_{cat}[enz][S]}{[S]\left(1 + \frac{k_{cat}}{k_x(x)}\right) + K_M} \quad \text{(Eq. 4.25)}$$

$$\text{or} \qquad i = \frac{i_{max}{}^{APP}[S]}{[S] + K_M{}^{APP}} \quad \text{(Eq. 4.26)}$$

$$\text{with} \quad i_{max}{}^{APP} = 2FAk_{cat}{}^{APP}[enz] \quad \text{(Eq. 4.26a)}$$

$$k_{cat}{}^{APP} = \frac{k_{cat}}{1 + \frac{k_{cat}}{k_x(x)}} \quad \text{(Eq. 4.26b)}$$

$$K_M{}^{APP} = \frac{K_M}{1 + \frac{k_{cat}}{k_x(x)}} \quad \text{(Eq. 4.26c)}$$

Eq. 4.26 presents the same form of the Michaelis-Menten equation for enzymatic reactions [142], with the difference that our equation applies for enzymatic reactions at the electrode surface and, therefore, the dependent parameter here is the current rather than the reaction rate. Eq. 4.26 is actually the equation that has been used to fit the experimental data in the previous chapter (Eq. 3.5): therefore, the parameters extracted from the fitting in Chapter 3 are actually apparent i_{max} and K_M.

4.2 Simulations of catalytic voltammograms

4.2.1 Definition of parameters and constants

Using the software Excel 2013, we wrote the final equation for the current that has been obtained in the previous section, Eq. 4.25. As we can see in the equation, the current depends on the applied potential through the term $k_x(x)$, which is expressed in Eq. 4.23. In fact, $k_x(x)$ depends on the kinetic constants of the IET and flavin/mediator kinetics (k_{int} and k_{med}), on the concentration of ferrocenium (Fc^+) and the amount of haem in the oxidised state (Φ_{FeIII}). The two latter parameters provide the dependence of the current on the potential, since the amount of ferrocene and haem in their respective oxidised forms depends on the applied potential as we can see from Eq. 4.9 and 4.11.

The constant parameters that have been used to build Eq. 4.25, which depends on Eq. 4.23 for the term $k_x(x)$, which in turn depends on Eq. 4.9 and 4.11 for the terms $[Fc^+]$ and Φ_{FeIII}, are reported in Table 4.2.

Table 4.2. *Constant parameters used in the equation for the current (Eq. 4.25).*

Parameter	Value
F (Faraday constant)	96 485 A s mol^{-1}
R (Gas constant)	8.314 J K^{-1} mol^{-1}
T (room temperature)	293 K
E_{Fc}' (redox potential of ferrocene)*	0.275 V *vs.* SCE
E_{Fe}' (redox potential of haem)**	-0.13 V *vs.* SCE

**E_{Fc}' is the redox potential of ferrocenecarboxylic acid. The value reported here was experimentally measured at a CDH-modified GC/CNT electrode in 50 mM acetate buffer (pH 5.5) containing 30 mM $CaCl_2$ and 1 mM ferrocenecarboxylic acid, in the absence of substrate (see Figure 3.12 in Chapter 3). It is in agreement with values found in the literature [121] and is pH independent.*

***E_{Fe}' is the redox potential of MtCDH haem group in the conditions of our experiments. The value reported here was obtained from experimental CVs of CDH-modified GC/CNT electrodes in the absence of substrate, as reported in Section 3.2.1. Moreover, E_{Fe}' is also pH independent as shown in Figure 3.3.*

Another constant parameter in Eq. 4.25 is the electrode area, A. However, A may not be constant from electrode to electrode as we used home-made carbon nanotube electrodes, for which it is very difficult to exactly control the active area. Even though we tried to prepare the electrodes as much as possible in a reproducible way, we cannot certainly affirm that all the electrodes used in this work were exactly the same. This is because it has been a work of almost three years and, during the period, some conditions may have changed, for example the solution of carbon nanotubes used to prepare the electrodes. Another problem in defining A arises from the difficulty in measuring the active area of carbon nanotube electrodes. As we will explain in Section 5.1.1, we could only have an estimation of the surface area of our electrodes, which was about 14 cm^2 using two different methods.

Nevertheless, for our purpose it is not so important to know the real value of A, since in our system the enzyme is immobilised on the electrode, so that the enzyme concentration corresponds to the enzyme surface coverage, Γ_{enz}:

$$[\text{enz}] = \Gamma_{\text{enz}} = \frac{m_{\text{enz}}}{A} \qquad \text{(Eq. 4.27)}$$

where m_{enz} is the number of moles of the immobilised enzyme. For that, the electrode area can be eliminated from Eq. 4.25, by substitution of [enz] given by Eq. 4.27, becoming therefore:

$$i = \frac{2Fk_{\text{cat}}m_{\text{enz}}[\text{S}]}{[\text{S}]\left(1 + \frac{k_{\text{cat}}}{k_{\text{x}}(x)}\right) + K_{\text{M}}} \qquad \text{(Eq. 4.28)}$$

The other parameters to define are the kinetic constants and the Michaelis-Menten constant, since the concentration of substrate, mediator and the moles of enzyme depend on the specific experiment. A particular consideration has now to be made about the kinetic constants relative to the reoxidation reactions of FAD by haem ($k_{int(1)}$ and $k_{int(2)}$) and by the mediator ($k_{med(1)}$ and $k_{med(2)}$). As shown in Table 4.1, each of these constants represents the reaction rate of one semioxidation reaction of the FAD group, corresponding to a full reduction of the haem or mediator. Therefore, since they represent very similar reactions, they might have the same or very similar values (with k_{int} being however different from k_{med}).

In fact, we do not have any evidence that the oxidation of F_3 is faster or slower that the oxidation of F_2. The only example found in the literature is for a similar dehydrogenase belonging to the same hemoflavoprotein family as CDH, flavocytochrome b_2, which contains the two active sites FMN (flavin mononucleotide) and haem [143,144]. The authors reported that, after oxidation of the substrate by the FMN group, one electron is transferred from the reduced FMN to haem with a rate of 1500 s^{-1} [145]. Then, after the reoxidation of haem by cytochrome c, the second electron is transferred from FMN semiquinone to haem with a rate of 120 s^{-1} [144]. According to this study, the two kinetic constants for the semioxidation reactions of the flavin group by haem are different, with the first reaction being faster than the second one. However, we have to take into account that those rate constants were measured for the free enzyme in solution transferring electrons to its natural electron acceptor, cytochrome c. Moreover, the authors reported also that the reaction product, pyruvate, acts as an inhibitor binding to the FMN semiquinone and slowing down the second electron transfer between FMN and haem [143]. Therefore, this is not necessarily a good model for our case, considering also that *i*) the enzyme used in the cited study was different from CDH, and *ii*) in our case the haem is oxidised at the electrode surface, not by an electron acceptor in solution.

Therefore, for simplicity we will consider the rates of the two semioxidation reactions of FAD by haem and the mediator being the same, so that we can write:

$$k_{\mathrm{int}(1)} = k_{\mathrm{int}(2)} = k_{\mathrm{int}} \qquad \text{(Eq. 4.29a)}$$

$$\text{and} \quad k_{\mathrm{med}(1)} = k_{\mathrm{med}(2)} = k_{\mathrm{med}} \qquad \text{(Eq. 4.29b)}$$

In the following sections, we will estimate these kinetic constants as well as the rate constants relative to the substrate/enzyme reaction, starting from the kinetic constant of the flavin/mediator reactions, k_{med}.

4.2.2 Estimation of k_{med}

We decided to start our estimation of the kinetic constants from k_{med} because this parameter can affect the potential of the MET catalytic current and also, in some particular conditions, the current itself. In fact, as we have shown in Section 3.3.3 (Figure 3.14), the MET catalytic current shifts towards cathodic potentials by increasing the concentration of mediator in solution. This unusual behaviour was explained by the fact that the FAD oxidation and, therefore, the catalytic current, is actually due to the oxidised form of ferrocene, Fc^+, whose concentration depends on the applied potential for the Nernst equation (Eq. 3.9 or 4.8). We found that a very small amount of ferrocenium ion (around 1 μM) was enough to react with the enzyme and, therefore, produce the catalytic current. This made us think that the kinetic constant for the reaction between the CDH flavin domain and Fc^+ must be very high, probably of the order of millions L mol^{-1} s^{-1}.

Nevertheless, since k_{med} can affect also the current intensity, we need to look at it in order to have a first rough estimation of this constant. However, in the MET mechanism, for relatively high concentrations of mediator, i_{max} is limited only by the reaction between the enzyme and the substrate and, as we can see from Eq. 4.26a or Eq. 4.28, will be given by:

$$i_{max} = 2Fm_{enz}k_{cat} \qquad \text{(Eq. 4.30)}$$

Only for the smallest concentrations of ferrocene the current can be affected by the reaction between CDH and the mediator, so that in Eq. 4.30 we can substitute the catalytic constant k_{cat} with the rate constant representing the reoxidation kinetics of FAD by the mediator ($k_x^{med}(x)$), given by Eq. 4.24b:

$$i_{max} = 2Fm_{enz}k_x^{med}(x) = 2Fm_{enz}\frac{k_{med}}{2}[Fc^+] \qquad \text{(Eq. 4.31)}$$

The smallest concentration of ferrocene we have used was 1 μM, which produced a catalytic current of about 2 μA (see Figure 3.14 in Chapter 3). We can rearrange Eq. 4.31 in order to find k_{med}:

$$k_{med} = \frac{i_{max}}{Fm_{enz}[Fc^+]} \qquad \text{(Eq. 4.32)}$$

Using the value of the catalytic current found in Figure 3.14 for i_{max}, the value of 8 pmol found in Section 3.2.1 for m_{enz}, and considering [Fc^+] equal to the total concentration of mediator in solution (1 μM), k_{med} was found to be equal to 2.6 $\times 10^6$ L mol^{-1} s^{-1}. Using this value for k_{med}, we simulated a first catalytic voltammogram (red line in Figure 4.3-A), which did not match very well with the experimental CV recorded at a E522-CDH modified GC/CNT electrode in the presence of 200 mM glucose and 1 mM ferrocene (black line in Figure 4.3-A). The simulated CV was shifted by about 26 mV at more cathodic potentials compared with the experimental one. This can be due to an imprecise estimation of k_{med} using Eq. 4.32, since m_{enz} could have been different for the electrode used in this experiment and also [Fc^+] may not have been exactly 1 μM. However, a more precise estimation can be done by using the observed potential shift: in fact, according to the Nernst equation for ferrocene (Eq. 4.8), the difference between the two potentials is given by:

$$\Delta E = E^{a} - E^{b} = \frac{0.059}{n}\left(\mathrm{Log}\frac{[Fc^+]_a}{[Fc]} - \mathrm{Log}\frac{[Fc^+]_b}{[Fc]}\right) \qquad \text{(Eq. 4.33)}$$

where $[Fc^+]_a$ is the concentration of ferrocenium at the first potential (E^a) and $[Fc^+]_b$ is its concentration at the second potential (E^b). Substituting the concentration of Fc^+ with the expression given by Eq. 4.24b, assuming n = 1, and [Fc] and $k_x(x)$ being constant in this potential range, we will have:

$$\Delta E = 0.059\ \mathrm{Log}\left(\frac{2k_x(x)}{{k_{med}}^{a}[Fc]} \cdot \frac{{k_{med}}^{b}[Fc]}{2k_x(x)}\right)$$

$$\Longrightarrow \quad {k_{med}}^{b} \cong {k_{med}}^{a} \cdot 10^{\left(\frac{\Delta E}{0.059}\right)} \qquad \text{(Eq. 4.34)}$$

Therefore, the correct value for k_{med} was found to be smaller than the initial one, being 9.4 $\times 10^5$ L mol^{-1} s^{-1}, which can be approximated to 1 $\times 10^6$ L mol^{-1} s^{-1}. The voltammogram simulated using this value overlapped perfectly with the experimental CV (Figure 4.3-B), so that we will keep this value of k_{med} for the following simulations. Note that the values of the other parameters used to simulate the CVs in Figure 4.3 were roughly estimated in order to better match the simulation with the experimental CV. A more accurate estimation of these parameters will be carried out in the following sections: for the moment it was

not necessary to have very accurate values of K_M, k_{cat} and k_{int} since these parameters should not have a significant effect on the shift of the MET catalytic current and, therefore, on the value of k_{med}.

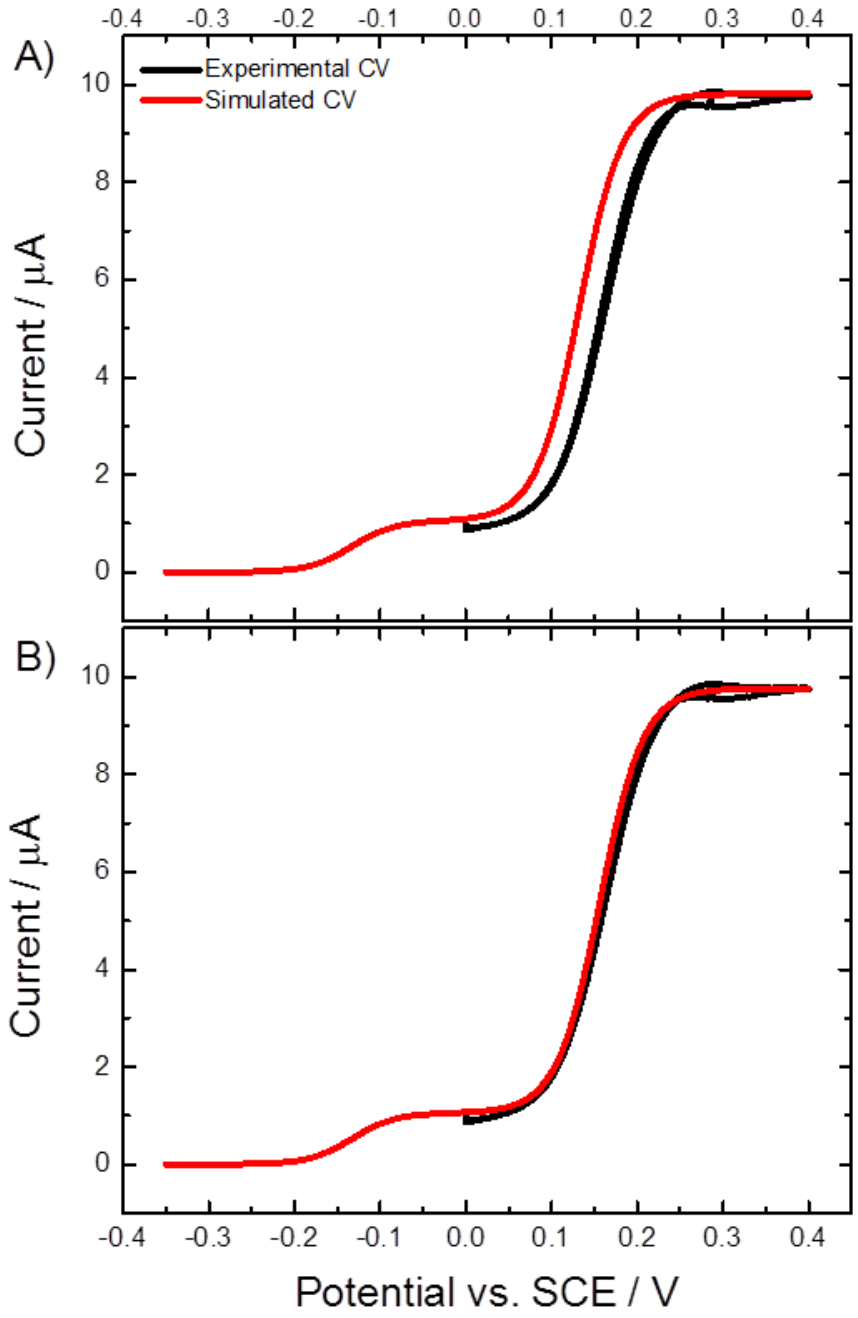

Figure 4.3. *Black line: experimental CV, background subtracted, recorded at a E522-CDH modified GC/CNT electrode in 50 mM acetate buffer (pH 5.5) containing 30 mM $CaCl_2$, 1 mM ferrocene and 200 mM glucose, scanning the electrode potential at 2 mV/s from 0 to 0.4 V vs. SCE. Red lines: CVs simulated using Eq. 4.28 with the following parameters: [M] = 1 mM, [S] = 200 mM, k_{cat} = 5.6 s^{-1}, K_M = 70 mM, k_{int} = 1 s^{-1}, m_{enz} = 12.3 pmol, k_{med} = (A) 2.6 ×10^6 L mol^{-1} s^{-1} and (B) 1 ×10^6 L mol^{-1} s^{-1}.*

A further confirmation of the value of 1 ×10^6 L mol^{-1} s^{-1} for k_{med} was provided by simulating a catalytic voltammogram recorded at a different concentration of mediator, since this will shift the potential for the catalytic current. Figure 4.4 shows an experimental CV (after background subtraction, black line) recorded at a E522-CDH modified GC/CNT electrode in the presence of 70 mM glucose and 20 µM ferrocene. The red line represents the voltammogram simulated using the same conditions and k_{med} = 1 ×10^6 L mol^{-1} s^{-1}. The two CVs overlap perfectly, meaning that this value for the flavin/mediator kinetic constant is still valid. In addition, note that the voltammograms in Figure 4.4 are shifted by about +82 mV compared with the CVs in Figure 4.3-B. This can be explained using again Eq. 4.33, assuming the concentration of Fc^+ to be the same at the two different potentials and [Fc] to be similar to the total concentration of mediator, [M]. Therefore, the potential difference is given by:

$$\Delta E = 0.059 \text{ Log} \frac{[\text{M}]_\text{b}}{[\text{M}]_\text{a}} = 0.059 \text{ Log} \frac{1000 \text{ µM}}{20 \text{ µM}} = 0.1 \text{ V} \qquad \text{(Eq. 4.35)}$$

The value obtained with Eq. 4.35 is close enough to the experimental one of 82 mV, given that there may be some errors in the actual concentration of ferrocene.

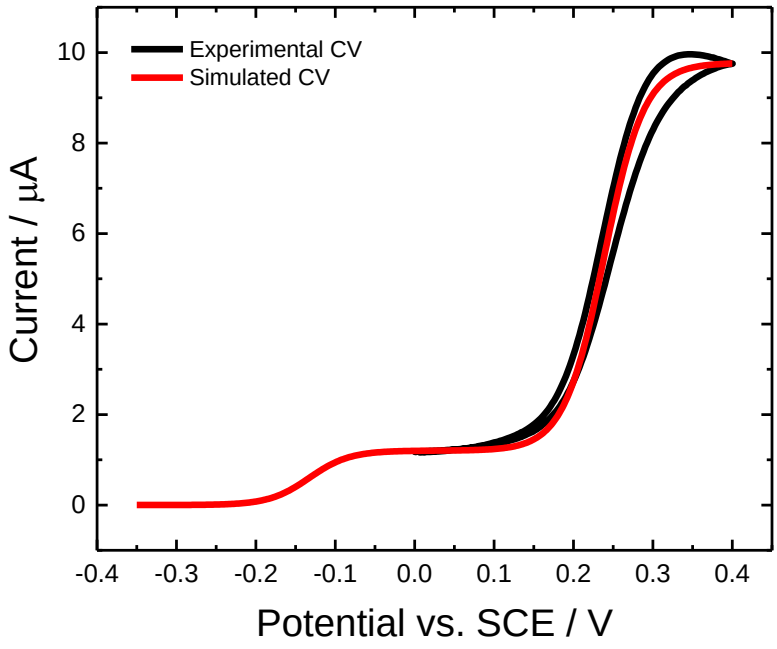

Figure 4.4. *Black line: experimental CV, background subtracted, recorded at a E522-CDH modified GC/CNT electrode in 50 mM acetate buffer (pH 5.5) containing 30 mM $CaCl_2$, 20 µM ferrocene and 70 mM glucose, scanning the electrode potential at 2 mV/s from 0 to 0.4 V vs. SCE. Red line: CV simulated using Eq. 4.28 with the following parameters: [M] = 20 µM, [S] = 70 mM, k_{cat} = 5.6 s^{-1}, K_M = 70 mM, k_{int} = 0.6 s^{-1}, m_{enz} = 23 pmol, k_{med} = 1 ×10^6 L mol^{-1} s^{-1}.*

4.2.3 Estimation of K_M

Another parameter to define is the Michaelis-Menten constant, K_M. This is an inverse measure of the affinity of the enzyme for the substrate, as it indicates the substrate concentration at which the reaction rate, or the current in our case, is half of its maximum value. Therefore, smaller K_M values suggest higher affinity between the enzyme and the substrate, meaning that the reaction rate, or the current, will approach the maximum more quickly.

In Chapter 3, Section 3.3.2, we reported the values of K_M extracted from the fitting of the data for the different CDH variants in the DET and MET experiments. At that point, we could not explain why the K_M values for DET were so different from the ones obtained in MET experiments, with the latter ones being higher than the first ones (at least for pH 5.5 experiments). However, we now know that the K_M extracted from the fitting is actually a K_M^{APP}, as we can see in Eq. 4.26.

K_M^{APP} is defined in Eq. 4.26c: it depends on the "real" K_M, k_{cat} and $k_x(x)$. Assuming K_M and k_{cat} being constant, we know that $k_x(x)$ depends on the kinetic constants of the mediator and interdomain electron transfer and on the concentrations of ferrocene and haem in their oxidised forms, which in turn depend on the applied potential. Therefore, in the potential range where IET is the dominant process (between -0.35 and +0.05 V), $k_x(x)$ will be relatively small as it mainly depends on k_{int}, the kinetic constant for the FAD/haem reaction (see Eq. 4.24a). We have not defined k_{int} yet, but we can assume that it will be in the order of a few s^{-1}. On the other hand, when MET is the dominant process (between 0.15 and 0.4 V), $k_x(x)$ will be higher as it mainly depends on k_{med}, which was previously found to be 1×10^6 L mol^{-1} s^{-1} (see Eq. 4.24b). For Eq. 4.26c, K_M^{APP} is almost directly proportional to $k_x(x)$, therefore it will be smaller for DET and higher for MET, as we found experimentally.

But what would be the value for the "real" K_M? Some authors report a value of 250 mM for *Mt*CDH with glucose [73,123,146], however this would be also a K_M^{APP} since it must have been calculated using the same equation we used to fit our experimental data, Eq. 4.26. Probably a better estimation of K_M would arise from the K_M^{APP} extracted by fitting the MET data. In fact, as we have discussed here above, in the potential region where MET is the dominant process, $k_x(x)$ is

given by Eq. 4.24b and can be called $k_x(x)^{med}$. In this potential range (and in particular at 0.4 V *vs.* SCE, where we normally take the value of the current to plot against the glucose concentration), using the value of k_{med} determined in the previous section (1×10^6 L mol^{-1} s^{-1}) and considering [Fc$^+$] equal to the total concentration of mediator, it follows that, for [M] = 1 mM, $k_x(x)^{med}$ is equal to 500 s^{-1}. We can now rearrange Eq. 4.26c in order to find K_M:

$$K_M = K_M{}^{APP} \cdot \left(1 + \frac{k_{cat}}{k_x(x)}\right) \qquad \text{(Eq. 4.36)}$$

Since k_{cat} would have a value rather small, which will be defined in the following section but will be certainly smaller than 500 s^{-1}, we can write that:

$$\text{for} \quad k_{cat} \ll k_x(x)^{med} \quad \Longrightarrow \quad K_M \cong K_M{}^{APP/MET} \qquad \text{(Eq. 4.37)}$$

This leads us to consider that K_M will have a value quite similar to the $K_M{}^{APP}$ extracted by fitting the MET data. Given that the average value between the experimental $K_M{}^{APP/MET}$ of the four CDH variants (reported in Table 3.1, Chapter 3) is 85 mM, we can try to use a value slightly higher for K_M, such as 90 mM. With this value of K_M and the k_{med} previously found, we simulated a set of cyclic voltammograms at different concentrations of substrate and with 1 mM mediator, adjusting the remaining parameters in order to better match with the experimental CVs recorded for the MET of a E522-CDH modified electrode. Figure 4.5 shows the plots of the catalytic current taken at 0.4 V in the experimental (black squares) and simulated voltammograms (red circles) *vs.* glucose concentration. The two sets of data match each other quite well and the $K_M{}^{APP}$ extracted by fitting the data with the Michaelis-Menten equation, Eq. 4.26 (black and red lines), are quite similar: 75 and 89 mM for the experimental and simulated data, respectively. Note that the $K_M{}^{APP}$ extracted from the fitting of the simulated data, 89 mM, is almost the same as the K_M used in the equation to simulate those data, 90 mM, as predicted by Eq. 4.37.

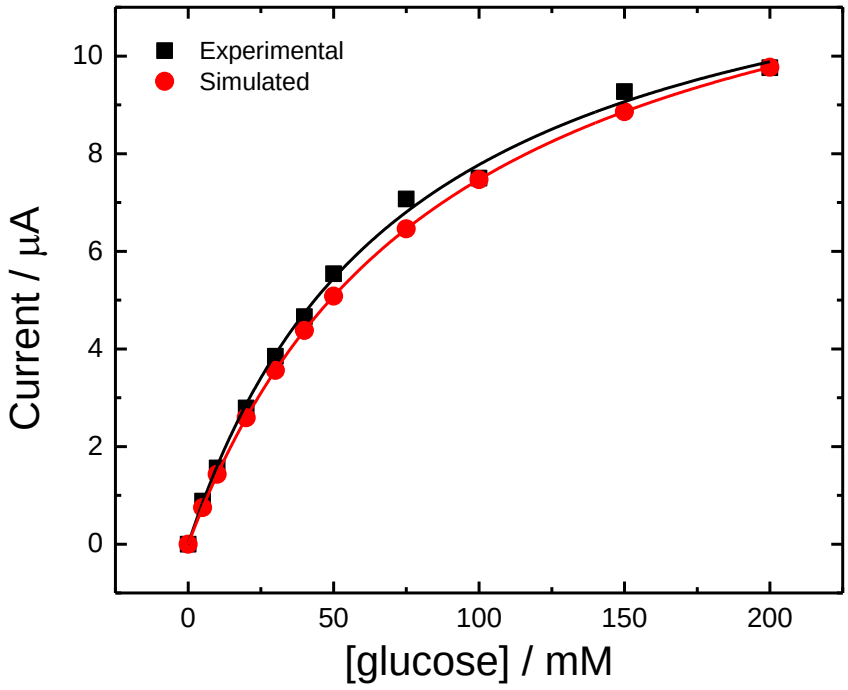

Figure 4.5. *Black squares: experimental data recorded for the MET of a E522-CDH modified GC/CNT electrode in 50 mM acetate buffer (pH 5.5) containing 30 mM $CaCl_2$, 1 mM ferrocene and different concentrations of glucose. Red circles: data simulated using Eq. 4.28 with the following parameters: [M] = 1 mM, k_{med} = 1 ×10^6 L mol^{-1} s^{-1}, K_M = 90 mM, k_{cat} = 7.2 s^{-1}, m_{enz} = 10.3 pmol, and different concentrations of substrate. The current was taken at 0.4 V vs. SCE in both cases. Lines: fitting curves using Eq. 4.26.*

However, to verify that this value of K_M can be used in our following simulations, we will need to simulate also the results of the DET. Figure 4.6 shows the data of the current taken at 0.0 V in experimental CVs recorded for the DET of the same electrode previously used (E522-CDH, black squares) and in CVs simulated using the same parameters as before (red squares), at different glucose concentrations. Apart for the concentration of mediator that was changed to 0 mM, the only other parameter we had to change to match the simulated data with the experimental ones was m_{enz}: we used 10.3 pmol for Figure 4.5 and 2.9 pmol for Figure 4.6. This fact will be discussed in more details in Sections 4.3.3 and 4.3.4, for now we want just to observe that using the same values for K_M, k_{cat} and the other parameters, except m_{enz}, we can simulate very well our experimental results both for the DET and MET of the same electrode. Note that in the caption of Figure 4.6 we added a parameter, k_{int}, which was not very relevant in the previous simulation of the MET data (Figure 4.5): we used a value of 5 s^{-1}, however this will be estimated more precisely in Section 4.2.6. Note also that, in the DET case, the K_M^{APP} extracted by fitting the data with the Michaelis-Menten equation are quite

similar: 24 and 23 mM for the experimental and simulated data, respectively, being however very different from the "real" K_M for the reason explained here above.

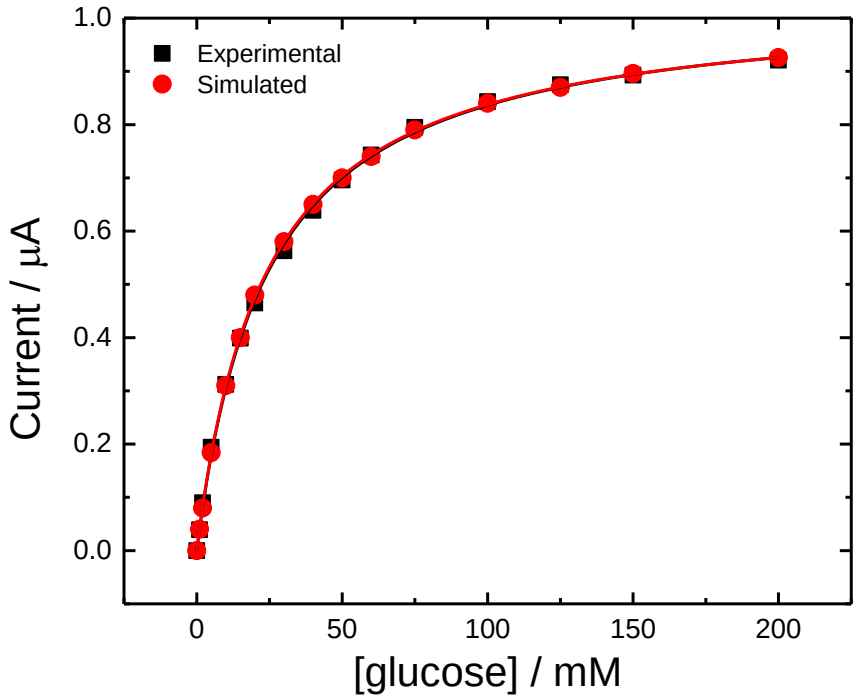

Figure 4.6. *Black squares: experimental data recorded for the DET of a E522-CDH modified GC/CNT electrode in 50 mM acetate buffer (pH 5.5) containing 30 mM $CaCl_2$ and different concentrations of glucose. Red circles: data simulated using Eq. 4.28 with the following parameters: [M] = 0 mM, k_{med} = 1 ×10⁶ L mol⁻¹ s⁻¹, K_M = 90 mM, k_{cat} = 7.2 s⁻¹, k_{int} = 5 s⁻¹, m_{enz} = 2.9 pmol, and different concentrations of substrate. The current was taken at 0.0 V vs. SCE in both cases. Lines: fitting curves using Eq. 4.26.*

4.2.4 Estimation of k_{cat}

k_{cat} (catalytic constant) is defined in Table 4.1 as the kinetic constant for the breakdown of the enzyme-substrate complex to yield the product. It is also called "turnover number" as it represents the maximum number of substrate molecules converted to product per enzyme molecule per second. Further addition of substrate does not increase the reaction rate, which is said to be saturated.

Similarly to K_M^{APP}, k_{cat}^{APP} can also be extracted by fitting the experimental data with the Michaelis-Menten equation (Eq. 4.26), which gives the values of i_{max}^{APP}. From i_{max}^{APP}, knowing the amount of immobilised enzyme it is possible to calculate k_{cat}^{APP} using Eq. 4.26a. However, a precise estimation of the amount of

immobilised CDH is not easy: in Section 3.2.1 we found a value of about 8 pmol for the electrode used in that analysis, but it might not be the same for all of the electrodes used in this work because of the problems already discussed in Section 4.2.1 about the preparation of reproducible CNT surfaces. It follows that a precise estimation of k_{cat}^{APP} is also difficult.

Nevertheless, in Chapter 3 we found that i_{max}^{APP} extracted for DET experiments is always much lower than the one obtained for MET (see Table 3.1). This must be due to k_{cat}^{APP}, which depends on the "real" k_{cat} and $k_x(x)$ as described in Eq. 4.26b. At this point, we can make the same considerations as we made for K_M^{APP} in the previous section: k_{cat}^{APP} is almost directly proportional to $k_x(x)$, which has a smaller value in the potential range where DET is the dominant process and a higher value when MET is dominant. It follows that k_{cat}^{APP} and, consequently, i_{max}^{APP} will be lower for the DET and higher for the MET, as we found experimentally.

Again, what would be the value for the "real" k_{cat}? The authors previously cited in the discussion of K_M, reported a value of k_{cat} for the oxidation of glucose by *Mt*CDH of 14 s^{-1} [73,146]. However, also this value would be actually a k_{cat}^{APP} as it was extracted by fitting experimental data. In the previous section, to match the simulated data with the experimental ones, for both DET and MET, we used a value of 7.2 s^{-1} for k_{cat}, which is rather close to the one reported in the literature, taking into account that it may be different at different pH. A better estimation of k_{cat} would be made using k_{cat}^{APP} extracted by fitting the MET data, as previously done for K_M. However, since the fitting provides only the value of i_{max}^{APP}, we cannot have a good estimation of k_{cat}^{APP} and, therefore, k_{cat} given that we do not know the exact value of m_{enz} as we have already discussed here above. Therefore, we will keep for now the value of 7.2 s^{-1} and verify it with other simulation experiments.

Other sets of cyclic voltammograms were simulated, for both the DET and MET of a E522-CDH modified electrode, using different values for k_{cat}, while keeping all the other parameters the same as before. The results are reported in Figure 4.7: it is clear that the best value of k_{cat} in order to match the simulated data with the experimental ones for both DET and MET is 7.2 s^{-1}, while using values even

slightly lower or higher, such as 4 or 12 s^{-1}, the curves of current/glucose concentration drastically change. Moreover, there are some other considerations to make: in fact, changing the value of k_{cat} produces a very different effect on the DET current (Figure 4.7-B) if compared with the MET current (Figure 4.7-A).

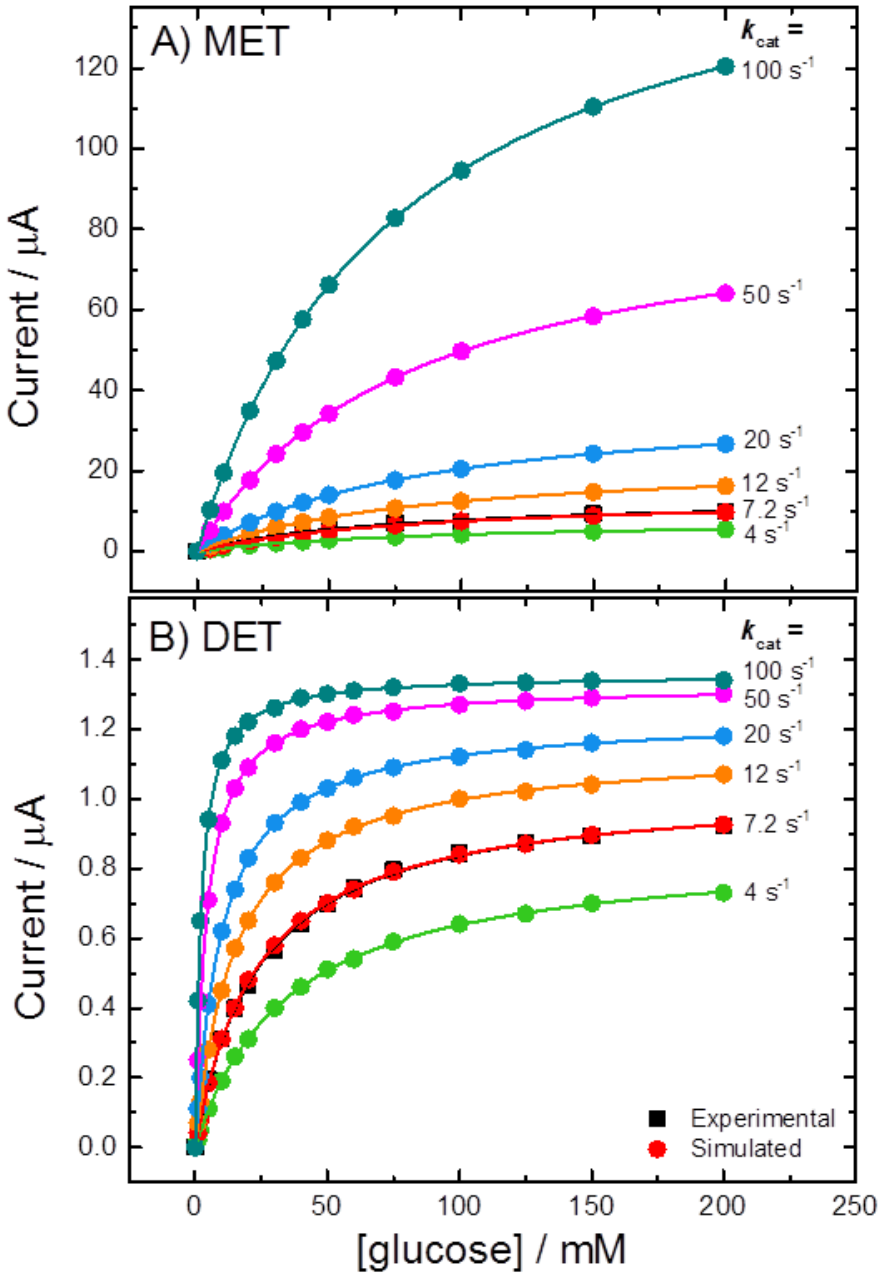

Figure 4.7. *Experimental and simulated data for the (A) MET and (B) DET of a E522-CDH modified GC/CNT electrode. Black squares: experimental data recorded in 50 mM acetate buffer (pH 5.5) containing 30 mM $CaCl_2$ (B), and with the addition of 1 mM ferrocene (A), at different concentrations of glucose. Coloured circles: data simulated using Eq. 4.28 with the following parameters: [M] = (A) 1 mM and (B) 0 mM, k_{med} = 1 ×10^6 L mol^{-1} s^{-1}, K_M = 90 mM, k_{int} = 5 s^{-1}, m_{enz} = (A) 10.3 and (B) 2.9 pmol, and different concentrations of substrate. k_{cat} was: (green) 4, (red) 7.2, (orange) 12, (blue) 20, (pink) 50 and (dark green) 100 s^{-1}. The current was taken at (A) 0.4 and (B) 0.0 V vs. SCE. Lines: fitting curves using Eq. 4.26.*

Table 4.3. *Values of K_M^{APP} and i_{max}^{APP} extracted by fitting the data in Figure 4.7 with Eq. 4.26.*

k_{cat} (s^{-1})	MET		DET	
	K_M^{APP} (mM)	i_{max}^{APP} (µA)	K_M^{APP} (mM)	i_{max}^{APP} (µA)
4	89	7.89	35	0.86
7.2	89	14.1	23	1.03
12	88	23.3	15	1.15
20	86	38.0	10	1.24
50	82	90.4	4.3	1.32
100	75	165	2.2	1.36

If we look at Figure 4.7-A, we can see that the MET current increases proportionally with k_{cat}. This is even more clear if we look at the values of i_{max}^{APP} (Table 4.3, 3rd column) extracted by fitting the data with the Michaelis-Menten equation: i_{max}^{APP}, in the case of MET, is almost linear with k_{cat}. In fact, according to Eq. 4.26a, i_{max}^{APP} is directly proportional to k_{cat}^{APP}. At this point, we can make the same consideration previously made for K_M and $K_M^{APP/MET}$. Using Eq. 4.26b, we can write that:

$$\text{for} \quad k_{cat} \ll k_x(x)^{med} \quad \Longrightarrow \quad k_{cat}^{APP/MET} \cong k_{cat} \qquad \text{(Eq. 4.38)}$$

Therefore, when MET is the dominant process, i_{max}^{APP} is directly proportional to $k_{cat}^{APP/MET}$ and, consequently, k_{cat}. These mathematical considerations explain that, in the case of MET and with a sufficiently high concentration of mediator, the current is limited only by the reaction between the enzyme and the substrate, which is described by the kinetic constant k_{cat}. Therefore, if we could increase the turnover number of the enzyme, k_{cat} indeed, we would increase the rate of the glucose oxidation and, thus, the current. The reaction between the enzyme and the mediator, instead, does not represent a limit since it is very fast, having a very high kinetic constant (1×10^6 L mol^{-1} s^{-1}). The same can be said about the reaction between the mediator and the electrode, which is fast and reversible and, therefore, does not limit the current.

K_M^{APP} (Table 4.3, 2nd column), instead, for the MET does not vary a lot by changing k_{cat}: it decreases only of the 16 % (passing from 89 to 75 mM) for increasing k_{cat} from 4 to 100 s^{-1}. This is because $K_M^{APP/MET}$ has always a value very close to the "real" K_M, as described by Eq. 4.37, and it becomes lower than K_M only for higher values of k_{cat}, such as 100 s^{-1}. In this case, indeed, the approximation made for Eq. 4.37 does not apply any longer and we have to calculate K_M^{APP} using Eq. 4.26c.

On the other hand, in the case of DET the current does not increase proportionally with k_{cat} (Figure 4.7-B): increasing k_{cat}, the current increases slowly until reaching almost a limiting value so that, even if we double k_{cat} from 50 to 100 s^{-1}, i_{max}^{APP} increases only by 0.04 μA (see Table 4.3, 5th column). This is because, in the case of the DET of CDH, there must be some other factors limiting the current, other than the reaction between the enzyme and the substrate. This other factor is represented by the interdomain electron transfer, which is the reaction between the haem and FAD, described in Table 4.1 by the kinetic constant k_{int}. We have not defined k_{int} yet, but in the simulations performed until now we have used a value of 5 s^{-1}, which is of the same magnitude order as k_{cat} (7.2 s^{-1}). Therefore, the two reactions substrate/FAD and FAD/haem are in competition between each other as limiting step and, depending on the specific values we give to their kinetic constants, the current will be limited by one or the other, or both of them. Note that we did not consider the haem/electrode reaction as a potential limiting step since in Section 3.2.2 we have proved that it is fast and reversible.

From a mathematical point of view, this can be explained by i_{max}^{APP} that, according to Eq. 4.26a, is directly proportional to k_{cat}^{APP}, which in turn depends on k_{cat} and $k_x(x)$ for Eq. 4.26b. When DET, and therefore IET, is the dominant process, $k_x(x)$ mainly depends on k_{int} and, according to Eq. 4.24a, when the haem is completely oxidised, $k_x(x)^{int}$ is equal to $k_{int}/2$. As we used a value of 5 s^{-1} for k_{int}, it follows that $k_x(x)$ is 2.5 s^{-1}. Therefore, for values of k_{cat} relatively small, k_{cat}^{APP} and, consequently, i_{max}^{APP} will depend on both k_{cat} and k_{int}, so the current will be determined by both the reactions substrate/FAD and FAD/haem.

However, for higher values of k_{cat} (such as 100 s^{-1}), we can rearrange Eq. 4.26b and Eq. 4.26a as follow:

$$\text{for } k_{cat} \gg k_x(x) \implies {k_{cat}}^{APP} = \frac{k_{cat} \cdot k_x(x)}{k_{cat} + \cancel{k_x(x)}} = k_x(x) \qquad \text{(Eq. 4.39)}$$

$$\implies {i_{max}}^{APP} = 2Fm_{enz}k_x(x) = 2Fm_{enz} \cdot \frac{k_{int}}{2} \qquad \text{(Eq. 4.39a)}$$

This means that, even if we could increase the turnover number of the enzyme and, therefore, the rate of glucose oxidation, the DET current will not increase above a certain limiting current that is determined by the kinetic constant k_{int}, hence by the interdomain electron transfer rate. In this case, using the values of the parameters employed for Figure 4.7-B, such limiting current will be equal to 1.4 µA: we could infinitely increase k_{cat}, but ${i_{max}}^{APP}$ will never overcome this limit.

Finally, ${K_M}^{APP}$ for the DET (see Table 4.3, 4th column), contrarily to the MET case, varies a lot by changing k_{cat}. This is clear if we look at Eq. 4.26c: in fact, increasing k_{cat}, ${K_M}^{APP}$ will decrease. Moreover, it is well visible in Figure 4.7-B: when we increase k_{cat}, the current increases more for the lower concentrations of glucose but then, at higher substrate concentrations, it is not free to increase further (as it was in the MET case) because it is limited by the IET. As a consequence, it looks like the current reaches its maximum more rapidly and the enzyme has a higher affinity for the substrate, which is however not true.

To conclude, in this section we have established that the best value for k_{cat} in order to match the simulated data with the experimental results is 7.2 s^{-1}, both for the DET and MET. However, during the estimation of k_{cat}, we have not changed any other parameter so that it was probably easy to find the value of k_{cat} that would perfectly fit into our simulations. In the next section, we will see what is the relationship between k_{cat} and K_M and what will happen if we change both of them at the same time.

4.2.5 Relationship between k_{cat} and K_M

Another parameter to consider is the so-called catalytic efficiency, k_{cat}/K_M, which was 0.08 mM^{-1} s^{-1} for the best set of simulated data reported in Figure 4.7 (with k_{cat} = 7.2 s^{-1} and K_M = 90 mM). In theory, if we kept the same catalytic efficiency, even changing k_{cat} and K_M, the results should not change. To prove that, other sets of cyclic voltammograms were simulated, for the DET and MET again, using values of k_{cat} equal to 4, 7.2 and 12 s^{-1}. In addition, K_M was changed in order to maintain the ratio k_{cat}/K_M constant and equal to 0.08 mM^{-1} s^{-1}. Therefore, values of 50, 90 and 150 mM were used for K_M.

The results reported in Figure 4.8 show again a significant difference between the DET and MET. In the case of MET (Figure 4.8-A), the three sets of data are very different between each other even if the ratio k_{cat}/K_M is the same. In this case, in fact, i_{max}^{APP} depends only on k_{cat} as discussed in the previous section, therefore we will have the same i_{max}^{APP} as before for the same value of k_{cat} used in the simulation (compare Tables 4.3 and 4.4). Moreover, K_M^{APP} will always have a value very close to K_M as described by Eq. 4.37 and reported in Table 4.4 (see 2nd and 3rd columns). It follows that, as K_M and k_{cat} act independently on the values of K_M^{APP} and i_{max}^{APP}, respectively, changing these two parameters, although keeping constant their ratio, will change completely the shape of the curve current/glucose concentration for the MET case.

On the other hand, the curves current/glucose concentration for the DET are more similar to each other (see Figure 4.8-B), even though the values of i_{max}^{APP} are the same as before since this depends only on k_{cat}^{APP} (compare Tables 4.3 and 4.4). However, the values of K_M^{APP} are very close to each other (see Table 4.4, 5th column) since this depends on both K_M and k_{cat} as described by Eq. 4.26c: decreasing or increasing in the same way both K_M and k_{cat} will not change significantly the value of K_M^{APP}.

We can conclude that the catalytic efficiency, k_{cat}/K_M, is not a good parameter to define an enzymatic reaction or enzymatic electrode since changing the values of K_M and k_{cat}, although keeping constant their ratio, will drastically change the results. As a consequence, we can use only one value for K_M and k_{cat} (or values very close to that one) to match the simulated data with the experimental ones.

This is more evident in the case of the MET but, given that the enzyme and the catalysed reaction are the same, we should use the same values of K_M and k_{cat} also in the case of the DET. The best values that were found in the previous sections were 90 mM for K_M and 7.2 s^{-1} for k_{cat}: these will be used in the following simulations, unless otherwise stated.

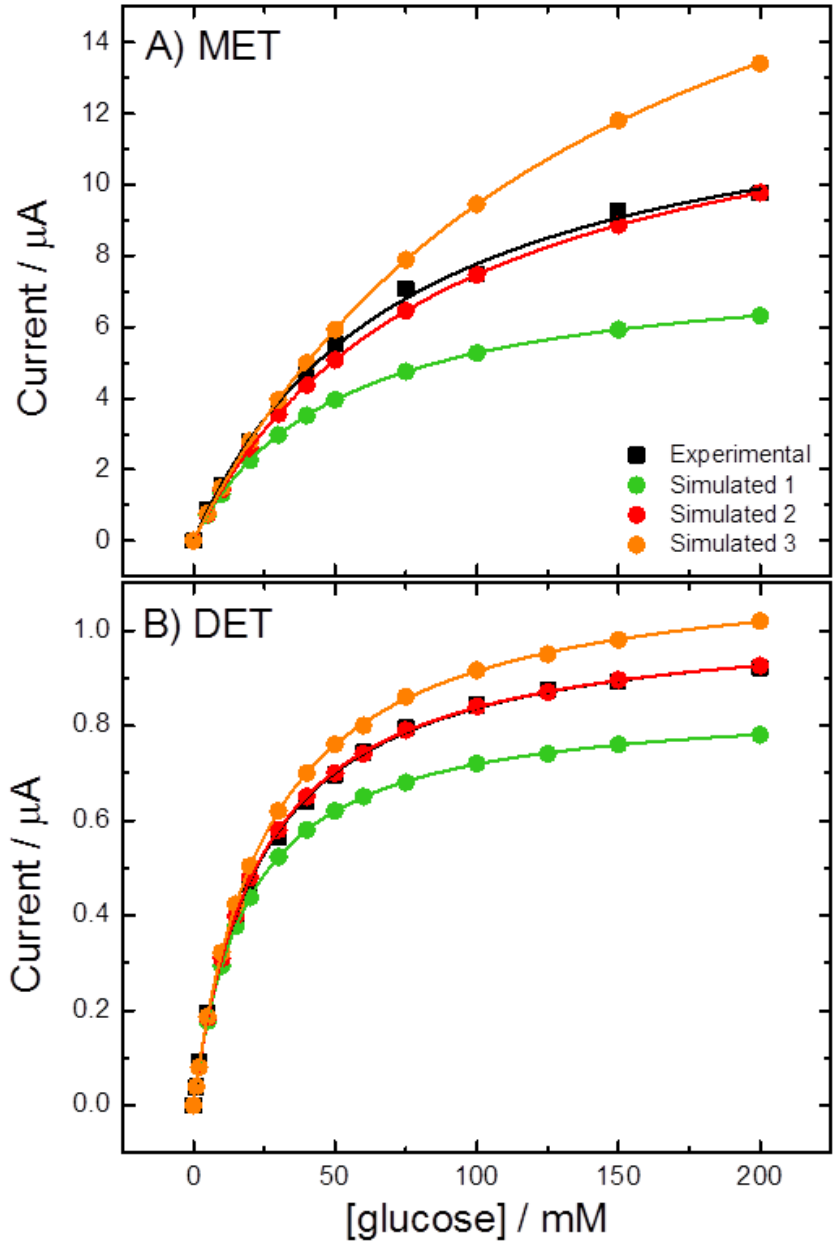

Figure 4.8. *Experimental and simulated data for the (A) MET and (B) DET of a E522-CDH modified GC/CNT electrode. Black squares: experimental data recorded in 50 mM acetate buffer (pH 5.5) containing 30 mM $CaCl_2$ (B), and with the addition of 1 mM ferrocene (A), at different concentrations of glucose. Coloured circles: data simulated using Eq. 4.28 with the following parameters: [M] = (A) 1 mM and (B) 0 mM, k_{med} = 1 ×10⁶ L mol^{-1} s^{-1}, k_{int} = 5 s^{-1}, m_{enz} = (A) 10.3 and (B) 2.9 pmol, and different concentrations of substrate. Green: k_{cat} = 4 s^{-1}, K_M = 50 mM; red: k_{cat} = 7.2 s^{-1}, K_M = 90 mM; orange: k_{cat} = 12 s^{-1}, K_M = 150 mM. The current was taken at (A) 0.4 and (B) 0.0 V vs. SCE. Lines: fitting curves using Eq. 4.26.*

Table 4.4. *Values of K_M^{APP} and i_{max}^{APP} extracted by fitting the data in Figure 4.8 with Eq. 4.26.*

k_{cat} (s^{-1})	K_M (mM)	MET		DET	
		K_M^{APP} (mM)	i_{max}^{APP} (µA)	K_M^{APP} (mM)	i_{max}^{APP} (µA)
4	**50**	50	7.89	19	0.85
7.2	**90**	89	14.1	23	1.03
12	**150**	145	23.2	26	1.15

4.2.6 Estimation of k_{int}

As described in Table 4.1, $k_{int(1)}$ and $k_{int(2)}$ are the kinetic constants of the reoxidation reactions of FAD by haem. They represent the process of the interdomain, or internal, electron transfer (IET). As we have already said in Section 4.2.1, we consider the rates of the two FAD semioxidation reactions being the same, therefore we assume $k_{int(1)}$ and $k_{int(2)}$ to be equal (Eq. 4.29a), so that we will refer to both of them as k_{int}.

Since k_{int} characterises the IET process, it will be affected by several factors, such as solution pH and presence of divalent cations. In fact, as we have already explained in Section 3.4.1 (Chapter 3), pH and divalent cations, like Ca^{2+}, play an important role in the efficiency of the interdomain and, therefore, direct electron transfer of CDH. The optimum pH for the DET of *Mt*CDH was reported to be around 5.0-5.5 [73,78,123,147,148]: within this pH range, indeed, there is the best interaction between the two CDH domains resulting in the most efficient IET. This is because at acidic pH there is a smaller electrostatic repulsion between the flavin and cytochrome domains than at neutral pH, resulting in the enzyme being in a closer conformation and having a shorter IET distance. A similar effect occurs with divalent cations: it was reported in the literature [76-78], and we showed in Section 3.4.1, that the addition of Ca^{2+} or other similar ions strongly enhances the DET current. This is because divalent alkali earth metal cations exert a bridging effect between the two CDH domains, thereby neutralising electrostatic repulsion and increasing IET rate.

It is not easy to find in the literature a value for k_{int}. Rogers *et al.* reported an interdomain electron transfer rate of 0.2 s^{-1} for *Pc*CDH at pH 6 (in the absence of divalent cations) [149]. Kracher *et al.* reported an apparent haem reduction rate for *Mt*CDH increasing from 0.25 to 1.37 s^{-1} upon addition of 30 mM $CaCl_2$ at pH 4.5 [78]. Given that k_{int} represents the kinetic constant for one semioxidation reaction of FAD/reduction of haem, the apparent (or observed) interdomain kinetic constant would be equal to $k_x(x)$ (when IET is the dominant process and the haem is completely in the oxidised form, see Eq. 4.24a) and given by:

$$k_{int}^{obs} = \frac{k_{int}}{2} \qquad \text{(Eq. 4.40)}$$

Therefore, k_{int} would be the double of k_{int}^{obs}. The value of k_{int} used in our previous simulations, which was 5 s^{-1}, seems quite reasonable taking into account that the experimental data we tried to match were recorded at pH 5.5 with 30 mM $CaCl_2$ (the best condition for the IET of *Mt*CDH).

But how can we estimate a precise value for k_{int}? This time we cannot use the data of the MET current, as we did for the estimation of K_M and k_{cat}, since k_{int} will affect only the DET current. However, the DET current depends on m_{enz} and k_{int}, when k_{cat} is much higher than k_{int} (see Eq. 4.39a), otherwise it depends on m_{enz}, k_{int} and k_{cat}. Even though we have already estimated k_{cat}, we cannot say the same for m_{enz}, also because we have seen that the amount of enzyme may be different between the MET and DET, as we will analyse in more details in Sections 4.3.3 and 4.3.4. Nevertheless, we can try to estimate k_{int} using the equation for K_M^{APP} (Eq. 4.26c), which depends on K_M, k_{cat} and $k_x(x)$ that, in the case of DET, depends only on k_{int}. Rearranging Eq. 4.26c to find $k_x(x)$, we will have:

$$k_x(x) = \frac{k_{cat} \cdot K_M^{APP}}{K_M - K_M^{APP}} \qquad \text{(Eq. 4.41)}$$

Using the values of k_{cat} and K_M previously found and the K_M^{APP} extracted by fitting the experimental data for the DET of the E522-CDH modified electrode used until now (24 mM), it follows that $k_x(x)$ is equal to 2.6 s^{-1}. In the absence of mediator $k_x(x)$ is given by Eq. 4.24a that, when the haem is completely oxidised, becomes $k_{int}/2$. From that we obtain that k_{int} is equal to 5.2 s^{-1}, which is very close to the value we used in our simulations until now (5 s^{-1}). We will decide later in Section

4.3.3 which value is the best to use for the simulation of the DET experiments. For the moment, we will carry on using 5 s^{-1} for k_{int}, which is however close enough to the value calculated using Eq. 4.41, considering also that the values of k_{cat} and K_M used in the equation are just estimations.

As we said here above, k_{int} will change for different pH or concentrations of divalent cations in solution. To prove that, we simulated the cyclic voltammograms recorded at a E522-CDH modified electrode with different concentrations of $CaCl_2$ in solution (reported in Figure 3.17-A in Chapter 3). The simulations were performed by keeping all the parameters constant except for k_{int}, which was fixed at 5 s^{-1} for 30 mM $CaCl_2$ and was increased or decreased to simulate the other CVs. The data of the current taken at 0.0 V in the simulated voltammograms, as well as in the experimental ones, are reported in Figure 4.9, together with the values of k_{int} used, which goes from 0.35 s^{-1} to simulate the absence of $CaCl_2$ up to 7.8 s^{-1} to simulate 50 mM $CaCl_2$. Note that m_{enz} here is different from the previous simulations (3.6 pmol instead of 2.9 pmol) because the electrode used to record the experimental data at different $CaCl_2$ concentrations was another electrode and it may have presented a higher amount of enzyme, probably due to a higher surface area.

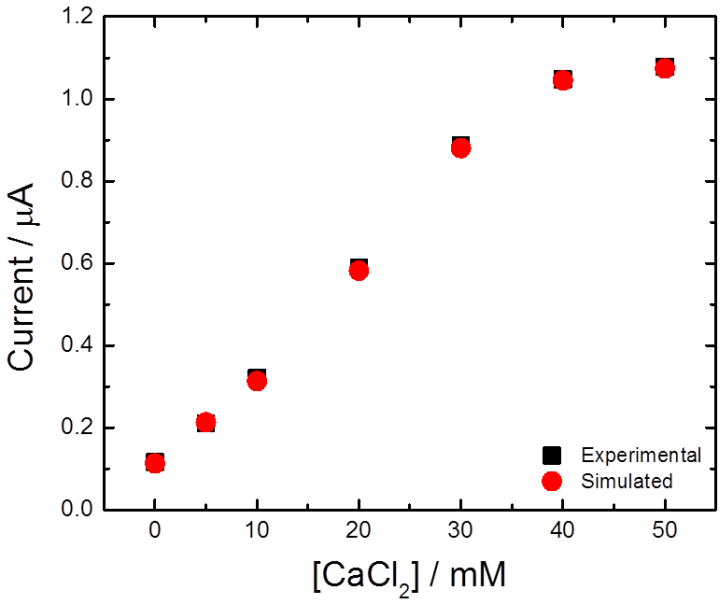

$[CaCl_2]$ (mM)	k_{int} (s^{-1})
0	0.35
5	0.7
10	1.1
20	2.5
30	**5.0**
40	7.3
50	7.8

Figure 4.9. *Black squares: experimental data recorded at a E522-CDH modified GC/CNT electrode in 50 mM acetate buffer (pH 5.5) containing 50 mM glucose and different concentrations of $CaCl_2$. Red circles: data simulated using Eq. 4.28 with the following parameters: [M] = 0 mM, k_{med} = 1 ×10⁶ L mol^{-1} s^{-1}, K_M = 90 mM, k_{cat} = 7.2 s^{-1}, m_{enz} = 3.6 pmol, [S] = 50 mM and different k_{int} (reported in the Table). The current was taken at 0.0 V vs. SCE in both cases.*

We can presume that k_{int} will also change with the pH. However, the solution pH will also affect the catalytic activity of FAD towards glucose oxidation: it was reported, indeed, that the FAD domain of *Mt*CDH has its highest catalytic ability at pH 8 [78,123]. Therefore, the kinetic constants responsible for the reaction between FAD and the substrate, which are k_{cat} and K_M, will also be different changing the pH. For that, we will not simulate the CVs at a different pH to see how k_{int} would vary, since too many parameters would need to be changed at the same time.

To summarise, in this Section 4.2 we have defined the main constants and parameters used in the equation to simulate the CDH catalytic voltammograms. Concerning the parameters, we have found the best value for:

- k_{med} (1×10^6 L mol^{-1} s^{-1}), using first the current obtained with a very small concentration of mediator (1 µM), and then adjusting the value according to the potential shift of the MET catalytic current;
- K_M (90 mM), using the K_M^{APP} extracted by fitting the experimental data for the MET with the Michaelis-Menten equation;
- k_{cat} (7.2 s^{-1}), because this was the value that better matched the simulated data with the experimental ones for the MET using the K_M previously found;
- k_{int} (5 or 5.2 s^{-1}), because this was the value that better matched the simulated data with the experimental ones for the DET using the K_M and k_{cat} previously found. This was confirmed by a calculation using the K_M^{APP} extracted by fitting the experimental data for the DET of a CDH-modified electrode. However, the role of k_{int} will be further discussed in the next section.

In the following section, we will simulate the experimental results obtained from different CDH variants to see what would change in that case. For that, we will use the values of the parameters defined until now, unless otherwise stated.

4.3 Simulation of different CDH variants

4.3.1 Introduction

At this point, the question is: what would change using different CDH variants bearing the free cysteine in different position and, therefore, being immobilised on the electrode with different orientations? We would presume k_{cat} and K_M to be the same, since they characterise the reaction between FAD and the substrate that, in theory, should not change by changing the enzyme orientation. Also k_{med} would be the same since the reaction between the mediator and FAD should not change either. Given that, the only parameters that would vary are k_{int} and the amount of immobilised enzyme, m_{enz}.

It is not obvious that k_{int} and, therefore, the IET rate should change by changing the orientation of the enzyme on the electrode. The four CDH variants used in this work present the free cysteine, responsible for the attachment on the electrode, at the surface of the flavin domain, but far from the interfacial region between it and the cytochrome domain. Therefore, the immobilization on the electrode surface via the cysteine should not directly interfere with the interdomain electron transfer. On the other hand, the great flexibility of the peptide linker connecting the two domains should be taken into account. In fact, the haem domain could slightly move around to find the best position on the electrode surface and such "movement" could be different for the different CDH variants. This would result in different distances between the two domains and, therefore, different IET rates and k_{int}. This hypothesis has been already mentioned in Sections 3.4.2 and 3.5.2, when we compared the DET of two CDH variants (E522 and T701) at different concentrations of $CaCl_2$ and different pH. At that point, we supposed that the variant E522 might better accommodate on the electrode surface with the two domains more apart from each other when they are freer to move, at neutral pH or in the absence of Ca^{2+}. To clarify that, we could simulate the experiment performed at different concentrations of $CaCl_2$ with the variant T701 (reported in Figure 3.19), as we did for the variant E522 in the previous section (Figure 4.9).

The results are reported in Figure 4.10: also in this case, the simulations were performed by keeping all the parameters constant except for k_{int}, which was fixed at 5 s^{-1} for 30 mM $CaCl_2$ and was increased or decreased to simulate the other CVs. We used the value of 5 s^{-1} also with this variant, since the results reported in Figure 3.11 showed that the DET current of E522 and T701 were very similar at pH 5.5 and with 30 mM $CaCl_2$, so that we can suppose that in these conditions they have the same IET rate. However, in the table in Figure 4.10 we can see that, decreasing the concentration of calcium, k_{int} decreases more rapidly for the variant E522 than for T701, reaching 0.35 s^{-1} in the first case and 1.1 s^{-1} in the second case to simulate the absence of $CaCl_2$. This would support the hypothesis that the variant E522 prefers to lie on the electrode with the two domains farther apart from each other when they are freer to move, resulting in a bigger IET distance and, therefore, lower k_{int} in the absence of $CaCl_2$ (or at neutral pH), if compared with the variant T701.

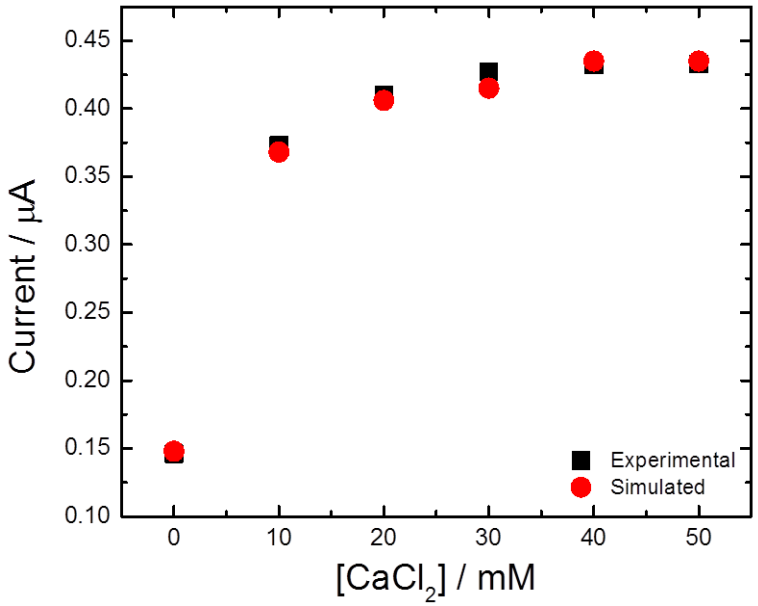

$[CaCl_2]$ (mM)	k_{int} (s^{-1}) E522	T701
0	0.35	1.1
10	1.1	4.0
20	2.5	4.8
30	**5.0**	**5.0**
40	7.3	5.5
50	7.8	5.5

Figure 4.10. *Black squares: experimental data recorded at a T701-CDH modified GC/CNT electrode in 50 mM acetate buffer (pH 5.5) containing 50 mM glucose and different concentrations of $CaCl_2$. Red circles: data simulated using Eq. 4.28 with the following parameters: [M] = 0 mM, k_{med} = 1 ×10^6 L mol^{-1} s^{-1}, K_M = 90 mM, k_{cat} = 7.2 s^{-1}, m_{enz} = 1.7 pmol, [S] = 50 mM and different k_{int}. The current was taken at 0.0 V vs. SCE in both cases. The Table shows the values of k_{int} used in this simulation (T701) and, for comparison, in the simulation of E522 (Figure 4.9).*

Nevertheless, almost all our experiments have been carried out at pH 5.5 and in the presence of 30 mM $CaCl_2$. In such conditions, we would expect the enzyme in the closest conformation possible, with the shortest distance between the two domains, and the cytochrome domain having limited freedom to move around. Given that, for the moment, in our simulations we will use the same k_{int} for all the CDH variants, which was found 5 s^{-1} in the case of 30 mM $CaCl_2$.

Therefore, the only parameter left to change is m_{enz}. In this way, we are assuming that the difference in the current/glucose concentration plots of the four CDH variants (reported in Figure 3.11 in Chapter 3) is uniquely due to a different amount of enzyme. However, a different amount of enzyme could mean: *i*) different amount of enzyme immobilised on the different electrodes (because of a different active area of the electrodes due to different amount of CNTs), or *ii*) different amount of enzyme capable of direct electron transfer with the electrode surface. Obviously, in the case of MET, if there were any difference between the curves of the four CDH variants, this would be attributed only to different amounts of immobilised enzyme. Therefore, we will start our simulations from the MET of the four CDH variants, adjusting m_{enz} in order to better match the simulated data with the experimental ones while keeping constant all of the other parameters.

4.3.2 Simulation of the MET of the four CDH variants

Using the values of k_{med}, K_M and k_{cat} previously defined, four sets of cyclic voltammograms were simulated and the data of the current taken at 0.4 V are reported in Figure 4.11 (coloured circles), together with the experimental data for the MET of the four CDH variants (black squares, already reported in Figure 3.13 in Chapter 3). The simulated data match very well with the experimental ones: the only parameter that was changed to have a good fit was m_{enz}. The amount of enzyme used in the simulations was about 10 pmol for E522, T701 and D813: in fact, these three CDH variants produced sets of data very similar to each other (see Figures 3.13 and 4.11-A, B and D). In the case of E674, instead, m_{enz} was 13.7 pmol since the current obtained with this variant was slightly higher (Figure 4.11-C). This may be due to a higher surface area of the electrode, probably because of a greater amount of CNTs adsorbed on it. Note that in the

caption of Figure 4.11 k_{int} was not mentioned, in fact it is not relevant in the simulation of MET experiments.

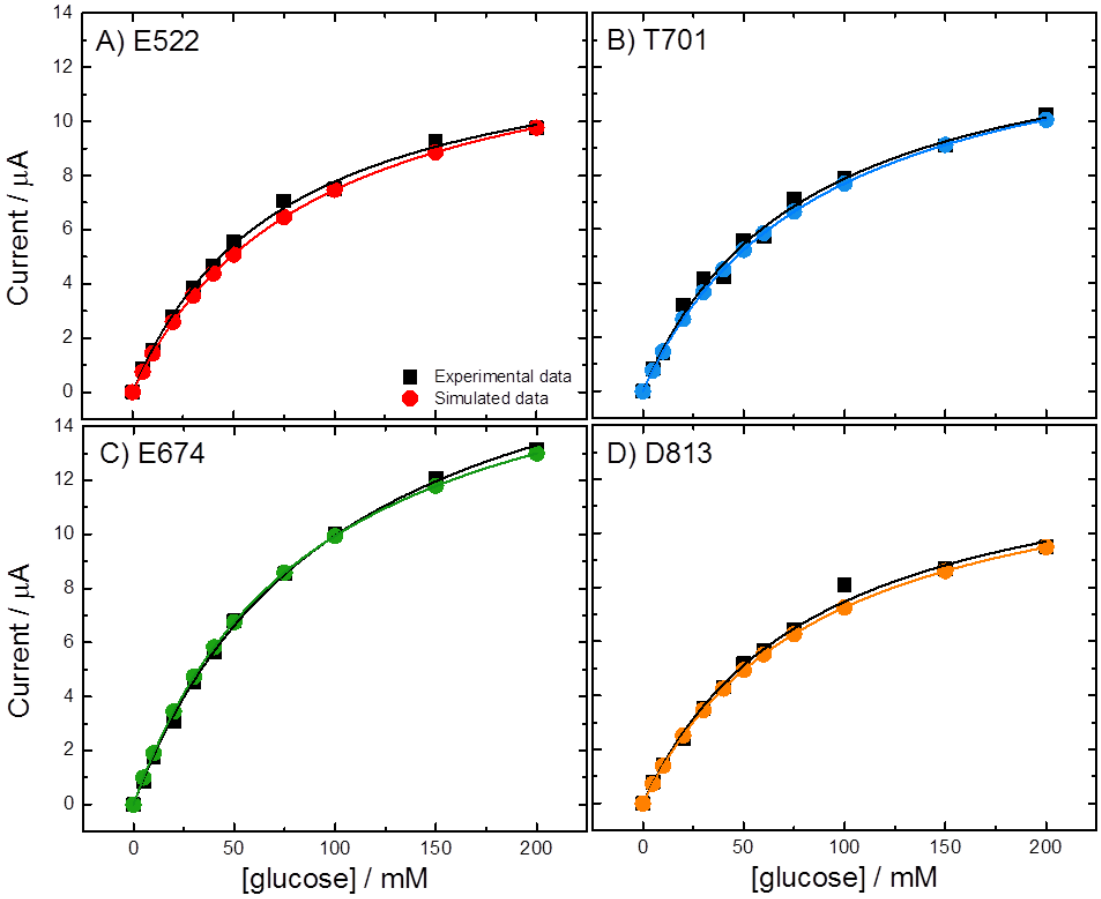

Figure 4.11. *Black squares: experimental data recorded for the MET of (A) E522, (B) T701, (C) E674 and (D) D813-CDH modified GC/CNT electrodes in 50 mM acetate buffer (pH 5.5) containing 30 mM $CaCl_2$, 1 mM ferrocene and different concentrations of glucose. Coloured circles: data simulated using Eq. 4.28 with the following parameters: [M] = 1 mM, k_{med} = 1 ×10^6 L mol^{-1} s^{-1}, K_M = 90 mM, k_{cat} = 7.2 s^{-1} and different concentrations of substrate. m_{enz} was (A) 10.3 pmol, (B) 10.6 pmol, (C) 13.7 pmol and (D) 10 pmol. The current was taken at 0.4 V vs. SCE. Lines: fitting curves using Eq. 4.26.*

K_M^{APP} extracted by fitting the simulated data (about 89 mM for all of the variants) is very close to the K_M used for the simulation (90 mM) and to the experimental K_M^{APP}, which is 75 mM for E522, 80 mM for T701, 101 mM for E674 and 85 mM for D813.

In conclusion, using the MET results, we have found that three of the four electrodes modified with different CDH variants presented roughly the same amount of enzyme, which was about 10 pmol. The fourth electrode presented a higher amount of CDH (13.7 pmol). At this point, we can carry on with the

simulation of the DET results of the four CDH variants. However, first we need to find out which values of m_{enz} and k_{int} are the best to use in our simulations and what is the relationship between them.

4.3.3 Estimation of m_{enz} and k_{int} for DET data

In Section 4.2.6 we have already estimated k_{int} for the variant E522, which was found to be 5.2 s^{-1} using Eq. 4.41, value very close to the one we have been using in our previous simulations (5 s^{-1}). However, our previous simulations of the DET results were performed using a value of m_{enz} (2.9 pmol) smaller than the one used to simulate the MET results (10.3 pmol). We have not studied what is the relationship between m_{enz} and k_{int} yet, and whether we could use, also in the case of the DET, the same m_{enz} found for the MET. For that, we will now simulate the data of the DET current of one CDH variant (always E522) using different combinations of m_{enz} and k_{int}.

The results of the simulations are reported in Figure 4.12 and the simulation parameters can be found also in Table 4.5. The first experiment (Figure 4.12-A) was carried out using the same value of m_{enz} found for the MET of the same electrode (10.3 pmol) and the same k_{int} used in our previous simulations of the DET (5 s^{-1}), which is however very close to the one calculated in Section 4.2.6. It is clear that the simulated data do not match at all with the experimental ones: also in Table 4.5 we can see that i_{max}^{APP} for the simulation A is much higher than the experimental one. In fact, i_{max}^{APP} depends on m_{enz} and k_{cat}^{APP} (see Eq. 4.26a), which in turn depends on k_{int}. Therefore, a too high value of m_{enz} or k_{int} will result in a higher current. However, K_M^{APP} extracted from the fitting of the simulated data is quite close to the experimental one. Since this depends only on k_{int} (in addition to k_{cat} and K_M), we can think that the value used for k_{int} is quite correct.

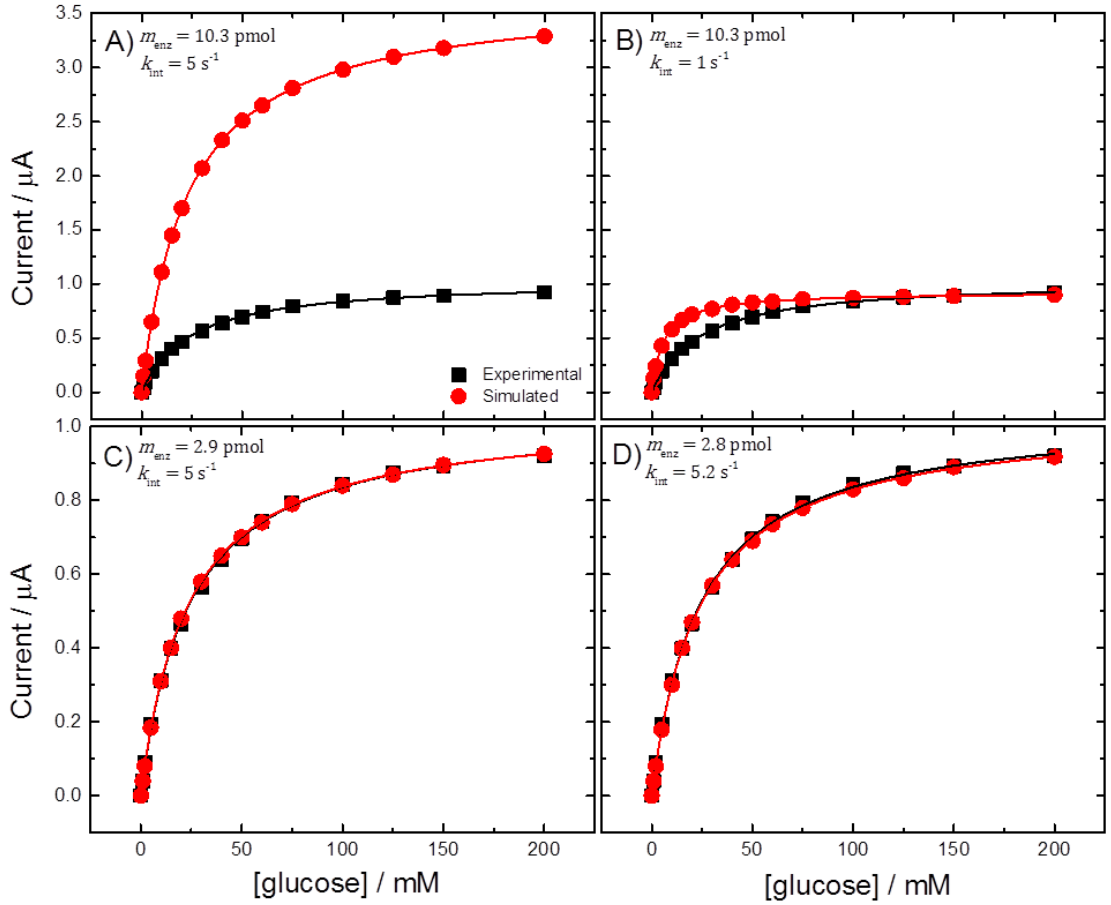

Figure 4.12. *Experimental and simulated data for the DET of a E522-CDH modified GC/CNT electrode. Black squares: experimental data recorded in 50 mM acetate buffer (pH 5.5) containing 30 mM $CaCl_2$ and different concentrations of glucose. Red circles: data simulated using Eq. 4.28 with the following parameters: [M] = 0 mM, k_{med} = 1 ×10^6 L mol^{-1} s^{-1}, K_M = 90 mM, k_{cat} = 7.2 s^{-1} and different concentrations of substrate. A) m_{enz} = 10.3 pmol, k_{int} = 5 s^{-1}; B) m_{enz} = 10.3 pmol, k_{int} = 1 s^{-1}; C) m_{enz} = 2.9 pmol, k_{int} = 5 s^{-1}; D) m_{enz} = 2.8 pmol, k_{int} = 5.2 s^{-1}. The current was taken at 0.0 V vs. SCE. Lines: fitting curves using Eq. 4.26.*

Table 4.5. *Values of K_M^{APP} and i_{max}^{APP} extracted by fitting the data in Figure 4.12 with Eq. 4.26. The values of m_{enz} and k_{int} used for the simulation are also reported.*

	Simulation parameters		**Fitting parameters**	
	m_{enz} (pmol)	**k_{int} (s^{-1})**	**K_M^{APP} (mM)**	**i_{max}^{APP} (µA)**
Experimental data	-	-	**24.0**	**1.04**
Simulation A	10.3	5	23.1	3.67
Simulation B	10.3	1	5.8	0.92
Simulation C	2.9	5	23.5	1.03
Simulation D	2.8	5.2	24.0	1.03

Since i_{max}^{APP} in the first simulation was too high, we tried to decrease the value of k_{int}. Simulation B was performed using again the same m_{enz} found for the MET and adjusting k_{int} in order to have roughly the same i_{max}^{APP} as the experimental one (so by having the same current intensity for the highest glucose concentration). For that, the best value of k_{int} was found to be 1 s^{-1}. However, also in this case, the simulation does not match very well with the experimental data (Figure 4.12-B). Even though the values of i_{max}^{APP} are quite similar, K_M^{APP} for the simulated data is much lower than the experimental one: in fact, the simulated data tend to reach the maximum more quickly than the experimental ones. This is because, according to Eq. 4.26c, decreasing k_{int} and, consequently $k_x(x)$, will decrease K_M^{APP}.

The third simulation was carried out using the value of k_{int} previously used (5 s^{-1}) and adjusting m_{enz} accordingly in order to have the best match with the experimental data: for that, a value of 2.9 pmol was used. This time, the simulated and experimental data match very well with each other (Figure 4.12-C), and also the values of i_{max}^{APP} and K_M^{APP} are very similar (see Table 4.5). Finally, simulation D was done using the value of k_{int} calculated using Eq. 4.41 (5.2 s^{-1}) and adjusting m_{enz} accordingly, so that a value of 2.8 pmol was used, which is very similar to the one used in simulation C. Also this simulation is very good, and the values of i_{max}^{APP} and K_M^{APP} are the closest ones to the experimental ones. Since there are no relevant differences between the two last simulations (Figure 4.12-C and D), we can assume that changing k_{int} from 5 to 5.2 s^{-1} had not a big effect on the current, as well as changing m_{enz} from 2.9 to 2.8 pmol. Therefore, we could use one or the other set of values: for the moment we will keep k_{int} equal to 5 s^{-1} (and consequently m_{enz} equal to 2.9 pmol for E522).

To conclude, we proved that the value of m_{enz} used to simulate the MET results is not suitable for the DET, for which instead we need to use a lower value. Even if the MET voltammograms were recorded the day after the ones for the DET (and during that time the electrodes could have lost some enzyme molecules), it looks like the amount of enzyme able to produce MET current is always more than the one able to give the DET current. This could be due to different factors, or a combination of them, considering that the mediator used in this work, ferrocene, interacts directly with the FAD group, so that the haem would be excluded from

the MET mechanism. First, we can imagine that not all the immobilised CDH molecules might be in the right orientation with the haem close enough to the electrode surface and, therefore, able to transfer electrons to it. Second, some of the CDH molecules could have lost the cytochrome domain so that they are not able to give DET, while they are still capable of catalysing the oxidation of glucose and producing MET current by interaction with the ferrocene.

For these reasons, we can suppose that there are two different populations of immobilised enzyme: one able to give DET and MET, $m_{enz}{}^{D+M}$, and another that can give only MET, $m_{enz}{}^{M}$. Given that, we need to change Eq. 4.28 as it depends only on one amount of enzyme and, while it can be used to simulate independently the data for DET or MET by changing m_{enz}, it cannot be employed if we want to simulate a full voltammogram matching with the experimental one in DET and MET at the same time.

4.3.4 New equation to simulate two enzyme populations

To address the problem highlighted in the previous section, we developed a new equation for the current that takes into account the presence of two different populations of enzyme on the electrode surface, $m_{enz}{}^{D+M}$ and $m_{enz}{}^{M}$:

$$i = \frac{2Fk_{cat}[S]m_{enz}{}^{D+M}}{[S]\left(1+\frac{k_{cat}}{k_x{}^{D+M}(x)}\right)+K_M} + \frac{2Fk_{cat}[S]m_{enz}{}^{M}}{[S]\left(1+\frac{k_{cat}}{k_x{}^{M}(x)}\right)+K_M} \qquad \text{(Eq. 4.42)}$$

where $k_x{}^{D+M}(x)$ contains the terms k_{int} and k_{med} and is given by Eq. 4.24, and $k_x{}^{M}(x)$ contains only the term k_{med} and is given by Eq. 4.24b.

This new equation was tested to simulate the cyclic voltammograms (background subtracted) recorded at a E522-CDH modified electrode in DET and MET, with 200 mM glucose (Figure 4.13-A). For the simulation (red line in Figure 4.13) we used the values of k_{med}, K_M and k_{cat} previously defined, the value of k_{int} that was found in the previous section to better match with the experimental data (5 s^{-1}), $m_{enz}{}^{D+M}$ = 2.9 pmol and $m_{enz}{}^{M}$ = 7.4 pmol (the difference between m_{enz} used to simulate the MET data and the one used for the DET). The simulated CV matches very well with the two experimental CVs for DET and MET (grey and black lines).

Figure 4.13-B shows the same simulated CV (red line) together with the single terms for the current that form Eq. 4.42: the first term depending on m_{enz}^{D+M} (blue line) and the second term depending on m_{enz}^{M} (green line). Note that the first CV presents both a direct and mediated catalytic current, while the second

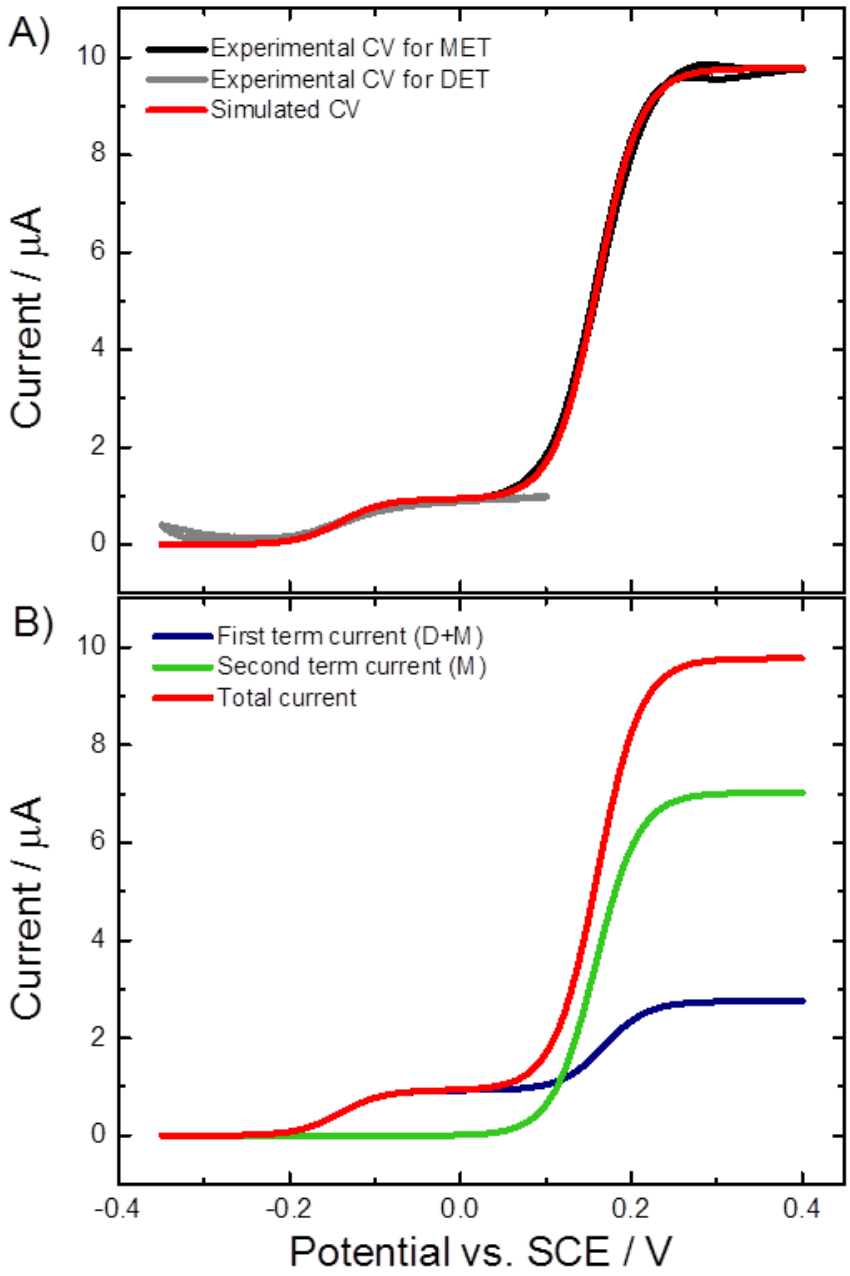

Figure 4.13. *A) Black and grey lines: experimental CVs, background subtracted, recorded at a E522-CDH modified GC/CNT electrode in 50 mM acetate buffer (pH 5.5) containing 30 mM $CaCl_2$ and 200 mM glucose (grey), and with the addition of 1 mM ferrocene (black), scanning the electrode potential at 1 (grey) and 2 mV/s (black). Red line: CV simulated using Eq. 4.42 with the following parameters: [M] = 1 mM, k_{med} = 1 ×10^6 L mol^{-1} s^{-1}, K_M = 90 mM, k_{cat} = 7.2 s^{-1}, k_{int} = 5 s^{-1}, [S] = 200 mM, m_{enz}^{D+M} = 2.9 pmol, m_{enz}^{M} = 7.4 pmol. B) Red: same as before; blue: first term in Eq. 4.42 depending on m_{enz}^{D+M}; green: second term in Eq. 4.42 depending on m_{enz}^{M}.*

CV presents only a mediated catalytic current. The total current (red line) is the sum of the two terms. This equation seems perfect to simulate the DET and MET experiments together, or the MET experiments alone where, however, also the DET current is always present at lower potential. However, in the simulations of the DET alone, we will carry on using Eq. 4.28 since also the experimental results were recorded in the absence of mediator and, therefore, MET current.

4.3.5 Simulation of the DET of the four CDH variants

Finally we will simulate the DET results for the three remaining CDH variants (T701, E674 and D813). In Section 4.3.3, we proved that the value of m_{enz} used to simulate the MET results is not suitable for the DET, for which instead we need to use a lower value. Since m_{enz} is not known, we will first fix a value for k_{int}, and then adjust m_{enz} accordingly in order to match the simulated data with the experimental ones. As we have discussed earlier, we do not know whether k_{int} is the same for all the different variants or not. For the moment we will suppose that it is the same, so we will use the same value of k_{int} previously employed with the variant E522, which was 5 s^{-1}.

Figure 4.14 shows all the simulations (coloured circles) together with the experimental data (black squares) for the three remaining CDH variants. For the first three simulations (A, B and C) we used k_{int} = 5 s^{-1}, adjusting m_{enz} in order to better match the simulated data with the experimental ones (all the parameters used are reported in Table 4.6). We can note that for the variants T701 and D813 (Figure 4.14-A and B) the simulations match quite well with the experimental data. In fact, as we can see in Table 4.6, for these two variants the experimental K_M^{APP} are very similar, being 21 and 19 mM, respectively. Therefore, since K_M^{APP} depends on k_{int}, we would expect similar values of k_{int} for these two enzymes, as well as for the variant E522. The values of m_{enz} used were 2.9 and 3.4 pmol for T701 and D813, respectively: in fact, T701 presents a curve current/glucose concentration very similar to the variant E522, while for D813 the current is slightly higher (see also Figure 3.11).

On the other hand, for the variant E674, the first simulation performed using the same k_{int} as for all the other variants did not match very well with the

experimental data (Figure 4.14-C). In fact, also the K_M^{APP} extracted from the simulated data (23 mM) is quite different from the experimental one (33 mM). Using Eq. 4.41, we obtained a value of 8.3 s^{-1} for k_{int}, which can be approximated to 8 s^{-1}. The simulation performed with that new value (Figure 4-14-D) matched better with the experimental data, and also the K_M^{APP} extracted from the fitting is very close to the experimental one (see Table 4.6).

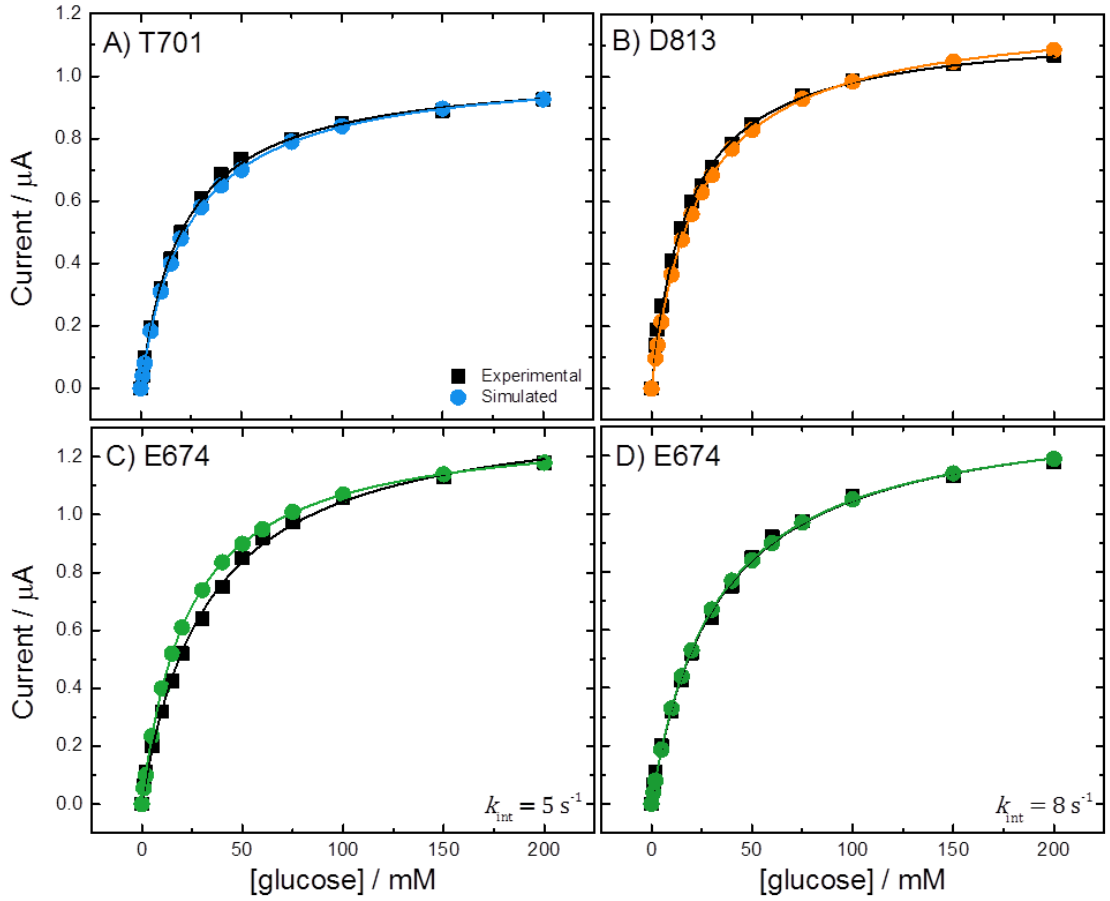

Figure 4.14. *Black squares: experimental data for the DET of (A) T701, (B) D813 and (C-D) E674-CDH modified GC/CNT electrodes in 50 mM acetate buffer (pH 5.5) containing 30 mM $CaCl_2$ and different concentrations of glucose. Coloured circles: data simulated using Eq. 4.28 with the following parameters: [M] = 0 mM, k_{med} = 1 ×10^6 L mol^{-1} s^{-1}, K_M = 90 mM, k_{cat} = 7.2 s^{-1} and different [S]. k_{int} was (A, B, C) 5 s^{-1} and (D) 8 s^{-1}. m_{enz} was: (A) 2.9 pmol; (B) 3.4 pmol; (C) 3.7 pmol, and (D) 2.8 pmol. The current was taken at 0.0 V vs. SCE. Lines: fitting curves using Eq. 4.26.*

Table 4.6. *Values of K_M^{APP} and i_{max}^{APP} extracted by fitting the data in Figure 4.12-C for the variant E522 and Figure 4.14 for the other variants with Eq. 4.26. The values of m_{enz} and k_{int} used for the simulation are also reported.*

CDH variant	Data plot	Simulation parameters		Fitting parameters	
		k_{int} (s^{-1})	m_{enz} (pmol)	K_M^{APP} (mM)	i_{max}^{APP} (µA)
E522	Experimental	-	-	**24.0**	**1.04**
	Simulation	5	2.9	23.5	1.03
T701	Experimental	-	-	**21.0**	**1.02**
	Simulation	5	2.9	23.5	1.03
D813	Experimental	-	-	**18.6**	**1.16**
	Simulation	5	3.4	23.1	1.21
E674	Experimental	-	-	**32.7**	**1.39**
	Simulation C	5	3.7	23.1	1.32
	Simulation D	8	2.8	32.1	1.38

In conclusion, we found that k_{int} presents very similar values for three of the four CDH variants, namely E522, T701 and D813, for which we can use the value of 5 s^{-1}. The variant E674, instead, has probably a different value of k_{int}, which was found slightly higher than for the other three (8 s^{-1}). This would mean a faster IET rate for this variant, maybe because of a closer conformation of the enzyme. Probably, E674 better accommodates on the electrode surface with the FAD and haem domains closer to each other, maybe because of favourable interactions with the electrode surface (see Figure 3.10 for the different orientations of the CDH variants on the electrode). On the contrary, the other three variants would present the two domains slightly farther from each other, even if close enough to have a good IET rate, as the experiments were performed at pH 5.5 and in the presence of $CaCl_2$. Most probably, to find different values of k_{int} for all the CDH variants, we should simulate experiments performed in different conditions, such as neutral pH and absence of divalent cations. However, this goes beyond our intentions here and in this chapter we will only show the simulations carried out to match the experimental results obtained at pH 5.5.

Table 4.7 reports the best values of k_{int} found for the four CDH variants, together with the best values of m_{enz} found for the DET of the four enzymes, denominated as m_{enz}^{D+M} since this is the amount of enzyme able to give both DET and MET. If we compare it with the total amount of enzyme found for each electrode, m_{enz}^{TOT}, which would be the sum of m_{enz}^{D+M} and m_{enz}^{M} and was previously determined by simulating the MET results in Section 4.3.2 (Figure 4.11), we can calculate the percentage of enzyme capable of DET for each variant (Table 4.7, 5th column). We can see that the percentage is basically the same for E522 and T701 (28 and 27 %), while it is slightly lower for E674 and higher for D813.

At the beginning of this Section 4.3, we were wondering if the differences in the plots of current/glucose concentration for the four CDH variants was due to a different amount of enzyme immobilised on the electrodes, a different amount of enzyme molecules capable of direct electron transfer or a different IET rate. Now we can conclude that the total amount of immobilised enzyme was roughly the same at least for three of the electrodes (the ones with the variants E522, T701 and D813), while it was higher for the variant E674 since the MET current was also higher. Moreover, from the ratio $m_{enz}^{D+M}/m_{enz}^{TOT}$, we can say that the differences in the plots of the four CDH variants should be due to a different amount of molecules able to give DET current. This may be due to the different orientations of the CDH variants on the electrode surface, or to the loss of a different amount of cytochrome domain from the immobilised enzyme. In addition, at least for one of the variants (E674), the different plot observed in Figure 3.11 in the previous chapter, may be due also to a faster IET rate as the kinetic constant k_{int} was found to be higher than the other ones.

Table 4.7. *Best values of k_{int}, m_{enz}^{D+M} and m_{enz}^{TOT} obtained from the simulations, and percentage of m_{enz}^{D+M} over m_{enz}^{TOT} for the four CDH variants.*

CDH variant	Simulation parameters			Percentage
	k_{int} (s^{-1})	m_{enz}^{D+M} (pmol)	m_{enz}^{TOT} (pmol)	$m_{enz}^{D+M}/m_{enz}^{TOT}$ (%)
E522	5	2.9	10.3	28
T701	5	2.9	10.6	27
E674	8	2.8	13.7	20
D813	5	3.4	10.0	34

4.4 Interaction between CDH and ferrocene

4.4.1 Limit of our model

So far, our potential-dependent Michaelis-Menten equation seems to work very well, being able to simulate the experimental data collected for four different CDH variants in DET and MET experiments. However, there is still one experiment that our model is not able to reproduce, which is the one reported in Figure 3.14 in Chapter 3. In that section, we reported the unusual behaviour of ferrocene as mediator for our CDH-modified electrodes: we found that, increasing the concentration of ferrocene in solution, the catalytic current shifted at more cathodic potentials. This was explained by the fact that the FAD oxidation and, therefore, the catalytic current, is actually due to the oxidised form of ferrocene, whose concentration depends on the applied potential. This was also confirmed in Section 4.2.2 with the estimation of the kinetic constant responsible for the reaction between FAD and ferrocene, which was found to be very high (1×10^6 L mol^{-1} s^{-1}), indicating that a very small amount of ferrocenium ion (in the order of few μM) is sufficient to react with the enzyme and, therefore, produce the catalytic current.

In Section 4.2.2, we showed that our model was able to simulate the potential shift of the MET catalytic current when changing the concentration of mediator (see Figures 4.3-B and 4.4). However, there is another characteristic of Figure 3.14 that we cannot yet reproduce, which is the fact that the MET current reaches a maximum at about 20 μM ferrocene and, after that, does not increase anymore with increasing concentrations of mediator.

We will try now to simulate the voltammograms for different concentrations of mediator, using Eq. 4.42, keeping all the parameters constant and equal to the best values found so far, except for the amount of immobilised enzyme, which can be different since this experiment was carried out using a different electrode. If we start our simulations trying to match the experimental CV for 1 μM ferrocene, we need to use m_{enz}^{M} equal to 21 pmol, while m_{enz}^{D+M} will be given by the value of the DET current (between 0.0 and 0.1 V), which is around 0.3 μA, so that m_{enz}^{D+M} = 1.25 pmol (Figure 4.15). In this way, the simulated CV for 1 μM ferrocene matches perfectly with the experimental one (Figure 4.15-C) but,

increasing the concentration of mediator, the catalytic current in the simulations increases too much, so that for the highest values of [M] (100 and 200 µM) it is double of the experimental one (Figure 4.15-D).

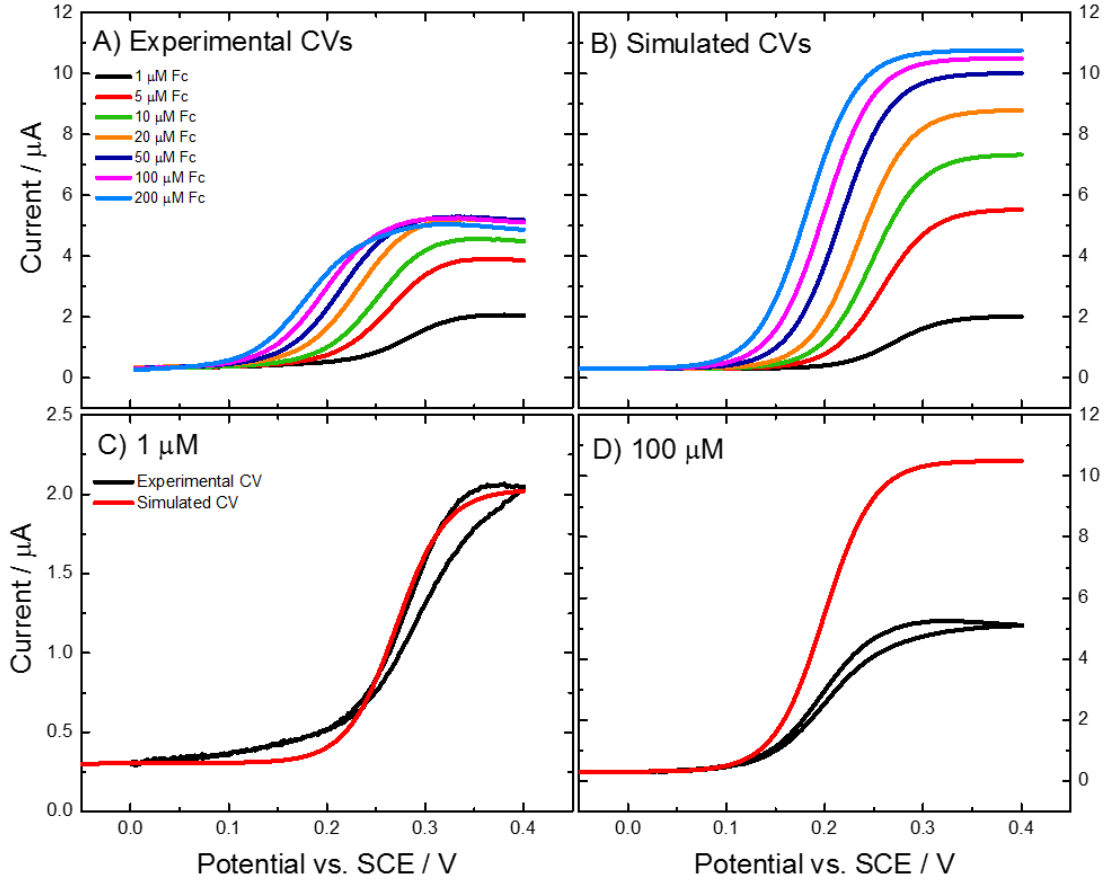

Figure 4.15. *A) Experimental CVs (forward scans only) recorded at a E522-CDH modified GC/CNT electrode in 50 mM acetate buffer (pH 5.5) containing 30 mM $CaCl_2$, 50 mM glucose and different concentrations of ferrocene. B) CVs simulated using Eq. 4.42 with the following parameters: [S] = 50 mM, k_{med} = 1 ×10⁶ L mol⁻¹ s⁻¹, K_M = 90 mM, k_{cat} = 7.2 s⁻¹, k_{int} = 5 s⁻¹, m_{enz}^{D+M} = 1.25 pmol, m_{enz}^{M} = 21 pmol and different concentrations of mediator. C and D) (Black) Experimental and (red) simulated CVs for (C) 1 µM and (D) 100 µM ferrocene.*

On the other hand, if we first try to match the voltammograms for the highest ferrocene concentrations, for example 100 µM, we need to use m_{enz}^{M} equal to 10 pmol, while keeping m_{enz}^{D+M} the same as before (Figure 4.16). This time, the simulated CV for 100 µM ferrocene matches perfectly with the experimental one (Figure 4.16-D), but this is not true for smaller values of [M]: for 1 µM ferrocene the simulated current is half of the experimental one (Figure 4.16-C). Note that, in any case, our model reproduces very well the potential shift of the catalytic current by varying the concentration of mediator.

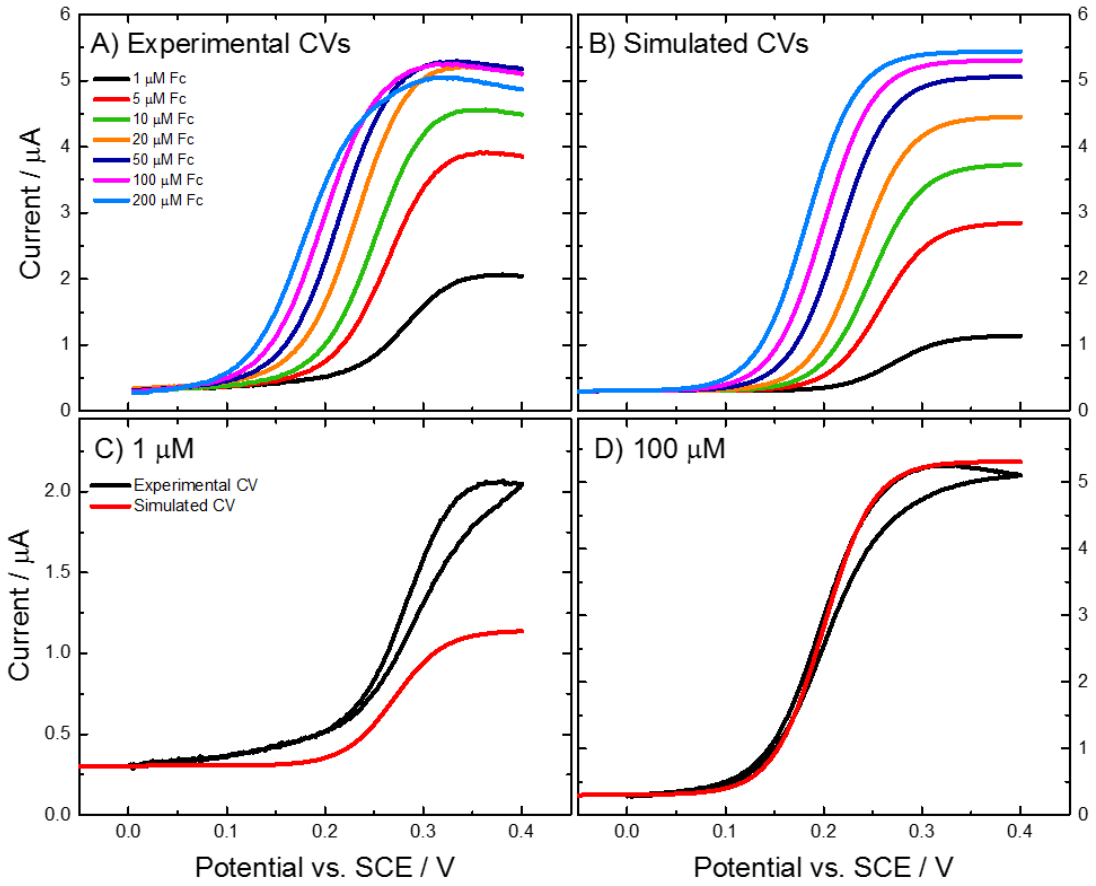

Figure 4.16. *A) Experimental CVs (forward scans only) recorded at a E522-CDH modified GC/CNT electrode in 50 mM acetate buffer (pH 5.5) containing 30 mM $CaCl_2$, 50 mM glucose and different concentrations of ferrocene. B) CVs simulated using Eq. 4.42 with the following parameters: [S] = 50 mM, k_{med} = 1 ×10^6 L mol^{-1} s^{-1}, K_M = 90 mM, k_{cat} = 7.2 s^{-1}, k_{int} = 5 s^{-1}, m_{enz}^{D+M} = 1.25 pmol, m_{enz}^{M} = 10 pmol and different concentrations of mediator. C and D) (Black) Experimental and (red) simulated CVs for (C) 1 µM and (D) 100 µM ferrocene.*

We might think that the different results between experimental and simulated data may be due to experimental error, since the concentration of ferrocene in solution was so small. In fact, if we plot the values of the current taken in the experimental and simulated voltammograms of Figure 4.16-A and B, we can see that the trend of the two sets of data is not so different (Figure 4.17): also in the simulations the current reaches a maximum and does not increase a lot after that. This is because, for relatively high concentrations of mediator (higher than 20 µM), i_{max} is limited by the reaction between the enzyme and the substrate and will be given by Eq. 4.30. Therefore, even increasing the concentration of ferrocene in solution, the current will not further increase because the rate of glucose oxidation does not change.

On the other hand, for concentrations of mediator smaller than 20 μM, the current is almost linear with [M]. This is because, in that case, k_{cat} is much higher than $k_x(x)$, which is given by Eq. 4.24b when MET is the dominant process: even if k_{med} has always a very high value (1×10^6 L mol^{-1} s^{-1}), $k_x(x)$ is directly proportional to the concentration of Fc^+. Therefore, for very small ferrocenium concentration, k_{cat}^{APP} will be equal to $k_x(x)$ as described by Eq. 4.39. By substituting this expression of k_{cat}^{APP} in Eq. 4.26a, we will have that i_{max}^{APP} is given by Eq. 4.31, and therefore the current depends on k_{med} and [Fc^+].

This explains that, for relatively low concentrations of mediator, the current is limited by the reaction between FAD and the ferrocene. However, looking more carefully at Figure 4.17, it looks like the current reaches its maximum more quickly in the experimental data than in the simulated ones. For that, we could think that there are some other factors playing a role here.

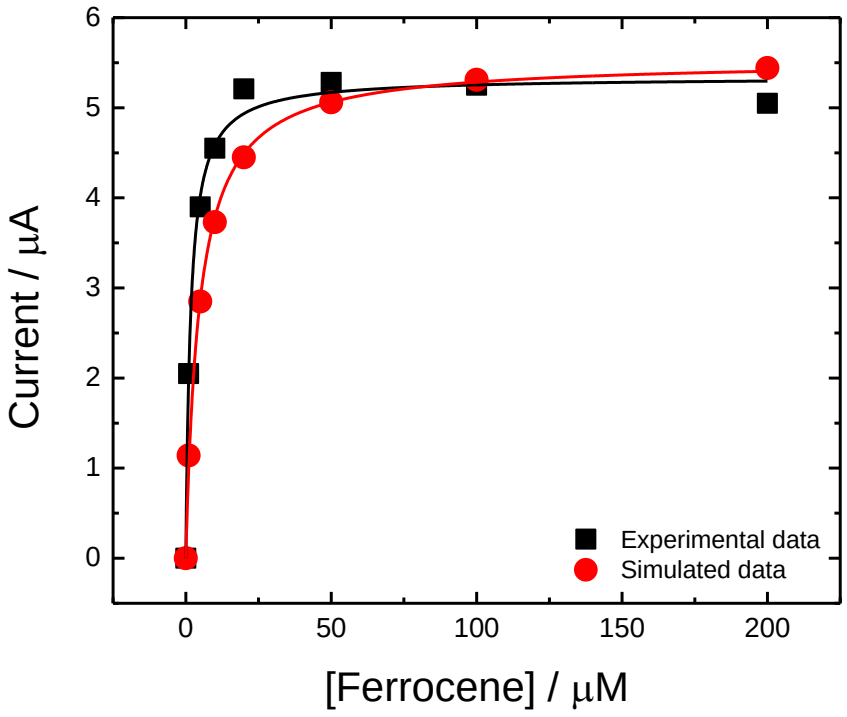

Figure 4.17. *Black squares: experimental data recorded at a E522-CDH modified GC/CNT electrode in 50 mM acetate buffer (pH 5.5) containing 30 mM $CaCl_2$, 50 mM glucose and different concentrations of ferrocene. Red circles: data simulated using Eq. 4.42 with the following parameters: [S] = 50 mM, k_{med} = 1 ×10^6 L mol^{-1} s^{-1}, K_M = 90 mM, k_{cat} = 7.2 s^{-1}, k_{int} = 5 s^{-1}, m_{enz}^{D+M} = 1.25 pmol, m_{enz}^{M} = 10 pmol and different concentrations of mediator. The current was taken at 0.4 V vs. SCE. Lines: fitting curves using Eq. 4.26.*

4.4.2 Michaelis-Menten interaction between CDH and ferrocene

As we have said in the previous section, the limiting current in Figure 4.17 is due to the enzyme-substrate reaction and, therefore, determined by the value of k_{cat} (for Eq. 4.30). However, we could imagine a Michaelis-Menten-like interaction between the enzyme and the mediator. For that, we fitted the data reported in Figure 4.17 with the Michaelis-Menten equation, already applied for the enzyme-substrate reaction, to extract the values of i_{max}^{APP} and K_M^{APP} for the ferrocene. i_{max}^{APP} is very similar between the experimental and simulated data: 5.3 and 5.5 μA, respectively. K_M^{APP} is quite different, being 1.6 μM for the experimental data and 4.6 μM for the simulated ones.

Such Michaelis-Menten-like interaction between CDH and mediators finds confirmation in the literature. Several authors reported that CDH oxidises sugars such as cellobiose, lactose and glucose (which act as electron donors) and, at the same time, reduces a very wide range of quinones, organic radical species, cytochrome c and complexes of metals like Fe, Cu and Mn (which act as electron acceptors) [150-152]. Both electron donors and acceptors can be considered as substrates for CDH, in fact several authors reported the Michaelis-Menten parameters, K_M and k_{cat}, for both categories of substrates [72,151,153]. In addition, while most of the publications report the use of CDH for glucose or lactose detection, Lindgren *et al.* showed that CDH can also be used for the amperometric detection of diphenols, which are reduced by the enzyme in the presence of an electron donor like cellobiose [87].

Many of the electron acceptors reported in the literature are used as mediators for CDH for the electrocatalytic oxidation of sugars, since they can help to transfer electrons between the reduced enzyme and the electrode surface [86,97,123,146]. Therefore, we can imagine that ferrocene, used as mediator in this work, could be considered also as a substrate for CDH and have its own values of K_M and k_{cat} for the interaction with the enzyme. In fact, in the literature there are evidences of the ferrocenium ion (the oxidised form of ferrocene) being used as electron acceptor for CDH. The authors report its values of K_M and k_{cat} for the interaction with different types of CDH: the K_M is always in the low μM range confirming that ferrocenium is a very good electron acceptor, being converted at

a fast rate, and that its kinetics is definitely of the Michaelis-Menten type [154-156].

If we imagine a Michaelis-Menten-like interaction between CDH and ferrocene, the reaction between them (already reported in Table 4.1, third step) becomes more complicate and we will need more kinetic constants to describe it. The new reactions for the reoxidation of FAD by ferrocene are reported in Table 4.8. Each of the two semioxidation reactions, oxidation of $FADH_2$ (F_3) and $FADH^{\cdot}$ (F_2), is divided in two steps: the formation of the enzyme-substrate complex and the breakdown of such complex to yield the products. Consequently, each step is associated with a kinetic constant of the type of K_M or k_{cat}. Note that for simplicity we have reported only K_M for the first step of each reaction, since it includes the two kinetic constants of the equilibrium reaction, k_f and k_b, as described in Eq. 4.1 or 4.1a.

Table 4.8. *Reaction steps for the reoxidation of FAD by ferrocene, with the relative kinetic constants.*

Step	Reaction	Kinetic constants
Reoxidation of FAD by mediator (step 1)	$F_3 + Fc^+ \rightleftharpoons \{F_3Fc^+\}$	${K_{M(1)}}^{med}$
	$\{F_3Fc^+\} \longrightarrow F_2 + Fc$	${k_{cat(1)}}^{med}$
Reoxidation of FAD by mediator (step 2)	$F_2 + Fc^+ \rightleftharpoons \{F_2Fc^+\}$	${K_{M(2)}}^{med}$
	$\{F_2Fc^+\} \longrightarrow F_1 + Fc$	${k_{cat(2)}}^{med}$

As we have previously said in Section 4.2.1, we assume the rates of the two semioxidation reactions of FAD to be the same, so that also their kinetic constants will be equal (Eq. 4.29b). Therefore, we can write:

$${K_{M(1)}}^{med} = {K_{M(2)}}^{med} = {K_M}^{med} \qquad \text{(Eq. 4.43a)}$$

$${k_{cat(1)}}^{med} = {k_{cat(2)}}^{med} = {k_{cat}}^{med} \qquad \text{(Eq. 4.43b)}$$

To keep things easier, we will not build another model to find a new equation for the current, as we have done in Section 4.1.3. To introduce the Michaelis-Menten-

like interaction between CDH and ferrocene we will just substitute k_{med} in Eq. 4.24 with the following expression:

$$k_{med} = \frac{{k_{cat}}^{med}}{{K_M}^{med} + [Fc^+]} \qquad \text{(Eq. 4.44)}$$

4.4.3 Estimation of K_M^{med} and k_{cat}^{med}

At this point, we need to estimate the values of K_M^{med} and k_{cat}^{med}. As we have already seen in the case of glucose, K_M would have a value quite similar to the K_M^{APP} extracted by fitting the MET data. Since the K_M^{APP} for the ferrocene extracted by fitting the experimental data in Figure 4.17 was 1.6 μM, we can imagine that K_M^{med} would have a value of the same magnitude order, probably a little bit higher than 1.6 μM. We will try then values between 5 and 10 μM. On the other hand, k_{cat}^{med} would depend on the value of K_M^{med} as we can see in Eq. 4.44. For concentration of ferrocenium very small (when the mediator is still in its reduced form at cathodic potentials), we could consider k_{med} as a sort of catalytic efficiency, which is the ratio k_{cat}/K_M. Therefore, we can rearrange Eq. 4.44 as follow:

$$\text{for } [Fc^+] \ll {K_M}^{med} \implies {k_{cat}}^{med} = k_{med} \cdot {K_M}^{med} \qquad \text{(Eq. 4.45)}$$

Keeping the best value of k_{med} previously found in Section 4.2.2, which was 1 $\times 10^6$ L mol^{-1} s^{-1}, we tried different values for K_M^{med} and, consequently, k_{cat}^{med}. Finally, the best compromise between the values of the catalytic current and the potential shift at the different concentrations of ferrocene was reached with K_M^{med} = 8 μM and, consequently, k_{cat}^{med} = 8 s^{-1}. Using such values, the cyclic voltammograms at different ferrocene concentrations were simulated (Figure 4.18): they match quite well with the experimental ones for both the current intensity and potential shift. To better compare the values of the current in the experimental and simulated CVs, they were plotted *vs.* the concentration of ferrocene and fitted with the Michaelis-Menten equation (Figure 4.19). The values of K_M^{APP} extracted from the fitting are quite similar: 1.6 μM for the experimental data and 2.7 μM for the simulated ones. The small difference between them can be due to experimental error since the concentration of

ferrocene added in the electrochemical cell was so small that it might have been difficult to control precisely. Note that the amount of enzyme able to give MET, m_{enz}^{M}, had to be increased from 10 to 17 pmol to simulate the voltammograms in Figure 4.18 using the new expression for k_{med} (Eq. 4.44).

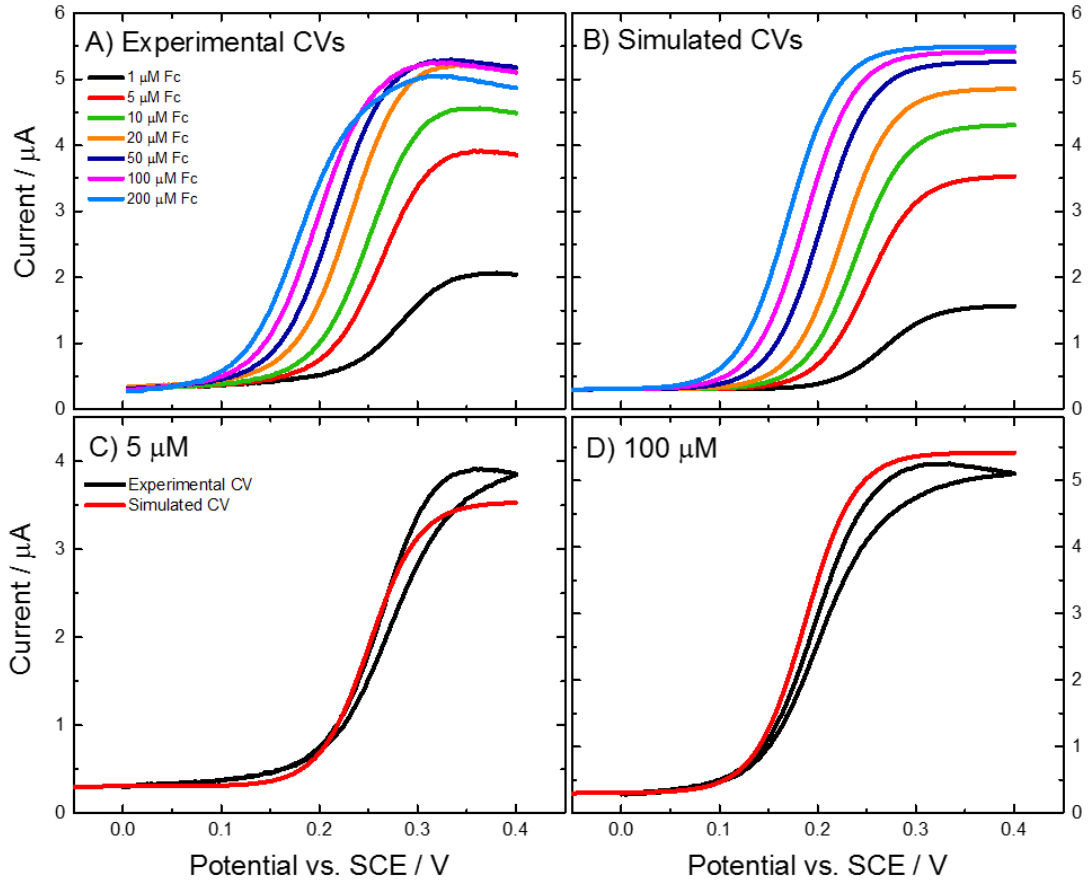

Figure 4.18. *A) Experimental CVs (forward scans only) recorded at a E522-CDH modified GC/CNT electrode in 50 mM acetate buffer (pH 5.5) containing 30 mM $CaCl_2$, 50 mM glucose and different concentrations of ferrocene. B) CVs simulated using Eq. 4.42 with the following parameters: [S] = 50 mM, K_M = 90 mM, k_{cat} = 7.2 s^{-1}, k_{int} = 5 s^{-1}, m_{enz}^{D+M} = 1.25 pmol, m_{enz}^{M} = 17 pmol, k_{cat}^{med} = 8 s^{-1}, K_M^{med} = 8 µM and different concentrations of mediator. C and D) (Black) Experimental and (red) simulated CVs for (C) 1 µM and (D) 100 µM ferrocene.*

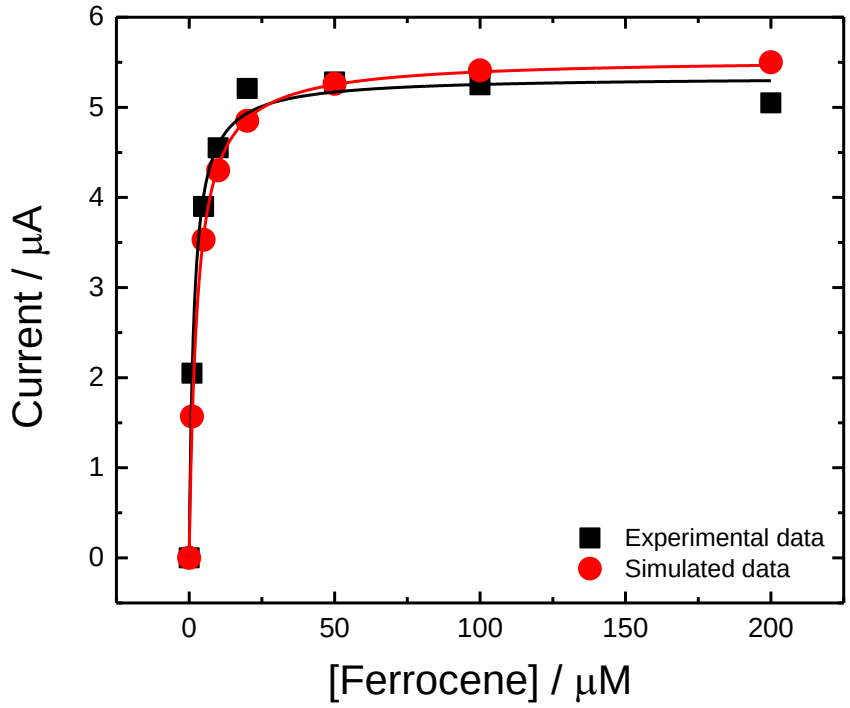

Figure 4.19. *Black squares: experimental data recorded at a E522-CDH modified GC/CNT electrode in 50 mM acetate buffer (pH 5.5) containing 30 mM $CaCl_2$, 50 mM glucose and different concentrations of ferrocene. Red circles: data simulated using Eq. 4.42 with the following parameters: [S] = 50 mM, K_M = 90 mM, k_{cat} = 7.2 s^{-1}, k_{int} = 5 s^{-1}, m_{enz}^{D+M} = 1.25 pmol, m_{enz}^{M} = 17 pmol, k_{cat}^{med} = 8 s^{-1}, K_M^{med} = 8 μM and different concentrations of mediator. The current was taken at 0.4 V vs. SCE. Lines: fitting curves using Eq. 4.26.*

4.4.4 New simulations of DET and MET experiments

Now we have established the new expression for k_{med}, we need to validate it for the simulation of the DET and MET experiments of the four CDH variants. We started by simulating the data of DET and MET for the variant E522, using Eq. 4.28 to keep things easier (in fact now $k_x(x)$ depends on more parameters than before, so it is better to avoid using Eq. 4.42 for two different populations of enzyme). Figure 4.20 reports the simulated data (red circles) together with the experimental ones (black squares) for E522-CDH: it is clear that the results of the MET do not match anymore, while the DET ones still do. In fact, the new expression for k_{med} will not affect the DET current, which does not depend on k_{med} since in the case of the DET experiments the concentration of mediator is zero, but only the MET current. Note that, since we used Eq. 4.28 for the simulations, we had to use two different amounts of enzyme to reproduce the

data in DET and MET, which were 2.9 and 18 pmol, respectively (m_{enz} for the MET was higher than the value previously used, 10.3 pmol).

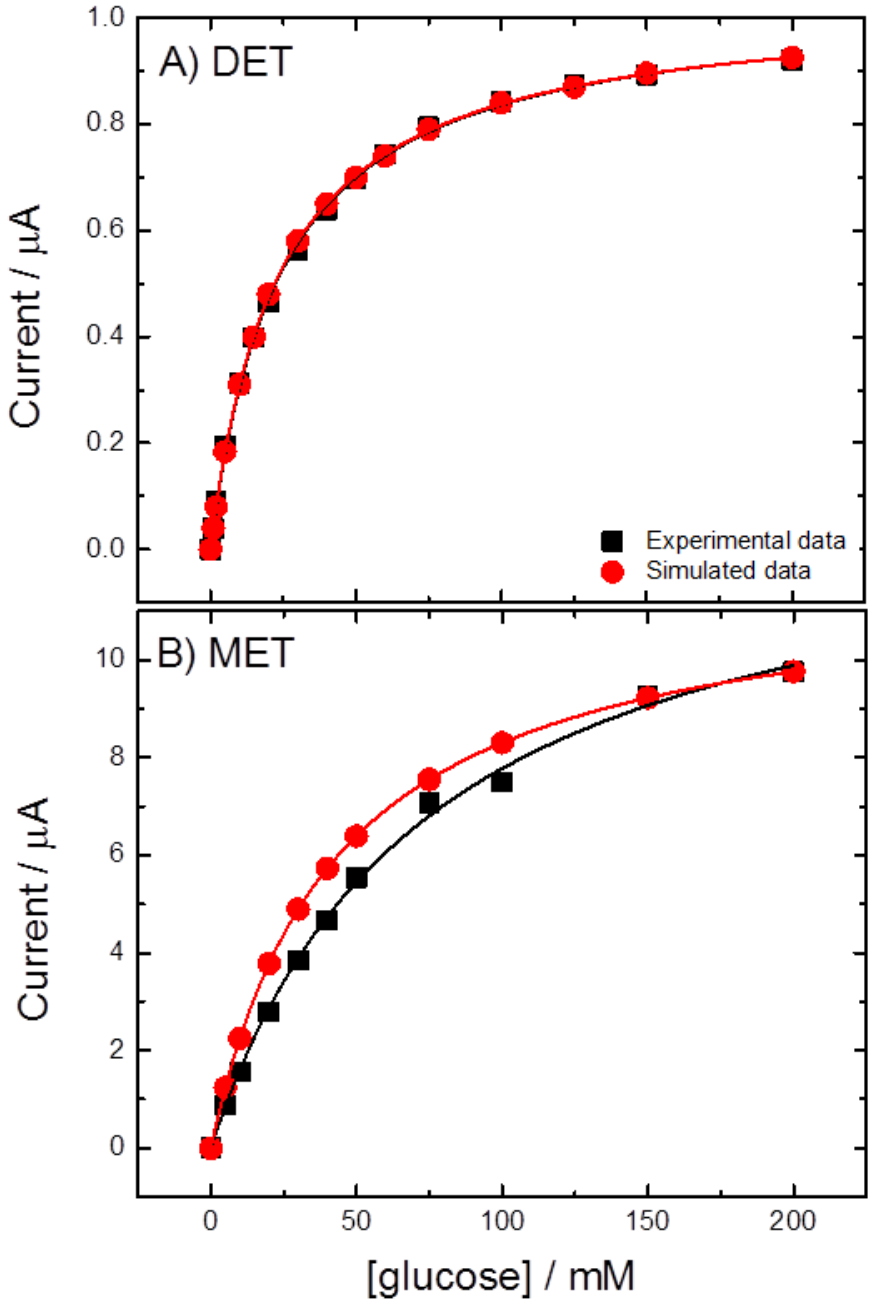

Figure 4.20. *Black squares: experimental data recorded at a E522-CDH modified GC/CNT electrode in 50 mM acetate buffer (pH 5.5) containing (A) 30 mM $CaCl_2$ and (B) with the addition of 1 mM ferrocene, at different concentrations of glucose. Red circles: data simulated using Eq. 4.28 with the following parameters: [M] = (A) 0 mM and (B) 1 mM, K_M = 90 mM, k_{cat} = 7.2 s^{-1}, k_{int} = 5 s^{-1}, m_{enz} = (A) 2.9 pmol and (B) 18 pmol, k_{cat}^{med} = 8 s^{-1}, K_M^{med} = 8 µM and different concentrations of substrate. The current was taken at (A) 0.0 and (B) 0.4 V vs. SCE. Lines: fitting curves using Eq. 4.26.*

Table 4.9. *Values of K_M^{APP} and i_{max}^{APP} extracted by fitting the data in Figure 4.20 with Eq. 4.26.*

	Data plot	Fitting parameters	
		K_M^{APP} (mM)	i_{max}^{APP} (μA)
DET	Experimental	**24.0**	**1.04**
	Simulation	23.5	1.03
MET	Experimental	**75**	**13.6**
	Simulation	42	11.8

Fitting the data of Figure 4.20 with the Michaelis-Menten equation, we can see that the values of K_M^{APP} (reported in Table 4.9) for the DET are very similar between the experimental and simulated data (as before), while the ones for the MET are very different. Note that the K_M^{APP} for the MET data is no longer similar to the K_M used to simulate the data (90 mM), as it was before. This is because $k_x(x)$, which depends on k_{int} and k_{med} (see Eq. 4.24), is very different from before: in particular, at 0.4 V *vs.* SCE it is equal to 6.5 s^{-1} using the parameters reported in Figure 4.20, while previously it was 500 s^{-1} for the same concentration of ferrocene. It follows that $k_x(x)$ is no longer much higher than k_{cat}, therefore the conditions of Eq. 4.37 are not valid anymore: with $k_x(x)$ having a value very close to k_{cat} (7.2 s^{-1}), the term at the denominator in the expression for K_M^{APP} (Eq. 4.26c) will be almost equal to 2 and, consequently, K_M^{APP} will be almost the half of K_M.

4.4.5 New estimation of K_M and k_{cat}

Since the term at the denominator in the expression for K_M^{APP} (Eq. 4.26c) has now a value close to 2 in the potential range where MET is the dominant process, K_M should be twice than given before. For that, we will try a value of 180 mM. Given that previously we found that the ratio k_{cat}/K_M (called also catalytic efficiency) was equal to 0.08 mM^{-1} s^{-1}, we can suppose k_{cat} to be equal to 14.4 s^{-1}. However, some preliminary simulations using K_M = 180 mM and k_{cat} = 14.4 s^{-1} did not work very well, so that we concluded that the catalytic efficiency needs to be changed too. By simulating the MET results (Figure 4.21), the best match between experimental and simulated data was found using the same k_{cat} as

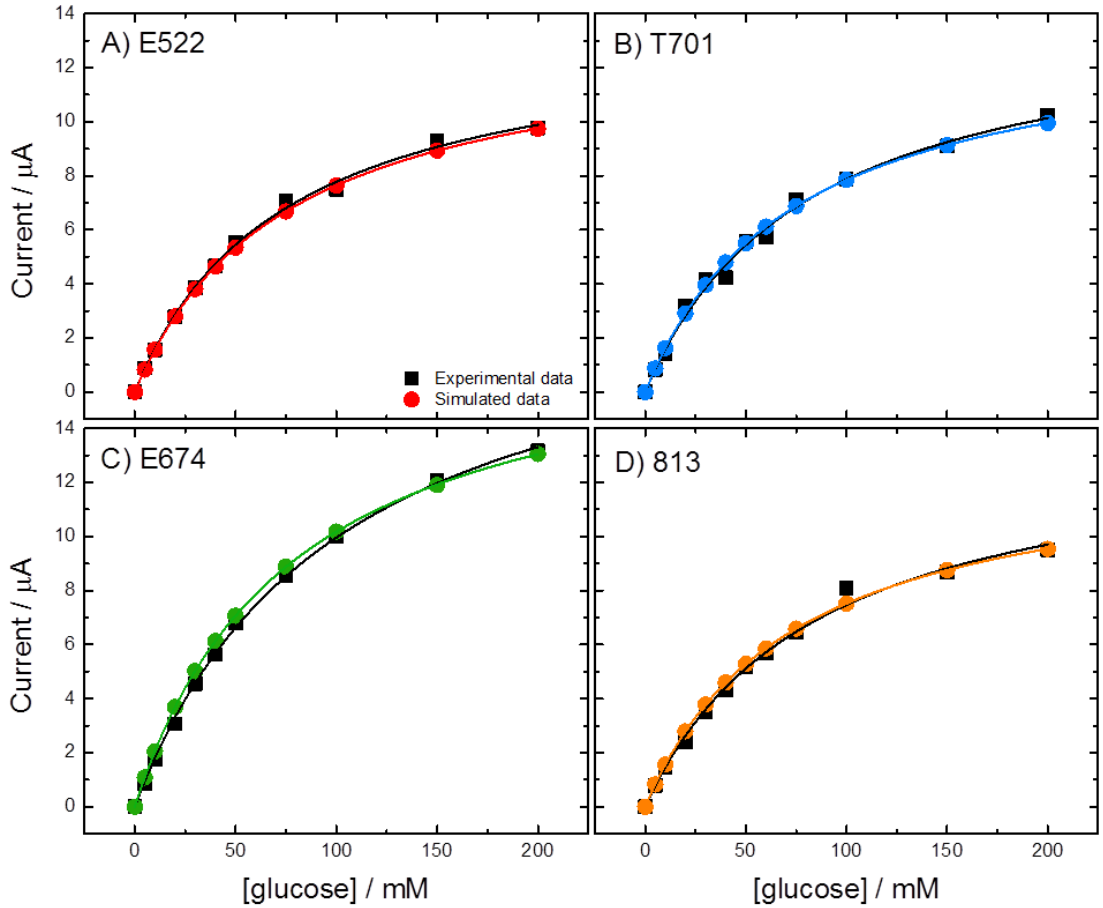

Figure 4.21. *Black squares: experimental data recorded for the MET of (A) E522, (B) T701, (C) E674 and (D) D813-CDH modified GC/CNT electrodes in 50 mM acetate buffer (pH 5.5) containing 30 mM $CaCl_2$, 1 mM ferrocene and different concentrations of glucose. Coloured circles: data simulated using Eq. 4.28 with the following parameters: [M] = 1 mM, K_M = 180 mM, k_{cat} = 7.2 s^{-1}, k_{cat}^{med} = 8 s^{-1}, K_M^{med} = 8 µM and different concentrations of substrate. k_{int} was: (A) 2.5 s^{-1}, (B) 2 s^{-1}, (C) 3.2 s^{-1} and (D) 2 s^{-1}. m_{enz} was: (A) 23, (B) 25, (C) 30 and (D) 23 pmol. The current was taken at 0.4 V vs. SCE. Lines: fitting curves using Eq. 4.26.*

before (7.2 s^{-1}), so that the new ratio k_{cat}/K_M is one half than before and equal to 0.04 mM^{-1} s^{-1}.

Using these values for K_M and k_{cat}, 180 mM and 7.2 s^{-1} respectively, the voltammograms for the MET of the four CDH variants were simulated and the data of the current taken at 0.4 V were plotted against the glucose concentration together with the experimental values (Figure 4.21). The simulations match very well with the experimental results, and also the values of K_M^{APP} and i_{max}^{APP} are very similar (see Table 4.10). Note that m_{enz} had to be increased if compared with the previous simulations of MET data in Section 4.3.2 (Figure 4.11): the new values reported in Table 4.10 are about the double than the previous ones. This is

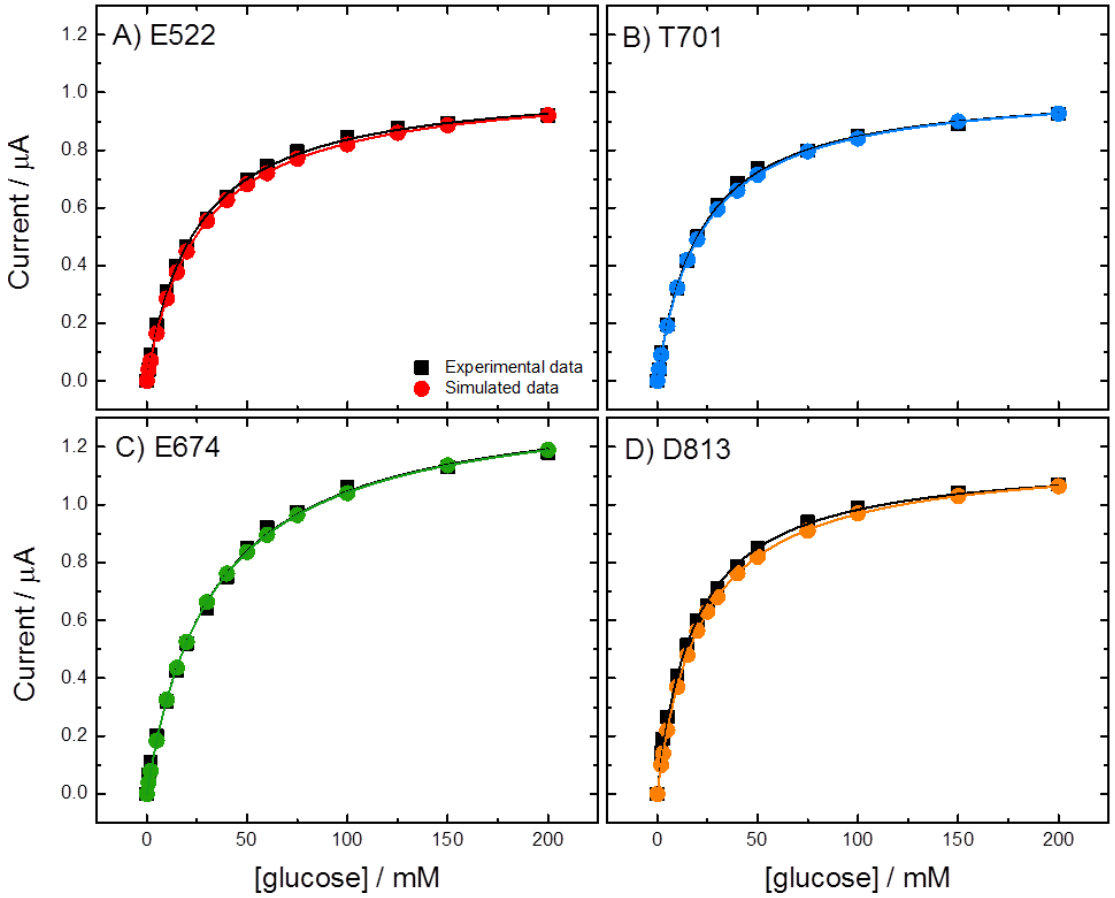

Figure 4.22. *Black squares: experimental data recorded for the DET of (A) E522, (B) T701, (C) E674 and (D) D813-CDH modified GC/CNT electrodes in 50 mM acetate buffer (pH 5.5) containing 30 mM $CaCl_2$ and different concentrations of glucose. Coloured circles: data simulated using Eq. 4.28 with the following parameters: [M] = 0 mM, K_M = 180 mM, k_{cat} = 7.2 s^{-1}, k_{cat}^{med} = 8 s^{-1}, K_M^{med} = 8 µM and different concentrations of substrate. k_{int} was: (A) 2.5 s^{-1}, (B) 2 s^{-1}, (C) 3.2 s^{-1} and (D) 2 s^{-1}. m_{enz} was: (A) 5.1, (B) 6.1, (C) 5.5 and (D) 7 pmol. The current was taken at 0.0 V vs. SCE. Lines: fitting curves using Eq. 4.26.*

because of the decrease of k_{cat}^{APP} due to the fact that $k_x(x)$ is now smaller (see Eq. 4.26b): therefore, to keep constant i_{max}^{APP}, according to Eq. 4.26a we need to increase m_{enz}.

Finally, the voltammograms for the DET of the four CDH variants were also simulated and the data of the current taken at 0.0 V were plotted together with the experimental values (Figure 4.22). Also in this case, the simulations match very well with the experimental results, and also the values of K_M^{APP} and i_{max}^{APP} are very similar (see Table 4.10). Note that k_{int} had to be change to match the simulated data with the experimental ones: in particular, it became almost one half of the value previously used. As a consequence, also in this case m_{enz} had to be increased to be almost double the value previously used (see Table 4.10 for all the simulation parameters).

Table 4.10. *Values of K_M^{APP} and i_{max}^{APP} extracted by fitting the data in Figure 4.21 and 4.22 with Eq. 4.26. The values of m_{enz} and k_{int} used to simulate the data are also reported.*

DET (Figure 4.22)		Simulation parameters		Fitting parameters	
		k_{int} (s^{-1})	m_{enz} (pmol)	K_M^{APP} (mM)	i_{max}^{APP} (µA)
E522	Experimental	-	-	**24.0**	**1.04**
	Simulation	2.5	5.1	26.5	1.04
T701	Experimental	-	-	**21.0**	**1.02**
	Simulation	2	6.1	21.9	1.03
E674	Experimental	-	-	**32.7**	**1.39**
	Simulation	3.2	5.5	32.6	1.38
D813	Experimental	-	-	**18.6**	**1.16**
	Simulation	2	7	21.9	1.18

MET (Figure 4.21)		Simulation parameters		Fitting parameters	
		k_{int} (s^{-1})	m_{enz} (pmol)	K_M^{APP} (mM)	i_{max}^{APP} (µA)
E522	Experimental	-	-	**75**	**13.6**
	Simulation	2.5	23	76	13.4
T701	Experimental	-	-	**80**	**14.2**
	Simulation	2	25	73	13.6
E674	Experimental	-	-	**101**	**20.0**
	Simulation	3.2	30	78	18.1
D813	Experimental	-	-	**85**	**13.8**
	Simulation	2	23	73	13.0

4.5 Conclusion

In this Chapter, we have described step by step the kinetics of the CDH electrode reactions, both for the direct and mediated electron transfer, assigning to each reaction a kinetic constant. From that, we have derived a potential-dependent Michaelis-Menten equation to be used with CDH or other enzymes with a similar kinetics for the simulation of their electrodic reactions. At this point, we needed to estimate the values of the kinetic constants used to build our equation, to be able to simulate the cyclic voltammograms that we have experimentally recorded at CDH-modified electrodes (reported in Chapter 3).

For the conditions used in our experiments, and that we wanted to recreate *in silico* (glucose as substrate, ferrocenecarboxylic acid as mediator, acetate buffer at pH 5.5 containing 30 mM $CaCl_2$), we found the best values for the kinetic parameters (reported in Table 4.11, 3rd columm):

- for k_{med}, using first the current obtained with a very small concentration of mediator (1 µM), and then adjusting the value according to the potential shift of the MET catalytic current;
- for K_M, by using the K_M^{APP} extracted by fitting the experimental data for the MET with the Michaelis-Menten equation;

- for k_{cat}, because 7.2 s^{-1} was the value that better matched the simulated data with the experimental ones for the MET using the K_M previously found;
- for k_{int}, looking at the value that better matched the simulated data with the experimental ones for the DET using the K_M and k_{cat} previously found. This was confirmed by a calculation using the K_M^{APP} extracted by fitting the experimental data for the DET (Eq. 4.41).

Table 4.11. *Best values of the kinetic parameters found in our simulations (of the first and second type) to match the simulated data with the experimental results for the four CDH variants.*

Kinetic parameter	CDH variant	1st Simulation (Sections 4.2-4.3)	2nd Simulation (MM interaction CDH-Fc, Section 4.4)
k_{med}	Same for all variants	1 ×10^6 L mol^{-1} s^{-1}	Given by Eq. 4.44 with K_M^{med} = 8 ×10^{-6} M and k_{cat}^{med} = 8 s^{-1}
K_M	Same for all variants	90 mM	180 mM
k_{cat}	Same for all variants	7.2 s^{-1}	7.2 s^{-1}
k_{int} (s^{-1})	E522	5	2.5
	T701	5	2.0
	E674	8	3.2
	D813	5	2.0
Ratio $m_{enz}^{D+M}/m_{enz}^{TOT}$ (%)	E522	28	22
	T701	27	24
	E674	20	18
	D813	34	30

In the literature, the K_M for *Mt*CDH with glucose was found of 250 mM [73,123,146], however this would be a K_M^{APP} since it was calculated using the same equation we used to fit our experimental data, Eq. 4.26. The same authors report a value of 14 s^{-1} for k_{cat}, which is probably a k_{cat}^{APP}, however it is quite

close to the value we found. k_{int} was found as an apparent haem reduction rate for *Mt*CDH increasing from 0.25 to 1.37 s^{-1} upon addition of 30 mM $CaCl_2$ at pH 4.5 [78]. In our simulations, we found values slightly higher for k_{int}, but still in the same range as the literature one, given also that it was an apparent haem reduction rate. Concerning k_{med}, we have not found in the literature this specific kinetic constant; however, we could compare it with the catalytic efficiency (k_{cat}/K_M) reported for the Michaelis-Menten interaction between ferrocenium and different types of CDH, which goes from 0.6 $\times 10^6$ to 181 $\times 10^6$ L mol^{-1} s^{-1} [154-156]. Therefore, our value for k_{med} is in this range.

During the simulations of the DET and MET experiments, we found that the amount of immobilised enzyme, represented by m_{enz}, could not be the same for the DET and MET simulations: in particular, for the DET m_{enz} was always much lower than in the case of the MET. This led to the conclusion that there are, on each CDH-modified electrode, two different populations of enzyme: one able to give DET and MET, the second one capable of only MET.

Given that, we successfully simulated the results for the DET and MET of the four different CDH variants. We found that the differences between them are due in part to k_{int}, therefore to a different IET rate: as we can see in Table 4.11, k_{int} was found to be 5 s^{-1} for three of the four CDH variants, while it was 8 s^{-1} for the variant E674. This means a better IET rate for this latter variant, maybe because of a closer conformation of the enzyme, probably due to a better orientation on the electrode surface, if compared with the other three variants. Moreover, from the ratio between the amount of enzyme capable of both DET and MET and the total amount of enzyme (see Table 4.11), we can conclude that the differences between the four CDH variants is due also to a different percentage of molecules able to give DET current. Also this may be attributed to the different orientations of the CDH variants on the electrode surface, otherwise to the loss of a different amount of cytochrome domain from the bound enzyme.

Finally, we investigated the relationship between CDH and the mediator used in this work, ferrocene. We concluded that there may be a Michaelis-Menten-like interaction between them, which finds confirmation also in the literature. Therefore, the rate constants K_M and k_{cat} for such interaction were estimated and

found to be 8 μM and 8 s^{-1}, respectively. Given that, the rate constant for the CDH-ferrocene reaction, k_{med}, was changed and given by Eq. 4.44. At this point, in order to simulate again the experimental results for the DET and MET of the CDH-modified electrodes, we had to change also the values of K_M, k_{int} and m_{enz}: in particular, K_M and m_{enz} almost doubled, while k_{int} became the half than before (see Table 4.11, 4th column). In any case, the relationship between the parameters k_{int} and m_{enz} of the four different variants remained almost the same, with E674 having always a higher k_{int} but a lower $m_{enz}^{D+M}/m_{enz}^{TOT}$ ratio than the other variants. The simulations were a success also in this case, so that we can conclude that both the methods can be used to simulate the cyclic voltammograms recorded at CDH-modified electrodes.

We can make another consideration by looking at the values of the k_{cat} found for the glucose/CDH and the ferrocene/CDH reactions, which were 7.2 and 8 s^{-1}, respectively. These two k_{cat} are very similar to each other, so that we can think that in the MET process the current is limited by the ferrocene/CDH reaction, not by the glucose oxidation by FAD. In fact, if the ferrocene-CDH reaction were the rate limiting step, it would mean that also the other reactions involved in the MET catalytic process have the same speed (once the steady state is achieved) and, consequently, a similar value for the catalytic constant. This hypothesis, true only if we consider valid the Michaelis-Menten interaction between ferrocene and CDH, would be confirmed by using a different mediator with a different k_{cat}^{med}, or a different substrate.

Some preliminary results obtained by simulating the MET data for the variant E522 using the Michaelis-Menten interaction between ferrocene and CDH (so Eq. 4.44 in substitution of k_{med}) and changing the value of k_{cat} for the glucose-FAD reaction, suggested indeed that the current is not limited only by the latter reaction. In fact, increasing k_{cat}, i_{max}^{APP} does not linearly increase with it like it did before we applied the ferrocene/CDH Michaelis-Menten interaction (see Figure 4.7-A). In the simulations of Figure 4.7-A, increasing k_{cat} up to 100 s^{-1} made i_{max}^{APP} increase up to 165 μA. On the contrary, substituting k_{med} with Eq. 4.44 would lead to a i_{max}^{APP} of just 22 μA for k_{cat} = 100 s^{-1}. This clearly suggests that there is another rate limiting step in the MET process, which must be the ferrocene/CDH reaction. However, it is probably more correct to say that the two reactions,

glucose/CDH and ferrocene/CDH, are in competition between each other, being both rate limiting steps, since we could still increase i_{max}^{APP} by increasing k_{cat} at values higher than 7.2 s^{-1}. This is a very interesting topic to be further investigated, and it would mean that the ferrocene/CDH reaction is not as fast as we thought at the beginning of this Chapter.

Chapter 5:

Covalent immobilization of CDH at flat electrodes

Since all the different CDH variants immobilised at GC/CNT electrodes showed high catalytic currents for the DET, we thought that a better discrimination between them could arise from their immobilization at flat electrodes. This is what will be shown in this Chapter, starting with the covalent immobilization of CDH at glassy carbon (GC) electrodes and then moving to flat gold electrodes. For the first ones, the same method already described for the modification of GC/CNT electrodes in Chapter 3 was employed. On the other hand, for the immobilization of CDH at gold electrodes some "bricks" of the molecular architecture were changed, keeping however unvaried the use of maleimide as the reactive group and the idea of a mixed monolayer to dilute the maleimide groups at the electrode surface.

5.1 Immobilization of CDH at flat GC electrodes

5.1.1 Comparison between GC and GC/CNT electrodes: covalent immobilization of anthraquinone

Before attempting the covalent immobilization of CDH onto flat GC electrodes, we wanted to compare these electrodes with the GC/CNT electrodes that have been already, successfully, used for the immobilization of this enzyme in Chapter 3. This comparison was carried out by immobilising a redox probe on both the electrodes using the same procedure employed for the covalent immobilization of CDH in Chapter 3, involving electrochemical and solid-phase synthesis. This will be useful to roughly estimate the amount of enzyme that could be immobilised onto one or the other type of electrode, so that we can also make an estimation of the active area of the GC/CNT electrodes.

The ideal redox probe for this experiment should present a reversible, well-defined redox system in order to be easily detected by cyclic voltammetry. In addition, it should bear a carboxylic group, essential for the coupling to amino-modified electrodes. For that, we chose anthraquinone-2-carboxylic acid (see Scheme 5.1 for the chemical structure) that has been used for several years as a redox probe in our group [64-67,111] as it presents a well-behaved redox system. In aqueous buffer, at acidic, neutral and alkaline pH, anthraquinone (AQ) undergoes a reversible one-step, two-electron reduction in which the reduction potential varies with pH in a straightforward Nernstian manner (Scheme 5.1) [157]. Therefore, the covalent immobilization of AQ through its carboxylic functionality will allow us to confirm the success of the modification procedure. In addition, through integration of its cyclic voltammogram we will be able to estimate its surface coverage.

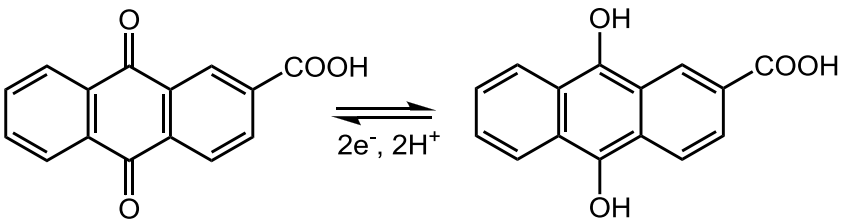

Scheme 5.1. *Reversible reduction of anthraquinone-2-carboxylic acid (AQ-COOH).*

The procedure for the modification of GC and GC/CNT electrodes with AQ was basically the same as used for the covalent immobilization of CDH, reported in Section 3.1.2, as they are both carbon electrodes. Briefly, two different amines (the linker and the passivating group) were grafted onto the electrode surface through electrochemical oxidation to form a mixed monolayer containing, in theory, 10 % of the linker and 90 % of the passivating group. Therefore, after Boc deprotection of the linker, the resulting amino-modified surface was made to react with a six-carbon-long spacer bearing a carboxylic group on one end and a Boc-protected amino group on the other end. Once the spacer was attached on the electrode, this second Boc protective group was also removed and the electrode was made react with anthraquinone-2-carboxylic acid dissolved in DMF (see Scheme 5.2).

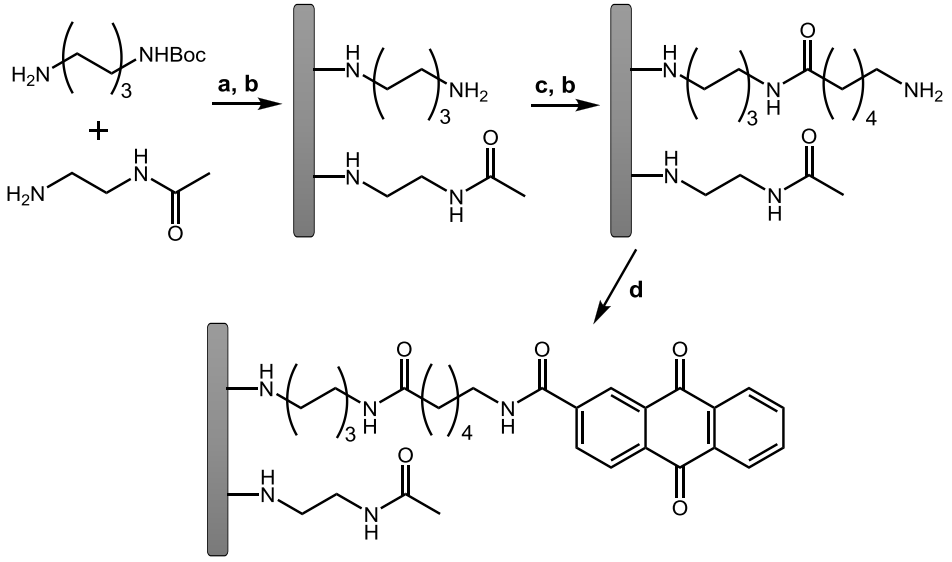

Scheme 5.2. *Sequential electrochemical and solid-phase modification of carbon electrodes with AQ. Reagents and conditions: a) 2 mM N-Boc-1,6-hexanediamine, 18 mM N-(2-aminoethyl)acetamide, 0.1 M TBATFB in deoxygenated acetonitrile, constant potential of +2 V vs. SCE for 180 s; b) 4 M HCl in 1,4-dioxane (45 min); c) 10 mM N-Boc-6-aminohexanoic acid, 0.1 M EDC, 60 mM NHS in DMF (16 h); d) 25 mM anthraquinone-2-carboxylic acid, 0.1 M EDC, 60 mM NHS in DMF (16 h).*

The AQ-modified electrodes were characterised by CV in 0.1 M phosphate buffer (pH 7), scanning the electrode potential from -0.25 V to -0.65 (or -0.7) V *vs.* SCE at different scan rates between 25 and 200 mV/s. Normally five complete cycles were recorded at each scan rate in order to reach a steady state condition, and the fifth cycle is shown in the graphs. Figure 5.1-A and C reports the cyclic voltammograms recorded at a GC electrode (A) and a GC/CNT electrode (C), both

modified with AQ as shown in Scheme 5.2. The characteristic redox peaks of anthraquinone are clearly visible around -0.48 V *vs.* SCE, confirming the successful modification of the carbon electrodes. Moreover, as shown in Figure 5.1-B, the anodic and cathodic peak currents increase linearly with the scan rate, as expected for a surface immobilised species [118].

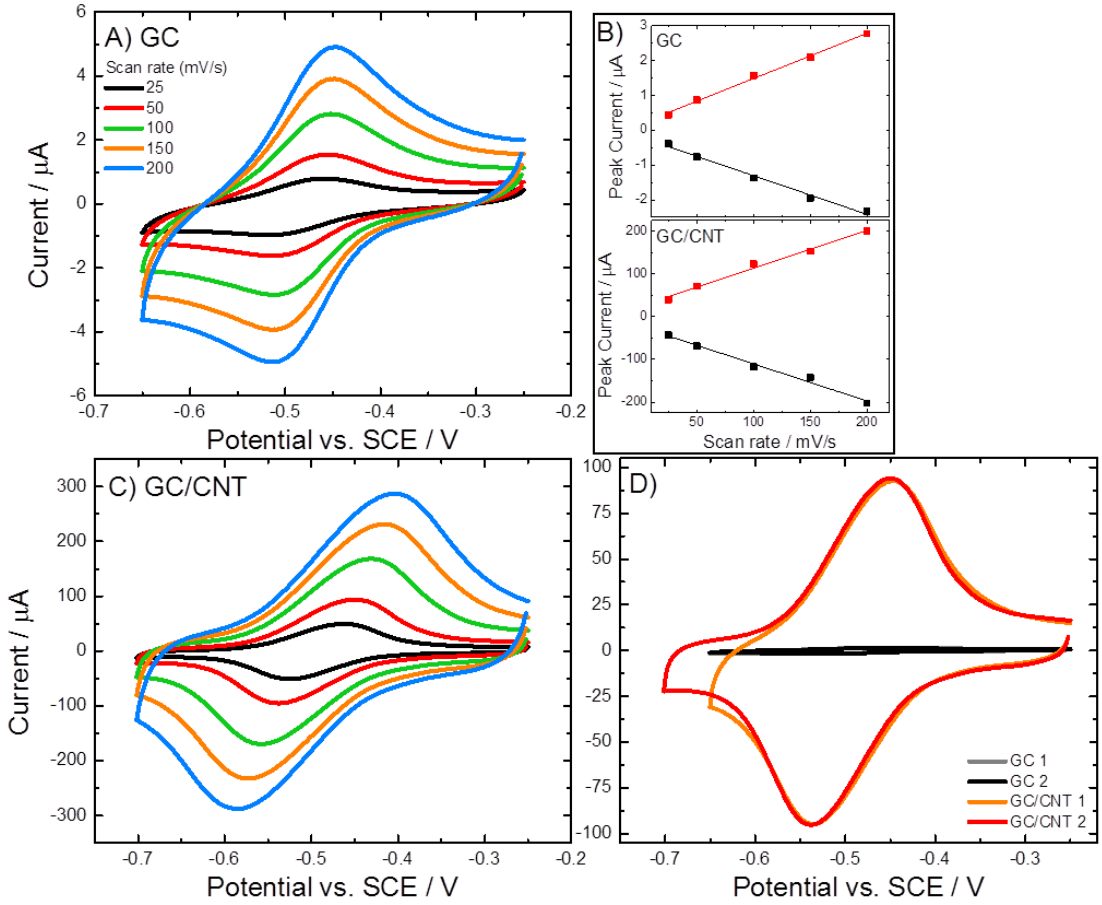

Figure 5.1. *Cyclic voltammograms at different scan rates for (A) a GC and (C) a GC/CNT electrode modified with AQ as shown in Scheme 5.2. CVs were carried out in argon-saturated 0.1 M phosphate buffer (pH 7). B) Anodic (red) and cathodic (black) peak currents vs. the scan rate for both the electrodes. D) CVs recorded at 50 mV/s for two GC and two GC/CNT AQ-modified electrodes.*

At first glance, we can observe that the current recorded at the GC electrode (Figure 5.1-A) is much lower than the one of the GC/CNT electrode (Figure 5.1-C). For a better comparison, Figure 5.1-D shows the CVs recorded at 50 mV/s for two GC electrodes (black and grey) and two GC/CNT electrodes (red and orange): the first two CVs are not even visible if compared with the ones recorded at the second type of electrode. This is a good indicator of the huge active area that GC electrodes gain once they are modified with CNTs (in this work, GC electrodes of

3 mm diameter were modified with 5 µL of a 1 g/L multiwall carbon nanotubes suspension in DMF, see Section 2.3.1 in the Experimental Part).

For a deeper comparison, the number of moles of anthraquinone immobilised at GC and GC/CNT electrodes can be calculated by integrating the anodic and cathodic peaks, as we have already done with CDH in Section 3.2.1. In fact, the area under the redox peaks represents the charge required for the full reduction or oxidation of the AQ monolayer at the electrode surface. In this work, we always used the CVs recorded at 50 mV/s for calculating m_{AQ} and the integration was performed using the software Origin 9. After selecting the peak to integrate using the "data selector" function, the integration was done by setting the "integrate peaks" mode in the "peak analyser" function. Therefore, an adequately high number of points (generally around 50) was manually placed on the curve, except for the potential range where the peaks are located. The points were interpolated using the "BSpline" function to produce the baseline, which is then subtracted to obtain the integrated area. The charge (Q) is given by:

$$Q = \frac{a_{\text{int}}}{v} \qquad \text{(Eq. 5.1)}$$

where a_{int} is the average integrated area between the anodic and cathodic peaks, and v is the scan rate (0.05 V/s in our case). The charge is then related to the number of moles of anthraquinone (m_{AQ}) through the Faraday law:

$$Q = n\, m_{\text{AQ}}\, F \qquad \text{(Eq. 5.2)}$$

where F is the Faraday constant (96485 C mol^{-1}) and n is the number of electrons exchanged during the oxidation or reduction of each molecule of AQ, which is equal to 2 (see Scheme 5.1). Table 5.1 reports the values of m_{AQ} obtained for the two GC and two GC/CNT electrodes used in this work. We can see that the amount of AQ immobilised on the two GC electrodes, as well as on the two GC/CNT electrodes, was basically the same: this proves the great reproducibility of our modification method. In addition, as we can see also from the CVs in Figure 5.1-D, the great reproducibility in the preparation of GC/CNT electrodes should also be acknowledged, even though this is probably true only for electrodes prepared together (using the same CNTs solution, by the same operator, at the same temperature). In fact, as we have seen several times in this work, GC/CNT

electrodes prepared in different periods can have different active areas, thus being able to retain different amounts of enzyme and producing different catalytic currents. This can be due to the use of different CNTs suspensions, even though we tried to use always the same one during the entire course of this work. However, even a different mixing of the same suspension, a different use of the micropipette to take 5 µL of it, a different temperature or evaporation time could produce some variations in the amount of CNTs adsorbed on the electrodes.

Table 5.1. *Number of moles of anthraquinone (m_{AQ}) for GC and GC/CNT electrodes, calculated using Eq. 5.2, and average value of m_{AQ} between two GC and two GC/CNT electrodes.*

Electrode type	Electrode number	Moles of AQ (pmol)	Average m_{AQ} (pmol)
GC	1	8.09	8.47
	2	8.86	
GC/CNT	3	890	901
	4	912	

This problem is emphasised by the difficulty of measuring the actual active area of each GC/CNT electrode using a simple method like we could do with other types of high active area electrodes, such as porous gold substrates. The specific area of carbon nanotubes is usually determined by measurements of gas adsorption (generally N_2 at 77 K) and calculations using the Brunauer–Emmett–Teller (BET) isotherm [158-160]. However, these measurements become more challenging once the CNTs are adsorbed on an electrode, so that it is not possible to control the exact specific area of each GC/CNT electrode. For that reason, in this discussion, we have not talked about the AQ surface coverage, for which we need to know the electrode active area, but only about the number of anthraquinone moles immobilised on the electrodes. Nevertheless, we could use this parameter to roughly estimate the active area of our GC/CNT electrodes, knowing the value for the GC electrodes, assuming the surface density to be the same in both cases.

From Table 5.1 we can see that the number of AQ moles immobilised at GC/CNT electrodes is, on average, 100 times higher than that for GC electrodes. If we assume the same AQ surface coverage for both types of electrode, it follows that the active area of the GC/CNT electrodes is roughly 100 times higher than that of the GC electrodes. However, the active area of a GC electrode (A_{GC}) does not normally correspond to its geometrical area (A_{geom}), but is given by:

$$A_{GC} = A_{geom} \cdot \rho \qquad \text{(Eq. 5.3)}$$

where ρ is called the roughness factor. Only when ρ = 1 the two areas coincide, but generally the roughness factor has a value between 2 and 3 for well-polished GC surfaces [161]. Given that the GC electrodes used in this work were 3 mm in diameter (therefore the geometrical area is about 0.07 cm^2), if we assume ρ = 2, the active area of these electrodes will be about 0.14 cm^2. Therefore, if we assume the active area of GC/CNT electrodes to be 100 times higher as we said here above, it would be around 14 cm^2. This is in agreement with the value obtained through a geometrical calculation described by A. Peigney *et al.* [162]: given that the CNTs used in this work had, on average, 7-9 walls and a diameter of 9.5 nm, we can use the curve for 10-walls CNTs in the plots developed by Peigney. In this way, the specific area of our CNTs is around 200 m^2/g (or probably a little bit more since our CNTs presented fewer walls). Given that for each electrode we used 5 µL of a 1 g/L CNTs suspension, which is equivalent to 5 µg of CNTs, the specific area of the CNTs adsorbed on each electrode will be around 10^{-3} m^2, which is equal to 10 cm^2, a value very close to the 14 cm^2 found using the AQ surface coverage (taking into account that we rounded it down using the plot for 10-walls CNTs).

A value around 10-14 cm^2 is a huge active area for a 3 mm diameter electrode, which explains the high catalytic current observed with CDH-modified GC/CNT electrodes in Chapter 3. However, this is not the only reason why electrodes modified with CNTs are so efficient: another factor is represented by their relatively low capacitance. Figure 5.2 can help to explain this: the CVs recorded at 50 mV/s at a GC (black) and a GC/CNT electrode (red) modified with AQ are reported not on the same scale. The scale of the two CVs was adjusted in order to have roughly the same capacitive current (represented by the dashed lines). We

can see that, even if the two electrodes had the same capacitance, they would not have the same faradaic current. Looking at the two scales for the current in Figure 5.2, black for the GC and red for the GC/CNT electrode, we can see that the ratio of the capacitive currents between the two electrodes is about 1:25 (since the black scale goes from -4 to +4 µA and the red scale from -100 to +100 µA). However, above we established that the ratio of the active areas between the same two electrodes was around 1:100. This means that, the active area being the same, GC/CNT electrodes have a lower capacitance (by about a factor of 4) than GC electrodes. It follows that species producing a very small current, such as enzymes, are more easily detected at GC/CNT electrodes than at GC electrodes.

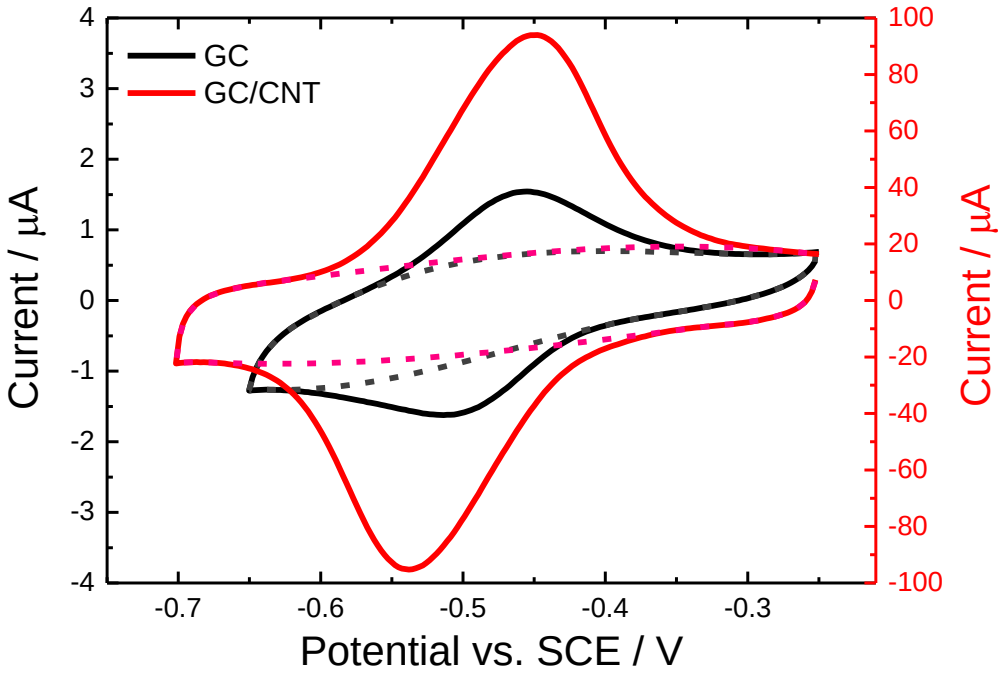

Figure 5.2. *Solid lines: cyclic voltammograms recorded at (black) a GC and (red) a GC/CNT electrode modified with AQ. CVs were carried out in argon-saturated 0.1 M phosphate buffer (pH 7), scanning the potential at 50 mV/s. Dashed lines: baselines (capacitive current) created with Origin 9. The two CVs are not on the same scale.*

For that reason, after immobilization of CDH at flat GC electrodes, we should not expect to see very nice catalytic voltammograms as those observed at GC/CNT electrodes in Chapter 3. In reality, we should not even expect to detect any DET current because the capacitive current of the electrode might be even higher than the enzyme catalytic current. Another problem could be the orientation of the CDH variants on the electrode. In fact, while with GC/CNT electrodes we were able see the DET current for all the CDH variants, maybe also thanks to the

porous structure of the CNTs network, with flat GC electrodes we might see the DET current only for some of the variants. This is because our procedure involves covalent immobilization of CDH through maleimide/cysteine bonds, which should keep the enzyme in a fixed orientation on the electrode surface. Therefore, some CDH variants might be in the right orientation to exchange electrons with the electrode surface, with the haem group in contact with it, while some others might not. In the next Section we show the immobilization of two different CDH variants at GC electrodes, and the tests of the resulting electrodes for DET and MET.

5.1.2 Immobilization of CDH at flat GC electrodes

As mentioned before, flat electrodes should be more suitable to discriminate between different CDH variants bearing free cysteine residues in different positions at the surface of the flavin domain. For that, the covalent immobilization of two different CDH variants, namely E522 and T701, was attempted at flat glassy carbon electrodes. Compared to GC/CNT electrodes, bare GC electrodes present a much smaller active area and a relatively higher capacitance, as we saw in the previous Section. Therefore, only a small number of CDH molecules will be immobilised at this type of electrode.

The immobilization of the enzyme was carried out using the same procedure already employed with GC/CNT electrodes, described in Section 3.1.2. The same amount of CDH solution at pH 7.0 (3 μL) was drop cast on each maleimide-modified GC electrode and left at 4 °C overnight. Afterwards, the electrodes were tested for DET and MET in acetate/$CaCl_2$ buffer (pH 5.5), with the addition of 20 μM ferrocenecarboxylic acid in the case of MET.

Figure 5.3 shows the cyclic voltammograms for the DET (A-C) and the MET (B-D) of the two different CDH variants immobilised at GC electrodes: E522 (A-B) and T701 (C-D). Looking at the experiments for the DET, we can immediately note that T701 showed a catalytic current in the presence of 50 mM glucose (Figure 5.3-C), while E522 did not (Figure 5.3-A). For the latter, the small shift up of the red line could have been due to the shift up of the background current as there is not a visible increase in the current in the region between -0.2 and -0.1 V, as in the case of T701. Note that, to test the DET of these electrodes, we used a lower

scan rate than the one employed with CDH-modified GC/CNT electrodes in Chapter 3: 0.5 mV/s instead of 1 mV/s. This change does not affect the catalytic current, since for sufficiently low scan rates it only depends on the rate of the enzymatic reaction, as we saw in Chapter 4, but it should affect the capacitive current. In fact, because the capacitive current is directly proportional to the scan rate, decreasing the latter should lower the capacitance. In this way, it should be easier to detect a very small catalytic current.

A second observation is that the analysis was performed only for one concentration of glucose (50 mM, red curves in Figure 5.3-A and C), in addition to the background without substrate (black curves). This is because the catalytic current with 50 mM glucose was so low that it would have been useless to test it with different substrate concentrations. Moreover, since the scan rate was decreased to 0.5 mV/s, recording a full CV going from -0.35 to 0.1 V takes 30 min. Given that we normally recorded two full cycles for each experiment, it took 1

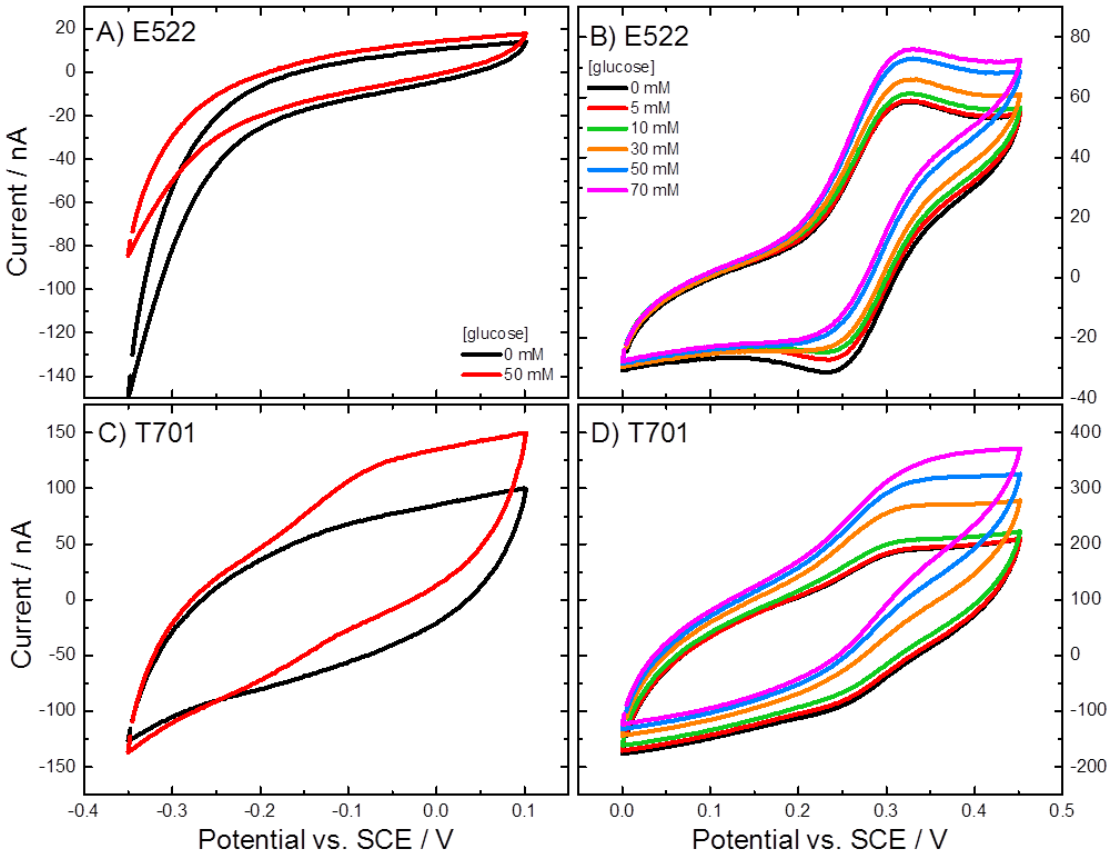

Figure 5.3. *Cyclic voltammograms for (A-B) E522 and (C-D) T701-CDH modified GC electrodes recorded in argon-saturated 50 mM acetate buffer (pH 5.5), containing 30 mM $CaCl_2$ and different concentrations of glucose. B and D contained also 20 µM ferrocenecarboxylic acid. The electrode potential was swept at (A-C) 0.5 mV/s and (B-D) 2 mV/s.*

hour for each single CV. For that reason, it would have been too long, and even useless, to test the DET for more than one glucose concentration.

From the DET experiment we could suppose that the variant T701 is lying on the electrode surface with a better orientation than E522, so that the haem group of the first variant is able to exchange electrons with the electrode. However, it could also be possible that the variant E522 was not immobilised on the electrode and, for that reason, we could not detect any DET current. To exclude this possibility, MET experiments were performed with both electrodes. We used ferrocenecarboxylic acid as mediator in a lower concentration than before with GC/CNT electrodes: 20 μM instead of 1 mM. We thought that a high concentration of ferrocene, such as 1 mM, would produce too high a faradaic current so that it could hide the small catalytic current of the enzyme. As shown in Figures 3.14 or 4.17, for concentrations of ferrocene ≥ 20 μM, the catalytic current is rather constant meaning that it does not depend on the mediator concentration but only on the enzyme/substrate reaction. For that reason, the lowest concentration of ferrocene that we can use is 20 μM. Smaller concentrations would produce a catalytic current, but it would be limited by both the enzyme/substrate reaction and the enzyme/ferrocene reaction.

The experiment with the mediator (Figure 5.3-B and D) showed a MET catalytic current increasing with the glucose concentration for both electrodes, thus proving that the enzyme was present on both of them. The only difference we can observe between the two electrodes is that the CVs for E522 (Figure 5.3-B) present the typical “duck shape”, while for the second electrode with T701 (Figure 5.3-D) the CVs are more flattened. If we look more closely, we can see that the background (or capacitive) current of the two electrodes is quite different: around 30 nA and 200 nA for the first and second electrodes, respectively. For that reason, the small faradaic current produced by 20 μM ferrocene is more visible at the first electrode than at the second one. The same difference in the capacitive current can be observed also in the DET experiments: the first electrode presents a background current of about 15 nA (Figure 5.3-A), while for the second electrode it is about 110 nA (Figure 5.3-C). The ratio between the capacitive currents of the two electrodes is roughly the same in the DET and MET experiments, with the capacitances being smaller in the DET case as the scan rate used was lower (0.5 mV/s for the DET and 2 mV/s for the MET).

The difference in the capacitive currents is probably due to a different active areas of the two electrodes: the one with T701 might have presented a higher roughness if compared with the other electrode, so that its active area was bigger. It follows that a higher amount of T701 would have been immobilised on the electrode. However, this should not be the reason why a DET current was detected at the electrode modified with T701, and not at the electrode with E522. In fact, the MET catalytic current was easily observed at both electrodes, even though it was higher for the variant T701 (160 nA with 70 mM glucose) and lower for E522 (17 nA with 70 mM glucose). Moreover, the background current in the DET experiment was so small for the electrode modified with E522 (just 15 nA) that we should have been able to detect even a very small catalytic current. The fact that we did not is most probably related to the different orientations of the two variants covalently immobilised at the electrode surface. As shown in Figure 3.10 in Chapter 3, the mutation E522, to give DET, would require the haem domain not only to move away from the flavin domain, but also to rotate to contact the electrode with its haem cofactor. On the other hand, the mutation T701 requires only a small movement of the haem domain and no reorientation towards the electrode. This would make the DET easier for the variant T701, when immobilised on a flat electrode, while it would be more difficult for E522.

We can conclude that the immobilization at flat electrodes would allow a better discrimination between different CDH variants bearing the free cysteine in different positions at the surface of the flavin domain. Unfortunately, it was not possible to perform this experiment with more than two variants since these enzymes were only available in limited amount from our collaborators at the BOKU-University of Vienna (Austria), and some of them were almost finished after the experiments carried out with GC/CNT electrodes (reported in Chapter 3). However, some other tests could be performed in the future, after the production and purification of new CDH variants, to confirm the results shown here above. In the next Sections we will show the use of a different electrode material, such as gold, for the covalent immobilization of CDH. Gold is an interesting electrode material, highly conductive, and the electrodes can be either flat or nanostructured (with a high surface area). Moreover, it is highly biocompatible, an important characteristic for implantable devices.

5.2 Covalent modification of gold electrodes

5.2.1 Method: electrochemical grafting of a diazonium salt

Before introducing the covalent immobilization of CDH at gold electrodes, we need to describe and characterise the covalent modification of these substrates. In fact, we cannot use exactly the same method employed with carbon electrodes (described in Section 3.1.2) as the electrochemical grafting of amines does not work on gold. Therefore, the gold electrodes will be modified using the electrochemical grafting of a diazonium salt, which works on both carbon and gold substrates.

This method followed previous work by our group that described the electrochemical grafting of a Boc-protected diazonium salt onto glassy carbon and gold electrodes [64,67,112,163]. The monolayer of diazonium salt onto the gold electrodes was formed by electrochemical reduction of BocNH-CH_2-C_6H_4 diazonium tetrafluoroborate from an acetonitrile solution (see Scheme 5.3). Once immobilised, the Boc protecting group can be easily removed by immersion in an HCl solution, resulting in a monolayer of free amino groups on the electrode surface. Therefore, a wide range of molecules can be coupled to the amino-modified surface by simple amination reactions.

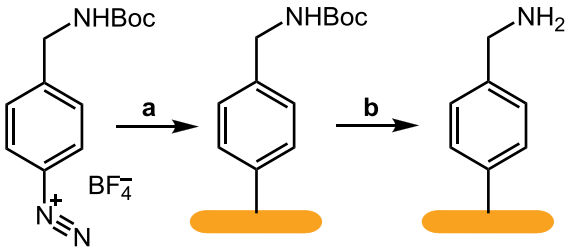

Scheme 5.3. *Modification of gold electrodes with diazonium salt. Reagents and conditions: a) 5 mM BocNHCH$_2$C$_6$H$_4$ diazonium tetrafluoroborate, 0.1 M TBATFB in deoxygenated acetonitrile, CV from 0.0 to -0.7 V vs. SCE at 50 mV/s (10 cycles); b) 4 M HCl in 1,4-dioxane (45 min).*

There are several advantages in using a Boc-protected diazonium salt. First, the conditions for the covalent attachment to the electrode can be separately optimised. Second, the reaction is easily controlled electrochemically and monitored through the current passed. In addition, the presence of the bulky Boc group on the diazonium salt discourages the formation of polymeric layers on the

surface by blocking coupling of further aryl radicals at the 3 and 5 positions of the aryl groups already attached to the surface. Finally, this approach allows using a single diazonium salt to couple a wide range of molecules to the electrode surface, avoiding the necessity of synthesising a variety of different diazonium salts and overcoming problems of poor stability for some of these salts. Indeed, the Boc protective group is readily and cleanly removed in acid to leave a free primary amine, which can be reacted using a variety of well-characterised solid phase coupling reagents.

The procedure employed in this work begins with the electrochemical reduction of the diazonium salt at a gold electrode, by cycling the potential between 0.0 and -0.7 V *vs.* SCE for 10 full cycles at 50 mV/s (see Scheme 5.3). Figure 5.4 shows a typical cyclic voltammogram of this reaction. In the first cycle, a broad irreversible reduction peak at about -0.45 V is visible. This peak is attributed to the reduction of the diazonium salt and formation of the corresponding aryl radical in solution, which then couples to the gold surface. Subsequent cycling of the potential in the same solution leads to the complete disappearance of the cathodic current, which tends to zero. This current decay is due to the

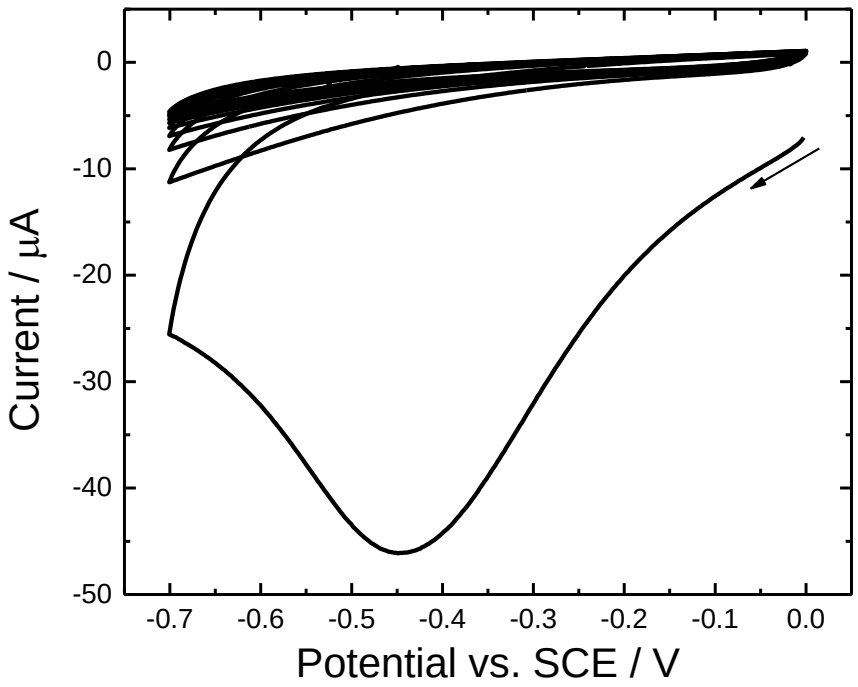

Figure 5.4. *Typical cyclic voltammogram for the reduction of 5 mM $BocNHCH_2C_6H_4$ diazonium tetrafluoroborate in acetonitrile, containing 0.1 M TBATFB, at a gold electrode (area was about 0.14 cm^2). The electrode potential was swept at 50 mV/s from 0.0 to -0.7 V vs. SCE, for 10 cycles.*

attachment of the linker, which bears the bulky Boc group, completely blocking the electrode surface. Note that the current intensity of the reduction peak depends on the active area of the electrode employed. Afterwards, the electrodes are immersed in a concentrated solution of HCl in dioxane, under gently stirring for 30-45 minutes, to remove the Boc protecting group and leave the free amine immobilised at the electrode surface.

5.2.2 Characterization by anthraquinone coupling and CV

The success of the modification process can be monitored by reacting a redox probe bearing a carboxylic group with the amino-modified surface, and characterising the resulting electrode by cyclic voltammetry. The redox probe chosen for the characterization was anthraquinone-2-carboxylic acid, already employed to characterise amino-modified GC electrodes in Section 5.1.1.

Anthraquinone-2-carboxylic acid was reacted with the amino-modified electrodes dissolved in DMF, employing well-known coupling reagents, such as EDC and NHS (see Scheme 5.4). The reaction is quite slow, so it was normally performed overnight. Then, the AQ-modified gold electrodes were characterised by CV in 0.1 M phosphate buffer (pH 7). Figure 5.5 shows the typical cyclic voltammograms recorded at an AQ-modified flat gold electrode, using different scan rates from 25 to 200 mV/s. The characteristic redox peaks of anthraquinone are clearly visible around -0.47 V *vs.* SCE, confirming the successful modification of the gold surface. Moreover, as shown in the inset, the anodic and cathodic peak currents increase linearly with the scan rate, as expected for a surface immobilised species.

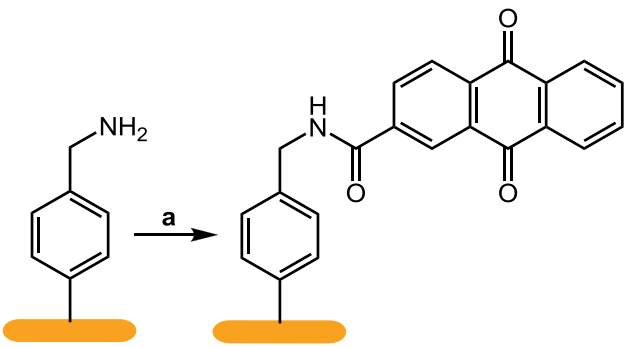

Scheme 5.4. *Coupling of anthraquinone at an amino-modified gold electrode. Reagents and conditions: a) 25 mM anthraquinone-2-carboxylic acid, 0.1 M EDC, 60 mM NHS in DMF (16 h).*

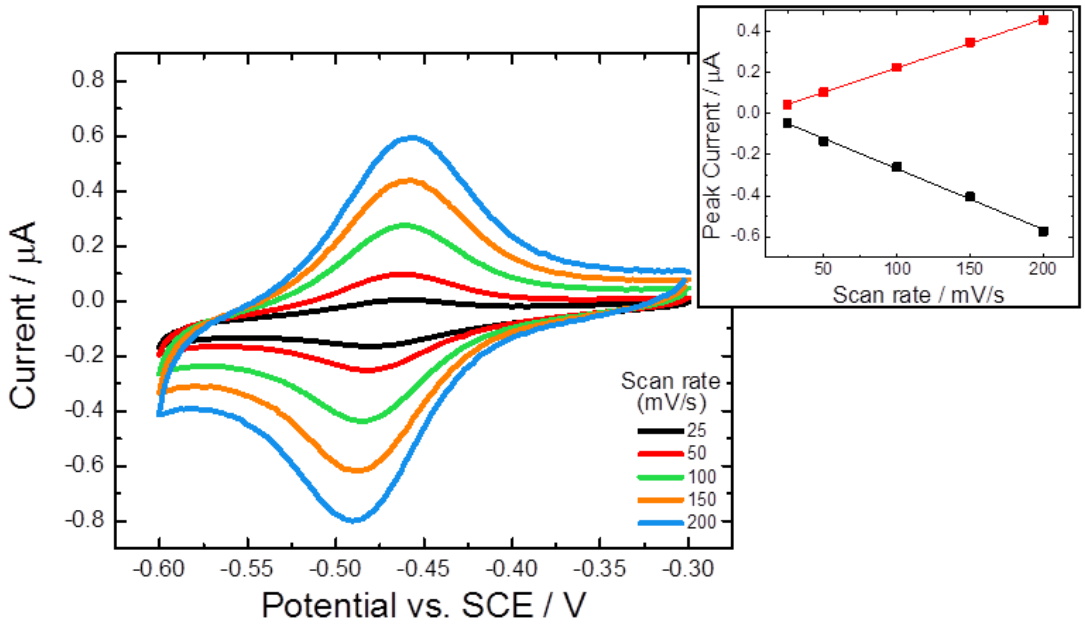

Figure 5.5. *Typical cyclic voltammograms at an AQ-modified gold electrode (area was about 0.14 cm²) in 0.1 M phosphate buffer (pH 7). The electrode potential was swept from -0.3 to -0.6 V vs. SCE (5 cycles) at different scan rates. The inset shows the anodic (red) and cathodic (black) peak currents vs. the scan rate.*

Through integration of the reduction and oxidation peaks visible in the cyclic voltammograms, the amount of anthraquinone immobilised at the electrode surface (m_{AQ}) and, therefore, its surface coverage (Γ_{AQ}) can be calculated. The integration of the AQ redox peaks was performed as already explained in Section 5.1.1 and m_{AQ} was calculated using Eq. 5.2. Therefore, knowing the electrode active area (A), Γ_{AQ} is given by:

$$\Gamma_{AQ} = \frac{m_{AQ}}{A} \qquad \text{(Eq. 5.4)}$$

The surface coverage for four different gold electrodes was found around 5-10 pmol/cm² (Table 5.2). In a previous work by or group the surface coverage of AQ molecules immobilised at gold electrodes using the same method with diazonium salt was found around 1.4 nmol/cm² [67], which is about 100 times higher than what we found here. However, in the work cited, nanostructured sphere segment void (SSV) gold substrates were used, so that there could have been some differences in the calculation of the electrode active area.

Table 5.2. *AQ surface coverage for four flat gold electrodes, calculated using Eq. 5.4, considering* $A = A_{geom} \cdot \rho$ *(with* $\rho = 1.25$*, see Section 2.1.5).*

Electrode	Geometrical area (cm^2)	Surface coverage ($pmol/cm^2$)
1	0.135	10
2	0.14	4.4
3	0.105	7.2
4	0.14	5.4

5.2.3 Characterization of gold functionalization by ToF-SIMS

Another characterization method that was tried is time-of-flight secondary-ion mass spectrometry (ToF-SIMS). Secondary-ion mass spectrometry (SIMS) is a technique used to analyse the composition of solid surfaces and thin films by sputtering the surface of interest with a focused primary ion beam, and collecting and analysing the ejected secondary ions. ToF-SIMS is an acronym for the combination of the analytical technique SIMS with time-of-flight (ToF) mass analysis. The technique provides detailed elemental and molecular information about the surface, thin layers and interfaces of the sample [164,165]. The ToF-SIMS analysis was carried out at the University of Limerick (Ireland) in the laboratory of Prof Edmond Magner, with the help of Till Siepenkoetter (PhD student) and Serguei Belochapkine (technician).

In order to be analysed with this technique, flat gold substrates were modified with the diazonium salt as described in Scheme 5.3. The substrates were analysed by ToF-SIMS before and after removing of the Boc group. For comparison, a silicon wafer spin-coated with the same diazonium salt was also analysed by ToF-SIMS in order to have the mass spectrum of the original compound not covalently attached to the substrate. Figure 5.6 shows the average positive mass spectra of the three substrates analysed, with the chemical structure of the molecules coated or immobilised on each substrate shown in the inset of each spectrum, and the structure of the most characteristic positive fragments. Only the positive mass spectra are reported here, being the most

characteristic spectra to define the organic species. However, Table 5.3 reports all the main peaks (positive and negative) with the possible assignments.

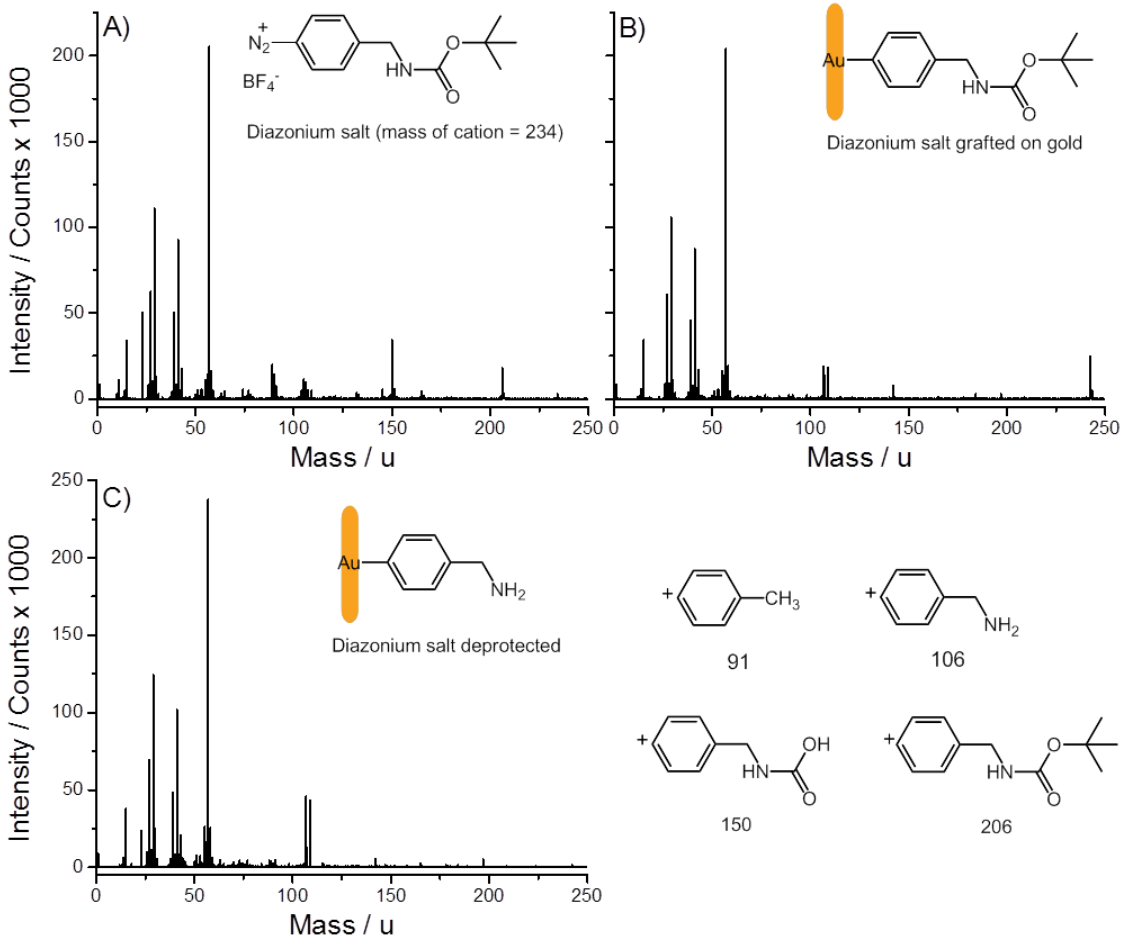

Figure 5.6. *Positive ToF-SIM spectra of (A) diazonium salt spin-coated on a silicon wafer, (B) diazonium salt grafted on a gold substrate and (C) diazonium salt on a gold substrate after Boc deprotection. The structures of some of the main fragments are reported as well.*

Table 5.3. *Molecular mass, assignment and intensity of the main peaks found in the positive and negative ToF-SIM spectra of the substrates: (A) diazonium salt spin-coated on silicon wafer, (B) diazonium salt grafted on gold substrate and (C) diazonium salt on gold substrate after Boc deprotection.*

Mass (u)	Assignment	Intensity (% toward the most intense peak)		
		sub. A	sub. B	sub. C
29	$C_2H_5^+$	54.2	51.7	52.5
39	$C_3H_3^+$	24.6	22.4	20.4
41	$C_3H_5^+$	45.0	42.7	42.8
57	$C_4H_9^+$ (butyl)	100.0	100.0	100.0
89	$C_7H_5^+$	9.7	1.0	1.8
90	$C_7H_6^+$	6.8	0.5	1.1
91	$C_7H_7^+$	3.6	1.1	2.0
104	$C_7H_6N^+$	2.5	0.5	0.7
105	$C_7H_7N^+$	5.5	0.5	0.6
106	$C_7H_8N^+$	4.7	1.0	1.2
107	$^{107}Ag^+$	-	9.3	19.4
109	$^{109}Ag^+$	-	8.8	18.1
150	$C_8H_8NO_2^+$	16.7	0.2	0.3
184	$C_{12}H_{26}N^{+\#}$	-	1.6	0.7
197	Au^+	-	1.3	2.2
206	$C_{12}H_{16}NO_2^+$	8.7	0.1	-
234	$C_{12}H_{16}N_3O_2^+$	1.4	-	-
242	$C_{16}H_{36}N^{+\#}$	-	12.1	0.6
287	$Au\text{-}C_7H_6^+$	-	0.1	0.4

 # from TBATFB used as supporting electrolyte during diazonium salt grafting

Mass (u)	Assignment	Intensity (% toward the most intense peak)		
		sub. A	sub. B	sub. C
19	F^-	100.0	-	-
26	CN^-	9.5	100.0	100.0
35	$^{35}Cl^-$	0.1	12.2	32.2
37	$^{37}Cl^-$	0.2	4.0	11.6
42	CNO^-	4.9	60.2	62.7
57	$C_3H_5O^-$	1.6	5.6	5.2
73	$C_4H_9O^-$	0.3	1.2	1.6
86	$^{10}BF_4^-$	34.4	-	-
87	$^{11}BF_4^-$	73.0	-	-
197	Au^-	-	5.8	13.1
224	$Au\text{-}C_2H_3^-$	-	2.2	4.3
274	$Au\text{-}C_6H_5^-$	-	0.8	1.4

From Table 5.3 and the spectra in Figure 5.6, it is evident that the most intense positive fragment in all the three substrates was the butyl cation (57 u). This can be explained in the case of substrates A and B, which present the butyl in the Boc protecting group of the diazonium salt. However, its peak was very intense also after the Boc deprotection (substrate C). This is not very surprising, as the butyl cation, especially in the form of *tert*-butyl $\{C(CH_3)_3^+\}$, is a relatively stable organic cation and can be formed by the fragmentation of many different organic species (the diazonium salt as well as organic contaminants present on the substrates). Some more characteristic positive fragments are the benzyl cation (89, 90 and 91 u) and the benzylamine cation (104, 105 and 106 u), which are present in the spectra of all three substrates, as expected. In spectrum A (pure diazonium salt) also the characteristic fragments of mass 150, 206 and 234 (see Figure 5.6 for the structures) are clearly visible. Such fragments are present to a much lesser extent, or completely absent, in spectra B and C: this was expected since substrates B and C should not present the pure diazonium salt (234 u), and substrate C should not have the Boc group (present in the fragments 150 and 206). Moreover, in spectra B and C, the fragment of mass 287 u was observed, even though not very intense, which could be assigned to the complex gold-benzyl cation. Fragments with mass greater than 300 u are not reported due to very low intensity.

In the positive spectra of substrates B and C, some fragments not directly related to the diazonium salt were also found, such as the peaks at 107 and 109 u, clearly due to the two silver isotopes. It was not clear why we had such a big amount of silver, but it was probably present as a contaminant on the gold slides, as they were prepared by magnetron sputtering with the same machine used to prepare Ag or Ag-Au alloy substrates (at the University of Limerick, Ireland). Other fragments not due to the diazonium salt were the ones of mass 184 and 242 u, probably due to TBATFB used as the supporting electrolyte during the diazonium salt grafting.

The negative spectra are less characteristic for the diazonium salt. The most intense peak in spectrum A is at mass 19 u, due to the fluoride present in the counter ion of the diazonium salt (BF_4^-), which also shows very intense peaks (86 and 87 u, as boron has two main isotopes: ^{10}B and ^{11}B). Such peaks are not

present in spectra B and C, meaning that the diazonium salt counter ion went away after the electrochemical grafting. The most intense peaks in spectra B and C are CN^- and CNO^- (26 and 42 u, respectively), which can be due in part to the diazonium salt, but most probably to other organic species, such as the acetonitrile used as solvent during the preparation and cleaning of the substrates, or other organic contaminants. The peaks of mass 35 and 37 u are also very intense in the last two substrates, especially in substrate C: they are probably due to the two isotopes of chlorine, which is a ubiquitous contaminant and, in the case of substrate C, can be present also because of the use of HCl for the Boc deprotection. Finally, in spectra B and C the gold anion (197 u) and some complexes of gold and organic species (224 and 274 u) are also observable, which can confirm the grafting of the diazonium salt on gold.

These results showed a rather accurate characterization of the pure diazonium salt (substrates A) by ToF-SIMS. However, we cannot say the same for the characterization of the diazonium salt grafted onto a gold substrate and the successive step of Boc deprotection. This could be due to a different amounts of the species of interest on the substrates: in fact, the sample spin-coated with the diazonium salt may have had a higher amount of the compound on the surface as compared with the substrates electrochemically grafted. Therefore, in the latter case, the presence of organic contaminants or other species used during the preparation of the substrates might have played a relevant role in the mass spectra.

Although the grafting of the diazonium salt can be proved by the ToF-SIM spectra thanks to the presence of some characteristic fragments and complexes of gold with organic species, the characterization of the successive steps of the gold modification, such as the Boc deprotection, is not very clear. Indeed, the small amount of the species electrochemically grafted, the possible relatively high amount of contaminants (reagents, by-products and solvents used in the preparation of the substrates), together with the impossibility of drastically cleaning the substrates once modified (for example using plasma cleaning procedures) make this technique poorly suited for the characterization of our gold modification procedure.

5.2.4 Characterization of gold functionalization by SPR

Another technique employed to characterise the covalent modification of gold electrodes was surface plasmon resonance (SPR) spectroscopy. SPR is an optical phenomenon which is sensitive to changes in the optical properties of the medium in the immediate vicinity of a metal surface [166,167]. The detection system of a SPR spectroscope essentially consists of a monochromatic and p-polarized light source, a glass prism coated with a thin metal film (normally gold), and a photodetector [168] (Figure 5.7). The p-polarised laser beam is shined through the cylindrical prism and becomes reflected from the thin gold layer (≈ 30 nm) deposited on top of the glass. The internal reflection of the light will cause an evanescent field that can couple to an electromagnetic surface wave (the surface plasmon) at the metal/liquid interface. Coupling is achieved at a specific angle of incidence, the SPR angle, which depends on the optical properties of the prism, the metal and the medium in contact with the metal (usually a liquid), and on the thickness of the organic films on the metal surface.

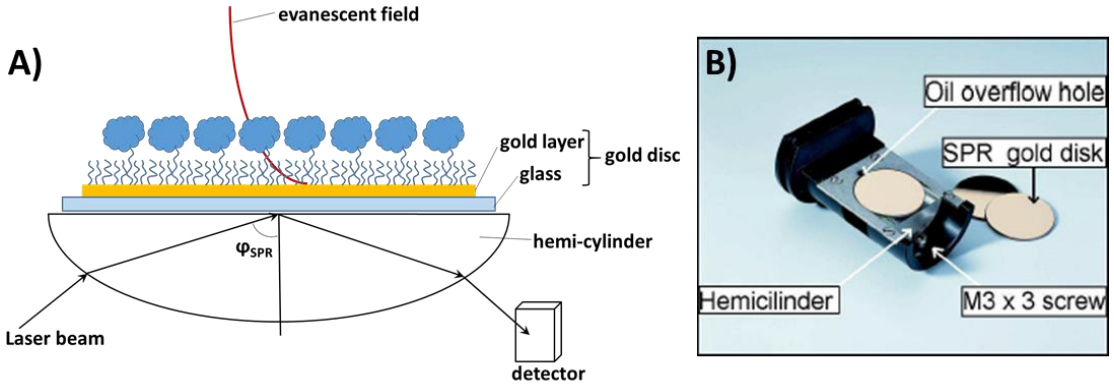

Figure 5.7. *A) Kretschmann configuration of a SPR sensor. B) Picture of gold-coated glass slides with hemi-cylinder (adapted from the Autolab ESPRIT manual).*

The SPR angle is highly sensitive to changes in the refractive index (RI) of a thin layer adjacent to the metal surface. For example, when a protein layer is adsorbed on the metal surface (and all the other parameters are kept constant) an increase in the surface concentration occurs and the SPR angle shifts to higher values. Therefore, the SPR angle shift can be used as a response unit to monitor and, eventually, quantify adsorption of molecules or functionalization of metal

surfaces [169]. For this study, it is enough to know that the resonance angle is, to a good approximation, a linearly increasing function of the adsorbed mass at the gold surface.

All the SPR measurements, reported in this Section and in Sections 5.3.10, 5.3.11 and 5.3.12, were carried out at the University of Lund (Sweden) in the laboratory of Prof Lo Gorton, in collaboration with Dr Jani Tuoriniemi (Goteborg University, Sweden) and Dr Su Ma (BOKU-University, Vienna, Austria).

SPR spectroscopy was used to monitor in real time the principal steps of our procedure for the covalent modification of gold surfaces: the electrochemical reduction of a Boc-protected diazonium salt, its subsequent deprotection and the solid phase coupling of a carboxylic acid (in this case Boc-β-alanine, which will be used as a three-carbon-long spacer later in this Chapter, see Scheme 5.5). The diazonium salt functionalization was performed on SPR gold substrates as only these particular substrates can be analysed at the SPR spectroscope. These were glass disc slides coated with a very thin gold layer (≈ 30 nm) that can reflect the laser beam (see Figure 5.7-B). Since we wanted to follow in real time the different steps of our modification procedure, the diazonium salt reduction and the successive steps were carried out on a gold substrate inside the SPR spectroscope. Given the delicate materials of the instrument and, also, the very thin gold layer of the substrates, the solvents normally employed in our procedure were slightly changed to avoid damages of the instrumentation. The diazonium salt was dissolved in a solution of water and acetonitrile (1:1), instead of using pure acetonitrile. The electrochemical reduction was then performed as usual by CV, since the SPR channels were also small electrochemical cells provided with a pseudo Ag/AgCl reference electrode and a platinum disc counter electrode. Also the Boc deprotection (step b in Scheme 5.5) was carried out using milder conditions: 1 M HCl dissolved in water, instead of 4 M HCl in dioxane. Finally, the carboxylic acid used to test the solid phase coupling (Boc-β-alanine, step c in Scheme 5.5) and the coupling reagents (EDC and NHS) were dissolved in ethanol instead of the usual solvent, DMF.

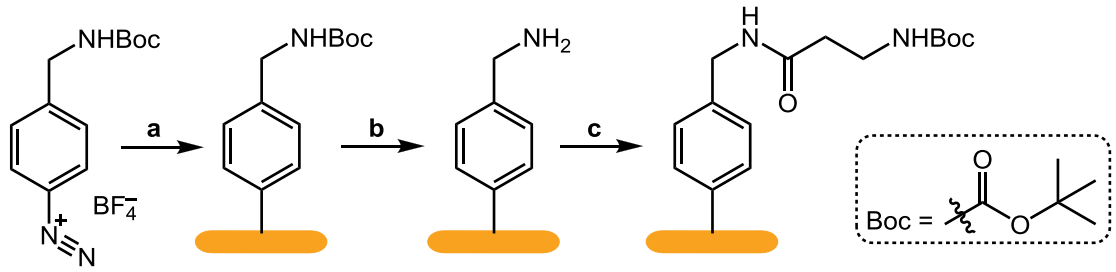

Scheme 5.5. *Sequential electrochemical and solid phase modification of SPR gold substrates. Reagents and conditions: a) 5 mM BocNHCH₂C₆H₄ diazonium tetrafluoroborate, 0.1 M TBATFB in acetonitrile/water (1:1), CV from 0.0 to -0.8 V vs. Ag/AgCl at 50 mV/s (8 cycles); b) 1 M HCl in water (30 min); c) 25 mM Boc-β-alanine, 0.1 M EDC, 60 mM NHS in ethanol (16 h).*

Figure 5.8-A shows the SPR sensorgram of the first step, the electrochemical reduction of the diazonium salt by cyclic voltammetry (step a in Scheme 5.5). At the beginning only the solvent, a solution of water and acetonitrile (ACN) 1:1, was present on the substrate. Then, at about 200 s, the solution with diazonium salt and TBATFB (supporting electrolyte) in the same solvent H_2O/ACN was added in the channels: the angle shift increased of about 0.29 degrees (deg or °) as the RI of the solution changed. At about 350 s the cyclic voltammetry was started (CV is reported in Figure 5.8-B): a significant increase in the SPR angle was immediately observed, followed by a staircase-like trend with eight steps. The first big increase in the angle shift (about 1.04 °) is due to the first cycle of the CV causing the major attachment of the reduced diazonium salt to the gold surface (as you can see in the CV in Figure 5.8-B, the first cycle has the biggest reduction peak). Further cycling the potential (eight cycles in total) increased again the angle shift and eight clear steps can be observed in the SPR sensorgram. In fact, during the CV, the SPR angle increased when the applied potential was more negative than -0.5 V (that is when the diazonium salt is reduced), while for more positive potentials it was constant or slightly decreasing, producing the staircase trend. After the end of the CV, at 675 s, the channels were washed with the solvent H_2O/ACN to remove the remaining diazonium salt and supporting electrolyte: the angle shift decreased as the RI of the solution changed again.

A complete quantitative interpretation of these results would be difficult, and probably exceeding our purpose. We can just report that, after the electrochemical grafting of the diazonium salt, the SPR angle has increased of about 2.26 °, when measured in the same liquid phase (the H_2O/ACN solution),

confirming that the gold surface has been functionalised. Moreover, we can note that the cyclic voltammogram and the SPR sensorgram perfectly match, showing that most of the diazonium salt reduction occurs at the first cycle, with probably further attachment of molecules between the second and fourth cycle. After that, the diazonium salt can still be reduced but, not having any space to be attached at the surface, it is probably washed away at the end. Lastly, this experiment confirms that the diazonium salt does not spontaneously react with the gold surface (at least not in the short time of this experiment), but it begins to be grafted on the electrode only when the potential becomes more negative than -0.5 V *vs.* SCE for the first time.

Figure 5.8-C shows the sensorgram of the second step, the deprotection of the Boc group (step b in Scheme 5.5). At the beginning only water was present at the

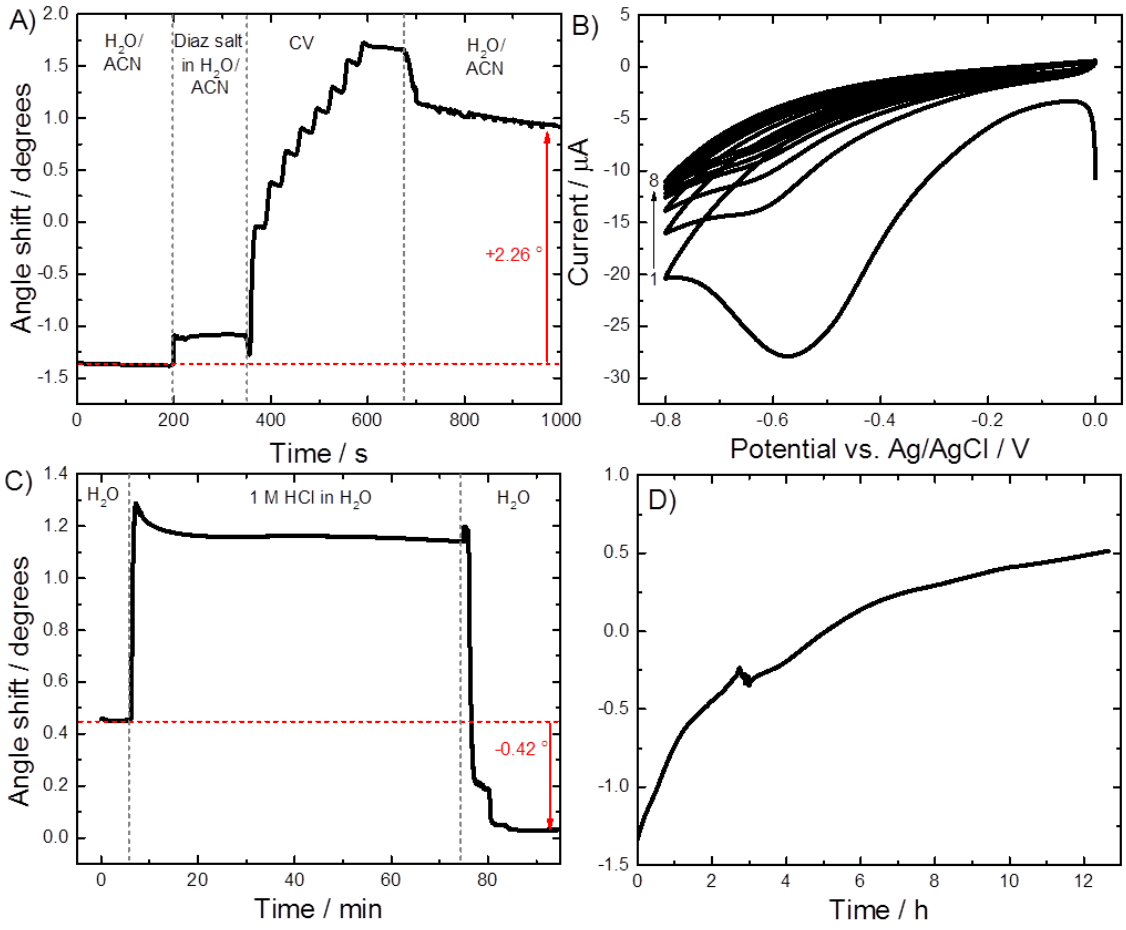

Figure 5.8. *(A) SPR sensorgram and (B) cyclic voltammogram for the diazonium salt reduction at a gold electrode (step a in Scheme 5.5). C and D) SPR sensorgrams for (C) Boc deprotection (step b in Scheme 5.5) and (D) NHS/EDC coupling of 3C-spacer (step c in Scheme 5.5). The substrate was a SPR glass slide coated with gold (the area of the gold disc was about 3.1 cm²).*

substrate surface. At about 6 min, 1 M HCl was added in the channels and the angle shift increased instantly (of about 0.83 °) because of the change in the RI of the solution. Immediately after, we can note that the SPR angle shift decreased very rapidly during the first 15 min from the addition of the acid, reaching then a kind of plateau. The acid was washed away with water at the 75th min and the angle shift immediately decreased, reaching a value even lower than before the addition of HCl. This was due both to the change in the solution RI, passing from 1 M HCl to pure water, and to the deprotection of the diazonium salt that occurred in the HCl solution. Measuring the angle shift in the same solvent (water) before and after the Boc deprotection, we can see that it has decreased of about 0.42 °. This confirms that the Boc protective group, which is a quite big group (see Scheme 5.5), was removed from the surface. In addition, this experiment showed that *i*) this process is quite fast, as the biggest decrease occurred during the first 15 min and after 30 min it seems already completed; and *ii*) a 1 M HCl solution in water is sufficient to deprotect the amino groups attached on a substrate, so that we could also avoid the use of organic solvents (such as dioxane) or more concentrated HCl.

Figure 5.8-D shows the sensorgram of the third step, the solid phase coupling of a carboxylic acid to the amino-modified surface (step c in Scheme 5.5). A solution containing Boc-β-alanine, EDC and NHS in ethanol was added in the channels of the SPR spectroscope and left it overnight. The instrument monitored the angle shift for about 12 hours. The SPR sensorgram confirmed that it is a long process and it is reasonable to leave the reaction overnight (or for about 16 hours). However, the results cannot be considered completely reliable: in particular, the great increase in the SPR angle shift (around 1.8 °) could be due also to changes in the temperature during the night and/or evaporation of the solvent (ethanol) with consequent concentration of the reagents in solution.

To conclude, both SPR spectroscopy and the coupling of a redox probe, such as anthraquinone, were useful techniques to analyse our procedure for the covalent modification of gold electrodes. SPR spectroscopy, in particular, will be used again in Section 5.3.10 to study the immobilization of CDH variants at maleimide-modified gold electrodes. Therefore, in the next Section, we will introduce the covalent immobilization of CDH at gold electrodes.

5.3 Immobilization of CDH at gold electrodes

5.3.1 Procedure

The procedure for the covalent immobilization of CDH variants at gold electrodes was adapted from that previously employed with carbon electrodes (see Sections 3.1.1 and 3.1.2). The benefit of that procedure, described for the first time in a previous work by our group [70], is its modular approach that allows the single elements of the modification to be independently varied. Therefore, applying this method to gold electrodes, we maintained the same spacer (*N*-Boc-6-aminohexanoic acid) and reactive group (maleimide) previously used with carbon electrodes, while the linker and passivating group were changed. In fact, the linker and the passivating group used before were amines that can be grafted on carbon surfaces by electrochemical oxidation, but cannot be grafted on gold surfaces. For this reason, a Boc-protected diazonium salt was chosen as the linker since it can be grafted on gold electrodes by electrochemical reduction, as described in Section 5.2.

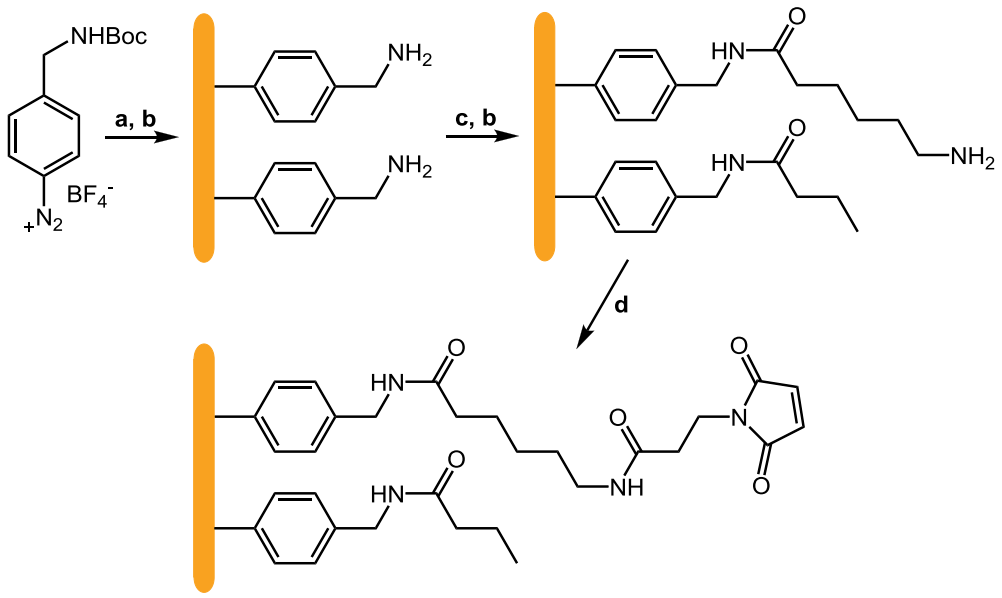

Scheme 5.6. *Sequential electrochemical and solid-phase preparation of maleimide-modified gold electrodes. Reagents and conditions: a) 5 mM* $BocNHCH_2C_6H_4$ *diazonium tetrafluoroborate, 0.1 M TBATFB in deoxygenated acetonitrile, CV from 0.0 to -0.7 V vs. SCE at 50 mV/s (10 cycles); b) 4 M HCl in 1,4-dioxane (45 min); c) 5 mM N-Boc-6-aminohexanoic acid, 45 mM butyric acid, 0.1 M EDC, 60 mM NHS in DMF (16 h); d) 25 mM N-maleoyl-β-alanine, 0.1 M EDC, 60 mM NHS in DMF (16 h).*

As already said in Section 5.2.1, the use of a Boc protected diazonium salt presents many advantages. One of these is using a single diazonium salt to couple a wide range of molecules to the electrode surface, avoiding the necessity to synthesise a variety of different diazonium salts and overcoming problems of poor stability for some of these. For that, we decided to use only one diazonium salt, thus forming a uniform monolayer at the electrode surface (see Scheme 5.6, step a). In order to reach a partial coverage of the reactive group (maleimide), important to avoid steric restrictions and better accommodate the enzyme on the surface, as explained in Section 3.1.1, a passivating group was added after the diazonium salt attachment. This was a short carboxylic acid without any other functionality that was added in the solution of the spacer so that the two compounds should react together with the amino-modified electrode, thus forming a mixed two-component layer (Scheme 5.6, step c). On this layer, the reactive group will be attached only in some positions, where there is the spacer, while the other positions will be blocked and unreactive (see Scheme 5.6, step d). Therefore, the schematic representation of a modified electrode shown in Scheme 3.1 must be changed in the case of gold electrodes and given by Scheme 5.7.

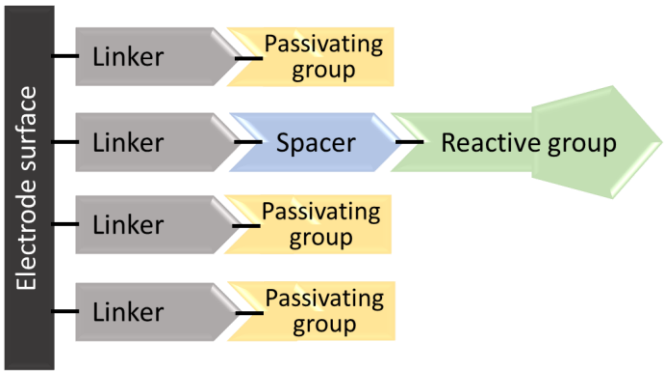

Scheme 5.7. *Schematic representation of the stepwise modification of a gold electrode, with the key elements highlighted.*

As shown in the second step in Scheme 5.6, the electrode modified with the diazonium salt was reacted with a mixture of 10 % six-carbon-long spacer (*N*-Boc-6-aminohexanoic acid) and 90 % passivating group (butyric acid). At this point, it is not sure if the two carboxylic acids in the mixture (the spacer and the passivating group) present the same reactivity toward the reaction with amines and, therefore, if the ratio of their surface coverage will be similar to the ratio of

their solution concentrations. In theory, they are quite similar carboxylic acids, differing mainly in the molecular weight (88 g/mol for butyric acid and 231 g/mol for *N*-Boc-6-aminohexanoic acid), so their reactivity should be quite similar. In any case, we will perform some control experiments before using this new procedure for the immobilization of CDH on gold electrodes.

After the coupling of the passivating group and the spacer, and subsequent Boc deprotection of the latter, *N*-maleoyl-β-alanine was reacted with the electrode to obtain the maleimide-modified gold surface (third step in Scheme 5.6). Lastly, the *Mt*CDH variant of choice, genetically engineered to bear a free cysteine in different positions at the surface of the flavin domain, was reacted with the maleimide-modified electrode by drop casting few μL of the enzyme solution (at pH 7.0) on the electrode.

5.3.2 Control experiment with a GC/CNT electrode

In order to verify the efficacy of the procedure described in the previous Section, a preliminary control experiment was performed using a GC/CNT electrode and applying the diazonium salt modification method to covalently immobilise a CDH variant. In fact, GC/CNT electrodes have been extensively used in this work (Chapter 3) to immobilise CDH through a hexanediamine (HDA) linker, grafted on the carbon surface by electrochemical oxidation (see Section 3.1.2). Since the electrochemical reduction of diazonium salts works both on gold and carbon electrodes, as described in previous works by our group [64,67,112], GC/CNT electrodes can be employed to test the new procedure developed to prepare maleimide-modified electrodes that uses a diazonium salt as the linker.

A GC/CNT electrode was modified as described in Scheme 5.6. Then, the CDH variant D813 was immobilised on it and the DET current was detected by cyclic voltammetry. Figure 5.9 shows the CVs (original and after background subtraction) recorded at this electrode in Tris/$CaCl_2$ buffer (pH 7.4), at different concentrations of D-glucose. The current taken at 0.0 V *vs.* SCE in the subtracted CVs (Figure 5.9-B) was then plotted versus the glucose concentration (black squares in Figure 5.10). For comparison, we plotted together the values of the current taken in CVs recorded at another GC/CNT electrode modified with the

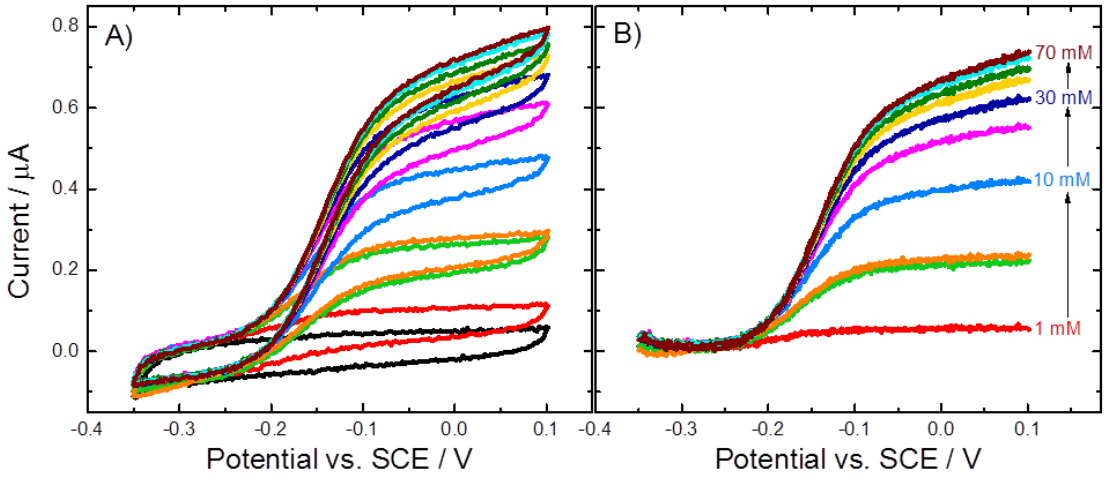

Figure 5.9. *(A) Original and (B) background subtracted CVs recorded at a D813-CDH modified GC/CNT electrode (modified with diazonium salt linker as described in Scheme 5.6), in argon-saturated 50 mM Tris buffer (pH 7.4), containing 30 mM $CaCl_2$ and different concentrations of D-glucose from 0 to 70 mM. The potential was swept at 1 mV/s.*

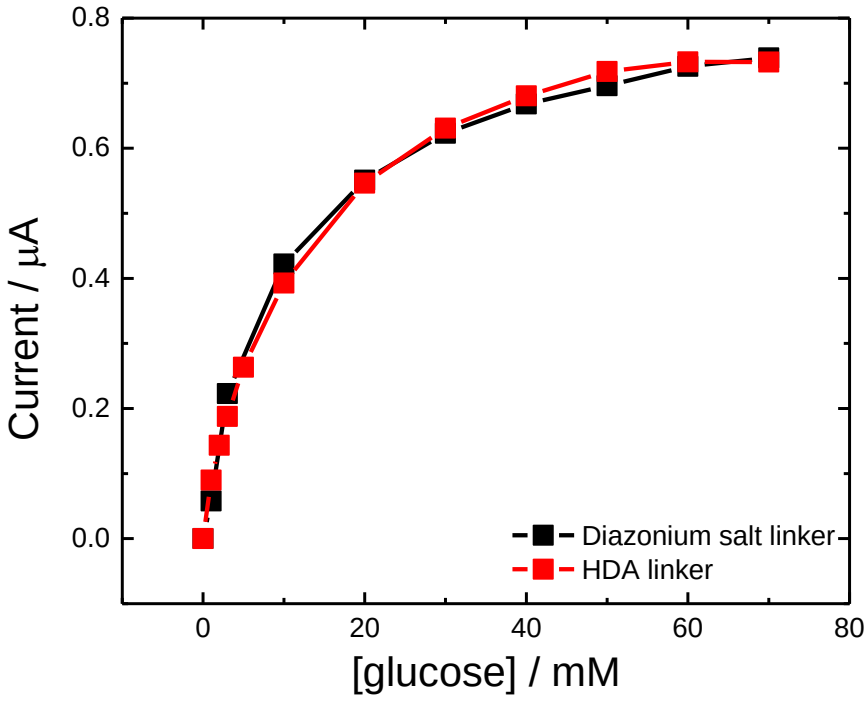

Figure 5.10. *Values of DET current taken at 0.0 V in CVs recorded at D813-CDH modified GC/CNT electrodes, in 50 mM Tris buffer (pH 7.4), containing 30 mM $CaCl_2$ and different concentrations of D-glucose. Black: electrode modified with diazonium salt linker as described in Scheme 5.6 (CVs are reported in Figure 5.9). Red: electrode modified with HDA linker as described in Scheme 3.3 (CVs not reported, performed by Firas Al-Lolage).*

same CDH variant, but using the procedure with HDA linker (described in Scheme 3.3). Note that the values reported here (red squares in Figure 5.10) are not the same as the ones in Figure 3.11 for the variant D813, although immobilised at a GC/CNT electrode using the HDA linker, because those CVs were recorded in acetate buffer (pH 5.5). The analysis reported here in Figure 5.9 was carried out in Tris buffer (pH 7.4); the data were then compared with the ones recorded under the same conditions (CVs not shown, performed by my colleague Firas Al-Lolage).

Although the two experiments reported in Figure 5.10 have been performed at different times, the two electrodes modified with D813, one using the diazonium salt linker and one with the HDA linker, showed exactly the same trend of the current *vs.* glucose concentration, meaning that the amount of immobilised enzyme was the same, as well as their active area. This proves the great reproducibility in the preparation of GC/CNT electrodes, in addition to the efficacy of the new method for the immobilization of CDH using diazonium salt chemistry, which seems capable of immobilising the same amount of enzyme as the previous method. The stability of this new immobilization procedure was also tested: this electrode presented the 50 % of its initial activity after 50 days from the preparation (data not shown), in line with what reported for electrodes prepared using the HDA linker (see Figures 3.23 or 3.25).

5.3.3 MET of CDH immobilised at flat gold electrodes

After the preliminary experiment with a GC/CNT electrode described in the previous Section, the procedure shown in Scheme 5.6 was applied to gold electrodes. We chose to use gold screen-printed electrodes (AuSPEs) from DropSens (Oviedo, Spain) as they are easy to use and clean, in addition they should all have roughly the same active area (≈ 0.125 cm^2, 4 mm diameter, see Figure 2.2-B). The only problem in using AuSPEs is that they are quite delicate and can be easily damaged by strong solvents or concentrated acids, as they are mainly made of plastic materials and inks. For that reason, the procedure described in Scheme 5.6 was slightly changed to avoid damaging the screen-printed electrodes. Since in Section 5.2.4 it was shown that the modification also

works using milder solvents and less concentrated acids, the conditions reported in Scheme 5.6 were changed as follows: the reduction of the diazonium salt (step a) was carried out in a solution of water and acetonitrile (1:1), instead of using pure acetonitrile; the Boc deprotection (step b) was performed in 1 M HCl dissolved in water, instead of 4 M HCl in dioxane; the coupling of the spacer and passivating group (step c) was carried out in water instead of DMF; finally, the coupling of maleimide (step d) was done in ethanol instead of DMF, as *N*-maleoyl-β-alanine was not soluble in water. Afterwards, 5-6 µL of the enzyme solution of choice (E522 in this case), in phosphate buffer pH 7, were drop cast on each electrode, placed in the fridge at 4 °C overnight.

Two AuSPEs modified in this way with the variant E522 were tested firstly for MET to see if the modification procedure was successful and the enzyme was effectively immobilised on the electrodes. The analysis was carried out by cyclic voltammetry in acetate buffer (pH 5.5), containing 30 mM $CaCl_2$ and 20 µM ferrocenecarboxylic acid as mediator. As in the case of flat GC electrodes (see Section 5.1.2), we used the lowest possible concentration of mediator in order to have a small faradaic current for the ferrocene and to be able to detect the catalytic current.

Figure 5.11 shows the CVs recorded at these two modified electrodes (AuSPE 1 and 2) using both glucose (A-B) and lactose (C-D) as substrate. From these, we can confirm that CDH was present on the electrodes since it produced very nice catalytic voltammograms in the presence of the mediator. The catalytic current taken at 0.4 V vs. SCE, after background subtraction, can then be plotted versus the sugar concentration (Figure 5.12). From these plots we can see that with glucose the saturation occurs at 100 mM or after (Figure 5.12-A), while 5 mM lactose is enough to saturate the same electrodes (Figure 5.12-B). By fitting the data with the Michaelis-Menten equation (Eq. 3.5), we can extract the values of K_M^{APP} (Table 5.4): these are very different between the two substrates, being however very similar for the two electrodes analysed. K_M^{APP} was found to be around 31 mM for glucose and 0.6 mM for lactose. This can be explained with a higher affinity of CDH for lactose, more similar to its natural substrate (cellobiose), than for glucose, as reported also in the literature [123,154,170]. However, the values of i_{max}^{APP} are quite similar between the two electrodes and

the two sugars (around 300 nA), meaning that *i*) the amount of CDH immobilised at the two different AuSPEs was basically the same confirming the great reproducibility of our modification method, and *ii*) the maximum current we can reach upon saturation does not depend on the sugar used as substrate. Note that with the first electrode, in the case of glucose, i_{max}^{APP} was slightly lower (250 nA) probably because the analysis was stopped after 30 mM glucose, so that there were not enough data for the fitting. This is because AuSPE 1 was the first CDH-modified gold electrode that was tested and, at the beginning, we thought it was not possible to reach the same high glucose concentrations as with GC/CNT electrodes. In any case, with the second electrode, the analysis was carried out until 100 mM glucose obtaining more accurate data.

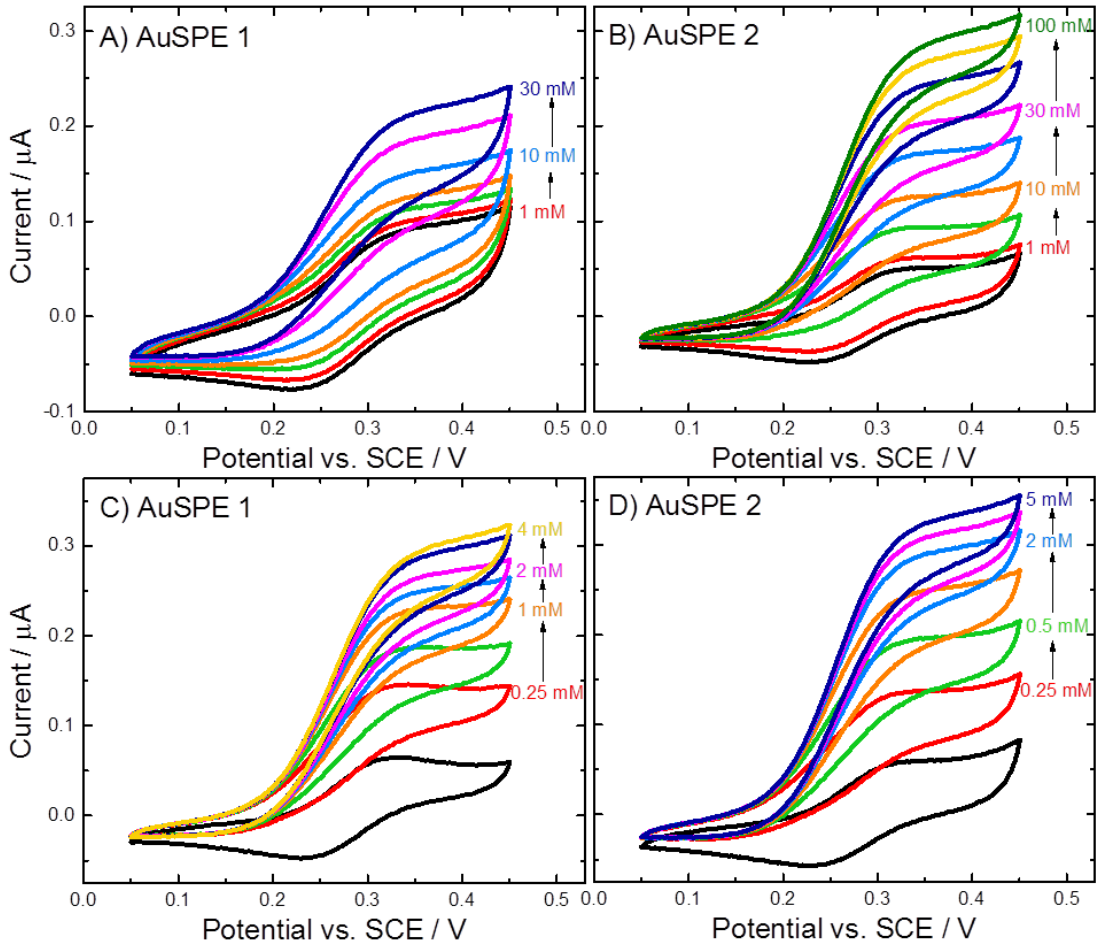

Figure 5.11. *CVs recorded at two E522-CDH modified AuSPEs (A and C: AuSPE 1; B and D: AuSPE 2), in argon-saturated 50 mM acetate buffer (pH 5.5), containing 30 mM $CaCl_2$, 20 µM ferrocenecarboxylic acid and different concentrations of (A-B) glucose or (C-D) lactose. The potential was swept at 2 mV/s.*

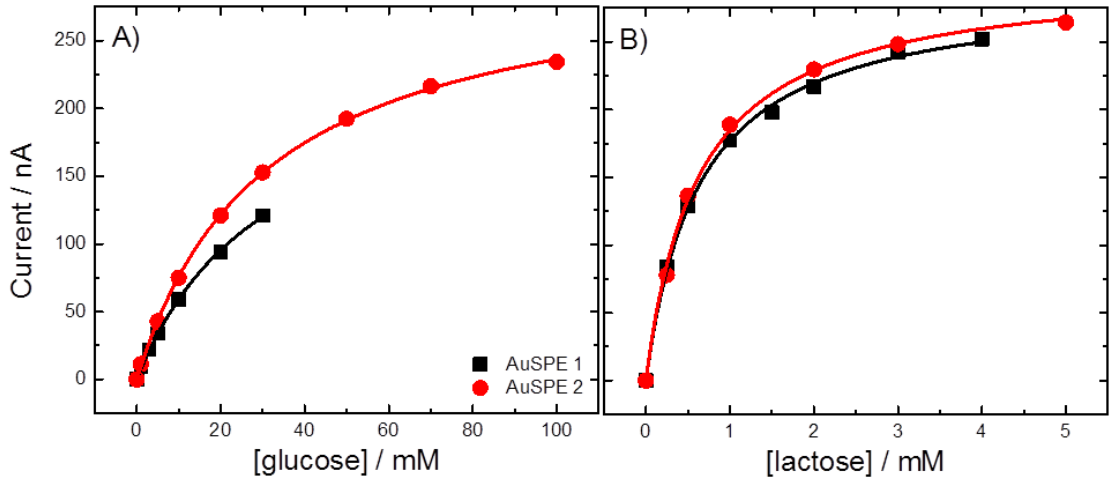

Figure 5.12. *Values of the MET current (after background subtraction) taken at 0.4 V in the CVs reported in Figure 5.11, versus the concentration of (A) glucose and (B) lactose. Black: AuSPE 1; red: AuSPE 2. Data were fitted with the Michaelis-Menten equation (Eq. 3.5, lines).*

Table 5.4. *Values of K_M^{APP} and i_{max}^{APP} for the MET of two AuSPEs modified with the CDH variant E522, analysed with glucose and lactose, extracted by fitting the data in Figure 5.12 with Eq. 3.5.*

Electrode	Glucose		Lactose	
	i_{max}^{APP} (nA)	K_M^{APP} (mM)	i_{max}^{APP} (nA)	K_M^{APP} (mM)
AuSPE 1	248 ± 9	32 ± 2	290 ± 4	0.64 ± 0.03
AuSPE 2	308 ± 2	30.7 ± 0.6	300 ± 5	0.62 ± 0.04

5.3.4 DET of CDH immobilised at flat gold electrodes

In the previous Section we proved that the immobilization method was successful, as the gold electrodes showed a catalytic current in the presence of mediator (further tests will be shown later in this Chapter). Therefore, the same two AuSPEs were tested also for DET using lactose as the substrate, since we found that CDH has a higher affinity for this sugar. Figure 5.13 reports the cyclic voltammograms recorded at the two AuSPEs modified with the variant E522 in the absence (black lines) and presence (coloured lines) of some amounts of lactose. Even though with both the electrodes the CVs recorded after the addition

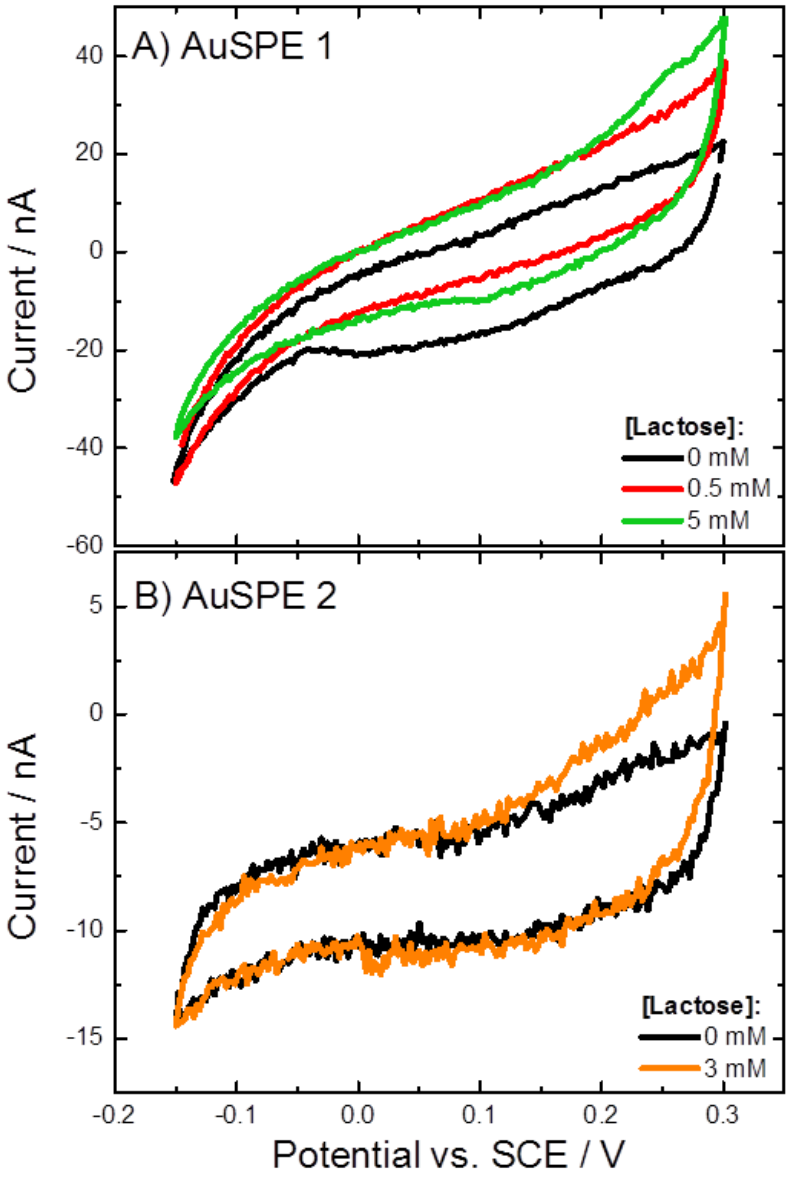

Figure 5.13. *CVs recorded at two E522-CDH modified AuSPEs, in argon-saturated 50 mM acetate buffer (pH 5.5), containing 30 mM $CaCl_2$ and different concentrations of lactose. The potential was swept at 1 mV/s.*

of lactose seem slightly different from the background CVs, we cannot certainly affirm that this was due to the DET of the enzyme. Probably, the background current changed a little bit between the first and second CV, as it is very small (around 10-15 nA for AuSPE 1 and 4-5 nA for AuSPE 2), giving the impression that the current was increasing. However, the results between the two electrodes are not consistent as the current increase seems to occur around -0.05 V for the first electrode (Figure 5.13-A) and around +0.15 V for the second one (Figure 5.13-B). Moreover, the addition of a second amount of sugar for the first electrode (green line) did not further increase the current, apart for a very late increase at 0.2 V. For that reason, it is difficult here to talk about DET.

Note that we used a different potential range if compared with the analysis for DET carried out at GC/CNT electrodes in Chapter 3, or also at GC electrodes in this Chapter (Figure 5.3): here the electrode potential was swept from -0.15 to 0.3 V *vs.* SCE, instead of between -0.35 and 0.1 V. This is because some preliminary experiments with gold electrodes seemed to show a DET current shifted to more anodic potentials than with carbon electrodes (see also Figure 5.25 later in this Chapter). Another observation we can make is that we used the variant E522 that, in the case of flat GC electrodes, did not show any DET current, while another CDH variant did (see Figure 5.3). It could be objected that this was not the best variant to test for DET at flat electrodes. However, we have to take into account that the conditions of the electrode surface may have changed if compared with GC electrodes as, in addition to the different electrode material, also the linker and the passivating group were different. Therefore, the interactions between the enzyme and the electrode may have changed too, as the charges at the electrode surface might be different. In this context, the CDH variants that had the highest probability of DET at flat carbon electrodes might not be the same in the case of gold electrodes, because their orientation on the electrode surface, due also to the surface charges, might be different.

To conclude, the two AuSPEs modified with the CDH variant E522 tested here did not show any clear DET current, even though the presence of the enzyme was confirmed by the MET catalytic current. However, other experiments will be shown later in this Chapter. For example, in the next Section we will test another modified gold electrode at a different pH, namely 7.4, to see if the DET could be

more easily detected in this condition. Furthermore, a control experiment using D- and L-glucose will be performed to verify that the observed MET catalytic current is effectively due to the immobilised enzyme.

5.3.5 Effect of a different pH

In order to see if the DET could be detected at neutral pH, another AuSPE covalently modified with the CDH variant E522 was tested in Tris buffer (pH 7.4), containing 30 mM $CaCl_2$. Firstly, the electrode was analysed for MET, in the buffer containing 20 µM ferrocenecarboxylic acid, to make sure that the enzyme was effectively present on the electrode surface. Figure 5.14 shows the CVs of this experiment, carried out using lactose as the substrate. Given the good results obtained, we can conclude that CDH was successfully immobilised on this electrode. The data of the catalytic current, taken at 0.4 V in the voltammograms of each lactose concentration (Figure 5.14-B), were fitted with the Michaelis-Menten equation to extract the values of i_{max}^{APP} and K_M^{APP}, which were 0.66 ± 0.02 µA and 1.6 ± 0.1 mM, respectively. While the K_M^{APP} was quite similar to those obtained with CDH-modified AuSPEs at pH 5.5 (see Table 5.4, for the lactose), the value of i_{max}^{APP} was twice that of the previous ones. However, this cannot be due to a doubling of the amount of enzyme immobilised on this new electrode, as the

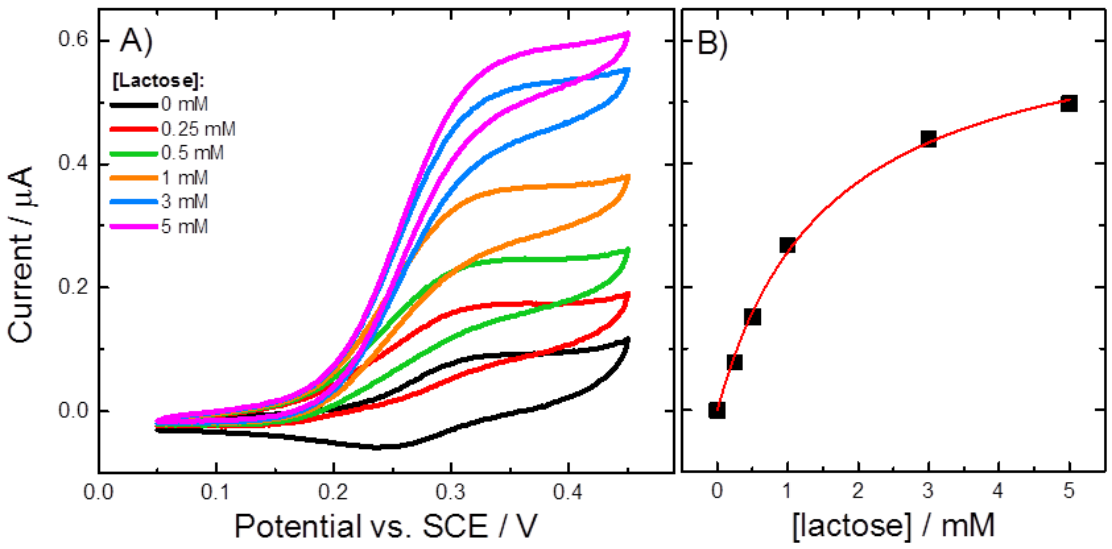

Figure 5.14. *A) CVs recorded at a E522-CDH modified AuSPE, in argon-saturated 50 mM Tris buffer (pH 7.4), containing 30 mM $CaCl_2$, 20 µM ferrocenecarboxylic acid and different concentrations of lactose. The potential was swept at 2 mV/s. B) Plot of the MET current (after background subtraction), taken at 0.4 V in the CVs in A, versus the lactose concentration. Data were fitted with Eq. 3.5 (red line).*

active area of the AuSPEs used should be roughly the same. Instead, the higher catalytic current observed here should be due to a higher rate constant for the substrate/FAD reaction at neutral pH, as we have already said [78].

While neutral pH can increase the MET current, since it increases the substrate/FAD reaction rate, it will not necessarily have the same effect on the DET current, which depends mainly on the IET rate and the possibility for the haem group to exchange electrons with the electrode surface. Figure 5.15 shows the cyclic voltammograms recorded at pH 7.4 for the DET of the same AuSPE modified with E522. After the addition of the first aliquot of lactose (0.25 mM, red line), the current seemed to increase at about -0.07 V, forming a kind of peak around +0.08 V. However, the addition of the second aliquot of sugar (1 mM, green line) did not produce a consistent increase, so that it is difficult to say whether the observed, small, current increase was due to DET of the enzyme or to a change in the background current, which is certainly very small (around 5 nA). To conclude, changing the solution pH did not produce any visible benefit for the DET current. Further experiments about that will be shown later in Section 5.3.12, using different gold electrodes under different conditions, with different CDH variants.

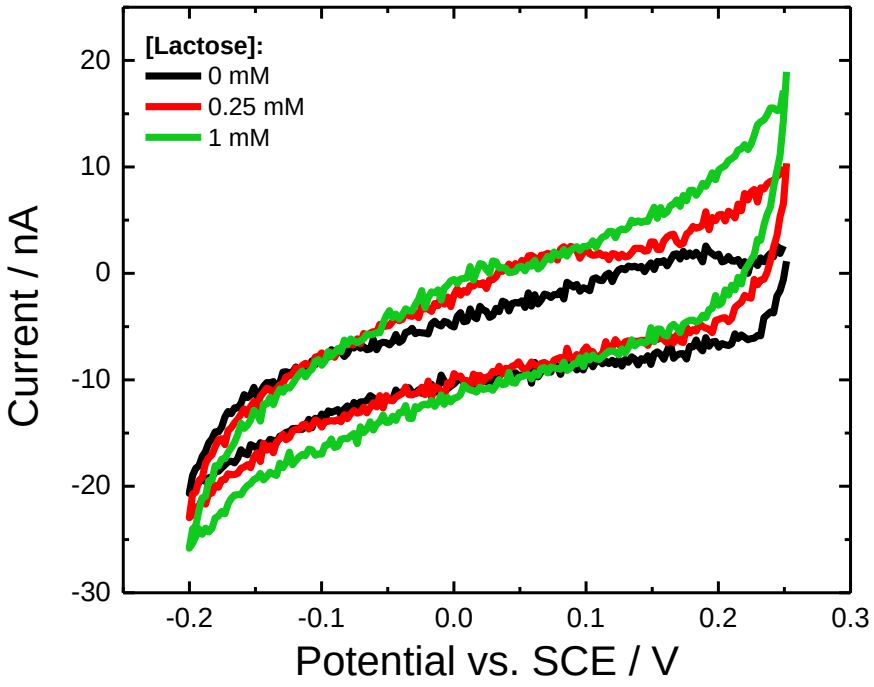

Figure 5.15. *CVs recorded at a E522-CDH modified AuSPE, in argon-saturated 50 mM Tris buffer (pH 7.4), containing 30 mM $CaCl_2$ and different concentrations of lactose. The potential was swept at 1 mV/s.*

5.3.6 Control experiment: effect of D- and L-glucose

As we have already done with CDH-modified GC/CNT electrodes in Section 3.2.4, to prove that the MET catalytic current observed in the previous Sections is due to the oxidation of a substrate by the immobilised enzyme, a control experiment using D- and L-glucose was performed. This experiment was not carried out with lactose as it is a disaccharide that, to our knowledge, is not commercially available in the L conformation. As we have already said, CDH is selective for the D-glucose, while it does not oxidise the other isomer, so that adding L-glucose in the electrochemical cell should not produce any increase in the catalytic current. This selectivity can only be attributed to the enzyme: indeed, other possible catalysts present in the cell or on the electrode, such as metals, would oxidise both the isomers of the sugar. Figure 5.16-A shows the voltammograms for the MET of the same electrode employed in the previous Section at pH 7.4, upon addition of different aliquots of L- and D-glucose in the cell. It is clear, also looking at Figure 5.16-B that shows the value of the current after every addition, that there is no change in the current upon addition of L-glucose in the cell (see dashed CVs in Figure 5.16-A). Contrarily, upon each addition of an aliquot of D-glucose the catalytic current increases (see solid CVs), confirming that the MET catalytic current was due to the immobilised enzyme.

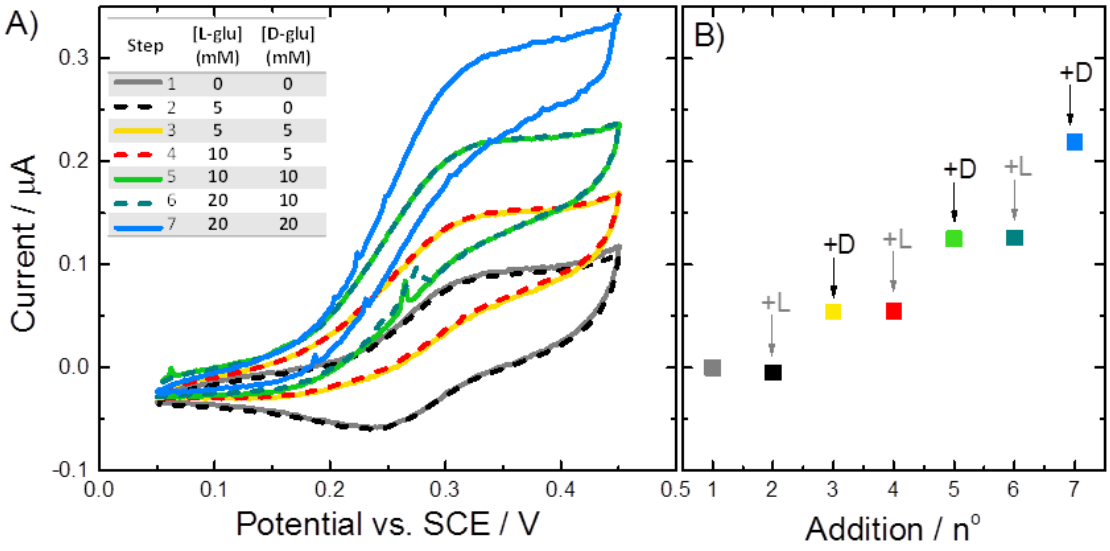

Figure 5.16. *A) CVs for a E522-CDH modified AuSPE, recorded in argon-saturated 50 mM Tris buffer (pH 7.4), containing 30 mM $CaCl_2$, 20 µM ferrocene (grey line) and increasing concentrations of L- and D-glucose. The solution compositions are reported in the inset. The electrode potential was swept at 2 mV/s. B) Background subtracted MET current measured at 0.4 V after each addition of D- and L-glucose.*

5.3.7 Covalent immobilization *vs.* physical adsorption

To verify that CDH was immobilised at the electrode surface through a covalent bond between its free cysteine residue and the maleimide, we carried out a test using the same CDH variant employed for the previous experiments (E522) physically absorbed at a AuSPE. For this experiment, a gold SPE was cleaned with ethanol and, once dry, 5-6 µL of the CDH solution were drop cast on it, leaving it in the fridge at 4 °C overnight. In theory, the CDH molecules should spontaneously adsorb on the unmodified gold electrode thanks to their cysteine residues, forming a self-assembled monolayer (SAM) [51,52]. Therefore, unlike with carbon electrodes, we could expect the cysteine-modified CDH variants to strongly bind at unmodified gold electrodes, thus making unnecessary the maleimide modification process. However, despite the fact that the SAM technique has been extensively employed to immobilise enzymes or other proteins at gold electrodes [171-173], the thiol-gold bonds lack of stability over a wide potential range, long periods or in other conditions (*e.g.* high temperature, exposure to UV light), as the thiol groups can be easily oxidised [54-57]. Moreover, the cysteine residues at the enzyme surface are probably not so inclined to react with the electrode surface because of steric restrictions: that is why our modification procedure includes the dilution of the maleimide groups on the electrode thanks to the use of a passivating group (see Scheme 3.2 in Section 3.1.1).

Figure 5.17 shows the CVs recorded for the MET of the AuSPE physically modified with E522-CDH, in acetate/$CaCl_2$ buffer (pH 5.5) containing 20 µM ferrocenecarboxylic acid. It is clear that the enzyme was present also on this electrode, since a catalytic current increasing with the glucose concentration was detected. However, if we compare the current of this electrode with the one obtained in the same conditions for a AuSPE covalently modified with the same CDH variant (reported in Figure 5.11-B), we can see a big difference. As shown in Figure 5.18, the covalently modified electrode (black) presented a catalytic current at least three times higher than the physically modified one (red). This is clear also if we compare the values of i_{max}^{APP} extracted by fitting the data in Figure 5.18 with the Michaelis-Menten equation (see Table 5.5).

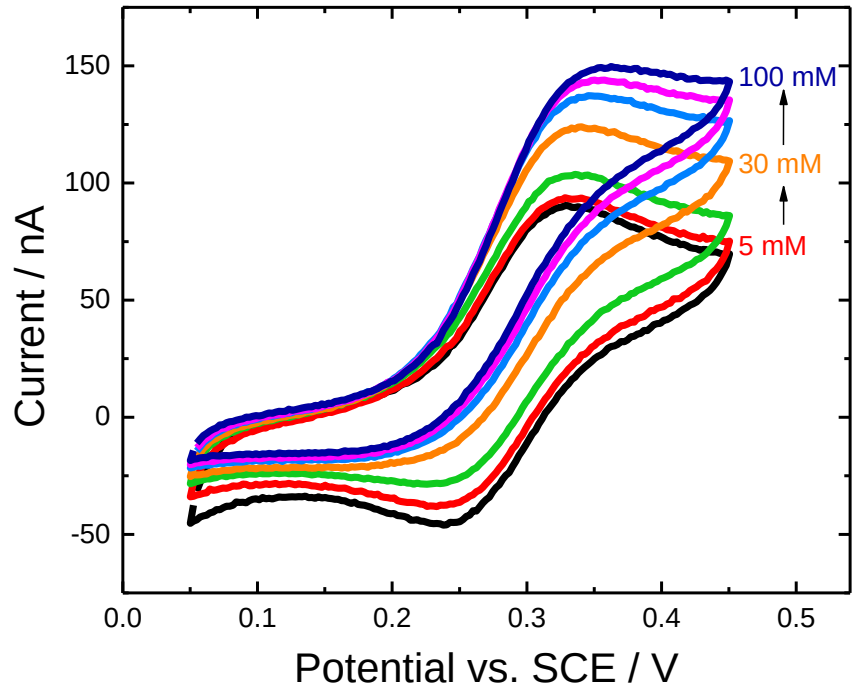

Figure 5.17. *CVs recorded at a AuSPE physically modified with E522-CDH, in argon-saturated 50 mM acetate buffer (pH 5.5), containing 30 mM $CaCl_2$, 20 µM ferrocenecarboxylic acid and different concentrations of glucose. The potential was swept at 2 mV/s.*

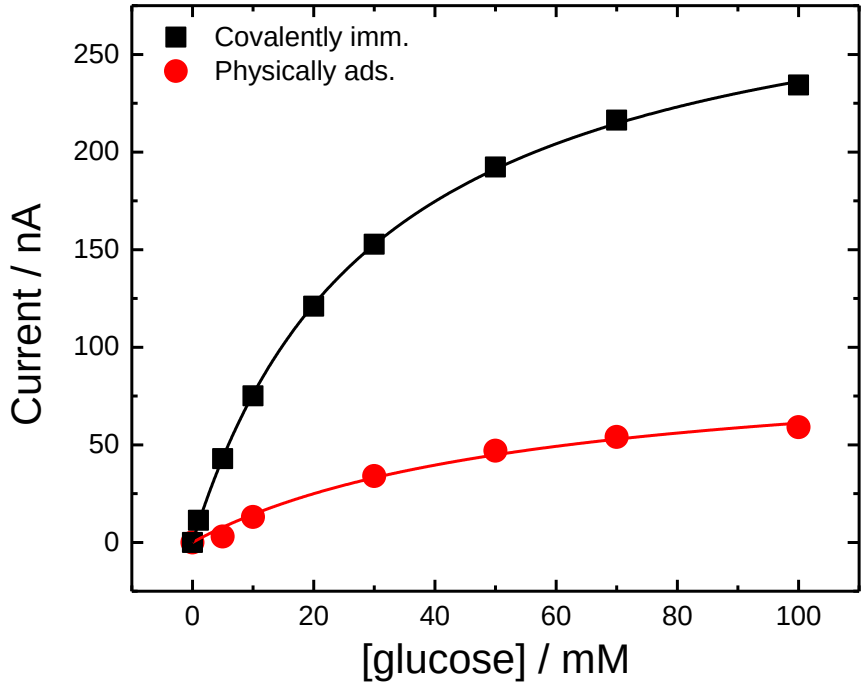

Figure 5.18. *Plot of the MET current (after background subtraction) versus glucose concentration, taken at 0.4 V in the CVs reported in Figure 5.11-B for the covalently immobilised CDH (black squares) and Figure 5.17 for the physically adsorbed one (red circles). Both experiments were carried out with E522-CDH, in 50 mM acetate buffer (pH 5.5), containing 30 mM $CaCl_2$ and 20 µM ferrocenecarboxylic acid. Data were fitted with the Michaelis-Menten equation (Eq. 3.5, lines).*

Such a big difference cannot be due to a different active area of the electrodes, as two different AuSPEs covalently modified with E522 produced basically the same current (see Figure 5.12), meaning that these electrodes have a very reproducible specific area. Therefore, we can explain this big difference with a much lower amount of CDH molecules that were retained at the unmodified electrode and/or denaturation of the enzyme adsorbed on bare gold. This confirms once again the great efficacy of our immobilization procedure, proving also that the maleimide modification is not superfluous to attach cysteine-modified enzymes at gold substrates, being instead more efficient than the pure thiol-gold bond.

Table 5.5. *Values of K_M^{APP} and i_{max}^{APP} for the MET with glucose of two AuSPEs covalently and physically modified with the CDH variant E522, extracted by fitting the data in Figure 5.18 with Eq. 3.5.*

Electrode	Glucose	
	i_{max}^{APP} (nA)	K_M^{APP} (mM)
Covalently mod.	308 ± 2	30.7 ± 0.6
Physically mod.	96 ± 10	57 ± 13

5.3.8 Stability over the time

A further evidence of the great efficacy of the maleimide-modified electrodes over unmodified gold electrodes was provided by the measurement of stability over the time. As already done with CDH-modified GC/CNT electrodes in Section 3.5.1, two gold electrodes, one covalently and one physically modified with the variant E522, were tested for MET in the acetate/$CaCl_2$ buffer (pH 5.5), containing 20 µM ferrocenecarboxylic acid and 70 mM glucose, at different times after the preparation. During that time, the electrodes were stored wet with the same buffer used for the tests, at 4 °C. The values of the MET current, taken at 0.4 V *vs.* SCE after background subtraction, were divided for the value on the first day to obtain a graph of the activity (in percentage) versus the time passed from the preparation of the electrodes (Figure 5.19). From this, we can see that the activity of the physically modified electrode (red) decreased quite rapidly reaching a value of zero after 28 days. On the other hand, the activity of the

electrode modified with maleimide and CDH (black) decreased quite sharply during the first few days, reaching 60 % of the initial activity, but then remained quite stable around this value for other 50 days, when we decided to end the experiment.

The first sharp decrease in the case of the covalently modified electrode is probably due to the loss of the physically adsorbed CDH molecules, or molecules immobilised through thiol-gold bonds, from the electrode surface. After that, the enzyme still bound at the electrode was quite stable, keeping the same activity for a very long period. The small fluctuations in the activity are probably due to experimental factors, such as slightly different temperature or concentration of glucose. In contrast, the unmodified electrode, with the enzyme retained through electrostatic interactions or thiol-gold bonds, lost quite rapidly its activity due to desorption of CDH from the surface. This is a further proof of the greater stability of the covalent bonds between maleimide-modified electrodes and CDH variants bearing a free cysteine at their surface.

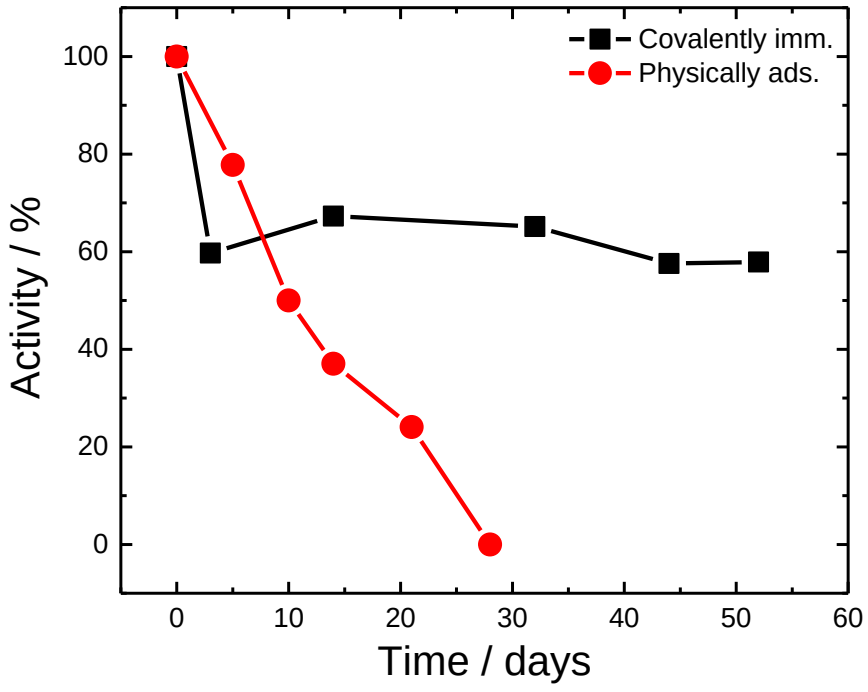

Figure 5.19. *Activity (expressed as percentage of MET current versus the current of the first day) of two gold electrodes (black) covalently and (red) physically modified with E522-CDH. All the experiments were carried out in argon-saturated 50 mM acetate buffer (pH 5.5), containing 30 mM $CaCl_2$, 20 µM ferrocenecarboxylic acid and 70 mM glucose. The current was measured at different times from the preparation of the electrodes, which were stored wet with the same buffer at 4 °C.*

5.3.9 Effect of different spacers

Another point we wanted to investigate is the architecture of the organic layer used for the covalent immobilization of CDH, in particular the length of the tether supporting the maleimide groups. Until now, we have always used the same compounds to modify the electrodes, changing only the linker and the passivating group for the modification of the gold electrodes, as the ones previously employed on carbon electrodes were no longer suitable. The use of these elements (linker, passivating group, spacer and reactive group) was established for carbon electrodes in a previous work by our group [70,110], so that we have not investigated the possibility of using different ones in Chapter 3, when we studied the covalent immobilization of CDH at GC/CNT electrodes. However, in this Chapter we have already changed two of them, the linker and the passivating group, to adapt the modification procedure to gold substrates. Therefore, we wondered if also other elements could be varied in order to better accommodate CDH onto flat gold electrodes. Since the reactive group cannot be changed as the cysteine-modified CDH variants react very well with maleimide, we can play only with the length of the tether by trying different spacers.

In this Section, we will study three different lengths of the tether for the immobilization of CDH at gold electrodes. In order to focus only on the different lengths of the modification, not on differences in the electrode active area, commercial gold disc electrodes (2 mm diameter) were used in this experiment instead of gold SPEs. This is because, with gold disc electrodes, the active area can be calculated by integrating the CV recorded in sulfuric acid (as explained in Section 2.1.5 in the Experimental Part). This procedure cannot be applied in the case of screen-printed electrodes since the concentrated sulfuric acid could damage them and, in addition, SPEs are made of a gold ink, not pure gold.

Three gold disc electrodes, after they were polished and the active area was calculated as already explained, were modified with maleimide as shown in Scheme 5.6. In particular, the first electrode (El. 1) was modified exactly as shown in Scheme 5.6 using a six-carbon-long spacer (*N*-Boc-6-aminohexanoic acid, here simply called “6C-spacer”), the second electrode (El. 2) was modified using a 3C-spacer (Boc-β-alanine) instead of the 6C-spacer, and the third

electrode (El. 3) was modified without any spacer by coupling the reactive group directly to the electrode with only the linker. A representation of the overall modification of the three electrodes is shown in Scheme 5.8, where the linker with the passivating group is reported in grey on each electrode for comparison. The ratio between spacer and passivating group was the same as before: 90 % passivating group and 10 % spacer (or reactive group in the case of El. 3).

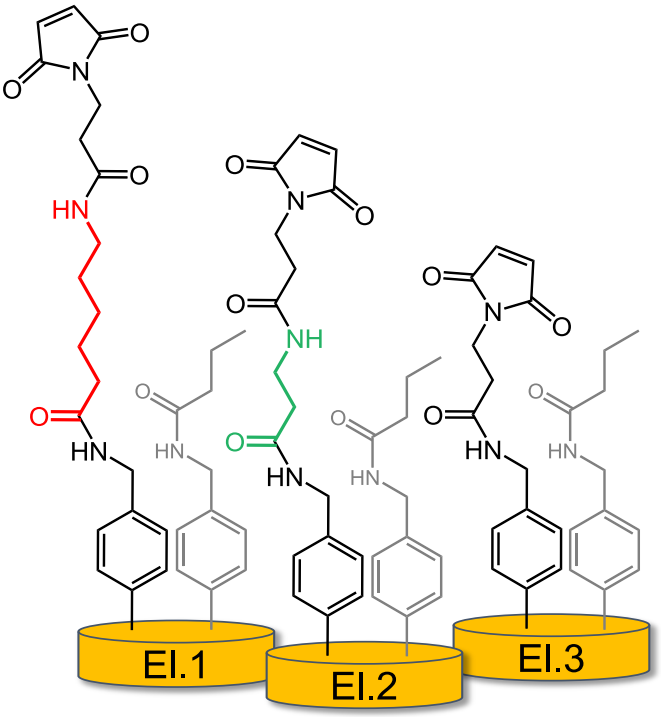

Scheme 5.8. *Representation of the maleimide modification on the three gold disc electrodes used in this experiment. El. 1: modified with 6C-spacer (N-Boc-6-aminohexanoic acid, red); El. 2: modified with 3C-spacer (Boc-β-alanine, green); El. 3: modified without any spacer. The passivating group is in grey for comparison.*

After the modification, the three electrodes were reacted with the CDH variant E522 and, then, analysed for MET, as DET did not produce good results in the case of gold electrodes. Figure 5.20 shows the CVs recorded at these three electrodes in Tris/$CaCl_2$ buffer (pH 7.4), containing 20 μM ferrocenecarboxylic acid, using lactose as the substrate. The background subtracted currents, taken at 0.4 V in Figure 5.20-B, D and F, were normalised for the active area of the electrodes to give the current density (*j*), which was plotted *vs.* the lactose concentration (Figure 5.21). We can immediately see that the electrode with the highest current density is the one modified with the 3C-spacer (green), followed by the one with the 6C-spacer (red) and, lastly, by the electrode without spacer

(black), which presents almost half of the current density of El. 2. The data in Figure 5.21 were fitted with the Michaelis-Menten equation to provide the values of j_{max}^{APP} and K_M^{APP}, reported in Table 5.6 together with the active area of each electrode measured before the modification. Concerning the active area, we can see that it is roughly the same for the three gold electrodes, being around 0.1 cm^2. Also the values of K_M^{APP} are basically the same for all the electrodes, being around

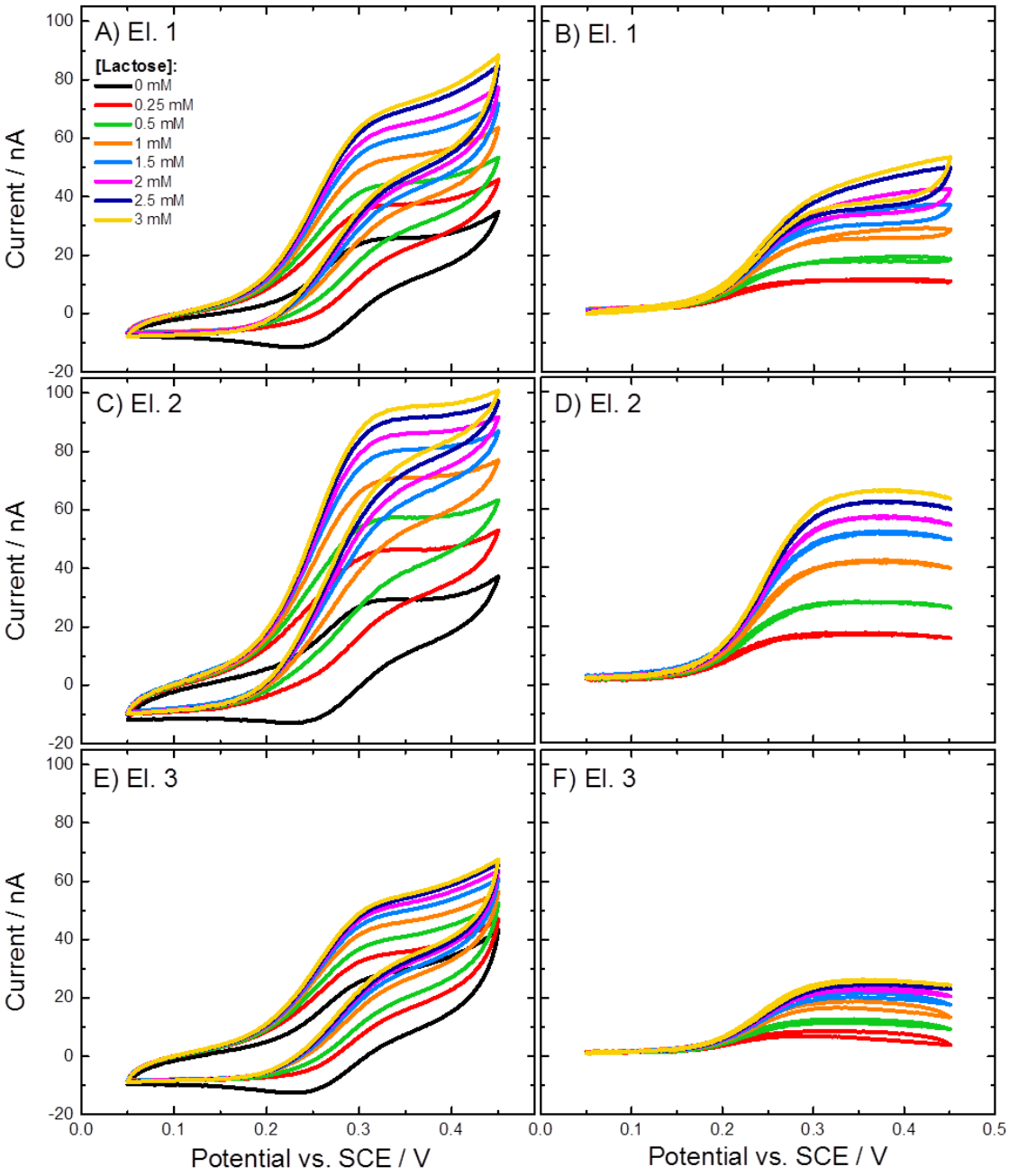

Figure 5.20. *(A, C, E) Original and (B, D, F) background subtracted CVs recorded at E522-CDH modified gold electrodes, in argon-saturated 50 mM Tris buffer (pH 7.4), containing 30 mM $CaCl_2$, 20 µM ferrocenecarboxylic acid and different concentrations of lactose from 0 to 3 mM. The potential was swept at 2 mV/s. The electrodes were modified as described in Scheme 5.8 using: (A-B) a 6C-spacer, (C-D) a 3C-spacer and (E-F) no spacer.*

1-1.2 mM, indicating that the enzyme has the same properties on the three different electrodes. However, the values of j_{max}^{APP} (note that in Figure 5.21 we plotted the current density, *j*, not the current) are different and reflect what we have already observed in Figure 5.21.

El. 3, modified without any spacer, presented the lowest current density probably because a lower amount of CDH molecules could be accommodated on it due to steric restrictions upon coupling between cysteine and maleimide, as the latter is basically at the same height as the passivating group (see Scheme 5.8). The other two electrodes, in fact, presented current densities decidedly higher than El. 3 since the maleimide groups rise up from the layer of the passivating group (see Scheme 5.8), facilitating the reaction with the cysteine residues at the enzyme surface. Among them, El. 2 modified with the 3C-spacer gave the best results. The reason for that is not clear, since this experiment was performed using a soluble mediator that can easily transfer electrons between the CDH and the electrode surface. In any case, the 3C-spacer instead of the 6C-spacer will be used to modify flat gold electrodes in the following experiments.

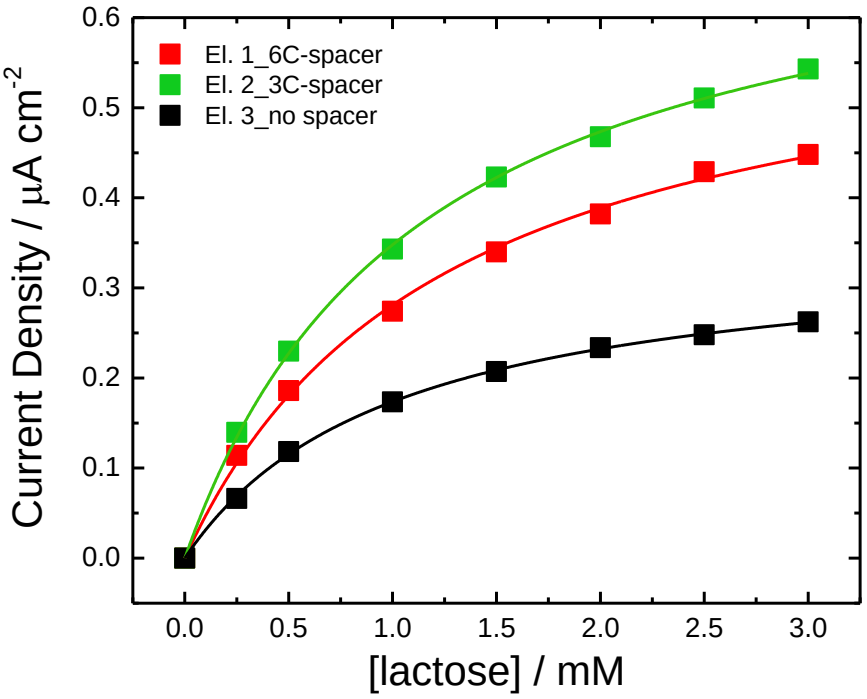

Figure 5.21. *Values of current density taken at 0.4 V in the background subtracted CVs reported in Figure 5.20 (divided for the electrode area). The electrodes were modified with E522-CDH as described in Scheme 5.8 using: (red) a 6C-spacer, (green) a 3C-spacer and (black) any spacer. Data were fitted with Eq. 3.5 (lines).*

Table 5.6. *Values of active area, K_M^{APP} and j_{max}^{APP} (current density) for three gold electrodes modified with E522-CDH as described in Scheme 5.8, extracted by fitting the data in Figure 5.21 with Eq. 3.5.*

Electrode	Modification	Electrode area (cm^2)	Fitting parameters	
			j_{max}^{APP} ($\mu A/cm^2$)	K_M^{APP} (mM)
El. 1	6C-spacer	0.100	0.63 ± 0.02	1.24 ± 0.08
El. 2	3C-spacer	0.121	0.74 ± 0.01	1.13 ± 0.04
El. 3	No spacer	0.098	0.35 ± 0.01	1.02 ± 0.03

5.3.10 Characterization of CDH immobilization by SPR

In Section 5.2.4 we employed surface plasmon resonance (SPR) spectroscopy to characterise the procedure for the covalent modification of gold electrodes, studying in particular the steps of diazonium salt reduction, Boc deprotection of the diazonium salt and solid phase coupling of a carboxylic acid (Boc-β-alanine, or 3C-spacer). In this Section we will investigate the immobilization kinetics of CDH variants using SPR spectroscopy, studying in particular the effect of the enzyme concentration during the immobilization and the effect of different CDH variants bearing the free cysteine in different positions. Afterwards, we will show the results obtained for the DET of CDH immobilised at the SPR gold substrates.

SPR substrates (glass disc slides coated with a very thin gold layer, ≈ 30 nm, see Figure 5.7-B) were modified with maleimide as described in Scheme 5.6. Due to the fragility of the substrates and SPR instrument, milder conditions were used during the modification process giving preference to solvents such as water or ethanol (instead of dioxane and DMF) and using less concentrated acid for the Boc deprotection, as already described in Section 5.3.3 for AuSPEs. Moreover, the 3C-spacer was used instead of the 6C-spacer since, in the previous Section, we observed higher MET currents when using this spacer, probably due to a higher surface coverage of the enzyme.

The maleimide-modified SPR substrates were placed inside the SPR spectroscope and used to follow in real time the immobilization of the CDH variant E522 at

different concentrations: 0.5, 1 and 10 g/L. The immobilization process was monitored though the SPR angle shift (Figure 5.22). At the beginning, in the first few minutes, only the 50 mM phosphate buffer (pH 7) was present on the substrate and the angle shift was constant. Then, around 10 µL of enzyme in the same phosphate buffer was placed on the substrate and the angle shift increased. The large sharp increase in the first few seconds of the process is due to the change in the reflective index when passing from the pure buffer solution to the buffer with the enzyme, and it depends on the concentration of the enzyme solution so that the increase is higher for 10 g/L CDH (black curve) than for the other two solutions. Afterwards, the angle increases more, but slower, because of the formation of covalent bonds between the maleimide and the cysteine residues of the enzyme. When the angle shift seemed rather constant (after 10 min for the 10 g/L solution, or a bit longer for the other two solutions), the immobilization process was stopped by washing the substrate with the buffer solution. At this point, the angle shift decreased rapidly because of the change in the solution RI. The process seems quite fast and already completed after 10 min for the highest concentration of CDH, or in 30-40 min for the lower concentrations. This means that the reaction between maleimide and cysteine at

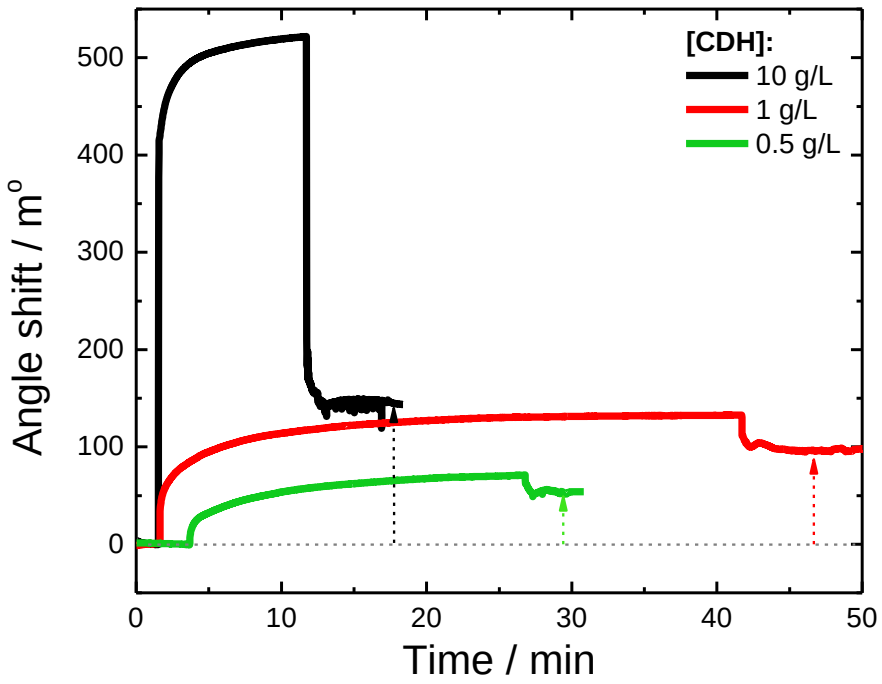

Figure 5.22. *SPR sensorgrams for the immobilization of E522-CDH at different concentrations (10, 1 and 0.5 g/L) at maleimide-modified SPR substrates. The dashed arrows represent the increase in the angle shift due to the immobilization.*

room temperature is very fast, so that it is not necessary to leave it react overnight since one hour seems more than enough.

The angle shift due to the enzyme immobilization can be measured in the SPR sensorgrams when the substrate is in phosphate buffer before and after the immobilization process (dashed arrows in Figure 5.22). The average values of angle shift between two experiments for each CDH concentration (except for 0.5 g/L, for which we had only one measure) are reported in Table 5.7. The angle shift is higher for the most concentrated solution, decreasing with the enzyme concentration. However, it is not directly proportional to the CDH concentration: in fact, leaving enough time for the reaction to occur, even the less concentrated solutions can produce the same surface coverage of enzyme as more concentrated solutions. On the other hand, a very concentrated solution cannot immobilise an infinite number of CDH molecules since the limit is represented by the amount of enzyme that can react with the maleimide at the electrode surface and form a monolayer. The enzyme in excess will be washed away at the end of the process.

From the considerations above we can see that there is a correlation between the angle shift and the surface coverage of the enzyme. In fact, the RI of the sensor surface changes upon binding of macromolecules to the surface, and the SPR angle will change accordingly. There is a linear relationship between the amount of bound protein and the angle shift, given by the following equation:

$$122\ \text{m°} = 1\ \text{ng/mm}^2 \qquad \text{(Eq. 5.5)}$$

This equation was reported in the instrument manual (an Autolab ESPRIT SPR spectroscope), as well as in a publication by Gorton *et al.* [95]. The value of 122 m° derives from the angle shift calculated by a model that assumes the protein layer as a composite material for which the RI is given by the Lorentz-Lorentz equation [168,169,174], assuming the protein density equal to 1.35 g/cm^3 [175]. Therefore, the surface coverage of CDH (Γ_{CDH}) will be given by:

$$\Gamma_{\text{CDH}}(\text{ng/mm}^2) = \frac{AS\ (\text{m°})}{122} \qquad \text{(Eq. 5.6)}$$

where *AS* is the angle shift measured in the SPR sensorgrams.

To convert the surface coverage in ng/mm^2 to the unit normally used in this work, pmol/cm^2, we can use the following equation considering the molecular mass of *Mt*CDH equal to 94 kDa [73]:

$$\Gamma_{CDH}(\text{pmol/cm}^2) = \frac{\Gamma_{CDH}(\text{ng/mm}^2)}{0.94} \qquad \text{(Eq. 5.7)}$$

The values of CDH surface coverage in pmol/cm^2 are reported in Table 5.7. For the two higher concentrations (1 and 10 g/L), Γ_{CDH} was about 1 pmol/cm^2. For the 0.5 g/L solution, it was almost the half of this value, meaning that the immobilization time (25 min) was not sufficient for this concentration: probably one hour would have been required to complete the process. If we consider CDH like a sphere of 80 Å in diameter [74,176], the area that each CDH molecule occupies can be approximated as a square 80 Å large, which is 6.4 $\times 10^{-13}$ cm^2. Therefore, multiplying this for the Avogadro number (6.022 $\times 10^{23}$ mol^{-1}), the area that one mole of CDH can occupy will be equal to 3.85 $\times 10^{11}$ cm^2/mol. It follows that the maximum surface coverage for *Mt*CDH is around 2.5 pmol/cm^2 with the enzyme molecules forming a close-packed monolayer. However, this would require the enzyme to move around on the surface, which does not happen in this case once the enzyme is immobilised through the maleimide-cysteine bonds. Instead, the immobilization process of CDH in our case can be better explained by the theory of random sequential adsorption developed by Feder [177,178], who found that the coverage at the jamming limit is roughly half than a close packing coverage. Considering this theory, and taking into account also the errors in the angle shift measurement and in the generally assumed protein density (used to write Eq. 5.5), our values for the CDH surface coverage reported in Table 5.7 seem quite reliable.

Table 5.7. *Angle shift measured in phosphate buffer before and after CDH immobilization in the SPR sensorgrams of Figure 5.22; CDH surface coverage and rate constant for three different concentrations of E522-CDH.*

[CDH] (g/L)	Angle Shift (m°)	Surface coverage (pmol/cm^2)	Rate constant (s^{-1})
10	137 ± 7	1.19 ± 0.06	(1.4 ± 0.5) $\times 10^{-2}$
1	94 ± 4	0.82 ± 0.03	(3.0 ± 0.1) $\times 10^{-3}$
0.5	53	0.46	(2.5 ± 0.01) $\times 10^{-3}$

While the solution concentration does not significantly affect the surface coverage of CDH, it will affect the rate constant of the binding reaction, k. A pseudo-first-order rate constant for the CDH immobilization at maleimide-modified substrates can be extracted by fitting the SPR curves in Figure 5.22 with the following equation:

$$AS = AS_0 + (AS_{\max} - AS_0)(1 - e^{-kt}) \qquad \text{(Eq. 5.8)}$$

where AS is the angle shift, AS_0 is the starting angle shift, $AS_{\max}$ is the maximum angle shift and k the rate constant. This equation was developed for optical biosensor responses by Edwards *et al.* [179], assuming the concentration of the protein in solution to be in large excess over the immobilised reactive group, so that is can be considered constant during the experiment.

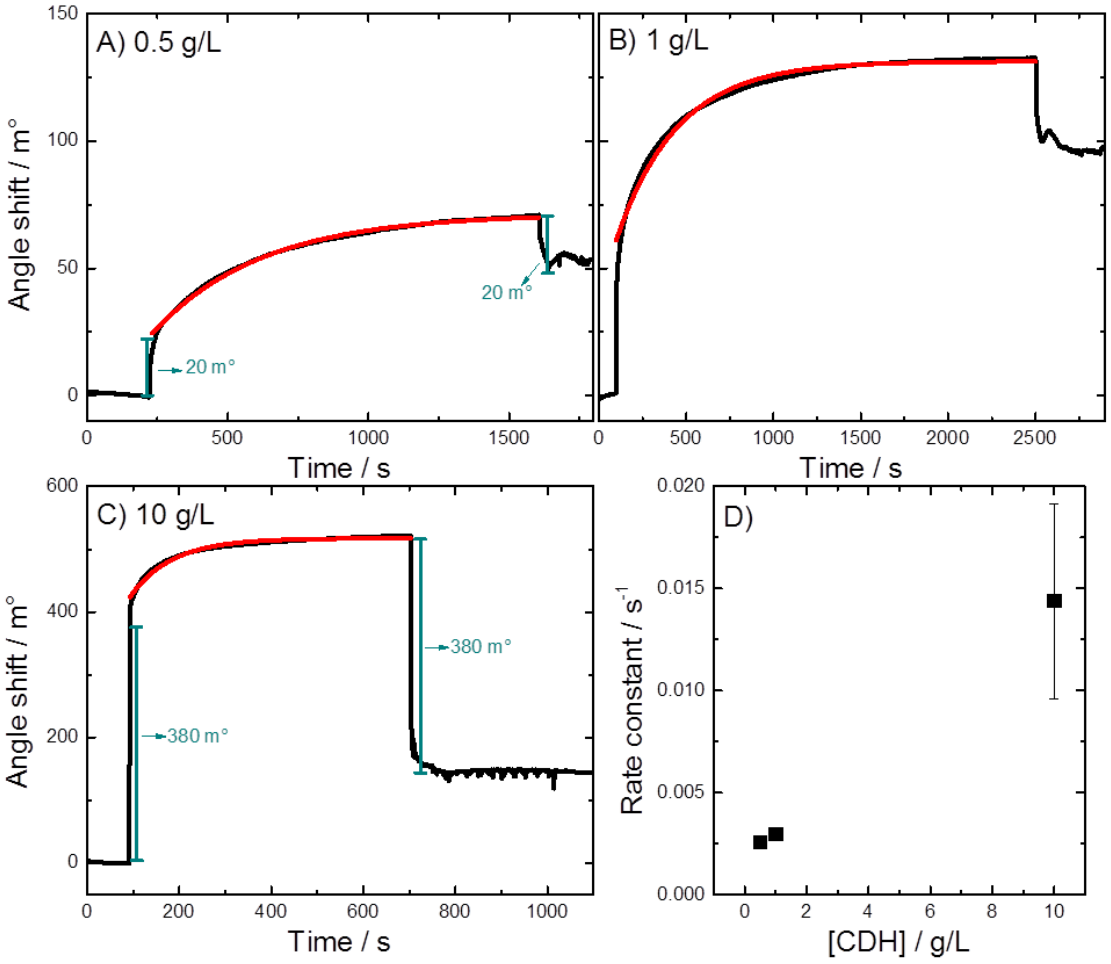

Figure 5.23. *A, B, C) SPR sensorgrams for the immobilization of E522-CDH at maleimide-modified SPR substrates, from solutions at different concentrations: (A) 0.5, (B) 1 and (C) 10 g/L. Red lines: fitting curves using Eq. 5.8 only for the portion of sensorgram corresponding to the enzyme immobilization. Green lines in A and C represent the changes in angle shift due to the change of solution on the substrate. D) Rate constant extracted by the fitting vs. CDH concentration.*

Eq. 5.8 was used to fit the portion of the SPR sensorgrams corresponding to the immobilization reaction (Figure 5.23), excluding the first sharp increase in the angle shift due to the change of the RI upon the addition, or removal, of the enzyme solution (represented by the green lines in Figure 5.23-A and C). The fitting was carried out on two sensorgrams for each CDH concentration, except for 0.5 g/L for which the second sensorgram was not usable because of technical problems during the experiment (Figure 5.23 shows one sensorgram for each concentration). The average values of rate constant extracted from the fitting are reported in Table 5.7 and Figure 5.23-D. As expected, they seem to be linearly correlated to the enzyme concentration meaning that, by increasing the CDH concentration, the immobilization reaction rate increases accordingly.

5.3.11 Effect of different CDH variants on the immobilization process

In this Section, we wanted to investigate the kinetics of the immobilization reaction for different CDH variants. In fact, the position of the free cysteine at the enzyme surface could affect the reaction with the maleimide immobilised on the substrates, making some of the CDH variants more reactive than others. For this experiment, two other variants (T701 and D574) were immobilised at maleimide-modified SPR substrates, following the process through the SPR angle shift. The enzyme concentration was 1 g/L since higher concentrations, such as 10 g/L, would make the immobilization reaction too fast for all the variants, so that the discrimination between them would be more difficult.

Figure 5.24 shows the SPR sensorgrams for the immobilization reaction of the three CDH variants used in this experiment (the one for E522 was already reported in Figure 5.23-B). The portion of the sensorgrams corresponding to the immobilization process, excluding the first sharp increase due to the addition of the enzyme solution, was fitted with Eq. 5.8 (red lines) to extract the rate constant. The average values of k obtained from the fitting of different sensorgrams for each CDH variant are reported in Figure 5.24-D and Table 5.8. We can note that the rate of immobilization is different for the three enzymes: this can be due in part to some differences in the concentration of the variants, but mainly to the different position of the cysteine that would be more or less accessible for the reaction with maleimide.

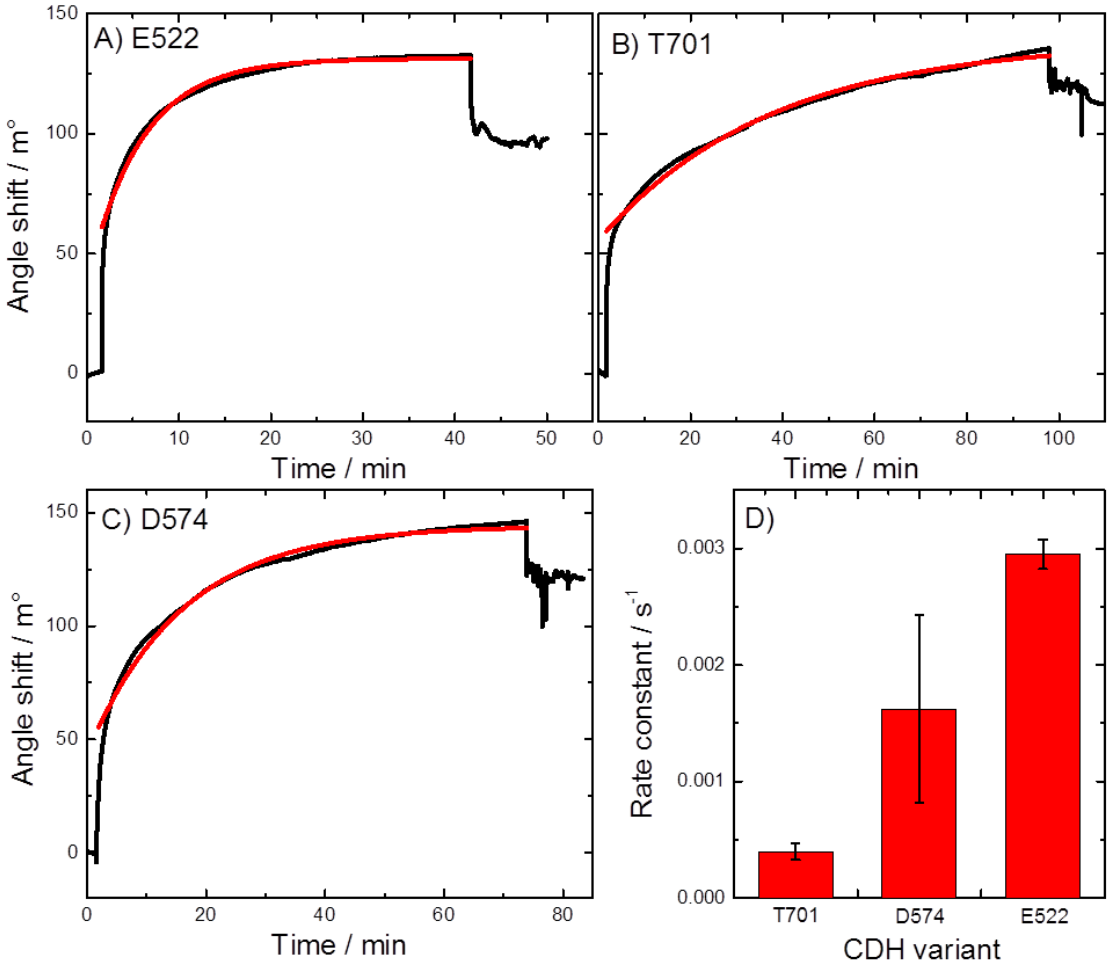

Figure 5.24. *A, B, C) SPR sensorgrams for the immobilization of different CDH variants (concentration = 1 g/L) at maleimide-modified SPR substrates: (A) E522, (B) T701 and (C) D574. Red lines: fitting curves using Eq. 5.8 only for the portion of sensorgram corresponding to the enzyme immobilization. D) Rate constant for the different variants extracted by the fitting.*

Table 5.8. *Rate constant for the immobilization reaction of three different CDH variants, extracted by fitting SPR sensorgrams with Eq. 5.8.*

CDH variant	Rate constant (s^{-1})
E522	$(3.0 \pm 0.1) \times 10^{-3}$
T701	$(4.0 \pm 0.7) \times 10^{-4}$
D574	$(1.6 \pm 0.8) \times 10^{-3}$

We can conclude that different CDH variants require different immobilization times. While one hour could be sufficient for the variants E522, as we have seen in the previous Section, the same time might not be enough for the other enzymes that seem to have a slower kinetics toward the reaction with maleimide. Therefore, it is recommended to leave the CDH solution on the electrodes for at least 2-3 hours at room temperature, or overnight in the fridge, as we have always done in this work. Note that the enzyme surface coverage was not calculated using the variation in the angle shift, as done in the previous Section, since this strongly depends on the reaction time. Given that the three variants were left on the SPR substrates for different times, the angle shift and, consequently, the surface coverage cannot be used to discriminate between the different enzymes.

5.3.12 Electrochemical analysis of CDH-modified SPR substrates

Some of the SPR substrates modified with CDH were analysed by cyclic voltammetry directly inside the SPR instrument. The analysis of two different substrates modified with the variants E522 and T701 was performed at pH 5.5 and 7.4, using the same buffer (50 mM Bis-Tris containing 30 mM $CaCl_2$) for both the pHs and lactose as the substrate. Figure 5.25 shows the CVs recorded for the DET of these two electrodes: the background current in black and the CVs for 10 mM lactose in red. A clearly visible catalytic current in the presence of lactose can be observed with E522 (Figure 5.25-A and B), while no catalytic current was detected with T701 (C and D).

These results are very different from the ones we found using flat GC electrodes, in Section 5.1.2. In fact, in Figure 5.3 we can see that only the electrode modified with the variant T701 produced a DET catalytic current, while the one with E522 did not. On the other hand, with flat gold electrodes the situation is the opposite. This fact could be related to the different orientation of the two CDH variants on the electrodes, due to the different positions of the free cysteine residues, combined with the different electrode materials they were immobilised on. For instance, the side of E522 oriented towards the electrode might have better electrostatic interactions with a gold surface (and with the passivating group

used on gold electrodes, which was butyric acid on diazonium salt) than with a carbon surface (and with the passivating group used with carbon, *N*-(2-aminoethyl)acetamide). This would result in the haem group of E522 being closer to the surface when immobilised on a gold electrode and farther in the case of carbon electrodes, thus giving DET only in the first case. On the other hand, the situation would be quite the opposite for the variant T701: in this case, the amino acids oriented towards the electrode when T701 is covalently immobilised might form better interactions with a carbon surface than with a gold one, therefore producing the DET current only in the first case.

Note that, when the enzymes were immobilised on GC/CNT electrodes, both these variants produced a DET current (see Figures 3.5, 3.8 or 3.11). In fact,

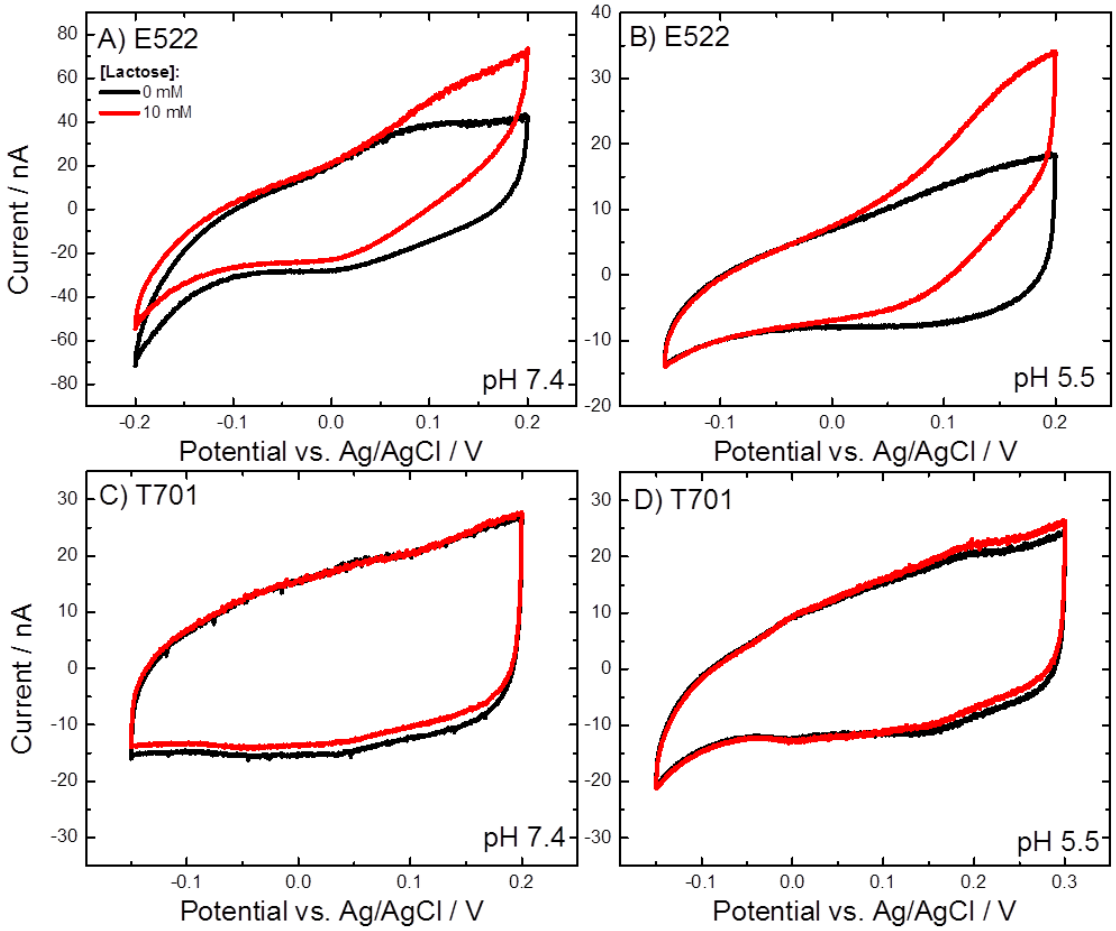

Figure 5.25. *CVs recorded at SPR substrates modified with (A-B) E522 and (C-D) T701-CDH, in 50 mM Bis-Tris buffer at pH (A-C) 7.4 and (B-D) 5.5, containing 30 mM $CaCl_2$ (black lines), and after the addition of 10 mM lactose (red lines). The CVs were carried out inside the SPR instrument by scanning the electrode potential at 1 mV/s.*

nanostructured electrodes facilitate the DET for all the different orientations of CDH. However, an experiment performed at pH 7.4 showed a higher DET current for T701 if compared with E522 (Figure 3.26). This was accounted for by a better orientation of the variant T701 (at least at neutral pH, when the two CDH domains are freer to move), which seems to have a better interaction with carbon electrodes than E522, as we found also in this Chapter.

Another question is: why the variant E522 showed DET in this experiment while before, when immobilised on gold screen-printed electrodes or gold disc electrodes, it did not? This could be due to the particular characteristics of the SPR substrates and the electrochemical SPR cuvette. The substrates present a very thin layer of gold (≈ 30 nm) having a large dimension (around 2 cm in diameter), even though the effective area used for the electrochemical and spectral measurements is defined by the two channels in the SPR cuvette and does not exceed 0.5 cm^2. These channels, in fact, form a very small electrochemical cell with the counter and reference electrodes fixed on the sides and very close to the underlying gold electrode (see Figure 2.6 in the Experimental Part). A few μL (around 20-30) of solution are sufficient to fill the channels. This set-up is probably very appropriate to study the DET of CDH as the relatively high active area of the working electrode can retain a great amount of enzyme, while the few drops of solution and the close vicinity of the counter and reference electrodes keep the solution resistance very low. In this way also very small currents can be detected. In fact, in one of the background CVs recorded at a E522-CDH modified substrate (black line in Figure 5.25-A), the redox peaks of the enzyme are visible at about 0.05 V: we have not seen this with any other flat electrode.

However, another concern regards the potential at which DET was detected. In Figure 5.25-A and B, we can observe the catalytic current starting around 0.05 V *vs.* Ag/AgCl. This potential is much more positive than that observed before for *Mt*CDH immobilised at carbon electrodes, which was around -0.15 V *vs.* SCE (see Figure 5.3-C in this Chapter or several other figures in Chapter 3). It is true that the reference electrode used in the SPR experiment (a pseudo Ag/AgCl electrode) was different than the one normally employed in this work, which was a SCE. However, the potential difference between the two reference electrodes was

measured to be around 20 mV, so this does not explain the bigger difference in the potential observed for the catalytic current. This fact would require a further investigation.

Another observation in Figure 5.25 concerns the effect of the solution pH. The DET current at acidic pH, at least for the variant E522 (Figure 5.25-B), seems higher than at neutral pH (Figure 5.25-A). This may be due to the different conformations that the enzyme assumes at different pH, and it is consistent with literature results reporting higher DET current for *Mt*CDH between pH 5.0 and 5.5 [73,74,123] due to a better interaction between the two domains at acidic pH.

In conclusion, SPR spectroscopy was useful to study the immobilization kinetics of cysteine-modified CDH variants at maleimide-modified gold substrates. The rate of the immobilization reaction strongly depends on the enzyme concentration in solution. However, allowing enough time for the reaction to occur, even the lowest concentrations can produce surface coverages comparable to the ones given by the most concentrated solutions, so that we can use very small amounts of the precious enzyme. Another thing to consider is that different CDH variants could have different rate constants for the immobilization reaction, since the free cysteine could be more or less accessible for the reaction with maleimide. Therefore, it is recommended to leave the CDH solution on the electrodes for at least 2-3 hours at room temperature, or overnight in the fridge. Finally, some SPR substrates modified with CDH were tested for DET, showing a catalytic current in the case of the variant E522, while T701 did not give any DET current. This point should be further investigated, possibly using similar gold electrodes with a similar set-up.

5.4 Conclusion

In this Chapter we showed the covalent, site-specific immobilization of CDH at flat electrodes, starting with glassy carbon electrodes and then moving on to gold electrodes. To begin, the GC electrodes were compared with GC/CNT electrodes by using a redox probe, anthraquinone (AQ), covalently immobilised at the carbon surfaces using the same procedure already employed to attach the maleimide groups in Chapter 3. The amount of immobilised AQ was used to estimate the active area of the GC/CNT electrodes, which was found to be about 100 times higher than that of GC electrodes, therefore around 14 cm^2. This was in agreement with the value obtained through a geometrical calculation described by A. Peigney *et al.* [162].

Afterwards, two different CDH variants (E522 and T701) were immobilised on GC electrodes using the same method, and tested for the direct and mediated electron transfer. Despite both the enzymes exhibited a MET current proving that the immobilization occurred, only T701 showed a DET catalytic current (Figure 5.3). This was explained with a better orientation of the variant T701, when immobilised at flat carbon electrodes, whose haem group would be able to exchange electrons with the electrode surface unlike the one of E522.

Subsequently, we moved on to the immobilization of CDH on gold, which has a great interest as electrode material for biosensor and biofuel cell applications, being highly biocompatible as well as very conductive. Firstly, we needed to develop a new procedure to be used with gold electrodes, since the electrochemical oxidation of amines, previously employed on carbon electrodes, does not work on gold. This new procedure uses instead the electrochemical grafting of a diazonium salt, which was our new linker. The new method was characterised with different techniques: cyclic voltammetry upon the immobilization of anthraquinone as redox probe, ToF-SIMS and SPR spectroscopy. CV and SPR were found useful methods to verify that the steps of diazonium salt grafting, Boc deprotection of the same and coupling of a carboxylic acid were working. In addition, the SPR spectroscopy proved that we can use “milder” conditions during the modification procedure, such as less concentrated acid for the Boc deprotection and, in general, solvents like water or

ethanol instead of DMF or dioxane. This is important in the case we use delicate electrodes or instruments that can be damaged by strong acids or organic solvents, but it is also a more sustainable solution.

Therefore, the new method was applied to the covalent immobilization of CDH variants at flat gold electrodes, testing them for the direct and mediated electron transfer, using both glucose and lactose as substrates. The MET experiments showed that the immobilization of the enzyme was successful and very reproducible. However, no DET catalytic current was detected for these electrodes (gold SPEs or gold disc electrodes), neither at pH 5.5 nor at pH 7.4. In any case, some control experiments were performed: the new immobilization procedure was tested on a GC/CNT electrode proving that it is comparable with the previous method used for carbon electrodes (Section 5.3.2); an experiment with D- and L-glucose verified that the observed MET catalytic current was effectively due to the enzyme (Section 5.3.6); finally, a gold electrode without any modification was compared with a maleimide-modified gold electrode for the immobilization of CDH, showing a much lower MET current that was not very stable for long periods, while the covalently immobilised enzyme exhibited a rather constant activity for more than 50 days (Sections 5.3.7 and 5.3.8).

The effect of different spacers in the construction of the CDH-modified gold electrodes was also studied (Section 5.3.9). The best results were obtained with a 3C-spacer, while the electrode modified without any spacer presented the lowest current density probably because a lower amount of CDH molecules could be accommodated due to steric restrictions upon coupling between cysteine and maleimide, as the latter was basically at the same height as the passivating group (see Scheme 5.8).

Finally, SPR spectroscopy was employed again to characterise the immobilization kinetics of CDH at maleimide-modified gold electrodes. We found that the rate constant of the immobilization reaction strongly depends on the enzyme concentration in solution, while this does not significantly affect the final surface coverage. Therefore, leaving enough time for the reaction to occur, even the less concentrated solutions can produce the maximum surface coverage. The reaction times, however, are different for different CDH variants, since different rate

constants were obtained for the immobilization reaction of three variants, with values going from 4 to 30 × 10^{-4} s^{-1}. It is therefore recommended to leave the CDH solution on the electrodes for the immobilization for at least 2-3 hours at room temperature, or overnight in the fridge. Lastly, some CDH-modified SPR gold substrates were tested for DET inside the electrochemical SPR cuvette: the variant E522 showed a DET catalytic current starting at 0.05 V *vs.* Ag/AgCl, while T701 did not (Figure 5.25). These results were the opposite of the ones obtained with flat GC electrodes in Section 5.1.2. This fact was accounted for different orientations of the two CDH variants, E522 and T701, immobilised at flat electrodes, due to the different positions of their cysteine residues, combined with the different electrode materials they were immobilised on. For instance, E522 would have a better interaction with a gold surface (and with the passivating group used on gold), while T701 would interact better with a carbon surface.

We can conclude that the site-specific immobilization at flat electrodes can allow a better discrimination between different CDH variants bearing the free cysteine in different locations, if compared with GC/CNT electrodes. In fact, the carbon nanotubes used in this work were 9.5 nm in diameter, which is roughly the same dimension of CDH, so that a CDH molecule attached to a nanotube could easily transfer electrons to another nanotube in close proximity. Probably this is the reason why all the four CDH variants used in this work showed a good DET on GC/CNT electrodes, even though their cysteine residues were located in opposite sides of the flavin domain. However, the experimental conditions for the electrochemical measurements should be improved since we could not detect the DET current for most of the gold electrodes used in this work.

Chapter 6:

Conclusions

In this thesis we showed the covalent, site-specific immobilization of a redox enzyme, cellobiose dehydrogenase, at carbon and gold electrodes. For the site-specific immobilization we employed the reaction between the thiol of enzymatic cysteine residues and maleimide groups attached on the electrode surface. The benefit of such reaction is that it occurs spontaneously at room temperature and neutral pH, without the need of any other reagent or catalyst. Moreover, the wild type of *Mt*CDH, like many other enzymes, does not present any surface cysteine residue, so that we could genetically engineer the enzyme to introduce only one cysteine residue at specific locations on the surface. This was performed through site directed mutagenesis by our co-workers at the BOKU-University of Vienna (Austria), who provided for this work four different *Mt*CDH variants with the cysteine in different positions.

The electrodes were modified with maleimide groups using a modular approach based on electrografting and solid-phase synthesis. The key point of this method is that the main elements of the modification can be independently varied to tune the architecture of the electrode surface as required, by simply changing the "bricks" of the structure. In this way, we could modify carbon electrodes employing the electrochemical oxidation of amines, and gold electrodes using instead the electrochemical grafting of a diazonium salt. For all the electrodes, however, the reactive group (maleimide) was unvaried, as well as the idea of forming a mixed two-component monolayer on the surface in order to dilute the reactive group and facilitate the reaction between it and the cysteine at the enzyme surface.

The CDH-modified electrodes were tested for direct and mediated electron transfer, confirming that the immobilization of the enzyme occurred. In addition, both carbon and gold electrodes covalently modified with CDH showed an excellent long-term stability, with a rather constant activity for about two months (or longer). This confirmed that an efficient immobilization method, such as the one employed in this work, can greatly extend the enzyme life-time, even outside its natural environment. Contrarily, the mere physical adsorption produced electrodes less stable over long periods and with lower amounts of biocatalyst if compared with the maleimide-modified ones.

The immobilization of CDH at GC/CNT electrodes, taken as a model for high surface area carbon electrodes, produced the best results for applications such as biofuel cells or biosensors. In fact, with these electrodes very high catalytic currents were obtained, even without the need of redox mediators, as the direct electron transfer between CDH and the electrode surface was very efficient. Therefore, the CDH-modified GC/CNT electrodes were used to perform many different tests, for example to verify that CDH was actually responsible for the observed DET catalytic current (using D- and L-glucose) and to study the mechanisms of the direct and mediated electron transfer. This was done by analysing the catalytic and non-catalytic cyclic voltammograms for CDH, which were due to a pH-independent one-electron process clearly attributable to the haem group of the enzyme, and by using divalent cations. This latter experiment further confirmed that the DET current is due to the haem group that shuttles

the electrons from the FAD to the electrode, since the catalytic current increased by adding calcium chloride in solution. On the other hand, in the MET pathway the mediator used in this work (a ferrocene derivative) was proven to interact directly with the FAD cofactor, thus excluding the haem group from this mechanism, as no increase in the catalytic current upon addition of $CaCl_2$ was observed.

The use of a ferrocene derivative, ferrocenecarboxylic acid, as mediator highlighted the occurrence of a potential shift for the MET catalytic current that depends on the mediator concentration. Using CDH-modified GC/CNT electrodes, such a potential shift was attributed to a very high rate constant for the reaction between the ferrocene and CDH, and the fact that the catalytic reaction is due to the oxidised form of the ferrocene, the ferrocenium ion. It was found that a very small amount of ferrocenium ions, around 1 μM, was sufficient to catalyse the reaction with CDH and produce the MET current. This was confirmed by the simulations of the catalytic voltammograms in Chapter 4, where the rate constant for the FAD/ferrocene reaction was found to have a really high value, which is 1×10^6 L mol^{-1} s^{-1}.

The simulations in Chapter 4 were carried out by using a potential-dependent Michaelis-Menten equation, which was derived by applying the Michaelis-Menten model for enzymatic reactions to the electrodic process of CDH. The computer simulations were a useful tool to study the kinetics of CDH at the electrode surface, have a better understanding of the Michaelis-Menten parameters extracted from the experimental data and give a value to the kinetic constants involved in the CDH catalytic reactions. In this way, we could find out which are the rate limiting steps that affect the current. For the DET, the current is mostly due to the IET as its rate constant was found to be the lowest one (around 5 s^{-1}), with also a contribution of the substrate/FAD reaction since its rate constant was just slightly higher (7.2 s^{-1}). In the MET, the rate limiting step is only the substrate/FAD reaction as the rate constant for the FAD/ferrocene reaction was found to be very high, as we said above, so that this step would not limit the current unless the concentration of mediator is very low (lower than 20 μM).

However, thanks to the simulations, a Michaelis-Menten-like interaction between CDH and the ferrocene was also supposed, as the ferrocene could act as a normal substrate for the enzyme. The simulations performed by applying this model suggested that also the ferrocene/CDH reaction could be a rate limiting step in the MET catalytic process, having a k_{cat} comparable to that of the glucose/FAD reaction (8 s^{-1} and 7.2 s^{-1}, respectively). In general, from the simulations, we concluded that the differences in the DET current observed between the four CDH variants immobilised at GC/CNT electrodes were mainly due to different IET rates, combined with different amounts of enzyme capable of DET. This was attributed to the different orientations of the four variants on the electrode surface, due to the different positions of their free cysteine residues.

However, a better discrimination between the different CDH variants was given by their immobilization at flat electrodes. Two variants covalently immobilised at flat GC electrodes proved that: in fact, only one (T701) showed a DET catalytic current, although both of them were immobilised on the electrode as confirmed by the MET experiment. Afterwards, we moved to flat gold electrodes since gold has a greater interest as an electrode material for biosensors and biofuel cells due to its high conductivity combined with a high biocompatibility, essential for medical implantable applications. As mentioned above, the immobilization procedure was slightly changed to be adapted to this new material. However, all the tests confirmed that CDH was effectively immobilised and in a more stable way if compared with physically adsorbed enzyme. Also in this case only one CDH variant showed a DET current, while the second one did not: however, the situation was inverted with respect to GC electrodes. This was attributed to the different orientations of the two variants (E522 and T701), combined with different interactions with the electrode material they were immobilised on.

The CDH-modified gold electrodes were tested to verify their stability, the effect of different pH and different substrates, and the best molecular architecture at the electrode surface (a 3C-spacer was found to produce the best results). Moreover, the kinetics of the immobilization reaction was studied using SPR spectroscopy: we found that the reaction between maleimide and cysteine-modified CDH is quite fast at room temperature and 2-3 hours are sufficient to fill the electrode surface with a monolayer of enzyme molecules, although the

reaction rate depends on the CDH concentration and position of the cysteine residue. However, other experiments could be performed in the future, as we will see in the next Section.

6.1 Future outlook

Some other experiments about the covalent immobilization of CDH at gold electrodes could be carried out. Firstly, the procedure developed in this work could be applied to nanostructured, high surface area gold electrodes with the aim of obtaining higher catalytic currents, comparable to those observed with GC/CNT electrodes in Chapter 3. Secondly, the DET of CDH immobilised on gold electrodes should be further investigated as, in Section 5.3.12, a DET catalytic current was observed at a potential much more positive than with carbon electrodes. Moreover, other different CDH variants should be tested for DET at flat electrodes (gold and carbon) to understand which mutations are capable of DET on a flat surface, and whether these two electrode materials always give different results. In fact, in this work it was not possible to perform such experiments with more than two CDH variants since these enzymes were only available in limited amounts from our collaborators at the BOKU-University of Vienna (Austria), and some of them were almost finished after the experiments carried out with GC/CNT electrodes (reported in Chapter 3). Note that the experiments with flat gold electrodes should be preferably performed using similar conditions to the ones employed for the SPR experiments in Chapter 5: in fact, the small dimension of the electrochemical SPR cell, with the reference and counter electrodes in fixed positions very close to the gold substrate and immersed in few µL of solution, could give very good results.

Also the solid-phase functionalization of CNTs with maleimide (or with other potential reactive groups) could be further investigated. In this work, we showed mainly the method to produce these modified CNTs (in Section 3.6), and tested them only on a few gold electrodes. However, other experiments to verify the stability and applicability of these nanotubes could be performed, as this method presents some interesting advantages:

- a large amount of CNTs can be modified with maleimide or other functional groups, stored and, if proven stable, used when necessary;
- such modified CNTs can be drop cast on different types of electrodes and supporting materials, being very stable once dried, probably because of the functional groups introduced;
- the modification of the CNTs before placing them on the electrode avoids the risk of damaging the electrode itself during the modification procedure.

Finally, the method described in this work could be tested for the site-specific immobilization of other enzymes bearing one surface cysteine, naturally present or genetically introduced. For instance, a colleague has already examined this procedure for the covalent immobilization of three bilirubin oxidase (BOD) variants, which were also genetically modified to have a free cysteine at their surface [180]. The enzyme immobilization was successful, but the BOD-modified electrodes did not present the same long-term stability as the CDH-modified ones. Other redox proteins or enzymes could be used and our procedure could be varied so that it can be better adapted to different biocatalysts or electrode materials, as all the elements of the modification can be independently changed.

List of References

[1] S.C. Barton, J. Gallaway, P. Atanassov, *Chem. Rev.* **2004**, 104, 4867-4886.

[2] A. Heller, *Phys. Chem. Chem. Phys.* **2004**, 6, 209 –216.

[3] R.A. Bullen, T.C. Arnot, J.B. Lakeman, F.C. Walsh, *Biosens. Bioelectron.* **2006**, 21 (11), 2015-2045.

[4] J.A. Cracknell, K.A. Vincent, F.A. Armstrong, *Chem. Rev.* **2008**, 108, 2439–2461.

[5] M.H. Osman, A.A. Shah, F.C. Walsh, *Biosens. Bioelectron.* **2011**, 26 (7), 3087-3102.

[6] K. Rabaey, W. Verstraete, *Trends Biotechnol.* **2005**, 23 (6), 291-298.

[7] P. Cinquin, Gondran, F. Giroud, S. Mazabrard, A. Pellissier, F. Boucher, J.P. Alcaraz, K. Gorgy, F.S. Cosnier, *PLoS One* **2010**, 5 (5), e10476.

[8] N.M. Farandos, A.K. Yetisen, M.J. Monteiro, C.R. Lowe, S.H. Yun, *Adv. Healthc. Mater.* **2014**, 4 (6), 792-810.

[9] M. Falk, V. Andoralov, Z. Blum, J. Sotres, D.B. Suyatin, T. Ruzgas, T. Arnebrant, S. Shleev, *Biosens. Bioelectron.* **2012**, 37 (1), 38-45.

[10] J. Kim, M. Kim, M.S. Lee, K. Kim, S. Ji, Y.T. Kim, J. Park, K. Na, K.H. Bae, H. Kyun Kim, F. Bien, C. Young Lee, J.U. Park, *Nat. Commun.* **2017**, 8, 14997.

[11] M. Southcott, K. MacVittie, J. Halamek, L. Halamkova, W.D. Jemison, R. Lobel, E. Katz, *Phys. Chem. Chem. Phys.* **2013**, 15 (17), 6278-6283.

[12] S. Clot, C. Gutierrez-Sanchez, S. Shleev, A.L. De Lacey, M. Pita, *Electrochem. Commun.* **2012**, 18, 37-40.

[13] A. Le Goff, M. Holzinger, S. Cosnier, *Cell. Mol. Life Sci.* **2015**, 72 (5), 941-952.

[14] C. Di Bari, S. Shleev, A.L. De Lacey, M. Pita, *Bioelectrochemistry* **2016**, 107, 30-36.

[15] N. Mano, *Appl. Microbiol. Biotechnol.* **2012**, 96 (2), 301-307.

[16] M. Cadet, X. Brilland, S. Gounel, F. Louerat, N. Mano, *Chem. Phys. Chem.* **2013**, 14 (10), 2097-2100.

[17] G.T.R. Palmore, H.H. Kim, *J.Electroanal. Chem.* **1999**, 464, 110–117.

[18] A.E.G. Cass, G. Davis, G.D. Francis, H.A.O. Hill, W.J. Aston, I.J. Higgins, E.V. Plotkin, L.D.L. Scott, A.P.F. Turner, *Anal. Chem.* **1984**, 56 (4), 667-671.

[19] P. Kavanagh, D. Leech, *Phys. Chem. Chem. Phys.* **2013**, 15 (14), 4859-4869.

[20] P. Bartlett, F.A. Al-Lolage, *J. Electroanal. Chem.* **2017**, (in press).

[21] A.A. Homaei, R. Sariri, F. Vianello, R. Stevanato, *J. Chem. Biol.* **2013**, 6 (4), 185-205.

[22] T. Tosa, T. Mori, N. Fuse, I. Chibata, *Enzymologia* **1966**, 31 (4), 214-224.

[23] T. Tosa, T. Shibatani, *Ann. N. Y. Acad. Sci.* **1995**, 750 (1), 364-375.

[24] N.R. Mohamad, N.H. Marzuki, N.A. Buang, F. Huyop, R.A. Wahab, *Biotechnol. Biotechnol. Equip.* **2015**, 29 (2), 205-220.

[25] L. Ma, X.T. Wang, D.L. You, S. Tang, Z.L. Huang, Y.H. Cheng, *Appl. Biochem. Biotechnol.* **1996**, 56, 223-233.

[26] B.M. Brena, F. Batista-Viera, *Immobilization of enzymes. A literature survey* in: *Methods in Biotechnology: Immobilization of Enzymes and Cells, Second Edition*, J.M. Guisan (Ed.), Humana Press Inc., Totowa, NJ (USA), **2006**, p. 15-30.

[27] P.N. Bartlett, *Bioelectrochemistry - Fundamentals, Experimental techniques and Applications*, P.N. Bartlett (Ed.), John Wiley & Sons Ltd, Chichester (UK), **2008**.

[28] R.J. Yon, *Biochem. J.* **1974**, 137, 127-130.

[29] B. Solomon, Z. Hollaander, R. Koppel, E. Katchalski-Kazir, *Use of monoclonal antibodies for the preparation of highly active immobilized enzymes* in: *Methods in Enzymology*, K. Mosbach (Ed.), Academic Press, London (UK), **1987**, p. 160-170.

[30] J.M.S. Cabral, J.M. Novais, J.F. Kennedy, *Appl. Microbiol. Biotechnol.* **1986**, 23, 157-162.

[31] N.C. Foulds, C.R. Lowe, *J. Chem. Soc. Faraday Trans. 1* **1986**, 82, 1259-1264.

[32] S. Cosnier, *Biosens. Bioelectron.* **1999**, 14, 443–456.

[33] Z. Salamon, J.T. Hazzard, G. Tollin, *Proc. Nat. Acad. Sci. USA* **1993**, 90, 6420-6423.

[34] R. Santucci, T. Ferri, L. Morpurgo, I. Savini, L. Avigliano, *Biochem. J.* **1998**, 332, 611–615.

[35] M. Guauque Torres, M.L. Foresti, M. Luján Ferreira, *AMB Express* **2013**, 3 (25).

[36] W. Liu, L. Wang, R. Jiang, *Top. Catal.* **2012**, 55 (16-18), 1146-1156.

[37] J. Kalia, R.T. Raines, *Chembiochem* **2006**, 7 (9), 1375-1383.

[38] J.E. Moses, A.D. Moorhouse, *Chem. Soc. Rev.* **2007**, 36 (8), 1249-1262.

[39] J. Kalia, N.L. Abbott, R.T. Raines, *Bioconjugate Chem.* **2007**, 18, 1064-1069.

[40] A. Tam, R.T. Raines, *Methods Enzymol.* **2009**, 462, 25-44.

[41] M. Kohn, R. Breinbauer, *Angew. Chem. Int. Ed.* **2004**, 43 (24), 3106-3116.

[42] L. Zhang, N. Vila, T. Klein, G.W. Kohring, I. Mazurenko, A. Walcarius, M. Etienne, *ACS Appl Mater Interfaces* **2016**, 8 (27), 17591-17598.

[43] L.R. Paborsky, K.E. Dunn, C.S. Gibbs, J.P. Dougherty, *Anal. Biochem.* **1996**, 234 (50), 60-65.

[44] M. Oshige, K. Yumoto, H. Miyata, S. Takahashi, M. Nakada, K. Ito, M. Tamegai, H. Kawaura, S. Katsura, *OJPChem.* **2013**, 3 (1), 6-10.

[45] M. Campas, B. Prieto-Simon, J.L. Marty, *Semin. Cell. Dev. Biol.* **2009**, 20 (1), 3-9.

[46] K. Hernandez, R. Fernandez-Lafuente, *Enzyme Microb. Technol.* **2011**, 48 (2), 107-122.

[47] R.F. Lane, A.T. Hubbard, *J. Phys. Chem.* **1973**, 77 (11), 1401-1410.

[48] P.R. Moses, L. Wier, R.W. Murray, *Anal. Chem.* **1975**, 47 (12), 1882-1886.

[49] C.M. Elliott, R.W. Murray, *Anal. Chem.* **1976**, 48 (8), 1247-1254.

[50] R.W. Murray, *Acc. Chem. Res.* **1980**, 13, 135-141.

[51] C.D. Bain, E.B. Troughton, Y.T. Tao, J. Evall, G.M. Whitesides, R.G. Nuzzo, *J. Am. Chem. Soc.* **1989**, 111, 321-335.

[52] A. Ulman, J.E. Eilers, N. Tillman, *Langmuir* **1989**, 5, 1147-1152.

[53] C.J. Zhong, M.D. Porter, *Anal. Chem.* **1995**, 67, A709-A715.

[54] M. Lewis, M. Tarolov, K. Carron, *J. Am. Chem. Soc.* **1995**, 117 (9574-9575).

[55] E. Delamarche, B. Michel, H. Kang, C. Gerber, *Langmuir* **1994**, 10, 4103-4108.

[56] W.R. Everett, T.L. Welch, L. Reed, I. Fritsch-Fades, *Anal. Chem.* **1995**, 67, 292-298.

[57] T. Kawaguchi, H. Yasuda, K. Shimazu, M.D. Porter, *Langmuir* **2000**, 16, 9830-9840.

[58] B. Barbier, J. Pinson, G. Desarmot, M. Sanchez, *J. Electrochem. Soc.* **1990**, 137, 1757-1764.

[59] A.J. Downard, *Electroanal.* **2000**, 12 (14), 1085-1096.

[60] M. DeIamar, R. Hitmi, J. Pinson, J.M. Savbnt, *J. Am. Chem. Soc.* **1992**, 114, 5883-5884.

[61] J. Pinson, F. Podvorica, *Chem. Soc. Rev.* **2005**, 34 (5), 429-439.

[62] D.M. Shewchuk, M.T. McDermott, *Langmuir* **2009**, 25 (8), 4556-4563.

[63] R.S. Deinhammer, M. Ho, J.W. Anderegg, M.D. Porter, *Langmuir* **1994**, 10, 1306-1313

[64] J.M. Chretien, M.A. Ghanem, P.N. Bartlett, J.D. Kilburn, *Chem. Eur. J.* **2008**, 14 (8), 2548-2556.

[65] M.A. Ghanem, J.M. Chrétien, A. Pinczewska, J.D. Kilburn, P.N. Bartlett, *J. Mater. Chem.* **2008**, 18 (41), 4917-4927.

[66] J.M. Chretien, M.A. Ghanem, P.N. Bartlett, J.D. Kilburn, *Chem. Eur. J.* **2009**, 15 (44), 11928-11936.

[67] A. Celiktas, M.A. Ghanem, P.N. Bartlett, *J. Electroanal. Chem.* **2012**, 670, 42-49.

[68] C.S. Lee, S.E. Baker, M.S. Marcus, W. Yang, M.A. Eriksson, R.J. Hamers, *Nano Letters* **2004**, 4 (9), 1713-1716.

[69] J.C. Harper, R. Polsky, D.R. Wheeler, S.M. Brozik, *Langmuir* **2008**, 24, 2206-2211.

[70] E.J. Wright, M. Sosna, S. Bloodworth, J.D. Kilburn, P.N. Bartlett, *Chem. Eur. J.* **2014**, 20 (19), 5550-5554.

[71] G. Henriksson, J. G., G. Pettersson, *J. Biotechnol.* **2000**, 78, 93-113.

[72] M. Zamocky, R. Ludwig, C. Peterbauer, B. Hallberg, C. Divne, P. Nicholls, D. Haltrich, *Curr. Protein Pept. Sci.* **2006**, 7 (3), 255-280.

[73] R. Ludwig, W. Harreither, F. Tasca, L. Gorton, *Chem. Phys. Chem.* **2010**, 11 (13), 2674-2697.

[74] R. Ludwig, R. Ortiz, C. Schulz, W. Harreither, C. Sygmund, L. Gorton, *Anal. Bioanal. Chem.* **2013**, 405 (11), 3637-3658.

[75] C. Schulz, R. Kittl, R. Ludwig, L. Gorton, *ACS Catal.* **2016**, 6 (2), 555-563.

[76] C. Schulz, R. Ludwig, P.O. Micheelsen, M. Silow, M.D. Toscano, L. Gorton, *Electrochem. Comm.* **2012**, 17, 71-74.

[77] A. Kadek, D. Kavan, A.K. Felice, R. Ludwig, P. Halada, P. Man, *FEBS Lett.* **2015**, 589 (11), 1194-1199.

[78] D. Kracher, K. Zahma, C. Schulz, C. Sygmund, L. Gorton, R. Ludwig, *FEBS J.* **2015**, 282, 3136-3149.

[79] G. Safina, R. Ludwig, L. Gorton, *Electrochimica Acta* **2010**, 55 (26), 7690-7695.

[80] F. Tasca, M.N. Zafar, W. Harreither, G. Noll, R. Ludwig, L. Gorton, *Analyst* **2011**, 136 (10), 2033-2036.

[81] M.N. Zafar, G. Safina, R. Ludwig, L. Gorton, *Anal. Biochem.* **2012**, 425 (1), 36-42.

[82] P. Bollella, L. Gorton, R. Ludwig, R. Antiochia, *Sensors* **2017**, 17 (8), 1912.

[83] H. Kanso, B.M. González García, S. Ma, R. Ludwig, P. Fanjul Bolado, D. Hernández Santos, *Electroanalysis* **2017**, 29 (1), 87-92.

[84] F. Lopez, S. Ma, R. Ludwig, W. Schuhmann, A. Ruff, *Electroanalysis* **2017**, 29 (1), 154-161.

[85] A. Yarman, C. Schulz, C. Sygmund, R. Ludwig, L. Gorton, U. Wollenberger, F.W. Scheller, *Electroanalysis* **2014**, 26 (9), 2043-2048.

[86] L. Stoica, A. Lindgren-Sjolander, T. Ruzgas, L. Gorton, *Anal. Chem.* **2004**, 76, 4690-4696.

[87] A. Lindgren, L. Stoica, T. Ruzgas, A. Ciucu, L. Gorton, *Analyst* **1999**, 124, 527-532.

[88] F. Tasca, L. Gorton, W. Harreither, D. Haltrich, R. Ludwig, G. Noll, *J. Phys. Chem. C* **2008**, 112, 13668-13673.

[89] V. Coman, R. Ludwig, W. Harreither, D. Haltrich, L. Gorton, T. Ruzgas, S. Shleev, *Fuel Cells* **2010**, 10 (1), 9-16.

[90] R. Ortiz, R. Ludwig, L. Gorton, *ChemElectroChem* **2014**, 1 (11), 1948-1956.

[91] E. Gonzalez-Arribas, T. Bobrowski, C. Di Bari, K. Sliozberg, R. Ludwig, M.D. Toscano, A.L. De Lacey, M. Pita, W. Schuhmann, S. Shleev, *Biosens. Bioelectron.* **2017**, 97, 46-52.

[92] P. Bollella, G. Fusco, D. Stevar, L. Gorton, R. Ludwig, S. Ma, H. Boer, A. Koivula, C. Tortolini, G. Favero, R. Antiochia, F. Mazzei, *Sens. Actuators B-Chem.* **2018**, 256, 921-930.

[93] A. Lindgren, L. Gorton, T. Ruzgas, U. Baminger, D. Haltrich, M. Schulein, *J. Electroanal. Chem.* **2001**, 496, 76-81.

[94] L. Stoica, N. Dimcheva, D. Haltrich, T. Ruzgas, L. Gorton, *Biosens. Bioelectron.* **2005**, 20 (10), 2010-2018.

[95] H. Matsumura, R. Ortiz, R. Ludwig, K. Igarashi, M. Samejima, L. Gorton, *Langmuir* **2012**, 28 (29), 10925-10933.

[96] A. Lindgren, T. Larsson, T. Ruzgas, L. Gorton, *J. Electroanal. Chem.* **2000**, 494, 105-113.

[97] D. Sarauli, R. Ludwig, D. Haltrich, L. Gorton, F. Lisdat, *Bioelectrochemistry* **2012**, 87, 9-14.

[98] U. Salaj-Kosla, M.D. Scanlon, T. Baumeister, K. Zahma, R. Ludwig, O.C. P, D. MacAodha, D. Leech, E. Magner, *Anal. Bioanal. Chem.* **2013**, 405 (11), 3823-3830.

[99] M. Shao, D.A. Guschin, Z. Kawah, Y. Beyl, L. Stoica, R. Ludwig, W. Schuhmann, X. Chen, *Electrochim. Acta* **2014**, 128, 318-325.

[100] J.Y. Damián-Almazo, G. Saab-Rincón, *Site-Directed Mutagenesis as Applied to Biocatalysts* in: *Genetic Manipulation of DNA and Protein - Examples from Current Research*, D. Figurski (Ed.), InTech, **2013**, p. 303-330.

[101] A. Zanghellini, L. Jiang, A.M. Wollacott, G. Cheng, J. Meiler, E.A. Althoff, D. Rothlisberger, D. Baker, *Protein Sci.* **2006**, 15 (12), 2785-2794.

[102] J. Meiler, D. Baker, *Proteins* **2006**, 65 (3), 538-548.

[103] A. Pavelka, E. Chovancova, J. Damborsky, *Nucleic Acids Res.* **2009**, 37 (Web Server issue), W376-W383.

[104] D.M. Mate, M. Alcalde, *Biotechnol. Adv.* **2015**, 33 (1), 25-40.

[105] D. Gonzalez-Perez, I. Mateljak, E. Garcia-Ruiz, F.J. Ruiz-Dueñas, A.T. Martinez, M. Alcalde, *Catal. Sci. Technol.* **2016**, 6 (17), 6625-6636.

[106] P. Molina-Espeja, J. Vina-Gonzalez, B.J. Gomez-Fernandez, J. Martin-Diaz, E. Garcia-Ruiz, M. Alcalde, *Biotechnol. Adv.* **2016**, 34 (5), 754-767.

[107] G. Canevascini, P. Borer, J.L. Dreyer, *Eur. J. Biochem.* **1991**, 198, 43-52.

[108] S. Trasatti, O.A. Petrii, *Pure Appl. Chem.* **1991**, 63 (5), 711-734.

[109] J. Lee, J. Lee, M. Kang, M. Shin, J.M. Kim, S.U. Kang, J.O. Lim, H.K. Choi, Y.G. Suh, H.G. Park, U. Oh, H.D. Kim, Y.H. Park, H.J. Ha, Y.H. Kim, A. Toth, Y. Wang, R. Tran, L.V. Pearce, D.J. Lundberg, P.M. Blumberg, *J. Med. Chem.* **2003**, 46, 3116-3126.

[110] E.J. Wright, PhD Thesis, University of Southampton (UK), **2014**.

[111] M.A. Ghanem, I. Kocak, A. Al-Mayouf, M. AlHoshan, P.N. Bartlett, *Electrochim. Acta* **2012**, 68, 74-80.

[112] M.A. Ghanem, J.M. Chretien, J.D. Kilburn, P.N. Bartlett, *Bioelectrochemistry* **2009**, 76 (1-2), 115-125.

[113] A. Pinczewska, M. Sosna, S. Bloodworth, J.D. Kilburn, P.N. Bartlett, *J. Am. Chem. Soc.* **2012**, 134 (43), 18022-18033.

[114] J. Mao, K. Hauser, M.R. Gunner, *Biochemistry* **2003**, 42 (33), 9829-9840.

[115] K. Hauser, J. Mao, M.R. Gunner, *Biopolymers* **2004**, 74 (1-2), 51-54.

[116] H.J. Lowe, W. Mansfield Clark, *J. Biol. Chem.* **1956**, 221, 983-992.

[117] S. Vogt, M. Schneider, H. Schafer-Eberwein, G. Noll, *Anal. Chem.* **2014**, 86 (15), 7530-7535.

[118] A.J. Bard, L.R. Faulkner, *Electrochemical Methods - Fundamentals and Applications, 2nd Edition*, Jonh Wiley & Sons Inc, New York (USA), **2001**.

[119] J.E. Frew, H.A.O. Hill, *Eur. J. Biochem.* **1988**, 172, 261-269.

[120] P.N. Bartlett, K.F.E. Pratt, *J. Electroanal. Chem.* **1995**, 397, 53-60.

[121] N.J. Forrow, G.S. Sanghera, S.J. Walters, *Dalton Trans.* **2002**, 16, 3187-3194.

[122] C. Schulz, R. Ludwig, L. Gorton, *Anal. Chem.* **2014**, 86 (9), 4256-4263.

[123] W. Harreither, V. Coman, R. Ludwig, D. Haltrich, L. Gorton, *Electroanalysis* **2007**, 19 (2-3), 172-180.

[124] E. Amri, F. Mamboya, *Am J. Biochem. Biotechnol.* **2012**, 8 (2), 99-104.

[125] G. Henriksson, G. Pettersson, G. Johansson, A. Ruiz, E. Uzcategui, *Eur. J. Biochem.* **1991**, 16, 101-106.

[126] J.D. Cohen, W. Bao, V. Renganathan, S. Sai Subramaniam, T.M. Loehr, *Arch. Biochem. Biophys.* **1997**, 341, 321-328.

[127] A.D. Baldwin, K.L. Kiick, *Bioconjug. Chem.* **2011**, 22 (10), 1946-1953.

[128] G. Arabaci, A. Usluoglu, *J. Chem.* **2013**, 2013, 1-6.

[129] A.B. Lowe, *Polym. Chem.* **2010**, 1 (1), 17-36.

[130] J.D. Gregory, *J. Am. Chem. Soc.* **1955**, 77 (14), 3922-3923.

[131] G.R. Grimsley, J.M. Scholtz, C.N. Pace, *Protein Sci.* **2009**, 18 (1), 247-251.

[132] S.S. Wong, E. Joselevich, A.T. Woolley, C.L. Cheung, C.M. Lieber, *Nature* **1998**, 394, 52-55.

[133] J.K. Towns, F.E. Regnier, *Anal. Chem.* **1991**, 63, 1126-1132.

[134] E. Dickinson, S. Tanai, *J. Agric. Food Chem.* **1992**, 40, 179-183.

[135] M. Shim, N.W. Shi Kam, R.J. Chen, Y. Li, H. Dai, *Nano Lett.* **2002**, 2 (4), 285-288.

[136] B. Huang, H. Wu, S. Kim, R.N. Zare, *Lab Chip* **2005**, 5 (10), 1005-1007.

[137] P. Abiman, G.G. Wildgoose, R.G. Compton, *Int. J. Electrochem. Sci.* **2008**, 3, 104-117.

[138] F. Barrière, A.J. Downard, *J. Solid State Electrochem.* **2008**, 12 (10), 1231-1244.

[139] M.A. Ghanem, I. Kocak, A. Al-Mayouf, P.N. Bartlett, *Electrochem. Commun.* **2013**, 34, 258-262.

[140] F. Lisdat, U. Wollenberger, A. Makower, H. Hortnagl, D. Pfeiffer, F.W. Scheller, *Biosens. Bioelectron.* **1997**, 12 (12), 1199-1211.

[141] F. Lisdat, W.O. Ho, U. Wollenberger, F.W. Scheller, T. Richter, U. Bilitewski, *Electroanal.* **1998**, 10 (12), 803-807.

[142] L. Michaelis, M.L. Menten, *Biochem. Z.* **1913**, 49, 333-369.

[143] M. Lesanavičius, O. Smutok, B. Valiauga, A. Marozienė, M. Gonchar, K. Krikštopaitis, N. Čėnas, *Chemija* **2016**, 27 (2), 123-127.

[144] S. Daff, W.J. Ingledew, G.A. Reid, S.K. Chapman, *Biochemistry* **1996**, 35, 6345-6350.

[145] S.K. Chapman, G.A. Reid, S. Daff, R.E. Sharp, P. White, F.D.C. Manson, F. Lederer, *Biochem. Soc. Trans.* **1994**, 22 (3), 713-718.

[146] F. Tasca, L. Gorton, M. Kujawa, I. Patel, W. Harreither, C.K. Peterbauer, R. Ludwig, G. Noll, *Biosens. Bioelectron.* **2010**, 25 (7), 1710-1716.

[147] M. Zamocky, C. Schumann, C. Sygmund, J. O'Callaghan, A.D. Dobson, R. Ludwig, D. Haltrich, C.K. Peterbauer, *Protein Expr. Purif.* **2008**, 59 (2), 258-265.

[148] S.A. Trashin, D. Haltrich, R. Ludwig, L. Gorton, A.A. Karyakin, *Bioelectrochemistry* **2009**, 76 (1-2), 87-92.

[149] M.S. Rogers, G.D. Jones, G. Antonini, M.T. Wilson, M. Brunori, *Biochem. J.* **1994**, 298, 329-334.

[150] B.P. Roy, T. Dumonceaux, A.A. Koukoulas, F.S. Archibald, *Appl. Environ. Microbiol.* **1996**, 62 (12), 4417-4427.

[151] U. Baminger, S.S. Subramaniam, V. Renganathan, D. Haltrich, *Appl. Environ. Microbiol.* **2001**, 67 (4), 1766-1774.

[152] F. Xu, E.J. Golightly, K.R. Duke, S.F. Lassen, B. Knusen, S. Christensen, K.M. Brown, B. S.H., M. Schulein, *Enzyme Microb. Technol.* **2001**, 28 (9-10), 744-753.

[153] S.S. Subramaniam, S.R. Nagalla, V. Renganathan, *Arch. Biochem. Biophys.* **1999**, 365 (2), 223-230.

[154] R. Ludwig, A. Salamon, J. Varga, M. Zamocky, C.K. Peterbauer, K.D. Kulbe, D. Haltrich, *Appl. Microbiol. Biotechnol.* **2004**, 64 (2), 213-222.

[155] W. Harreither, C. Sygmund, E. Dunhofen, R. Vicuna, D. Haltrich, R. Ludwig, *Appl. Environ. Microbiol.* **2009**, 75 (9), 2750-2757.

[156] C. Sygmund, D. Kracher, S. Scheiblbrandner, K. Zahma, A.K. Felice, W. Harreither, R. Kittl, R. Ludwig, *Appl. Environ. Microbiol.* **2012**, 78 (17), 6161-6171.

[157] P.S. Guin, S. Das, P.C. Mandal, *Int. J. Electrochem.* **2011**, 2011, 1-22.

[158] F. Li, Y. Wang, D. Wang, F. Wei, *Carbon* **2004**, 42 (12-13), 2375-2383.

[159] S. Chakraborty, J. Chattopadhyay, H. Peng, Z. Chen, A. Mukherjee, R.S. Arvidson, R.H. Hauge, W.E. Billups, *J. Phys. Chem. B* **2006**, 110, 24812-24815.

[160] A.A. Bakhtiary Davijani, H.C. Liu, K. Gupta, S. Kumar, *ACS Appl. Mater. Interfaces* **2016**, 8 (37), 24918-24923.

[161] M.T. McDermott, C.A. McDermott, R.L. McCreery, *Anal. Chem.* **1993**, 65, 937-944.

[162] A. Peigney , C. Laurent, E. Flahaut, R.R. Bacsa, A. Rousset, *Carbon* **2001**, 39, 507-514.

[163] M. Sosna, J.M. Chretien, J.D. Kilburn, P.N. Bartlett, *Phys. Chem. Chem. Phys.* **2010**, 12 (34), 10018-10026.

[164] A. Benninghoven, F.G. Rüdenauer, H.W. Werner, *Secondary Ion Mass Spectrometry: Basic Concepts, Instrumental Aspects, Applications, and Trends*, Wiley, New York (USA), **1987**.

[165] J.C. Vickerman, A. Brown, N.M. Reed, *Secondary Ion Mass Spectrometry: Principles and Applications*, Clarendon Press, Oxford (UK), **1989**.

[166] B. Liedberg, C. Nylander, I. Lundstrom, *Sens. Actuators* **1983**, 4, 299-304.

[167] R.P.H. Kooyman, H. Kolkman, J. Van Gent, J. Greve, *Anal. Chim. Acta* **1988**, 213, 35-45.

[168] E. Stenberg, B. Persson, H. Roos, C. Urbaniczky, *J. Colloid Interface Sci.* **1991**, 143 (2), 513-526.

[169] L.S. Jung, C.T. Campbell, T.M. Chinowsky, M.N. Mar, S.S. Yee, *Langmuir* **1998**, 14, 5636-5648.

[170] G. Henriksson, V. Sild, I.J. Szabo, G. Pettersson, G. Johansson, *BBA* **1998**, 1383, 48-54.

[171] M.J. Tarlov, E.F. Bowden, *J. Am. Che. Soc.* **1991**, 113, 1847-1849.

[172] J.J. Gooding, D.B. Hibbert, *Trend. Anal. Chem.* **1999**, 18 (8), 525-533.

[173] X. Chen, R. Ferrigno, J. Yang, G.M. Whitesides, *Langmuir* **2002**, 18, 7009-7015.

[174] J. Homola, *Chem. Rev.* **2008**, 108, 462-493.

[175] H. Fischer, I. Polikarpov, A.F. Craievich, *Protein Sci.* **2004**, 13 (10), 2825-2828.

[176] T.C. Tan, D. Kracher, R. Gandini, C. Sygmund, R. Kittl, D. Haltrich, B.M. Hallberg, R. Ludwig, C. Divne, *Nat. Commun.* **2015**, 6, 7542.

[177] J. Feder, *J. Theor. Biol.* **1980**, 87 (2), 237-254.

[178] E.L. Hinrichsen, J. Feder, T. Jossang, *J. Stat. Phys.* **1986**, 44, 793-827.

[179] P.R. Edwards, R.J. Leatherbarrow, *Anal. Biochem.* **1997**, 246, 1-6.

[180] F.A. Al-Lolage, PhD Thesis, University of Southampton (UK), **2018**.